EPA United States
Environmental Protection
Agency

Simulating Radionuclide Fate and Transport in the Unsaturated Zone: Evaluation and Sensitivity Analyses of Select Computer Models

Simulating Radionuclide Fate and Transport in the Unsaturated Zone: Evaluation and Sensitivity Analyses of Select Computer Models

by

Jin-Song Chen, Ronald L. Drake and Zhixun Lin
Dynamac Corporation
3601 Oakridge Boulevard
Ada, OK 74820

David G. Jewett
Subsurface Protection and Remediation Division
National Risk Management Research Laboratory
Ada, OK 74820

Project Officer

David S. Burden
Subsurface Protection and Remediation Division
National Risk Management Research Laboratory
Ada, OK 74820

NOTICE

The U.S. Environmental Protection Agency, through its Office of Research and Development, partially funded and collaborated in the research described here under Contract Number 68-C-99-256 to Dynamac Corporation. It has been subjected to the Agency's peer and administrative review and has been approved for publication as an EPA document. Mention of modeling codes does not constitute endorsement or recommendation for use.

FOREWORD

The U.S. Environmental Protection Agency is charged by Congress with protecting the Nation's land, air, and water resources. Under a mandate of national environmental laws, the Agency strives to formulate and implement actions leading to a compatible balance between human activities and the ability of natural systems to support and nurture life. To meet these mandates, EPA's research program is providing data and technical support for solving environmental problems today and building a science knowledge base necessary to manage our ecological resources wisely, understand how pollutants affect our health, and prevent or reduce environmental risks in the future.

The National Risk Management Research Laboratory is the Agency's center for investigation of technological and management approaches for reducing risks from threats to human health and the environment. The focus of the Laboratory's research program is on methods for the prevention and control of pollution to air, land, water, and subsurface resources; protection of water quality in public water systems; remediation of contaminated sites and ground water; and prevention and control of indoor air pollution. The goal of this research effort is to catalyze development and implementation of innovative, cost-effective environmental technologies; develop scientific and engineering information needed by EPA to support regulatory and policy decisions; and provide technical support and information transfer to ensure effective implementation of environmental regulations and strategies.

Mathematical models are useful tools for determining soil screening levels of radionuclides in the unsaturated zone. However, models require users to specify various parameters characteristic of the site and chemical of interest. These parameters are not known without error. Many parameters vary over time and space in manners which are unknown. This is especially true when models are used to predict future events. This uncertainty in input parameters is associated with an uncertainty in model output which should be recognized by the model user. This report analyzes several transport models for unsaturated soils and quantifies the sensitivity of model outputs to changes in input parameters. This information will help users understand the importance of different parameters, identify parameters which must be determined at the site, interpret model results and apply their findings to specific problems.

Stephen G. Schmelling, Acting Director
Subsurface Protection and Remediation Division
National Risk Management Research Laboratory

ABSTRACT

Numerical, mathematical models of water and chemical movement in soils are used as decision aids for determining soil screening levels (SSLs) of radionuclides in the unsaturated zone. Numerous transport and fate modeling codes exist for predicting movement and degradation of these hazardous chemicals through soils. Many of these codes require extensive input parameters which include uncertainty due to soil variability and unknown future meteorological conditions. The impacts of uncertain model parameters upon pertinent model outputs are required for sound modeling applications. Model users need an understanding of these impacts so they can collect the appropriate parameters for a given site and incorporate the uncertainties in the model predictions into the decision making process. This report primarily summarizes the findings which address the uncertainties and sensitivities of model outputs due to uncertain input parameters. However, the report also addresses the sensitivity of simulated results to conceptual model selection, and the comparison of sensitivity results between models, illuminating numerical differences and errors.

The objective of the parameter sensitivity studies was to determine the sensitivities and uncertainties of peak contaminant concentrations and time to peak concentrations at the water table, as well as those for the time to exceed the contaminant's MCL at a representative receptor well. The five models selected for these analyses were CHAIN, MULTIMED-DP 1.0, FECTUZ, CHAIN 2D, and HYDRUS. All of these are designed to estimate movement and fate of radionuclides through unsaturated soils. The models span a range in detail and intended use. This report presents information on the sensitivity of these codes to model conceptualization of radionuclide transport in the vadose zone, to numerical differences and errors, and to changes and uncertainties in input parameters, as well as presenting information concerning the analysis and interpretation of certain modeling components. The report does not intend to assess the appropriateness of any model for a particular use nor the uncertainty due to the model chosen, but it does indicate the problems and limits of using certain modeling components for certain physical applications.

Model parameters investigated include soil properties such as soil structure and texture, bulk density, water content, and hydraulic conductivity. Chemical properties examined include distribution coefficient, degradation half-life, dispersion coefficient, and molecular diffusion. Other site and soil characteristics such as equilibrium/nonequilibrium sorption sites, rooting depth, recharge rate, hysteretic effects, and precipitation/evapotranspiration were examined. Model parameter sensitivity was quantified in the form of sensitivity and relative sensitivity coefficients. The sensitivity coefficient is useful when calculating the absolute change in an output due to a known change in a single parameter. Relative sensitivity is useful in determining the relative change in an output corresponding to a specific relative change in one input parameter. Relative sensitivities are also used to compare the sensitivities of different parameters. These results are presented in graphical and tabular forms.

This study identified the limitations and advantages of using the selected codes for assessing the transport and fate of radionuclides in the unsaturated zone. This study also found the degree of uncertainty that exists in various model output parameters due to the combination of sensitivities of input parameters, high parameter variabilities, model type with its particular set of components, and the specific properties of the radionuclides. In addition, the study found that predicted movement of radionuclides was greater when the natural variability of daily rainfall was incorporated into the model than when only an annual flux was used. This is because major precipitation events (their daily averages in this case) result in larger fluxes of water and higher leaching rates that are essentially smoothed over when annual averaged fluxes are used. The study reaffirms that uncertainty is pervasive in natural systems and that results of modeling efforts presented in a deterministic fashion may be misleading, unless the results of modeling studies are presented in terms of probabilities of various outcomes. Further, this report evaluates model parameter sensitivity for a specific scenario, that is, radionuclide transport and fate through a 6 m homogeneous soil column at the Las Cruces Trench Site in New Mexico. For other scenarios, the general model user should take great care in the use of the results of the current study. Other sensitivity and uncertainty estimates may be required for the specific conditions and parameters of interest.

Contents

Figures

Tables

Section 1
Introduction

This report is concerned with the evaluation and sensitivity analysis of select computer models for simulating radionuclide fate and transport in the unsaturated zone. The work reported here was performed in support of the U.S. Environmental Protection Agency's (EPA's) project on Soil Screening Guidance (SSG) for Radionuclides (U.S. EPA, 2000ab). The models reviewed and evaluated in the current report form a small subset of the models available to the public, and those which are considered have not met U.S. EPA approval for the exclusive use in the Soil Screening Level (SSL) process. Other models also may be applicable to the SSL effort, depending on pollutant-and site-specific circumstances.

1.1. The Radionuclide SSL Effort

The U.S. EPA developed the Soil Screening Guidance for Radionuclides (U.S. EPA, 2000ab) as a tool to help standardize and accelerate the evaluation and cleanup of soils contaminated with radioactive materials at sites on the National Priorities List (NPL) with future residential land use. This guidance is intended for the appropriate environmental professionals to be able to calculate risk-based, site-specific, SSLs for radionuclides in soil, thus allowing them to identify areas needing further investigation at NPL sites. However, these SSLs alone do not trigger the need for response actions or define "unacceptable" levels of radionuclides in soil. In these guidance documents, "screening" refers to the process of identifying and defining areas, radionuclides, and physical conditions at a particular site that do not require further Federal action. Generally speaking, at sites where radionuclide concentrations fall below SSLs, no further action or study is warranted under the Comprehensive Environmental Response, Compensation and Liability Act (CERCLA). Where radionuclide concentrations equal or exceed SSLs, further study or investigation, but not necessarily cleanup, is generally warranted.

In identifying and managing risks at sites, EPA considers a spectrum of radionuclide concentrations (Figure 1-1). The level of concern associated with the concentrations in the figure depends on the likelihood of exposure to radioactive soil contamination at levels of potential concern to human health. As stated above, if the soil concentrations fall between zero and SSL, no further study is warranted under CERCLA. If the soil concentrations fall between SSL and RL (the response level), then further study and investigation are warranted, but response action may not be warranted. For sites requiring cleanup, the goal or level of cleanup, SSCG, must fall below RL and be such that no further action is required.
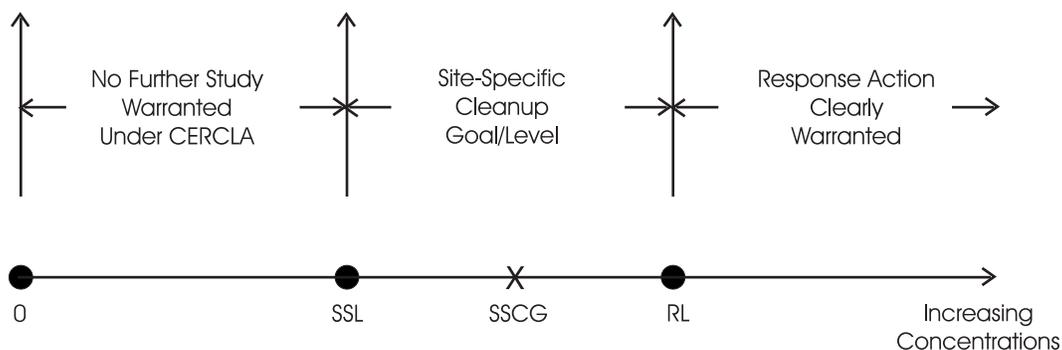
Figure 1-1. Conceptual risk management spectrum for contaminated soil, where SSL is the soil screening level, RL is the response level, and SSCG is a hypothetical, site-specific cleanup goal/level (from U.S. EPA, 2000a).

1

The soil screening process is a seven-step approach (U.S. EPA, 2000a) consisting of the following steps:

- Developing a conceptual site model (CSM),
- Comparing the CSM to the SSL scenario,
- Defining data collection needs,
- Sampling and analyzing soils at the site,
- Calculating site-specific SSLs,
- Comparing site soil radionuclide concentrations to calculated SSLs,
- Determining which areas of the site require further study.

In following this process, several exposure pathways are addressed by the SSLs for radionuclides, such as produce ingestion, soil ingestion, external radiation from soil and dust, and the consumption of drinking water. The models considered in this report are concerned with the pathway from a surface source of radionuclides, down through the unsaturated zone and finally leading to a ground-water aquifer which is a source of drinking water.

1.2 The Available Modeling Techniques for the Unsaturated Zone

Over the last ten to fifteen years, due in part to large increases in computer speed and memory, there has been an explosion in the number of modeling techniques and numerical computer codes applicable to the investigation and simulation of flow and transport through the unsaturated zone. The general discussion of subsurface contaminant hydrogeology is covered in many recent texts, among which are those of Zheng and Bennett (1995), Fetter (1999), Bedient et al. (1999) and Charbeneau (2000). In addition, there are several excellent books and reports concerned with individual processes (e.g., chemical reactions, sorption processes, and media interface problems) and modeling tools and their properties. These publications include texts on physicochemical hydrodynamics by Probstein (1994), environmental chemodynamics by Thibodeaux (1996), and a text on multicomponent fluids by Drew and Passman (1999). Two texts on modeling tools and their mathematical properties are those of Logan (2001) and Nirmalakhandan (2002). A compilation of simple mathematical models for the estimation of infiltration rates of water into the vadose zone is given in Ravi and Williams (1998) and Williams et al. (1998), while discussions of porous medium thermodynamics are given in Bear and Nitao (1995) and Spanos (2002). The dynamics of fluids in fractured rock, under both saturated and unsaturated conditions, have been covered in many references, such as Bear (1993), Clemo and Smith (1997), Stockman (1997), Pruess et al. (1999), and Faybishenko et al. (2000). Because of uncertainties in, lack of knowledge about, and the inherent randomness of subsurface hydrogeology, some investigators have forsaken the "deterministic world" of the subsurface and have concentrated on the "random" nature of subsurface processes and their stochastic simulation. Important references in this regard are those of Dagan (1989), Chilès and de Marsily (1993), and Gelhar (1993). To better understand flow and transport processes on the microscale, and how these processes affect macroscale flow and transport, investigators have applied cellular automata and fractal techniques in their analyses, techniques that are very adaptable to the current upsurge in parallel computational hardware and software. The use of fractal geometry in geology, geophysics and porous media is discussed in Turcotte (1992), Adler and Thovert (1993), Flury and Flühler (1995), and Gouyet (1996). Percolation theories, homogenization, pore network models, and lattice gas automata have been used to analyze flow and transport processes in homogeneous and heterogeneous porous media by authors such as Gao and Sharma (1994), Hornung (1997), Kaiser (1997), Vollmayr et al. (1997), and Yortsos and Shing (1999). Another tool for bridging the gap between molecular and macroscopic simulation of flows in porous media, multiphase flows, and colloidal suspensions is that called "dissipative particle dynamics." This technique is described in Coveney and Novik (1996), Groot and Warren (1997), and Boek and van der Schoot (1998).

In the first half of the 1990s, three comprehensive documents were published which were concerned with simulation codes for flow and the transport of solvents and heat in both saturated and unsaturated zones of the subsurface. In 1993, van der Heijde and Elnawawy authored a report on the compilation of ground-water models for saturated and unsaturated conditions. This compilation included analytical and numerical codes for the following areas: saturated flow, unsaturated flow, solute transport, heat transport, gas flow and vapor transport, flow and transport in fractured rock, hydrogeochemical models, optimization models for ground-water management, and multiphase flow models. In 1994, van der Heijde authored a report on the compilation of unsaturated /vadose zone models. This report considered about 90 modeling codes covering flow processes, solute transport and heat transport. The final report of this series, van der Heijde and Kanzer (1995), considered ground-water model testing: a systematic evaluation and testing of code functionality, performance, and applicability to practical problems. The procedures were exemplified by applying them to a specific three-dimensional flow and solution transport code.

Two other recent books on the flow and transport of pollutants in the subsurface environment are of interest. Corwin et al. (1999) edited a report on the assessment of non-point source pollution in the vadose zone. Papers in this report considered the application of geographic information systems (GIS), transfer functions, fuzzy logic, fractals/ scaling, hierarchical theory and uncertainty analysis to flow and solute transport through heterogeneous soil layers. Mackay (2001) detailed the intermedia transport of reactive organics through the environment using a series of multiple-compartment, mass-balance modules. The modules included those of air, water, soil, sediments, and biological entities.

1.3 Computer Model Uncertainty and Sensitivity

Model predictions are uncertain and erroneous because of uncertainties and errors that can occur at various points in the modeling process and in the model's structure. These points can be illuminated by considering the *modeling protocol* described in Bedient et al. (1999); namely:

1. Identify the purpose of the model and the site(s) to which it will be applied.
2. Develop a conceptual model of the system based on the model purpose and site application.
3. Select the governing conservation and constitutive equations describing the physical system, as well as the computer codes required to solve the system. Verify that the governing equations describe the physical, chemical and biological processes occurring in the physical system. Verify that the computer codes accomplish stated objectives by comparing model results to analytical solutions of know problems.
4. Design the model for the site(s) at hand, including the selection of initial and boundary conditions, grid design and grid size, time increments and parameters, and estimates of model parameters.
5. Calibrate the designed model by determining a set of model input parameters that approximate field-measured pressure heads, flows and/or concentrations, thus establishing that the model can reproduce field-measured values of the unknown variables.
6. Determine the effects of uncertainty on model results through the use of uncertainty and sensitivity analyses.
7. Verify the designed, calibrated model by testing the model's ability to reproduce another set of field measurements using the model parameter set developed in the calibration process.
8. Predict site results for desired scenarios using the designed, calibrated, verified model.
9. Determine the effects of uncertainty on model predictions.
10. Present modeling design and results for the site(s) and scenarios in question.
11. Post audit and redesign model as necessary. Modify and refine the site model if the comparison of model predictions against new sets of field data warrant such action.

The lists of modeling errors given by Guymon (1993), van der Heijde and Kanzer (1995), and Mulla and Addiscott (1999) are related to the various steps given in this 11-step modeling protocol. Errors in *conceptualization* or *model structure* occur when the processes and the assumptions represented by the model fail to represent reality. An example is a model, which simulates solute transport using the convective-dispersive equation over an area in which two-region, or macropore transport is significant. The failure of the model in this case may be compensated for by using unrealistic large values for saturated hydraulic conductivity and solute dispersivity, but this approach is usually not satisfactory. Errors in *experimental measurement* are also common due to biased sample collection, sample handling and storage errors, or sample analysis errors. Quality control and quality assurance procedures can be used to minimize such errors. Mulla and Addiscott (1999) state that a model can be considered properly validated if the goodness-of-fit criterion for validation is less than the experimental error among experimental replicates.

Since most mathematical systems require numerical, computer codes to solve them, the *discretization in space and time* introduces error. Further, there are *roundoff errors,* which represent the differences between the "true" representation of the dependent variables in the discretized formulas and the machine representation of those variables in the computer (van der Heijde and Kanzer, 1995). *Truncation errors* are the difference between the true, discretized representation of the variables and the exact value of the variables. Truncation errors are *algorithm errors* and often occur because the distribution of the unknown variables is represented by truncated polynomial expansions. As the number of polynomial elements increases in a particular expansion, the truncation errors tend to decrease. As one might expect, the *numerical solution technique* used for a given mathematical system may have a significant impact on the model results. For example, Mehl and Hill (2001) considered five common numerical techniques for solving the advection-dispersion equation (i.e., finite difference, predictor-corrector, total variation diminishing, method of characteristics, and modified method of characteristics). The results of their investigation indicate that, depending on the solution technique employed and the choice of solute model dispersivity, model calibration can produce significantly different estimated values of hydraulic conductivity that result in different

simulated flow fields and potentially very different solute concentration predictions. As Bedient et al. (1999) state, model calibration is very subjective, and in many cases, does not yield a unique set of parameters that reproduce field conditions.

Guymon (1994) states that ***boundary conditions*** and ***initial conditions*** are always a problem and a source of errors for unsaturated flow processes. For example, the land surface boundary condition for fluid flow is extremely difficult to specify in practical field problems. About the only thing that one can do to evaluate errors associated with boundary conditions is to conduct uncertainty analyses and sensitivity tests. The situation with respect to initial conditions is no better since these conditions are rarely known with confidence. The deterministic nonlinear equations that are used to describe fluid flux in the unsaturated zone may be sensitive to initial conditions; however, the dissipative nature of the soil system is such that solutions often appear to be insensitive to initial conditions, especially if sufficient time has elapsed since the start of the simulation.

Errors in ***model parameterization*** can result from a variety of sources and causes. One of the most important is the uncertainty due to spatial and temporal variability (Mulla and Addiscott, 1999). Within the calibration site, the relatively invariant soil properties of bulk density and soil pH can have coefficients of variation of 10% or so, while the relatively variable soil properties such as soil hydraulic conductivity and solute diffusivity can have coefficients of variation of 300% or greater. Solute velocities due to surface ponding and solute concentrations may have coefficients of variation from 60 to 200%.

Uncertainties in model prediction can also result from errors in ***spatial scale transitions*** (Mulla and Addiscott, 1999). One type of error occurs when the source and sink terms or the transport and fate processes operating at the scale of the calibration study (e.g., the field scale) are different from those operating at the prediction scale (e.g., the watershed or aquifer scale). In ground-water modeling, this type of problem may be evidenced as changes in dispersive or transformation processes, geological influences on transmissivity and flow direction, and recharge patterns. A second type of scale-transition error is due to errors in extrapolation caused by spatial and temporal averaging of model parameters, or due to bias caused when the calibration is not representative of the region over which predictions are to occur. Thus, careful selection of the size and location of the calibration site and the time scales for calibration are important. The essence of these spatial scale transition errors can be illustrated by the following two statements:

1. Processes that are significant at small scales may not be relevant at large scales.
2. New processes (e.g., dispersion) emerge in response to an increase in scale and the way to represent them may depend on the original assumed model structure.

Investigators have employed various methods of uncertainty analysis and sensitivity testing to quantify the uncertainties in model results due to the errors discussed in the above paragraphs. For example, Nofziger et al. (1994) used Monte Carlo techniques in their uncertainty analysis of four unsaturated zone models for Superfund site application. The sensitivity analysis invoked by these authors was the "informal approach" described by Helton (1993). The crux of this approach involves varying one parameter or member of a set of assumptions, one at a time, and observing the deviation in the resultant model prediction from a base-case prediction. In Helton's analysis in his 1993 paper, four "formal" uncertainty/sensitivity approaches were considered: differential analysis, Monte Carlo analysis, response surface methodology, and Fourier amplitude sensitivity test (FAST). These approaches are based on Taylor series, random sampling, response surface construction, and Fourier series, respectively. Although the implementation of the formal approaches is more complex than the informal sensitivity approach, Helton found that the formal approaches often yield more information concerning result uncertainty with less computational effort. Further, he felt that Monte Carlo analysis is the most widely applicable approach for use in performance assessment (e.g., for use in the performance assessment of radioactive waste disposal sites). In this regard, EPA has recently published a summary report on a workshop on Monte Carlo analysis, U.S. EPA Risk Assessment Forum (1996). Further, to aid in the implementation of the Monte Carlo uncertainty analyses of exposure estimates through the soil/ground-water pathway, Meyer et al. (1997) have published generic probability distributions for unsaturated and saturated zone soil hydraulic parameters. In addition, procedures are given for Bayesian updating of the generic distributions when site-specific field data are available. Other uncertainty analysis techniques have been employed; for example, reliability-based analysis given in Jang et al. (1994) and Hamed and Bedient (1999), optimization by data fusion described in Eeckhout (1997), and fuzzy-random analysis and neural network/learning techniques discussed in Ayyub (1998).

In the current report, the technique of uncertainty analysis will be the informal approach as defined by Helton (1993) and invoked by Nofziger et al. (1994). In the U.S. EPA Risk Assessment Form (1996) report, this technique

is called the simplest direct response method to explore changes in model output for a discrete or unit change in each of the inputs, one at a time. For each of the varied inputs, all other inputs to the model are held at their nominal or baseline values when the sensitivity is computed. These nominal values generally correspond to the means or medians in a subsequent probabilistic analysis, if one was to be applied (e.g., a Monte Carlo uncertainty analysis). Sensitivity analyses in this report will address process parameter sensitivity in general, and to some extent conceptual model choice and numerical error.

1.4. Report Organization

This report is organized into seven sections, along with nine appendices. *Section 2* is an overview of numerical models for simulating radionuclide transport in the vadose zone. The section discusses model selection and includes model description for the radionuclide SSL effort. *Section 3* addresses the sensitivity of simulated results to conceptual model selection. Model conceptualization and the effect of simplifying assumptions on model outcome are discussed. *Section 4* describes the basic elements and definitions of a sensitivity analysis. A simplified system is provided to demonstrate the intricacies of an analysis. *Section 5* provides the physical setting for the hypothetical modeling scenario (i.e., the Las Cruces Trench Site, NM) along with the development of the conceptual model for the site, and the baseline parameter selection for the various models to be tested. *Section 6* considers the implementation of the parameter sensitivity analysis and reports the results obtained from the analysis. The general impacts of the model's input parameters on the output quantities are specified and the relative sensitivity of each model output to each input parameter is described. *Section 7* compares the sensitivity results between the tested model codes and presents a discussion on various numerical modeling errors. *Section 8* gives the summary and conclusions of this study, while *Section 9* lists the cited references in alphabetical order by author.

The nine explanatory appendices cover features of the five tested model codes which are only briefly considered in the main text, or which require a more extensive analysis than that given in the main text. The features considered are as follows:

- *Appendix A* – Empirical models of the unsaturated soil hydraulic properties which are used in the various models.

- *Appendix B* – A discussion on the scaling of field soil-water behavior.

- *Appendix C* – An explanation of the hysteretic characteristics of soil-water properties.

- *Appendix D* – The first-order decay chains used in the various models.

- *Appendix E* – The impact of using a nonuniform moisture distribution versus a uniform distribution.

- *Appendix F* – The impact of using daily precipitation and evapotranspiration rates versus an annual average recharge rate.

- *Appendix G* – The impact of considering a layered soil column versus a homogeneous soil column.

- *Appendix H* – A detailed analysis of nonequilibrium sorption of pollutants, mainly for the radionuclide ^{90}Sr.

- *Appendix I* – Results from the transport and fate of other radionuclides not considered in the main text.

Section 2
Overview of Numerical Models for Simulating Radionuclide Transport

The transport mechanisms and loss pathways for chemicals in the soil consist of many elements (Jury and Valentine, 1986), such as:

- *Static Soil Properties* – porosity, bulk density, organic carbon content, pH, soil temperature.
- *Flow and Transport Variables and Properties* – saturated hydraulic conductivity, saturated water content, matrix head-water content function, hydraulic conductivity function, solute dispersivity.
- *Basic Chemical Properties* – molecular weight, vapor pressure, water solubility, Henry's constant, liquid diffusion coefficient in water, partition coefficient, decay rate of compound.
- *Contaminant Source Characteristic* – solute concentration of source, solute flux of source, solute source decay rate.
- *Time Dependent Parameters* – water content and flux, infiltration or evaporation rate, solute concentration and flux, solute velocity, volatilization flux, air entry pressure head.
- *Soil Adsorption Parameters* – distribution coefficient, isotherm parameters, organic carbon partition coefficient.
- *Tortuosity Functions* – vapor and liquid diffusion tortuosities.

These variables and properties are related to one another by conservation equations (e.g., conservation of mass, momentum and energy) and constitutive equations (e.g., state equations, sorption isotherms, dispersion relationships, unsaturated soil hydraulic properties). Further, these equations are supplemented by sets of auxiliary equations (e.g., boundary and initial conditions). In general, for specific site/process contaminant scenarios, these mathematical systems are sufficiently complex so that numerical solutions are required. Techniques and procedures as briefly outlined in Section 1.2 are employed. However, for some pedagogical and screening scenarios, simple systems employing analytical or semi-analytical solution techniques may be applicable. Such solutions can also be used to verify numerical computer codes developed for the more complex scenarios.

In Section 1.1, the aims and objectives of the radionuclide SSL effort were briefly outlined. Based upon these aims and objectives, the breadth of the modeling tools and codes outlined in Section 1.2 can be greatly reduced for current applications. For example, the SSL effort will probably not be concerned with stochastic modeling and stochastic codes, modeling and codes based on fractal geometry and percolation theory (i.e., discrete networks and cellular automata), and fractured rock flow modeling. Further, for the radionuclides of concern in this report, no vapor transport models will be explicitly required; however, there may be vapor modules in some of the candidate codes finally chosen. In general, the final candidate list of codes was chosen in part from the codes listed in publications such as van der Heijde and Elnawawy (1993), Nofziger et al. (1994), van der Heijde (1994) and Bedient et al. (1999).

2.1 Model Selection for the Radionuclide SSL Effort

The evaluation of models' applicability to the SSL process for radionuclides was based on the following considerations:

- Can the model be used to simulate the transport and fate of five selected radionuclides – tritium ^{3}H, technetium ^{99}Tc, uranium ^{238}U, strontium ^{90}Sr, and plutonium ^{238}Pu?
- Can the model simulate the transport and fate of the selected radionuclides for a specific site test case?
- Is the model appropriate for use in the SSL process?
- What are the limitations of the model and how do they impact its intended use?

Keeping these considerations in mind, a search was undertaken to locate and evaluate vadose zone flow and transport models to determine their suitability for inclusion in the SSG document for radionuclides. The search criteria sought to identify models which included at least first-order decay and radionuclide chain decay. Models were also selected based on evidence of current revisions and updates to eliminate the evaluation of obsolete codes. Whenever possible, the history of the models was also examined to determine if the codes had undergone name changes or inclusions into other codes in order to eliminate redundancy. Using these criteria and the above considerations, one-, two- and three-dimensional models in the public domain and the private sector were located through library resources, internet searches, and personal communications.

In general, the search focused on the identification and preliminary evaluation of relatively simple one-dimensional models which are most suited to the SSL process. The search produced four one-dimensional and two two-dimensional models in the public domain. All six of these models have decay-chain transport modules in the vadose zone, and all can calculate the leachate contaminant concentration entering the ground water. All four one-dimensional models were chosen for analysis and evaluation, and only one of the two-dimensional models was chosen. These five models are identified by the following acronyms:

- One-dimensional CHAIN Code (van Genuchten, 1985),
- One-dimensional MULTIMED-DP 1.0 Code (Liu et al., 1995; Sharp-Hansen et al., 1995; Salhotra et al., 1995)
- One-dimensional FECTUZ Code (U.S. EPA, 1995ab),
- One-dimensional HYDRUS Code (Šimúnek et al., 1998),
- Two-dimensional CHAIN 2D Code (Šimúnek and van Genuchten, 1994).

2.2 Model Description of the Selected Codes

The CHAIN Code is an analytical model which requires the assumption of uniform flow conditions. The MULTIMED-DP 1.0 and FECTUZ Codes are semi-analytic models which approximate complex analytical solutions using numerical methods such as numerical inverse transform modules. Transient and steady-state conditions can be accommodated in both the analytical and semi-analytical models, while layered media are usually only accommodated by the semi-analytical codes. The HYDRUS and CHAIN 2D Codes solve the pertinent sets of partial differential equations using finite-difference or finite-element methods. The resolution in space and time of these numerical models depends on the physical characteristics of the site in question, the computational resources available to the modeler, and the purposes of the simulation. Numerical codes are used when simulating time-dependent scenarios under spatially varying soil conditions and unsteady flow fields.

HYDRUS, CHAIN 2D, and CHAIN are stand-alone vadose zone models of the fate and transport of solutes in the liquid, solid and gaseous phases. FECTUZ is the unsaturated module of EPA's composite model for leachate migration with transformation products (EPACMTP), see USEPA 1995a and 1995b. This code is based on enhancements to the VADOFT Code (Huyakorn and Buckley, 1987). FECTUZ simulates migration of contaminants from a landfill or a surface impoundment through the unsaturated zone to an unconfined aquifer with a water table fixed some L units below the surface. MULTIMED-DP was initially developed as a multimedia fate and transport model to simulate contaminant migration from a waste disposal unit (e.g., from a landfill) through different pathways which include air, surface water, soil and ground water. In Version 1.0, it simulates the transport and fate of first- and second-generation transformation products through the saturated and unsaturated zones. This version has the option to allow it to be used for unsaturated zone migration alone. It is this version, MULTIMED - DP 1.0, and the unsaturated option that is analyzed in this report, see Liu, et al. (1995), Salhotra, et al. (1995), and Sharp-Hansen, et al. (1995).

Except for dimensionality, the most comprehensive code is HYDRUS, which contains the greatest number of physical processes. HYDRUS considers only the vertical dimension (z), while CHAIN 2D considers a vertical slab in two dimensions (x, z). For vadose zone modeling, it is not always clear that a two-dimensional, vertical slab model will give superior results to those obtained from a one-dimensional model for the real three-dimensional area being simulated. If the region to be simulated is reasonably uniform in the horizontal planes of the surface and subsurface layers, then a one-dimensional vadose zone model may suffice over that of the two dimensional model. If the region to be simulated is rather uniform in one horizontal direction, while being heterogeneous in the orthogonal horizontal direction (e.g., furrow irrigation of a field of row crops), then a two-dimensional, vertical slab model oriented along the heterogeneous direction (e.g., perpendicular to the crop rows) would be superior to a one-dimensional model. However, if the region to be simulated is rather heterogeneous and nonsymmetrical in the

horizontal, then the choice between a one-dimensional model and a two-dimensional, vertical slab model may tilt in the direction of the one-dimensional model being applied at several discreet, representative points within the region of interest. Then through the use of superposition, scaling and geostatistics, the results of the several one-dimensional solutions can be used to gain knowledge of the real three-dimensional system. Thus, one dimensional vadose zone models need not take an inferior role to a two-dimensional, vertical slab model. Since HYDRUS is the most comprehensive of the five models, the systems of equations discussed in this subsection with support from Appendices A to D will be those associated with HYDRUS (Šimúnek et al., 1998). Table 2-1 indicates the model components that will be discussed and the status of these components in each of the selected codes.

2.2.1 The Variably Saturated Water Flow

The variably saturated water flow in a vertical soil column (Figure 2-1) is governed by Darcy's Law:

$$q = -K \left[\frac{\partial h}{\partial z} + 1 \right],$$

(2-1)

and by the continuity of mass equation

$$\frac{\partial \theta}{\partial t} + \frac{\partial q}{\partial z} = -S ,$$

(2-2)

where $h = h(z,t)$ is the water pressure head in units of length (L), $q = q(z,t)$ is the Darcian fluid flux density in units of length over time (LT^{-1}), $K = K(z,t)$ is the unsaturated hydraulic conductivity (LT^{-1}), $\theta = \theta(z,t)$ is the volumetric moisture content (L^{3}L^{-3}), and $S = S(z,t)$ is the volume of water removed from a unit volume of soil per unit time due to plant water uptake (L^{3}L^{-3} T^{-1}). As shown in Figure 2-1, $z = 0$ defines the bottom of the soil column which could be taken as the water table of an unconfined aquifer. The value $z = L$ is the soil surface and $z = L - L_R$ defines the bottom of the root zone.

Combining Equations (2-1) and (2-2) leads to a modified Richards Equation (Richards, 1931):

$$\frac{\partial \theta}{\partial t} = \frac{\partial}{\partial z} \left[K \left(\frac{\partial h}{\partial z} + 1 \right) \right] - S .$$

(2-3)

For heterogeneous layers with time-independent properties, the soil hydraulic functions and K can be written as follows (Šimúnek et. al. 1998):

$$\theta = \theta(z,t) = \theta(h,z) ,$$

(2-4a)

$$K = K(z,t) = K(h,z) = K_s(z) \, K_r(h,z) ,$$

(2-4b)

where $K_s(z)$ is the saturated hydraulic conductivity (LT^{-1}), and $K_r(h,z)$ is the relative hydraulic conductivity (dimensionless). For homogeneous layers with time-independent properties, the parameters become:

$$\theta = \theta(z,t) = \theta(h), \quad K = K(z,t) = K(h) .$$

(2-5)

The moisture sink due to *root water uptake* is expressed as follows (Šimúnek et al., 1998):

$$S(z,t) = \alpha(h,h_\phi) \, S_p(z,t) ,$$

(2-6)

where $\alpha(h,h_\phi)$ is the water stress response function (dimensionless), $S_p(z,t)$ is the potential water uptake rate (T^{-1}), and h_ϕ is the osmotic head (L) which is a linear function of the concentrations of all solutes in the soil moisture. Two

Table 2-1. Comparison of the Model Components in Each of the Five Codes Being Analyzed in this Report.

MODEL COMPONENT	HYDRUS	CHAIN 2D	FECTUZ	MULTIMED_DP 1.0	CHAIN
Variably Saturated Water Flow	One-Dimensional Time Dependent Richards Equation with Sink Term	Two-Dimensional Time Dependent Richards Equation with Sink Term	One-Dimensional Steady State Constant Infiltration Rate Darcy's Law	One-Dimensional Steady State Constant Infiltration Rate Darcy's Law	One-Dimensional Steady State Constant Flux and Water Content Throughout Soil Column
Root Water Uptake	Sink in Richards Equation Which Depends on Osmotic Head, Water Stress, Root Distribution	Sink in Richards Equation Which Depends on Osmotic Head, Water Stress, Root Distribution	Not Considered in Model	To Some Extent, Considered in the Landfill Module, Not in the Unsaturated Flow Zone Module	Not Considered in Model
Unsaturated Hydraulic Properties	*See Appendix A* Brooks-Corey, van Genuchten, and Vogel-Cislerová Models	*See Appendix A* Vogel-Cislerová and van Genuchten Models	*See Appendix A* van Genuchten Model	*See Appendix A* Brooks-Corey and van Genuchten Models	Not Considered in Model
Scaling of Soil Hydraulic Functions	*See Appendix B* Linear Scaling of Pressure Head, Soil Moisture, and Hydraulic Conductivity	*See Appendix B* Linear Scaling of Pressure Head, Soil Moisture, and Hydraulic Conductivity	Not Considered in Model	Not Considered in Model	Not Considered in Model
Scaling for Temperature Dependence of Soil Hydraulic Functions	Scaling Due to Parameter Variations with Temperature Applied to Pressure Head and Hydraulic Conductivity	Scaling Due to Parameter Variations with Temperature Applied to Pressure Head and Hydraulic Conductivity	Not Considered in Model	Not Considered in Model	Not Considered in Model
Hysteresis in Soil Hydraulic Functions	*See Appendix C* Applied to van Genuchten and Vogel-Cislerová Models for Moisture Content and Hydraulic Conductivity	Not Considered in Model	Not Considered in Model	Not Considered in Model	Not Considered in Model
Initial and Boundary Conditions for the Water Flow System	Initial Condition on Pressure Head; Head and Flux Boundary Conditions; Ponding and Seepage	Initial Condition on Pressure Head; Head and Flux Boundary Conditions; Ponding and Seepage	Steady State, Thus no Initial Condition; Pressure Head Zero at Water Table, Pressure Head Consistent with Infiltration Rate at Surface	Steady State, Thus no Initial Condition; Pressure Head Zero at Water Table, Pressure Head Consistent with Infiltration Rate at Surface	Not Required Since Soil Moisture and Flux Are Specified Constants

Table 2-1. Comparison of the Model Components in Each of the Five Codes Being Analyzed in this Report.

MODEL COMPONENT	HYDRUS	CHAIN 2D	FECTUZ	MULTIMED_DP 1.0	CHAIN
Solute Transport Equations	*See Appendix D* One-Dimensional, Time-Varying; Gas, Liquid and Solid Phases; 0th Order Production, 1st Order Decay; Advection/ Dispersion; Equilibrium/ Nonequilibrium Sorption, Nonlinear Sorption	*See Appendix D* Two-Dimensional, Time-Varying; Gas, Liquid and Solid Phases; 0th Order Production, 1st Order Decay; Advection/ Dispersion; Equilibrium/ Nonequilibrium Sorption, Nonlinear Sorption	*See Appendix D* One-Dimensional, Time-Varying; Liquid and Solid Phases; 1st Order Decay; Advection/Dispersion; Linear/Nonlinear Equilibrium Sorption	*See Appendix D* One-Dimensional, Time-Varying; Gas, Liquid and Solid Phases; 1st Order Decay; Advection/ Dispersion; Linear Equilibrium Sorption	*See Appendix D* One-Dimensional, Time-Varying; Liquid and Solid Phases; 1st Order Decay; Advection/Dispersion; Linear Equilibrium Sorption
Initial and Boundary Conditions for the Solute Transport Equation	Initial Conditions for Liquid and Solid Phases; Dirichlet, Cauchy and Neumann Boundary Conditions; Volatile Solutes at Surface	Initial Conditions for Liquid and Solid Phases; Dirichlet, Cauchy and Neumann Boundary Conditions; Volatile Solutes at Surface	Initial Concentration for Liquid Phase; Dirichlet and Cauchy Boundary Conditions; Batemann Decaying Source Terms	Initial Concentration for Liquid, Gas and Solid Phases; Dirichlet and Cauchy, Separate and Mixed, Boundary Conditions	Initial Concentration for Liquid Phase; Dirichlet and Cauchy Boundary Conditions; General and Batemann Decaying Source Terms
Effective Dispersion Coefficients	Solute Dispersion Coefficient; Gas Diffusion Coefficient; Tortuosity Factors	Solute Dispersion Matrix in Two-Dimensions; Gas Diffusion Coefficient; Tortuosity Factors	Solute Dispersion Coefficient; Effective Molecular Diffusion Coefficient	Solute Dispersion Coefficient; Gas Diffusion Coefficient; Tortuosity Factor	Solute Dispersion Coefficient
Temperature Dependence of Transport and Reaction Coefficients	Modified Arrhenius Equation for Temperature Scaling of Production, Degradation, and Adsorption Coefficients	Modified Arrhenius Equation for Temperature Scaling of Production, Degradation, and Adsorption Coefficients	Not Considered in Model	Hydrolysis Rates Temperature Corrected Using Arrhenius Equation	Not Considered in Model
Heat Transport Equations	One-Dimensional Time-Varying, Convection, Dispersion Equation; Energy Uptake by Roots; Thermal Conductivity Coefficient; Heat Capacities	Two-Dimensional Time-Varying, Convection, Dispersion Equation; Energy Uptake by Roots; Thermal Conductivity Matrix in Two-Dimensions; Heat Capacities	Not Considered in Model	Not Considered in Model	Not Considered in Model
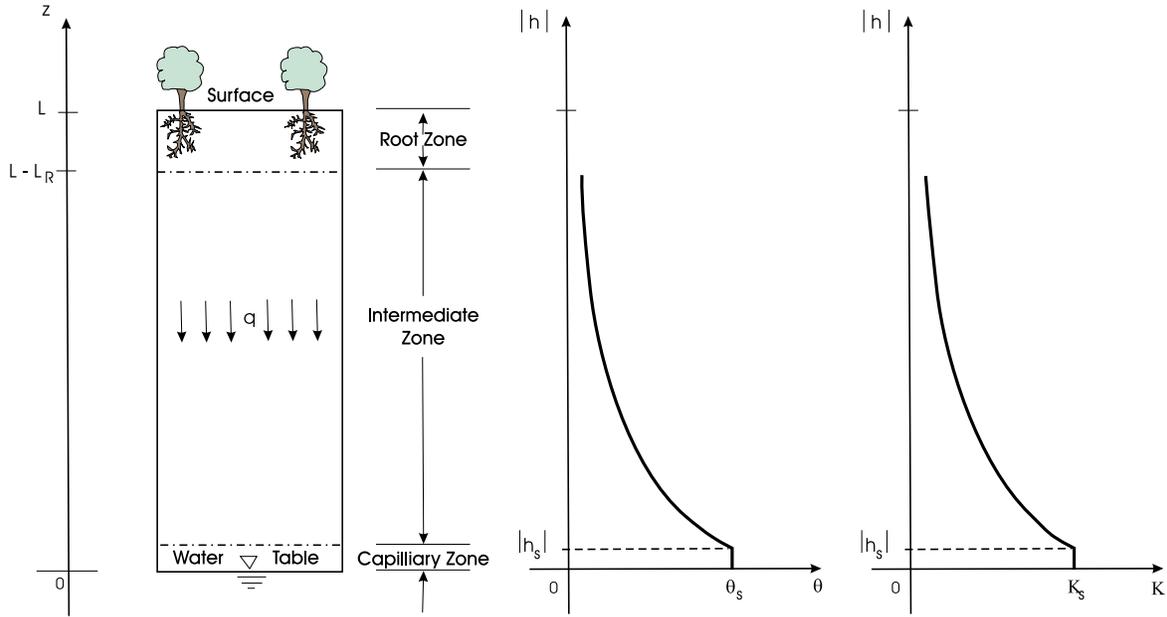
Figure 2-1. Schematic of an unsaturated soil column, soil-water retention curve, and hydraulic conductivity function, where subscript "s" indicates saturated conditions.

formulas for $\alpha(h,h_\phi)$ are given in terms of experimentally determined exponents and values of h and h_ϕ at which the water extraction is reduced by 50% during conditions of negligible stress. The quantity $S_p(z,t)$ is the product of the normalized water uptake distribution function b(z,t) in L^{-1} units and the potential transpiration rate $T_p(t)$ in LT^{-1} units. The quantity b(z,t) is related to a root distribution function and the rooting depth $L_R(t)$. In turn, the quantity $L_R(t)$ varies with a logistic-type growth function. Finally, the potential transpiration rate $T_p(t)$ is related to the actual transpiration rate obtained from field measurements.

In HYDRUS, three models of the ***unsaturated hydraulic properties***, $\theta(h)$ and K(h), are given: they are the Brooks and Corey (BC) Model (1964), the van Genuchten (VG) Model (1980), and the Vogel and Cislerová (VC) Model (1988). The equations for these models are given in Appendix A. In addition to giving the analytical forms of these models, Appendix A discusses two papers (Morel-Seytoux, et al. 1996; Nachabe, 1996) concerned with the interchangeability of the BC- and VG-Models for infiltration calculations. Further, it was suggested by Morel-Seytoux, et al., though not proved, that this interchange of models would be valid for drainage and evapotranspiration calculations, as well. The VC-Model, as shown in Appendix A, is a modification of the VG-Model to add flexibility in the description of the hydraulic properties near saturation. Also discussed in Appendix A is a new model for the soil-water retention curve, $\theta(h)$, which the authors, Assouline, et al. (1998), claim to be more flexible than the VG- or VC-Models.

The ***scaling features*** for soil-water behavior found in the HYDRUS and CHAIN 2D Models are part of the fundamental process of searching for symmetry in nature. The application of these features is to simplify calculations of soil-water behavior for vertically heterogeneous systems consisting of different homogeneous soil layers, and to simplify and make more consistent the superposition of discrete one-dimensional (vertical dimension) results distributed over a horizontally heterogeneous field. In Appendix B, the general topic of symmetry in nature is briefly discussed, along with the analytical concepts of similitude, transformation groups, inspectional analysis and self-similarity. Finally, Appendix B discusses the scale dependence and scale invariance in the field of hydrology. An excellent recent survey book on these topics is that edited by Sposito (1998).

One of the first papers on the similarity of soil-water behavior in unsaturated porous media is that of Miller and Miller (1956). This work is based on geometric similarity and requires that similar porous media will have the same porosities, a concept more fully satisfied in the laboratory than in the field. To account for the variation of porosity in the field, Warrick, et al. (1977) replaced the use of θ in the Miller and Miller Model by ratio θ/θ_s, where θ_s is the saturated moisture content. In essence, θ_s becomes a new scale factor which accounts for the different internal

11

geometries in field soils. Based on the results of these papers, as well as the principles of similitude and invariance, Vogel, et al. (1991) introduced the transformations that form the foundation of the scaling relationships in the HYDRUS and CHAIN 2D Codes. These transformations account for the linear variability in the soil moisture parameters and are defined by the following:

$$h = \alpha_h h^* , \tag{2-7}$$

$$\theta(h) - \theta_r = \alpha_\theta \left[\theta^*(h^*) - \theta_r^* \right], \tag{2-8}$$

$$K(h) = \alpha_k K^*(h^*) , \tag{2-9}$$

where θ_r is the residual soil moisture, the asterisks denote reference quantities, and the three scale factors, $(\alpha_h, \alpha_\theta, \alpha_k)$, are assumed to be independent of one another. These linear transformations will explain the variability due to soil structure within a given soil textural class, but will not account for the nonlinear phenomena expressed by different soil textural classes. Figure 2-2 illustrates an example of soil structure scaling for a set of scaling factors given by $(\alpha_h, \alpha_\theta, \alpha_k) = (3/2, 2, 7/4)$. Thus, the above transformations become

$$h = 3h^*/2, \tag{2-7a}$$

$$\theta(h) - \theta_r = \theta(3h^*/2) - \theta_r = 2 [\theta^* (h^*) - \theta_r^*] , \tag{2-8a}$$

$$K(h) = K(3h^*/2) = 7/4 \, K^*(h^*). \tag{2-9a}$$

The values of the scaling factors, $(\alpha_h, \alpha_\theta, \alpha_k)$, are determined from field sampling; and if representative of an area in question, allows one to coalesce data sets (see Figure B-3 of Appendix B) and allows one to transfer measured soil relationships to unsampled areas. For example, Rockhold et al. (1996) applied the transformations of equations (2-7) to (2-9) in the simulation of water flow and the transport of tritium measured at an initially unsampled domain of the Las Cruces Trench Site, the site which forms the physical setting of our analyses. These transformations allowed for successful transfer of soil-water properties from originally sampled areas at the site to the domain used by Rockhold, et al. This study is a good example of the power of the scaling features in the HYDRUS and CHAIN 2D Codes; however, in the present sensitivity analyses, these features will not be considered since we use a single homogenous soil layer.

In capillary theory the dependence of the pressure head, h, on temperature variations comes from the variation of surface tension with temperature, while those for the hydraulic conductivity, K, arise from the temperature dependence of the dynamic viscosity, μ (ML^{-1}T^{-1}), and the density, ρ(ML^{-3}), of the soil water. The ***temperature scaling factors*** are thus defined by:

$$h(T_a) = \frac{\sigma(T_a)}{\sigma^*} \, h^* = \bar{\alpha}_h h^*, \tag{2-10}$$

$$K(\theta, T_a) = \frac{\mu^*}{\mu(T_a)} \, \frac{\rho(T_a)}{\rho^*} K^*(\theta) = \bar{\alpha}_k K^*(\theta), \tag{2-11}$$

where $\sigma(T_a)$ is the surface tension at the air-water interface (MT^{-2}), T_a in the functional expressions is the temperature (^{0}K), $\bar{\alpha}_h$ is the temperature scaling factor for pressure head, and $\bar{\alpha}_k$ is the temperature scaling factor for hydraulic conductivity. For the current sensitivity analyses, the systems are taken to be isothermal and sensitivity to changes in h and K are obtained by variations in other parameters rather than from temperature variations.

The soil-water retention curve, and to some extent the hydraulic conductivity curve, for a draining (drying) soil is not the same as that for an imbibing (wetting) soil. Reasons for such a phenomenon in the unsaturated zone are the entrapment of air in the soil pores and the surface tension effects occurring in the pore throats. This phenomenon is called ***hysteresis*** and is a highly nonlinear characteristic which occurs in many mechanical, electrical, chemical, biological, and geophysical systems. The formulation and analysis of hysteretic systems has a history from the early 1900's to the present. Appendix C is concerned with the origins and applications of hysteretic phenomena; hysteresis loops, operators and models; and hysteresis in soil-moisture parameters. The study of hysteretic operators and
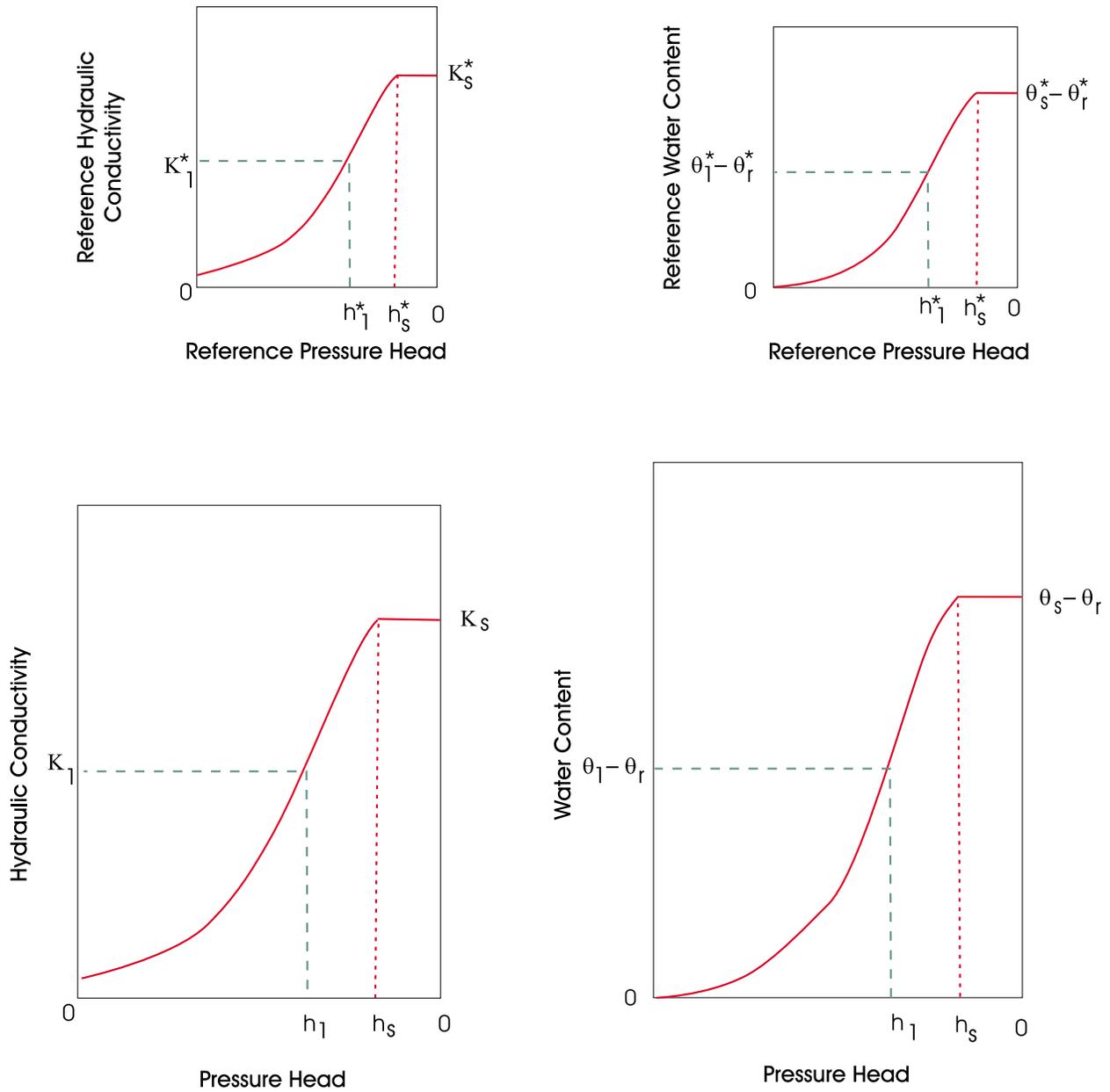
Figure 2-2. An example of soil structure scaling for scale factors $(\alpha_h, \alpha_\theta, \alpha_k) = (3/2, 2, 7/4)$. The ratios $h_s/h_s^* = h_1/h_1^* = 3/2$, $(\theta_s - \theta_r) \div (\theta_s^* - \theta_r^*) = (\theta_1 - \theta_r) \div (\theta_1^* - \theta_r^*) = 2$, and $K_1/K_1^* = K_s/K_s^* = 7/4$.

models lays the groundwork for the existence and uniqueness of solutions for hysteretic systems in soil physics, as well as in other disciplines. The principles and techniques developed in the other disciplines are useful in soil physics, and vice versa.

Appendix C discusses the background and theory for the hysteretic features presented in HYDRUS (Šimúnek et al., 1998). These features are based on the VG- and VC-Models for the soil-moisture parameters and the predominant feature that defines the difference between the main drying curve and the main wetting curve is the van Genuchten parameter α, the inverse of the air-entry value or the bubbling pressure. The α for drying, α^d, is less than that for wetting, α^w. A reasonable approximation is to let $\alpha^w = 2\alpha^d$. The drying scanning curves, as defined in Appendix C, are linearly scaled from the main drying curve, while the wetting scanning curves are scaled from the main wetting curve. In both cases, the scale factor α_h in Equation (2-7) is taken to be unity. In the current analyses, where a constant infiltration rate is postulated, the hysteretic features of the HYDRUS Model will not be invoked.

The *intial and boundary conditions* for the water flow system as given in HYDRUS (Šimúnek et al., 1998) consist of a prescribed pressure head distribution at time zero, $h_i(z)$, $0 < z < L$, and boundary conditions at the surface $z = L$ and the bottom of the soil profile $z = 0$. The type of boundary conditions possible are as follows:

Dirichlet Conditions

$$h(z,T) = h_o(t), \quad t > 0, \quad z = 0,L ,$$
(2-12)

Cauchy Conditions

$$-K\left[\frac{\partial h}{\partial z} + 1\right] = q_o(t), \quad t > 0, \quad z = 0, L ,$$
(2-13)

Neumann Conditions

$$\frac{\partial h}{\partial z} = 0, \quad t > 0, \quad \text{only at } z = 0 ,$$
(2-14)

where h_o is a specified head and q_o is a prescribed soil water flux. The boundary conditions in Equations (2-12) to (2-14) are assumed to be system-independent conditions. HYDRUS also considers the soil-air interface at $z = L$ under "current" atmospheric conditions of evaporation, precipitation, ponding, and infiltration. In addition, the code considers the case when seepage occurs at the bottom of the soil column, at $z = 0$.

2.2.2. Solute Transport Systems

All five models under consideration in this report have time-dependent *solute transport systems* involving first-order decay chains which are straight, branched and/or a combination of both, as well as systems where a set of species can evolve independent of one another. The various decay chains which each model addresses are described in Appendix D. The general form of the governing equations for the systems described in HYDRUS are as follows (Šimúnek et al., 1998):

$$\theta R_1 \frac{\partial c_1}{\partial t} + q\frac{\partial c_1}{\partial z} = \frac{\partial}{\partial z}\left[\theta D_1 \frac{\partial c_1}{\partial z}\right] + F_1(c_1)c_1 + G_1(s_1^*) ,$$
(2-15)

$$\theta R_2 c_{2,t} + q c_{2,z} = \left[\theta D_2 c_{2,z}\right]_{,z} + F_2(c_2)c_1 + G_2(c_1, s_1', s_2^*) ,$$
(2-16)

$$\frac{\partial s_i^*}{\partial t} = H(c_i, s_i^*) - (\mu_i + \mu_i')s_i^* + \gamma_i, \quad i = 1,2 ,$$
(2-17)

where the "1" index is for the parent species, "2" index is for the daughter species, R_i is the retardation factor

14

accounting for gaseous, equilibrium solid, and liquid phases of the solute, c_i is the concentration of the liquid phase, D_i is the dispersion coefficient for the ith species, s_i^* represents the concentration of the solute on the nonequilibrium sites of the soil matrix, μ_i is the degradation rate of s_i^* and represents material lost to the system, μ_i' is the rate of transfer of material from parent to daughter, and γ_i is the production of s_i^*. The function $F_i(c_i)$ represents the degradation of the solute (losses of material from the system) from gaseous, liquid and solid phases, transfer losses from the parent passed on to the daughter for the three phases, losses due to plant uptake, and changes due to temperature variations in the system. The function $G_1(s_1^*)$ accounts for the production of the solute in all three phases, losses due to plant uptake, and the amount of solid phase at the nonequilibrium sorption sites. The function $G_2(c_1, s_i^*, s_2^*)$ describes the amount of daughter material transferred from the parent in gaseous, liquid, equilibrium solid and nonequilibrium solid phases, accounts for the production of the daughter species in all phases, and accounts for root uptake losses. Finally, the function $H(c_i, s_i^*)$ in Equation (2-17) is a first order sorption rate of s_i^* produced by the difference between equilibrium and nonequilibrium concentrations.

The **initial conditions** corresponding to the system in Equation (2-15) to (2-17) require specifications of the concentrations of all liquid phase solutes in the decay chain, as well as the species at the nonequilibrium sites in the soil matrix; that is, we specify

$$c_i(z,0) = c_{io}(z), \; s_i^*(z,0) = s_{i0}^*(z), \; 0<z<L, \tag{2-18}$$

where c_{io} and s_{i0}^* are prescribed functions of z. The standard **boundary conditions** in the HYDRUS model are as follows:

Dirichlet Conditions

$$c_i(z,t) = \overline{c}_i(z,t), \quad t > 0, \quad z = 0, L, \tag{2-19}$$

Cauchy Conditions

$$-\theta D_i \frac{\partial c_i}{\partial z} + qc_i = \overline{q}\,\overline{c}_i, \quad t > 0, \quad z = 0, L, \tag{2-20}$$

Neumann Conditions

$$\frac{\partial c_i}{\partial z} = 0, \quad t > 0, \quad z = 0, L, \tag{2-21}$$

where $\overline{c}_i$ is the specified concentration at the boundaries or the specified concentration of the incoming/outgoing fluid in Equation (2-20), and $\overline{q}$ is the downward fluid flux at the boundary. In addition to the conditions in Equation (2-19) to (2-21), HYDRUS allows for vaporization losses of volatile solutes at the soil surface $z = L$.

The **effective dispersion coefficients** $D_i (L^2 T^{-1})$ in Equation (2-15) and (2-16) are defined by the following (Šimúnek et al., 1998):

$$\theta D_i = D_{iL} |q| + \theta D_{iw} \tau_w + a_v D_{ig} k_{ig} \tau_g, \tag{2-22}$$

where D_{iL} is the longitudinal dispersivity (L) of the ith species, D_{iw} is the molecular diffusion coefficient ($L^2 T^{-1}$) of the ith species in free water, τ_w is the dimensionless tortuosity factor in the liquid phase, a_v is the dimensionless air content, D_{ig} is the molecular gas diffusion coefficient ($L^2 T^{-1}$) of the ith species, k_{ig} is the dimensionless constant of proportionality linearly linking c_i to the gaseous solute concentration g_i, and τ_g is the dimensionless tortuosity factor in the gas phase. The sum of the air content, a_v, and the soil moisture content, θ, is equal to the saturated water content, θ_s. The empirical formulas for the tortuosity factors are given by:

$$\tau_w = \theta^{7/3} \theta_s^{-2}, \quad \tau_g = a_v^{7/3} \theta_s^{-2}. \tag{2-23}$$

HYDRUS assumes that several of the parameters in the governing equations for the transport and fate of solutes are **temperature dependent**, such as: the molecular diffusion coefficients, the zero-order production terms for all phases, the first-order degradation rates (both for system losses and transfers from parent to daughter), and the adsorption coefficients relating one phase to another phase. This dependency is given by a modified Arrhenius equation defined by (Šimúnek et al., 1998):

$$A(T_a) = \exp\left[\frac{E(T_a - T_a^*)}{RT_a T_a^*}\right], \tag{2-24}$$

where T_a is the absolute temperature under consideration, T_a^* is the absolute reference temperature, E is the activation energy of the particular reaction or process being modeled in units of $(ML^2T^{-2}M^{-1})$, and R is the universal gas constant in units of $(ML^2 \div T^2 M^o K)$. If a (T_a) is the coefficient or parameter varying with temperature and a * (T_a^*) is the corresponding reference quantity dependent on the reference temperature, T_a^*, then the relationship between a and a* is given by:

$$a(T_a) = a^*(T_a^*)\ A(T_a)\ . \tag{2-25}$$

However, for the current sensitivity analyses, the variations of the above parameters will be for isothermal conditions and will be due to causes other than temperature changes.

2.2.3. Heat Transport Equation

The last model component listed in Table 2-1 is the heat transport equation. For the HYDRUS Code, the governing equation for heat transfer is one-dimensional, time-varying, and with terms accounting for convection, dispersion, and energy uptake by plant root water uptake. It is assumed that no heat is transferred by water vapor diffusion and there is no latent heat transfer by vapor movement. The convection-dispersion equation takes the following form (Šimúnek et al., 1998):

$$\frac{\partial\left[c_p(\theta)T_a\right]}{\partial t} + c_w \frac{\partial[qT_a]}{\partial z} = \frac{\partial}{\partial z}\left[\lambda(\theta)\frac{\partial T_a}{\partial z}\right] - c_w S T_a\ , \tag{2-26}$$

where $c_p(\theta)$ is the volumetric heat capacity of the porous medium $\left(M \div LT^2 {}^o K\right)$, c_w is the volumetric heat capacity of the liquid phase $\left(M \div LT^2 {}^o K\right)$, and $\lambda(\theta)$ is the coefficient of the apparent thermal conductivity of the soil $\left(ML \div T^3 {}^o K\right)$. To a reasonable degree of accuracy, it can be shown that

$$\frac{dc_p(\theta)}{d\theta} \cong c_w\ . \tag{2-27}$$

Thus, combining Equations (2-2), (2-26) and (2-27) leads to the heat equation programmed in HYDRUS:

$$c_p(\theta)\frac{\partial T_a}{\partial t} + c_w q \frac{\partial T_a}{\partial z} = \frac{\partial}{\partial z}\left[\lambda(\theta)\frac{\partial T_a}{\partial z}\right]. \tag{2-28}$$

The apparent thermal conductivity coefficient $\lambda(\theta)$ is given by the empirical formula

$$\lambda(\theta) = b_1 + b_2\theta + b_3\theta^{1/2} + \beta c_w |q|\ , \tag{2-29}$$

where (b_1, b_2, b_3) are empirical constants with units of $\left(ML \div T^{3o}K\right)$ and β is the thermal dispersivity (L). The initial

16

conditions require that the temperature be specified throughout the soil column at time zero. The boundary conditions considered by HYDRUS are as follows:

<u>Dirichlet Conditions</u>

$$T_a(z,t) = T_0(t), \quad t > 0, \quad z = 0,L ,$$ (2-30)

<u>Cauchy Conditions</u>

$$-\lambda \frac{\partial T_a}{\partial z} + T_a c_w q = T_0(t) c_w q_0(t), \quad t > 0, \quad z = 0,L ,$$ (2-31)

<u>Neumann Conditions</u>

$$\frac{\partial T_a}{\partial z} = 0, \quad t > 0, \quad z = 0 ,$$ (2-32)

<u>Atmospheric Boundary Condition</u>

$$T_0(t) = \langle T_a \rangle + A \sin\left[\frac{2\pi t}{p} - \frac{7\pi}{12}\right], \quad t > 0, \quad z = 0 ,$$ (2-33)

where T_0 in Equation (2-31) is the temperature of the incoming fluid, $\langle T_a \rangle$ in Equation (2-33) is the average temperature at the soil surface during period p, and A is its amplitude. In fact, in Equation (2-33), $\langle T_a \rangle$ is the average daily temperature at the soil surface, p is one day, and A is the daily temperature amplitude. It is assumed that time zero is at midnight and that the maximum temperature occurs at 1:00 pm.

As with the other temperature dependent components in HYDRUS, and some of the other codes, the heat transfer equations are not considered in the current sensitivity analyses. It is believed that for radionuclide soil screening purposes the computer codes need not incorporate the additional effects due to temperature variations. Thus, all such corrections are dropped in the analyses which follow.

Section 3
Sensitivity of Simulated Results to Conceptual Model Selection

As introduced in Section 1.3, the conceptual model is a simplification of the "real world" into a set of mathematical equations (i.e., conservation equations, constitutive relationships, and auxiliary conditions) that represent the most relevant physico-chemical processes thought to govern the problem at hand, in this case, the fate and transport of radionuclides in the unsaturated zone. The reader should be aware that the "real world" itself is only a conceptual model, or a composite of many conceptual models, that investigators embrace based on their field, laboratory, theoretical and simulation studies. These more comprehensive models, which are called the "real world", evolve and change in time as new and more extensive knowledge of the physico-chemical processes is obtained. One should not think of the comprehensive models as one super computer code containing many interacting modules, allowing for highly nonlinear processes, and time and space variations on all scales of interest. Such super computer codes do not currently exist: and if they did, the interpretation of their results may be as complex as those seen in the real world. These comprehensive conceptual models of the "real world" usually consist of equations and/or inequalities relating physico-chemical variables and parameters for specific processes under various external influences (e.g., flow of water through porous media, multicomponent/multiphase chemical processes, biological processes, thermodynamic processes). When such a collection of comprehensive models is linked together into single computer codes for situations such as the fate and transport of radionuclides in the unsaturated zone, many simplifing assumptions are invoked in the individual comprehensive models or modules, and in the manner in which these modules are linked together. The subject of this section is the sensitivity of the simulated results of radionuclide fate and transport through the vadose zone to the simplifing assumptions of the individual modules as they may occur in the computer codes selected to generate the results.

3.1 Time and Space Scales

Subsurface water and pollutant fate analyses are difficult because of the variabilities in time and space. One can not easily see underground, and extensive measurements and observation are both difficult and expensive. The medium through which the subsurface vapors, gases, liquids, and solids move is usually extremely hetergeneous, and analyses often involve several spatial and temporal scales. Aquifers and their overlying soil layers many be on the scale of 10^4 meters or more, and large-scale hetergeneities within an aquifer and the overlying soil may range from 1 to 10^2 meters. Surface source areas of pollutants may also have scales of 1 to 10^2 meters. The soil and rock pores may have scales on the order of 10^{-2} to 10^{-4} meters or less, while cracks, fractures, worm holes and root channels may be 100 times these values. Colloids which may freely pass through many of these pores have scales less than 10^{-5} meters. If adsorption and chemical processes are of interest, then analyses may require looking at scales of the order of 10^{-7} meters, which is the order of the adhesive layers on the soil matrix. Added to these length scale variations are a variety of time scales (Logan, 2001).

For example, precipitation/runoff/infiltration events may occur over severe storm periods lasting several minutes to an hour or two, or may occur over moderate rainfall periods of a day or two. Water flow in soil and aquifers may be a few meters per day to as low as a few millimeters per year. Significant variations in water flow can occur over periods of several minutes to several hours. Certain chemical reactions may occur very rapidly, while radioactive decay may require days to thousands of days to be consequential. Mineral deposition and dissolution may take centuries or longer to have a substantial impact on subsurface processes. The mix of all these lengths and time scales, some of which appear to be over scale continua, makes the selection of a problem's time/space domain difficult, as well as making the problem's mathematical formulation and its solution difficult. In fact, the entire conceptual model selection process is strongly tied to these time and space considerations and/or strongly influenced by them.

These variability and heterogeneity effects are evidenced in many ways, such as:

- Affect gas and liquid flow in the subsurface.
- Determine the validity and practicality of the selection of the problem's time/space domain.
- Affect the choice of conditions on the boundaries of the space domain and affect the choice of the initial conditions within the domain.
- Dictate the presence or absence of the impacts of hysteretic effects and those of density and thermal gradients.
- Influence whether or not preferential flowpaths and facilitated transport (e.g., pollutant transport by colloids) should be considered.
- Affect the form of the dispersion processes for pollutant mass transport.
- Enhance or suppress the impacts of chemical sorption, reaction and decay processes.
- Influence multicomponent and multiphase systems.

Each of these items or concerns is important to the selection process of conceptual models, and they are discussed in the following subsections with the respect to fate and transport of radionuclides in the unsaturated zone.

3.2 Domain Selection, Boundary and Initial Conditions

The fluid and water quality dynamics within the unsaturated zone are governed by the migration processes within the zone and the interactions between this soil-water zone and the atmospheric/soil-surface zone, the surface-water zone, and the ground-water zone (Luckner and Schestakow, 1991). The atmospheric/soil-surface zone affects the soil-water dynamics through the processes of precipitation, infiltration, evaporation, transpiration, heat transfer, vapor diffusion, pollutant transfer, exfiltration and fluid transfer at seepage surfaces. The surface-water zone interacts with the soil-water zone by the process of interflow which transfers fluid, pollutants and heat between the two zones. The soil-water and ground-water zones interact with one another through the processes of percolation and capillary rise, and in so doing transfer fluids, pollutants and heat. Thus, the physical domain, D, for a given modeling scenario in the unsaturated zone is a finite, three-dimensional, heterogeneous volume of a solid soil matrix whose particles may have sorbed pollutants attached to them, and a soil void space containing air, vapors, and liquids with dissolved pollutants. In addition, domain D may possess density gradients that affect the fluid and water quality dynamics, the density gradients being produced by thermal effects, fresh/saline water interactions, and areas of free pollutant products with densities higher or lower than pure water. Since domain D is finite in the real world, it must possess a boundary, ∂D. Parts of the boundary, ∂D_1, may be fixed over the time domain, T, of interest in a given modeling scenario, boundaries such as the soil surface, streams or river channels, lake or reservoir shores. Other boundaries, ∂D_2, may be free, such as fresh/saline interfaces, water-table surfaces, and seepage zones. These free boundaries, ∂D_2, are determined as part of the solution process of the governing equations in a modeling scenario, thus highly complicating that solution process and often changing a linear system to a highly nonlinear system. There may also be internal boundaries, ∂D_3, within domain D if the domain consists of distinct soil layers possessing discontinuous properties as one moves from layer to layer, or if moisture and/or pollution fronts move through the domain. The head, moisture, temperature, and pollutant conditions specified on the boundaries, ∂D_1 and ∂D_2 couple the soil-water zone to the atmospheric/soil-surface, surface-water, and ground-water zones. These real world boundary conditions are time-varying, spatially-heterogeneous and often are highly uncertain. In addition, the fixed vertical boundaries of the domain D may not be determined by natural interfaces such as rivers and lakes or by anthropogenic interfaces such as walls and other structures, but may be chosen arbitrarily at some distance from the area of immediate interest in a modeling scenario. The conditions specified on these boundaries may be specified in terms of symmetry, periodicity or no-transport conditions, all of which may be contradictory to real world conditions. Since modeling scenarios for the subsurface zone usually involve time variations and thus some starting point in the time simulation, initial distributions of moisture content, hydraulic head, pollutant concentrations in solution, air and gaseous vapors, sorbed pollutants, and temperature within domain D are required. Thus, a comprehensive formulation of the fluid and pollutant dynamics in the unsaturated zone is often highly complex and highly uncertain. This complexity and uncertainty force unsaturated zone scientists to make several assumptions and simplifications in their investigations of specific physical systems.

Two trains of thought concerning choices for dimensionality and scale in the study of subsurface solute transport and fate are exemplified by Carrera (1993) and Logan (2001). Carrera states that the anomalies that can not be accounted for by the classical solute transport equations (Equations 2-15 to 2-17) are directly or indirectly caused by heterogeneity in the subsurface. He states that current approaches for dealing with heterogeneity can be divided into deterministic and stochastic procedures. Stochastic methods have been successful in explaining qualitatively some anomalies of solute transport and fate; but because of their restrictive assumptions (e.g., statistical homogeneity and

stationarity), they appear to be far from reaching a stage at which they can be used routinely for solving realistic field problems.   On the other hand, Carrera states that deterministic methods, when applied with care, have been successively used in actual problems. Yet, he says it can be argued that these methods fail to account for small-scale variability of concentration so that they would become ineffective when dealing with nonlinear processes, such as chemical reactions.

Logan (2001) states the obvious that "models do not include all the details of the physical reality". He says that in the best of all possible worlds, the model should give a reasonable description of some part of reality. This is why one often separates out specific mechanisms and studies equations with only diffusion, with only advection, or with only reaction-dispersion. Understanding the behavior of these simple models can then give one **clues** into the behavior of more general problems. For example, if one can show that some simple, nonlinear reaction-advection-dispersion equation possesses solutions that blow up (go to infinity, or have their derivatives go to infinity) in finite time, then one has succeeded in creating a **healthy skepticism** about such systems in the real world. Many of the systems in Logan (2001) are one-dimensional with semi-infinite or infinite domains, involving nonlinear equilibrium adsorption processes, non-instantaneous and multi-site adsorption kinetics, nonlinear advection and reaction rates, in situ bioremediation processes, or colloidal transport and porosity-reducing filtration processes. The similarity solutions (see Appendix B) and traveling-wave solutions, the solution blow ups, and the colloidal clogging of filtration media studied in these rather simplistic and ideal models may well be representative of such happenings in the real world. Thus, in choosing the dimensionality of the domain D, one must keep in mind the objectives of the study and the resolution of the heterogeneities that are to be considered.

One-dimensional models cannot simulate the curvatures and refractions of streamlines as water flows through layered soil with spatially varying hydraulic properties, and cannot simulate water flow in sloping soil layers (Miyazaki et al., 1993). These models cannot account for two- and three-dimensional soil heterogeneities and anisotropies, cannot account for the nonsymmetric location of surface-water bodies, cannot simulate the heterogeneous areal distribution of rainfall and vegetation cover, and cannot account for a heterogeneous source of radionuclides. For example, McCord et al (1997) presented a numerical modeling approach for assessing the impacts of geologic heterogeneity on groundwater recharge estimates derived from environmental tracers. They stated that common to many of the environmental tracer methods used to infer recharge in arid environments is an assumption of one-dimensional, vertical downward flow of water and solutes. However, it is known that fluid flux rates through geologic materials can be spatially variable in more than one dimension owing to heterogeneities in porous media properties. Local flow directions within the medium may not be vertical even when application of water at the surface is spatially uniform and hydraulic gradients are vertical. Consequently, environmental tracer movements are also spatially variable and the one-dimensional assumption involved to interpret unsaturated environmental tracer concentration profiles may be unrealistic. The results of the McCord et al (1997) simulations show that recharge inferred using environmental tracer methods is also highly spatially variable and the recharge estimates obtained by tracer profiles (using the one-dimensional model) tend to overestimate recharge and may only be accurate to within an order of magnitude, particularly in situations with significant media heterogeneity in two or three dimensions.

However, one- and two-dimensional models possessing scaling modules as given in Equations (2-7) to (2-9) can often efficiently treat linearly variable soil structures over field mapping units and thus present reasonable three-dimensional pictures of flow and solute transport (Rockhold et al, 1996; and Rockhold, 1999). For example, Figure 3-1a shows 13 locations in a field mapping unit where it is assumed that each location has a different soil-water behavior, but each behavior is linearly related to each other through similar soil structures (Figure 2-2).

Thus, a one-dimensional code, such as HYDRUS, through the use of its scaling component, can be efficiently applied at each location, and the results of the simulation can form a reasonable composite picture of radionuclide transport and fate over the entire field mapping unit, the composites being formed through the use of scaling, superposition, and geostatistical techniques. Similarly, a two-dimensional code, such as CHAIN 2D, can be used to form a good composite for the transport and fate of pollutants through the vadose zone underlying the field of row crops shown in Figure 3-1b. The vertical slab simulation along the four transects shown in the figure can be efficiently carried out through the use of the scaling module in the code. From these four transects, a composite for the field can be constructed as in the one-dimensional case.

Once the dimensionality of domain D is established, along with its dimensions in all directions, the next step is to determine realistic boundary conditions on all segments of the boundary, ∂D. These conditions may be constant in time, time-varying, or cyclic; and the type of conditions may be Dirichlet, Neumann, or Cauchy (Bear and Verruijt, 1987; van der Heijde, 1994). Conditions are required for fluid flow variables, solute transport variables,
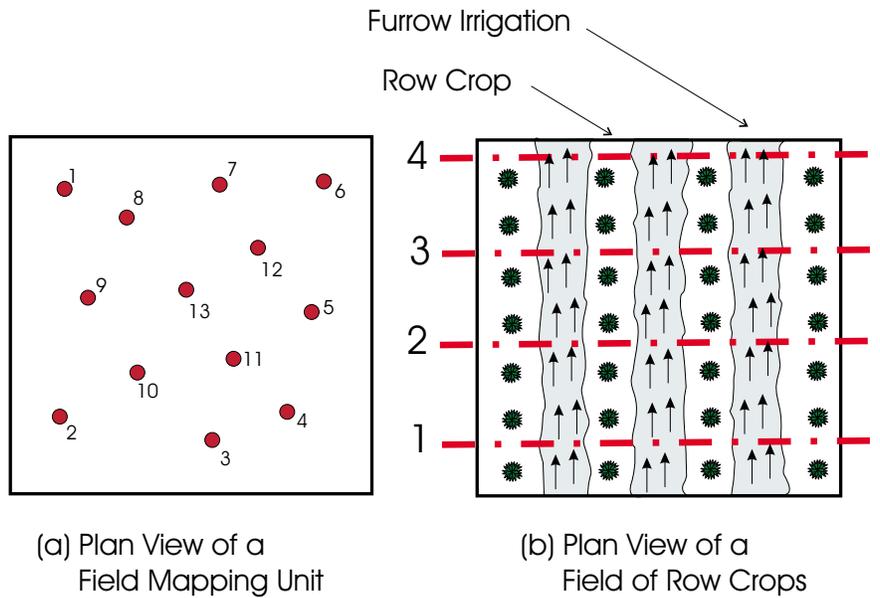
Figure 3-1 Schematic of modeling applications for simulating three-dimensional field mapping units using one-dimensional codes (a), and two-dimensional codes (b).

and heat transport variables. The boundary conditions dictate how the domain (i.e., the unsaturated zone) interacts with its environment (i.e., atmospheric/soil-surface zone, surface-water zone, ground-water zone). If the boundary conditions are time varying, then the corresponding environment is time varying; if the conditions are spatially heterogeneous, then there exist spatially heterogeneous environmental conditions; and if the boundary conditions are stochastically distributed, then there exists randomly variable environmental conditions. If the governing equations of a given model contains an internal (i.e., internal to domain D) source on sink term, such as the root water uptake term in Equation (2-3), then what happens in the external environment to domain D may influence the formation of the source or sink term, such as given in Equation (2-6). Thus, specific solutions of the governing equations of a given model are highly influenced by the specific conditions specified on the boundary, ∂D, of domain D. However, the influence of conditions on one part of the boundary may die off faster or slower, both spatially and temporarily, than the influence of conditions specified on another part of the boundary. Which part of the boundary and which boundary conditions are the most influential in a given model depends on the size, shape and dimensionality of domain D, and on the set of governing equations and constitutive relationships. The determination of these influences is part of the sensitivity analysis of conceptual model selection.

The initial conditions for a given model are the starting distributions of the flow variables and the heat and solute transport variables within the domain D, along with the starting distributions of any adsorbed pollutant species on the soil matrix. Usually for the pollutant species (e.g., radionuclides), a time-varying source of pollution is specified at the soil surface. If this is the case, it is convenient and often reasonably realistic to set the initial concentrations of the dissolved and adsorbed species at zero. The difficult initial distributions to determine are those for the flow variables. The pollutant species, except for background concentrations in the soil water and on the soil matrix, may well have a well-defined starting point; but the moisture content and hydraulic head within most unsaturated zone domains are constantly varying due to the constantly varying conditions in the environmental zones that influence these domains. What further complicates the specifications of the initial flow conditions is that these conditions possess a "history" component. The history component accounts for the hysteretic characteristics of the soil-water properties (see Visintin, 1994; Brokate and Sprekels, 1996; and Appendix C). For a given soil, the soil-water retention curve and the hydraulic conductivity function of Figure 2-1 take on different forms depending on whether the soil is drying or wetting. In addition, Fetter (1999) found from numerical simulation that the importance of the hysteretic mode appears to be greater for the pressure head and water content than for pore velocity and the solute front movement. Thus, the forms of the distribution of the flow variables at zero simulation time depend on the history of soil conditions prior to zero time.

In spite of the above difficulties, initial flow distributions must be specified. One common mode of specification is to assume a constant, steady flow through domain D. In this way, history components and hysteretic effects are eliminated, as well as time-varying infiltration rates at the soil surface. Miyazaki et al. (1993) assert that the **steady state** of water flow is the state where water is moving continuously without storage or consumption in the soil. They further state that saturated flows in groundwater and unsaturated flows in the vadose zone when suction is less that the air entry value can be considered steady flow provided that the flow boundary conditions do not fluctuate. In the field, vertical-down water flows under ponded water at the soil surface and lateral flows of groundwater are typical steady flows. However, a completely steady flow in unsaturated soil can only be generated in the laboratory where flow boundary conditions can be fixed. In nature, as stated above, flows of water in unsaturated soils are almost always in unsteady states due to changes in the flow boundary conditions (e.g., variable precipitation and evaporation rates, see Appendix F), changes in soil pore water storage, impacts of soil hysteresis, and the consumption of soil water by plant roots.

The water content distribution in a homogenous, unsaturated soil column under the influence of a steady downward flow (i.e., a constant recharge rate, q) may be taken as a constant value, as in the CHAIN Model, or it may be obtained from the steady-state solution of the Richards Equation (Equation 2-3, without the sink term S). This steady-state solution gives a nonuniform moisture distribution in the homogenous soil column and can be obtained from codes such as HYDRUS and CHAIN 2D. The differences of these two approaches on the fate and transport of radionuclides are discussed in Appendix E. For multi-layered, unsaturated soil columns under the influence of a steady downward flow, the water content distribution, as determined from the steady-state solution of the Richards Equation, can be highly variable, depending upon the variability of the hydraulic properties as one passes from layer to layer. These piecewise-continuous moisture distributions are shown for layered soils, with significant differences in hydraulic properties from layer-to-layer, in Miyazaki et al. (1993) and Rockhold et al. (1997). The affects that a layered soil under constant recharge versus that of a corresponding homogeneous layer on the fate and transport of radionuclides are shown in Appendix G. However, the layered soil in this case does not possess large differences in hydraulic properties as one passes from layer to layer. For example, the range of saturated hydraulic conductivities over the nine layered column considered in Appendix G is from 172 cm/d to 539 cm/d, with a harmonic mean of 245 cm/d. Thus, differences in pertinent output parameters for radionuclide transport through the homogenous column versus that of the nine-layered column vary from only 2 to 10 percent.

Appendix F compares the impacts on radionuclide fate and transport through a homogeneous soil column under the influence of a steady-state recharge rate, q, against the time-varying conditions of daily precipitation rates and daily evapotranspiration rates specified at the soil surface. As shown in Figure F-4, significant differences can occur when steady-state flow conditions replace the more realistic daily, time-varying conditions. In arid and semi-arid areas, the impacts are even more drastic when daily averages are replaced by storm event situations. For example, Litaor et al (1998), through the use of large-scale rain simulations, found that the highly immobile radionuclide species of plutonium and americium at the Colorado Rocky Flats Facility could be significantly remobilized under severe storm conditions. Thus, it is assumed, but not proved, that the differences in radionuclide movement between steady-state and time-varying flow conditions would even be greater than shown in Appendix F if daily averages were replaced by sequences of realistic storm events.

3.3 Density and Thermal Gradients

For the objectives and purposes of the current study (i.e., radionuclide transport in the unsaturated zone), density gradients produced by free pollutant products with densities greater than or less than pure water, and gradients produced by fresh/saline water interfaces are assumed to be of lower order importance and will not be further considered. Discussion of the importance of such gradients can be found in Domenico and Schwartz (1990) and Bedient et al (1999). However, density gradients due to thermal effects may be of importance.

The temperature gradients in the soil form a driving force for movement of both liquid water and water vapor. Therefore, a daily change in the temperature due to surface changes in wind velocity, net radiation from the atmosphere, relative humidity, and air temperature near the ground may influence water movement in the soil. Such temperature changes produce changes in soil water viscosity and surface tension which in turn change the hydraulic conductivity and pressure head (Equation 2-10 and 2-11). In addition, these temperature gradients affect several of the parameters (e.g., molecular diffusion coefficients, production coefficients, and decay rates) in the solute fate and transport equations, see Equations (2-24) and (2-25). Temperature changes in the subsurface may also occur due to the generation of heat during chemical reactions, the generation of heat by underground nuclear waste storage repositories, and the heat produced in deep geological formations by hydrothermal systems. Whenever heat is generated and temperature gradients produce significant changes in the flow of underground vapors and liquids, and

produce significant changes in solute fate and transport, the energy balance must be added to the governing system of equations, such as the balance given in Equation (2-26) to (2-28). Accounting for temperature variations in the upper soil layers is definitely important in geographical areas experiencing annual fluctuations in air temperatures from below freezing to above freezing. These fluctuations are, in turn, important for the fate and transport of radionuclides from surface sources. Even in the arid areas around the Mojave Desert, Nevada, Andraski (1997) found that both isothermal liquid and vapor flow, and nonisothermal vapor flow needed to be considered in the conceptualization of flow under natural vegetated sites, as well as under sites where the vegetation had been removed. Thus, the assumption of isothermal conditions (i.e., no heat flow considerations) for all fluid and solute flow may lead to uncertainties that could be eliminated if the effects of thermal gradients, and their induced density gradients are considered.

3.4 Facilitated Transport and Preferential Pathways

Facilitated transport of pollutants in the unsaturated zone, as well as in the ground-water zone, is the transport of adsorbed contaminants on suspended particles or colloidal particles that are able to pass through the connected pores of a porous medium. In Corapcioglu and Choi (1996), the simulation of colloid transport in the vadose zone consists of four phases: an aqueous phase, the stationary solid matrix phase, a carrier (i.e., colloidal particles) phase, and a stagnant air phase. The fact that colloidal particles can act as carriers enhances the transport of contaminants in porous media by effectively reducing retardation, the R_i value in Equations (2-15) and (2-16). McCarthy and Zachara (1989) indicated that the highly immobile species of plutonium and americium were transported over a mile from a liquid waste outfall at New Mexico's Los Alamos facility through preferential pathways by colloidal carriers. These results are supported by the work of Litaor et al (1998) at Colorado's Rocky Flats facility. In this study, the remobilization of large fluxes of americium and plutonium, initiated by severe storm events, was accomplished by carrier suspended and colloidal particles. The dynamics of suspended and colloidal particle systems are fully discussed in references such as van de Ven (1989) and Probstein (1994).

Colloids, other suspended particles, and microbial particles play another important role in the fate and transported of radionuclides in the unsaturated zone, namely the change of the medium's porosity with time. Logan (2001) calls this **filtration**. He says filtration occurs in a porous medium when the transported particles are actually sieved by the solid porous matrix, thereby decreasing the porosity and possibly clogging the medium. He states that this clearly can, and will, occur when the average size of the pores is smaller than the particles in solution, as is the case for large molecules, bacteria and colloids migrating through clayey soil. But filtration can also occur when smaller particles form sediments in domains with large porosities. In fact, Kretzschmar et al (1997) have evaluated four different experimental systems for determining colloid deposition rates and collision efficiencies in natural porous media. They found that colloid deposition generally followed a first-order kinetic rate law and they were able to calculate collision efficiencies for the colloid deposition. Logan (2001) studied the filtration process through the use of a one-dimensional, time-varying, deterministic system of equations in terms of the volume concentration of the transported colloid, the volume concentration of the retained or immobile colloid, and the changing porosity of the medium. Kaiser (1997) studied the clogging in a two-dimensional porous medium with small inhomogeneities through the use of directed percolation techniques, Monte Carlo simulations, and fractal pore clogging (i.e., the deposited colloids formed fractal clusters in the percolation network). The proposed models for study in the current report do not allow for either colloidal transport of radionuclides or for colloidal reduction of porosity. As indicated above, both phenomena under the right conditions could be very important.

The unsaturated zone is certainly not a homogeneous, porous medium. In the root zone there are numerous large pores and cracks formed by such agents as plant roots, shrinkage cracks, and animal burrows. These **macropores** can form **preferential pathways** for the movement of water and solute, both in the vertical and horizontal directions through the root zone. This situation can lead to what is called "short-circuiting" or "bypass flow" of the infiltrating water as it moves through the macropores at a rate much greater than would be expected from the hydraulic conductivity of the soil matrix (Fetter, 1999). This **bypass flow** only takes places when either the macropores and cracks are open to the atmosphere or the water pressure within the macropores and cracks is positive. On the other hand, when ponded water infiltrates a soil matrix within which macropores and cracks are buried and when the soil matrix is under suction, water will not infiltrate the buried macropores but will infiltrate only the soil matrix. In this case, macropores are not preferential pathways for flow but are obstacles of the water flow (Miyazaki et al, 1993).

A second type of preferential flow is **fingering** which occurs when a uniformly infiltrating solute front, or wetting front, is split into downward-reaching "fingers" due to instabilities in the wetting front. An instability often occurs, due to pore-scale permeability variations, when an advancing wetting front reaches a boundary where a finer

sediment overlies a coarser sediment. Under some conditions, fingering flows can also be generated in uniform soils. Yao and Hendrickx (1996) state that instabilities in wetting fronts occur under the following conditions:

- Infiltration of ponded water with compression of air ahead of the wetting front;
- Surface desaturation and redistribution of water in the soil profile;
- Water-repellent soils due to the plant litter and residues, organic fertilizers, and pesticides;
- A water content increasing with depth; and
- Continuous nonponding infiltration.

In several of these mechanisms which produce wetting front instabilities, **flow hysteresis** (Appendix C) plays a major role.

There have been several recent studies concerned with these various conditions producing wetting front instabilities. Wang et al (1997, 1998) considered the variations of water infiltration into the unsaturated zone under the influence of air compression, air counterflow, and flow hysteresis. The first paper deals with theoretical considerations and the second paper gives the results of testing this theory in the laboratory. Wang, Feyen and Elrick (1998) derived generalized linear instability criteria for finger formation applicable for field scale assessment. Wang, Feyen and Ritsema (1998) experimentally evaluated these criteria in the laboratory under the combined effects of air entrapment, surface desaturation, soil layering, and water repellency. Further studies on the effects of water repellency on infiltration, wetting front instability and vadose zone flow fingering were carried out by Wang et al (2000), and Wang, Wu and Wu (2000).

A third type of preferential flow is **funneling** (Fetter, 1999; and Miyazaki et al, 1993). Funneling occurs in the vadose zone below the root zone and is associated with stratified soil profiles. Sloping coarse-sand layers embedded in fine-sand layers can impede the downward flow of water. The sloping layer will collect the water like the sides of a funnel and direct the flow to the end of the layer. When the pressure of the funneled flow exceeds a critical value, fingering flow will be generated in the coarse layer and the water again percolates vertically.

Miyazaki et al (1993) state that preferential flows in soils are generally regarded as a type of saturated flow, and that evidence of unsaturated preferential flows is scarce. In addition, they state that the velocities and local quantities of preferential flows are large compared with other saturated flows in soils. In the review by Gee at al (1991), it is stated that some very heterogeneous soils exhibit little or no preferential flow when partially saturated. They considered a test at Las Cruces, New Mexico, where extremely heterogeneous soils were wetted at rates well below saturation and no preferential flow was observed. In general, the visual wetting front for these tests was relatively smooth and surprisingly uniform. However, Shurbaji and Campbell (1997) studied the phenomena of evaporation and recharge in desert soil at three sites in southeastern New Mexico and found that possibly 85% of the recharge occurs via movement of water through preferential pathways in the root zone. Preferential flow was evident at all three sampling sites, and the long-term recharge rates at these sites were calculated to be 0.5, 0.8, and 2.4 mm/yr. Yao and Hendrickx (1996) assert that worldwide it is thought that a major mechanism for ground-water contamination is the passage of pollutants through preferential flow pathways. For modeling purposes, it should be kept in mind that this is an event type phenomenon (e.g., storm events of tens of minutes to an hour or two) which is currently not well parameterized for large time-step simulation.

3.5 Scale Dependency in Heterogeneous Media

Most subsurface flow and transport models are not sufficiently detailed to allow an explicit representation of all dynamical scales in heterogeneous media. That is, most models are constructed at such a coarse scale of resolution that unresolved subgrid variablity often exists. It is therefore important to understand the interaction between unresolved dynamics and explicitly resolved dynamics. For example, Beckie et al (1994) examined when it is possible to construct an accurate model for the explicitly resolved large scales, without an explicit description of the subgrid scale dynamics; and they demonstrated how unresolved subgrid scale dynamics interact with resolved scale dynamics. They showed that a **universally** valid resolved scale model can be constructed if the resolved dynamics are sufficiently independent of the details of the subgrid scale dynamics; that is to say, there is a **spectual gap** between the subgrid scales and the resolving scales. In the event of a spectral gap, a resolved model is composed of a universal structure and accompanying model parameters, the parameters representing the effect of unresolved dynamics upon resolved dynamics. Beckie et al (1994) showed theoretically, and numerically, that a **local Darcy law** (Equation 2-1) for groundwater flow is a universally valid resolved scale model if the resolved and subgrid scales of the hydraulic conductivity are separated in scale by a spectral gap. However, if the hydraulic conductivity

possesses many scales of variability (which Neuman and DiFederico, 1998, assert is true of all real geologic media), then a more general **nonlocal Darcy law** is a more appropriate model structure. Using numerical experiments, Beckie et al (1994) found that when the nonlocal Darcy law is more appropriate, the errors in using the local Darcy law with effective parameters are most significant at the smallest resolving scale of the nonlocal model, and are minimal at scales between 8 and 16 times the resolving scale.

Carrera (1993) considered the applicability of the advection-dispersion-reaction equations in their standard form (Equations 2-15 to 2-17) for simulating solute transport in heterogeneous media. He identified several solute transport features observed in the field that are poorly simulated with such equations. The most notable of these is scale dependency of dispersivity (dispersivity tends to increase with the scale of measurement). Other features are long tails in breakthrough curves, skewness in spatial distribution of solutes, directional effects on arrival times, porosity, and dispersivity, and the inability to account for small-scale variability of concentrations which affects nonlinear processes such as chemical reactions. Carrera asserts that all of these effects are more or less caused by the spatially correlated variability of hydraulic conductivity. He states that spatial variability can be simulated using a **stochastic approach** and that this may be the correct framework for formulating solute transport. Even though stochastic hydrogeology has been successful in explaining some facts observed in the field, he says that its applicability to real problems is hampered by theoretical and practical difficulties, such as the stochastic stationarity of hydraulic conductivity. Carrera says this conflicts with observations. For example, the scale effects of hydraulic conductivity, small-scale variability of concentrations, and the possible unbounded growth of dispersivity suggest that the logorithm of the hydraulic conductivity is usually non-stationary. The alternative to stochastic formulations is a **deterministic approach** to solute transport, an approach based on the belief that dominant discrete heterogeneities can be identified and their effects can be explicitly built into the model. Hence, the main advantage of deterministic methods is their ability to incorporate qualitative information into their formulations, while the main disadvantages arise from the lack of procedures for representing such qualitative information in a given model. Thus, much effort is being expended to identify effective parameters for flow and solute transport models in heterogeneous environments.

The flow and transport in heterogeneous porous media is highly dependent on the spatial variability of soil and aquifer properties. However, it is impractical when modeling a real situation to obtain aquifer properties at the scale of each "grid block" of a given model. Hence, tools are required to move information between scales (e.g., upscaling from laboratory measurements to grid block scale), to incorporate the scale and location of test data when interpolating to a fine grid, and to fill in missing information around sparse data areas. Some tools that have been used, and are being used, for these purposes are given in the following books and papers:

- Transport and divergence theorems developed in the context of generalized functions for changing spatial scales in the analysis of subsurface flow and transport, Gray et al (1993).
- A multi-scale, hydraulic conductivity distribution, reconstruction method based on forward and inverse wavelet transforms in conjunction with a pseudo-fractal distribution for filling in missing information around sparse data areas, Brewer and Wheatcraft (1994).
- Comparison of two fast algorithms, one based on random walks and the other based on real-space renormalization group methods, for upscaling permeability data from cores to reservoir grid blocks in heterogeneous media, McCarthy (1995).
- A review of the various upscaling techniques used to calculate the equivalent permeability of a heterogeneous porous medium, and indicating in what circumstances they can be most suitably applied, Renard and de Marsily (1997).
- The use of the theory of homogenization as an upscaling procedure for modeling porous media on micro-, meso- and macro-scales; percolation, two-phase flow and miscible displacement are also considered, Hornung (1997).
- The application of fractals in the unsaturated zone for characterizing heterogeneity and for modeling soil moisture, biodegradation and solute transport, Crawford et al (1999).
- A current assessment of parameter upscaling procedures and techniques for addressing vadose zone heterogeneities, leading to an optimistic outlook on improving our ability to model pollutant transport in this complicated subsurface zone, Mayer et al (1999).

3.6 Chemical Adsorption, Chemical Reactions, and Decay Processes

According to some investigators, ideal solute transport is transport through a homogenous porous media under the influence of linear, instantaneous adsorption/desorption processes. Conversely, nonideal solute transport includes a host of complicating processes leading to solute transport complexity, processes such as (Brusseau and

Rao, 1989; Weber et al, 1991): nonlinear equilibrium sorption; partial, nonreversable sorption; linear and nonlinear, nonequilibrium sorption; sorption capacity variability and rate-limited sorption; facilitated transport; hydraulic conductivity variability due to heterogeneous media; vapor-phase processes; immiscible liquid phase processes; and transformation reactions and decay rates. Brusseau and Rao (1989) list several induced and natural gradient tracer experiments showing extended-tail breakthrough curves which were attributed to rate-limited sorption, hydraulic conductivity heterogeneity, sorption capacity limits, and/or rate-limited desorption. Thus, the subject of this subsection is the sensitivity of conceptual models based on varying chemical sorption, chemical transformation, and chemical decay processes.

Kuox et al (1993) and Thibodeaux (1996) describe the various processes involved in solid-liquid soil reactions, including those characterized as **adsorption/desorption**. Depending upon soil structure and texture, contaminant characteristics, and the flow characteristics, the characteristic time scales for simple physical sorption are known to vary from microseconds to months. In addition, experimental evidence has shown that often the solid-phase fraction of a contaminant on the desorption cycle behaves much different than when it is on the adsorption cycle. This leads to nonequilibrium states and hysteretic type adsorption/desorption cycles. For example, Knox et al (1993) states that such hysteretic cycles affect the amount of water required in pump-and-treat remediation of subsurface aquifers. Thibodeaux (1996) states that the validity of the ideal local equilibrium assumption (LEA) for solid-liquid reactions depends on the degree of interaction between the macroscopic transport processes of water and hydrodynamic dispersion, and the microscopic processes of molecular diffusion and sorbed-solute distribution in conjunction with soil aggregate size, shape and composition. When the rate of change of solute mass during the microscopic sorption processes is fast relative to the mean velocity of the bulk flow, the solid-liquid interactions are nearly instantaneous with reference to bulk-flow time scales, and they conform to the LEA. Deviations from the LEA occur as the interactions of the solute with the soil matrix become increasingly time dependent with respect to bulk-flow time scales. This divergence also occurs as soil aggregates increase in size and complexity and pore-class heterogeneity increases.

Several investigators have studied the effects of the deviations from LEA and linear adsorption/desorption, deviations based on nonlinear adsorption and those based on nonequilibrium solute transport. Common nonlinear, equilibrium isotherms are those of **Freundlich**,

$$s = \alpha c^n \ , \tag{3-1}$$

and **Langmuir**,

$$s = \alpha c \div (1 + \beta c) \tag{3-2}$$

where c is the concentration of the liquid phase in mg/L, s is the concentration of the solid phase on soil equilibrium sites in mg/kg, and α, β, and n are constants with consistent physical units. The linear, equilibrium isotherm,

$$s = K_d c \ , \tag{3-3}$$

arises from the Freundlich isotherm when $n = 1$ and $\alpha = K_d$, the distribution parameter in ml/g. Logan (2001) and Fetter (1999) list several other nonlinear equilibrium isotherms, such as the Langmuir two-surface sorption isotherm, the generalized Langmuir isotherm and the quadratic and exponential isotherms.

Using a one-dimensional, deterministic, advection-dispersion-sorption model, Fetter (1999) found that the Freundlich sorption isotherm with n>1 produced a spreading pollutant front, while for 0<n<1, the front was self-sharpening. For n=1 (i.e., the linear isotherm) the classical "Gaussian" breakthrough curve was produced. These results are supported by Logan (2001) and Sachdev (2000). Sachdev (2000) found that the asymptotic behavior of the solute plume differed for the following three ranges of n: 0<n<1, 1<n<2, and n>2. These differences were shown to occur for both one- and two-dimensional domains. In addition, Logan (2001) pointed out that the Langmuir isotherm limits the amount of material that can be adsorbed (i.e., $s < \alpha/\beta$), but the Freundlich isotherm does not. Thus, the use of the Freundlich isotherm should be done with extreme caution for realistic simulations. In other studies, Bai et al (1997) constructed a triple-porosity, one-dimensional model of contaminant migration with linear sorption in strongly heterogeneous media. They showed that extensive tailing in the breakthrough response occurred over that due to single-porosity approaches and that multiple breakthrough fronts with reverse diffusion also developed. Both behaviors were due to the strong heterogeneities. Berglund and Cvetkovic (1996) considered contaminant displacement in aquifers under the coupled effects of flow heterogeneity and nonlinear sorption, using five different isotherm equations, including those of Freundlich and Langmuir. They found that the effects of the

choice of sorption isotherm is very significant and strongly dependent on the heterogeneity of the particular data set considered.

The solute transport system of the HYDRUS Code, Equation (2-15) to (2-17), accounts for a two-site sorption structure (i.e., equilibrium and nonequilibrium sites). This model was developed by van Genuchten and his colleagues (van Genuchten and Wagenet, 1989; Toride et al, 1993). A two-dimensional version of this system also occurs in the CHAIN 2D Code. In Appendix H, the impact of nonequilibrium sorption on the fate and transport of radionuclides is considered. This impact can be great depending upon the mean recharge rate in the vadose zone, and the relative relationships between the first-order rate for nonequilibrium sorption, the radioactivity decay rate, and the linear distribution parameter K_d. In other studies, Simon et al (1997) and Logan (2001) determined the properties of exact and approximate traveling wave solutions for solute transport with nonlinear and nonequilibrium sorption. Often nonlinear sorption leads to the existence of moving concentration fronts of substances transported in porous media that do not change shape (i.e., traveling wave solutions). The cause for the existence of such solutions is a balance that develops between the self-sharpening effect of nonlinear sorption and the spreading effects of dispersion and sorption kinetics. Traveling wave solutions also occur for the combined processes of linear equilibrium and nonlinear nonequilibrium sorption. The nonequilbrium processes considered in Appendix H are linear and do not possess traveling wave solutions. Finally, Chen and Wagenet (1995) compared the two-site, equilibrium/nonequilibrium model with a continuously-distributed, sorption site heterogeneity. They found that the deviations between the two-site model and the continuously-distributed model tended to be more severe as time increases. Thus, as sorption-site heterogeneity increases, the applicability of the two-site model tends to decrease.

Murray (1989) and Logan (2001) have shown that **diffusion-dispersion-reaction systems** can have a variety of solution forms when the reaction terms are nonlinear. For example, solutions can blow up in finite time; traveling wave solutions can occur; solitons can be formed, which are special wave pulses which interact with one another so as to keep their basic identity and take on a "particle-like" character; deterministic solutions can become chaotic as time evolves and act as "random" quantities; and various stable and unstable spatial patterns can form. Even though Fetter (1999) demonstrates that the chemistry of dissolved uranium is somewhat complex, the possible chemical reactions of the five radionuclides listed in Section 2.1 will not be considered in this report. The only transformations that will be considered are those related to adsorption/desorption and **radioactive decay**.

In Appendix I, the effects on the pollutant breakthrough curves of the five radionuclides (Section 2.1) due to changing distribution coefficients (K_d of linear, equilibrium sorption), changing decay rates (μ), and varying recharge rates (q) were investigated using the CHAIN Model. The values of K_d and μ vary with the parent radionuclide under consideration. Also given in Appendix I is an example of the differences between the one-dimensional transport and fate of a parent and that of a daughter radionuclide. Oldenburg and Pruess (1996) indicate some daughter characteristics in their two-dimensional simulation of mixing with first-order decay in variable-velocity porous media flow that can not happen in the one-dimensional simulation given in Appendix I. These authors found that the mixing due to advective dilution, hydrodynamic dispersion, and molecular diffusion is stronger in regions of higher velocity and weaker in slower-moving regions. Further, they found that concentrations profiles normal to the flow direction are displaced toward regions of slower flow in fields possessing velocity gradients. Hence, they found for species undergoing first-order decay, that the effect of parent accumulation in regions of low velocity is enhanced for the daughter species because of the following factors:

- The rate of daughter production is proportional to the local concentration of the parent;
- Mixing is proportional to the local velocity; and the lower the velocity, the less mixing and longer time periods for decay.

Using a one-dimensional system, Logan (1996) studied the transport of a decaying tracer in a heterogeneous porous medium subjected to rate-limited adsorption with a linear equilibrium isotherm. The medium was semi-infinite and periodic boundary conditions of the Dirichlet and flux-type were examined. The heterogeneity was simulated by using a scale-dependent dispersion coefficient that increased exponentially with distance, up to some limiting value. The one-dimensional model was designed to give information about how adsorption and decay effects can interact with heterogeneities in the medium. For example, when both adsorption and decay are present, the amplitude of a pollutant wave in a homogeneous medium can exceed that in a heterogeneous medium, even though the later has smaller dispersivity. Somewhat contradictory evidence was given by Miralles-Wilhelm and Gelhar (1996), who performed a stochastic analysis of the transport and first-order decay of a solute plume in a three-dimensional heterogeneous aquifer. They found that the characteristic timescale of the transient development of all field-scale coefficients is reduced by the presence of a heterogeneous decay rate, and that all these trends are

accentuated with increasing decay rate variability. Increase peak concentrations, earlier arrival times, and decreased plume spreading are practical consequences of these derived results.

3.7 Summary

The selected models, identified in Section 2.1, are all deterministic and thus are incapable of stochastic simulation, except for Monte Carlo simulations for certain parameter or boundary condition distributions. In addition, four of the models (i.e., CHAIN, MULTIMED-DP 1.0, FECTUZ, and HYDRUS) are one-dimensional and only CHAIN 2D is two-dimensional. Thus, three-dimensional features cannot be easily simulated by these models, except for features such as those presented in Figure 3-1. Many two-dimensional features cannot be easily simulated, as well, even with the use of CHAIN 2D. Density gradient problems cannot be addressed by these models, as well as facilitated transport and preferential pathways. The scale dependency of hydraulic conductivity and dispersivity due to soil heterogeneities are not considered by these models. Other processes and features that are not addressed by these models are nonlinear reactions, nonlinear nonequilibrium sorption, nonequilibrium site heterogeneity, and variable decay processes. To address precipitation/evapotranspiration/infiltration processes on a storm event basis for the several-year periods required for some radionuclides will require extensive computational resources for the models in this group which are capable of performing such simulations. Table 2-1 summarizes the five models' capabilities and limitations with respect to the other features discussed in this section on conceptual model selection.

Section 4
Parameter Sensitivity Analysis: Basic Elements

The *process parameter sensitivity* analysis of a model is a measure of the change in a selected model output resulting from a specified change in an input parameter. Mathematically, the sensitivity coefficient, S_{ij}, of a model's output, y_i, to a model's input parameter, x_j, is given by

$$S_{ij} = \frac{\partial y_i}{\partial x_j} .$$

(4-1)

For a model with n output quantities and m input parameters, the total number of sensitivity coefficients that may be required in the analysis is given by the product, mn.

In the current analyses, the unsaturated zone model evaluation for the transport and fate of radionuclides, the model input parameters include such quantities as the hydraulic conductivity, K, the maximum depth of plant roots, L_m , the pore-size distribution index, n, the net infiltration rate, q, the first order rate constant, μ, and the dispersion coefficient, D. The model outputs of interest include such quantities as the peak concentration, C_{peak}, of a given radionuclide, the time, T_{peak}, at which peak concentrations reach the water table, and the time, T_{MCL}, at which a given radionuclide concentration will exceed a given quantity at a specified point. In this study the specified point is the water table, which is the point where the radionuclide in question is leached into the ground water. The given quantity is the product of the maximum critical level (MCL) of the contaminant in the ground water times a dilution attentuation factor (DAF) where DAF > 1. The DAF is used for back-calculation of the soil screening levels (SSLs). When the specified radionuclide's concentration exceeds the value (MCL)(DAF) at the water table, the contaminant at the downgradient receptor is considered to pose a risk to human health and environment.

The units of S_{ij} are those of y_i divided by those of x_j. Since S_{ij}, in general, is unit dependent, it may be difficult and confusing to compare sensitivities for different input parameters. These problems are overcome by introducing a normalized form of S_{ij}, called the **relative sensitivity coefficient**, defined by:

$$S_{rij} = \frac{x_j}{y_i} \frac{\partial y_i}{\partial x_j} .$$

(4-2)

By definition, S_{rij} is dimensionless and can be considered an absolute sensitivity coefficient in the sense that it reduces the difficulties and confusion inherent in the use of just S_{ij} for sensitivity analyses.

Suppose we have a simple model given by the following arbitrary equation:

$$y = F(p),$$

(4-3)

where p is the input parameter and y is the output of the model.

The sensitivity coefficient for this model is given by the ordinary derivative:

$$F_p = \frac{dy}{dp} \equiv \frac{dF}{dp} .$$

(4-4)

29

The relative sensitivity coefficient F_{rp} is defined by:

$$F_{rp} = \frac{p}{F(p)} \bullet \frac{dF}{dp} \;.$$

(4-5)

Suppose that the graph of F_{rp} versus p (Equation 4-5) is given by Figure 4-1. To aid in the interpretation of this figure, rewrite Equation (4-5) as

$$\frac{dF}{F(p)} = F_{rp}(p)\; \frac{dp}{p} \;.$$

(4-6)

Equation (4-6) states that a small percentage change in the input, 100 dp/p, in the neighborhood of p, produces a percentage change in the output, 100 dF/F(p), in the neighborhood of p equal to 100 dp/p times $F_{rp}(p)$. Thus, looking at Figure 4-1, one concludes the following:

1. A 10% increase in the input parameter p in the neighborhood of p_1 , based on the value of p_1 , produces a (10a)% decrease in the value of y_1, or the quantity $F(p_1)$.

2. A 10% increase in the input parameter p in the neighborhood of p_2, based on the value of p_2, produces a (10b)% increase in $F(p_2)$.

3. A 10% increase in the input parameter p in the neighborhood of p_3, based on the value of p_3, produces a (10c)% increase in $F(p_3)$.

4.1. Computing Sensitivity Coefficients

Often models are too complicated for one to obtain sensitivity coefficients by the direct analytical approach indicated in Equations (4-1) and (4-2). When this occurs, the sensitivity coefficients can be approximated by the following difference equations:

$$S_{ij} \cong \frac{\Delta y_i}{\Delta x_j} \;,$$

(4-7)

and
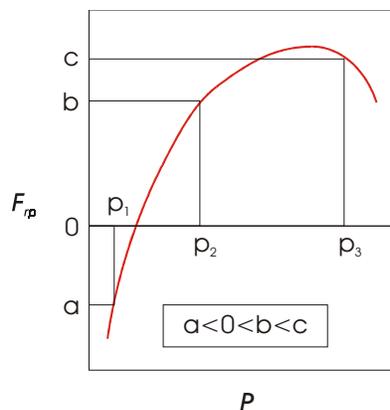
Figure 4-1.   The graph of the relative sensitivity F_{rp} in terms of the parameter p for a model defined by y = F(p).

30

$$S_{rij} \cong \frac{\Delta y_i x_j}{\Delta x_j y_i} = \frac{\Delta y_i}{y_i} \div \frac{\Delta x_j}{x_j} \, , \tag{4-8}$$

where Δy_i is the change in y_i due to a small change Δx_j in x_j. The above interpretation of the graph of F_{rp} versus p in Figure 4-1 follows directly from the last term in Equation (4-8); namely, the relative sensitivity can be expressed as the ratio of the relative change of the output parameter $\Delta y_i / y_i$ to the relative change of the input parameter $\Delta x_j / x_j$. For example, if the relative sensitivities are -1.0 for the time to reach peak concentration to recharge rate and +0.05 for the time to reach peak concentration to distribution coefficient, then it can be said that the time to reach peak concentration is much more sensitive to recharge rate than to the distribution coefficient.

4.2. An Application of Equations (4-1) and (4-2) to a Simple Model

Because of the complexity of many models, the meaning of the variations in the sensitivity S and the relative sensitivity S_r for a given output versus a given input parameter is often obscure. Thus, the choice of a simple model with a variety of nonsimilar components will aid the investigator in understanding variations in S and S_r. The simple model that we chose to present is one with a single output y and six input parameters (a,b,c,d,e,f). The defining equation for this model is arbitrarily chosen for pedagogical reasons and is not representative of any physical phenomenon. It is given by:

$$y = F(a,b,c,d,e,f) = \frac{a}{e}\left[b + cd + e\ell n(c^2 f)\right] \, . \tag{4-9}$$

For parameter a, the sensitivity of y with respect to a is denoted by F_a and the relative sensitivity is denoted by F_{ra}. This notation is used for the other 5 input parameters, as well. Table 4-1 lists the formulas for S and S_r corresponding to the expression in Equation (4-9).

For a numerical example corresponding to the arbitrary formulas in Table 4-1, we require a base case and a domain of definition for each of the input parameters. These numerical quantities are chosen as follows:

$$\text{Base Case} = F(a,b,c,d,e,f) = F(2,1,-1,3,4,5) \, , \tag{4-10}$$

$$-1 \le a \le 5, \quad 0 \le b \le 2, \quad -4 \le c \le 2, \tag{4-11}$$

$$1 \le d \le 5, \quad 1 \le e \le 7, \quad 2 \le f \le 8 \, . \tag{4-12}$$

The functional value, F, and the sensitivity and relative sensitivity of y with respect to a given input parameter are determined by letting the given input parameter be arbitrary and all other input parameters take on the values of the base case. Thus, if the given input parameter is c, the functional value and the sensitivities are

$$F(2,1,c,3,4,5), \quad F_c(2,1,c,3,4,5), \quad F_{rc}(2,1,c,3,4,5), \tag{4-13}$$

similarly for the other five parameters. Table 4-2 lists the forms of F, F_α and $F_{r\alpha}$, where α represents the parameters a,b,c,d,e,f. The characteristics of the relationship between the output y and the input α dictate the forms of the sensitivities F_α and $F_{r\alpha}$ over the domain of the input α. Figures 4-2 to 4-4 show the variations of F, F_α and $F_{r\alpha}$ over the domain of the input α.

From Figure 4-2, we note that F(a,1,-1,3,4,5) is homogeneous in *a* and linearly varies with *a*, thus both F_a and F_{ra} are constants over the domain of *a*. In fact, F_{ra} must be equal to unity. Also from this figure, we see that F(2,b,-1,3,4,5) is linear in b, not homogeneous, and possesses a positive slope. Linearity guarantees that F_b is a constant over the domain of b, but F_{rb} is a strictly monotonically increasing function of b which would approach a horizontal asymptote ($F_{rb}=1$) if the domain of b was great enough. In Figure 4-3, we note the F(2,1,-1,d,4,5) is linear in d, not homogeneous, and possesses a negative slope. The linearity guarantees that F_d is a constant, actually negative, while F_b was positive. Further, F_{rd} is now a strictly monotonically decreasing function of d and approaches a vertical asymptote at

$$d = 1 + \ell n(625) \approx 7.438 \, , \tag{4-14}$$

Table 4-1. Sensitivities and Relative Sensitivities of Output F with Respect to the Six Input Parameters, for Arbitrary Values of the Inputs.

Parameter	Sensitivity, S	Relative Sensitivity, S_r
a	$\dfrac{1}{e}\left[b + cd + e\ell n\left(c^2f\right)\right]$	1
b	$\dfrac{a}{e}$	$\dfrac{b}{b + cd + e\ell n(c^2f)}$
c	$\dfrac{a}{e}\left[d + \dfrac{2e}{c}\right]$	$\dfrac{dc + 2e}{dc + b + e\ell n(c^2f)}$
d	$\dfrac{ac}{e}$	$\dfrac{cd}{cd + b + e\ell n(c^2f)}$
e	$-\dfrac{a}{e^2}\left[b + cd\right]$	$-\dfrac{b + cd}{e\ell n(c^2f) + b + cd}$
f	$\dfrac{a}{f}$	$\dfrac{e}{e\ell n(c^2f) + b + cd}$

which is outside the domain of d. From these three input parameters (a,b,d), we can see the effects of linearity, homogeneity and sign of the slope, as well as the domains of definition of the input parameters. Also in Figure 4-3 is the plot of F(2,1,c,3,4,5) versus c. Because of the particular domain of c and the presence of $\ell n(c^4)$ in F, there is a vertical asymptote at c = 0 in the graph of F versus c. In addition the linear-logarithmic variation of c in F results in two zeros, one at α and one at β. The vertical asymptote shows up as a vertical asymptote in F_c but a zero in F_{rc}. The zeros (α, β) in F have no particular effect on F_c but become vertical asymptotes in F_{rc}. The γ zero in F_c carries over into a zero of F_{rc}. These zero/asymptotic relationships will exist between F, F_α, and $F_{r\alpha}$ as long as we do not run into indeterminant forms, 0/0 or ∞/∞. For these cases, the asymptote and zeros in F_α, and $F_{r\alpha}$ may disappear. Finally, in Figure 4-4, we note that for the domain of definition in F(2,1,-1,3,e,5) there is a zero at α which produces a vertical asymptote in F_{re}. The quantity F(2,1,-1,3,4,f) has no zeros because of the restricted domain of definition for f. One can also note the different characteristics in F_{re} and F_{rf} at the right side of the domains of definition of e and f, respectively. This is because the quantity F(2,1,-1,3,e,5) approaches a horizontal asymptote (F$\approx$3.219) for sufficiently large e, while F(2,1,-1,3,4,f) approaches $+\infty$ in a logarithmic manner as f becomes large. Thus, by studying these simple forms, one can better interpret the sensitivity and relative sensitivity results for the five models being analyzed in this report.

Table 4-2. Sensitivity and Relative Sensitivity of Output F to Individual Input Parameters with Reference to the Base Case Given in Equation (4-10).

Parameter	Output F		Sensitivity S	Relative Sensitivity S_r
	Formula	Characterization		
a	$\left[\ln(5) - \dfrac{1}{2}\right] a$	Linear and Homogeneous in a.	$\ln(5) - \dfrac{1}{2}$	1
b	$\dfrac{b}{2} - \dfrac{3}{2} + \ln(25)$	Linear and Non-homogeneous in b.	$\dfrac{1}{2}$	$\dfrac{b}{b - 3 + \ln(625)}$
c	$\ln(c^4) + \dfrac{3c}{2} + \ln(25) + \dfrac{1}{2}$	Linear-Logarithmic and Nonhomogeneous in c.	$\dfrac{4}{c} + \dfrac{3}{2}$	$\dfrac{c + \dfrac{8}{3}}{c + \ln(c^{8/3}) + \dfrac{1}{3} + \dfrac{4}{3}\ln(5)}$
d	$-\dfrac{d}{2} + \dfrac{1}{2} + \ln(25)$	Linear and Nonhomogeneous in d.	$-\dfrac{1}{2}$	$\dfrac{d}{d - 1 - \ln(625)}$
e	$-\dfrac{4}{e} + \ln(25)$	Nonhomogeneous in e, Inverse Variation with e.	$\dfrac{4}{e^2}$	$\dfrac{2}{\ln(5)\, e - 2}$
f	$2\,\ln(f) - 1$	Logarithmic and Nonhomogenous in f.	$\dfrac{2}{f}$	$\dfrac{1}{\ln(f) - \dfrac{1}{2}}$
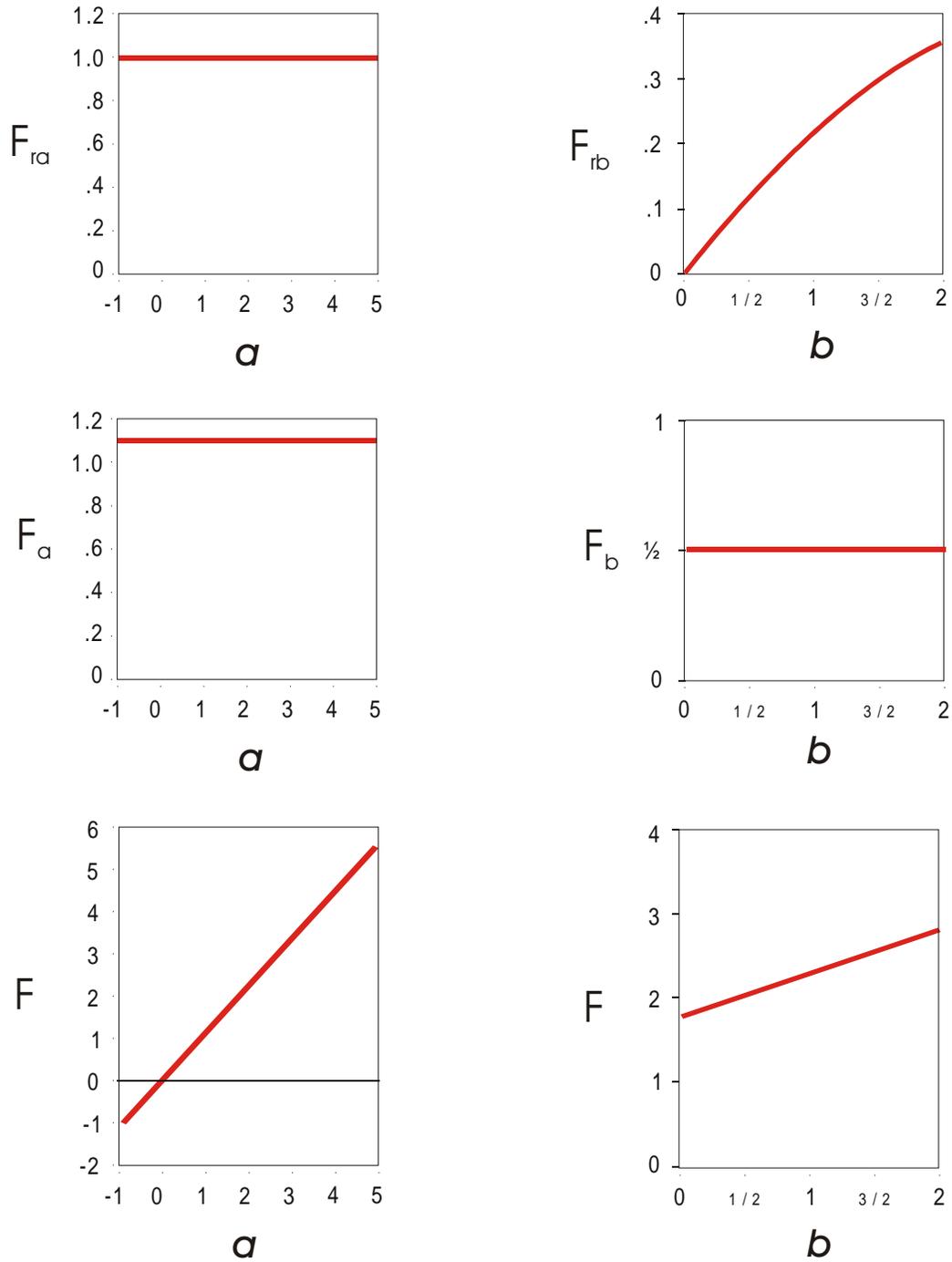
Figure 4-2. Sensitivities and relative sensitivities of F with respect to a and b, with reference to the base case in Equation (4-10).
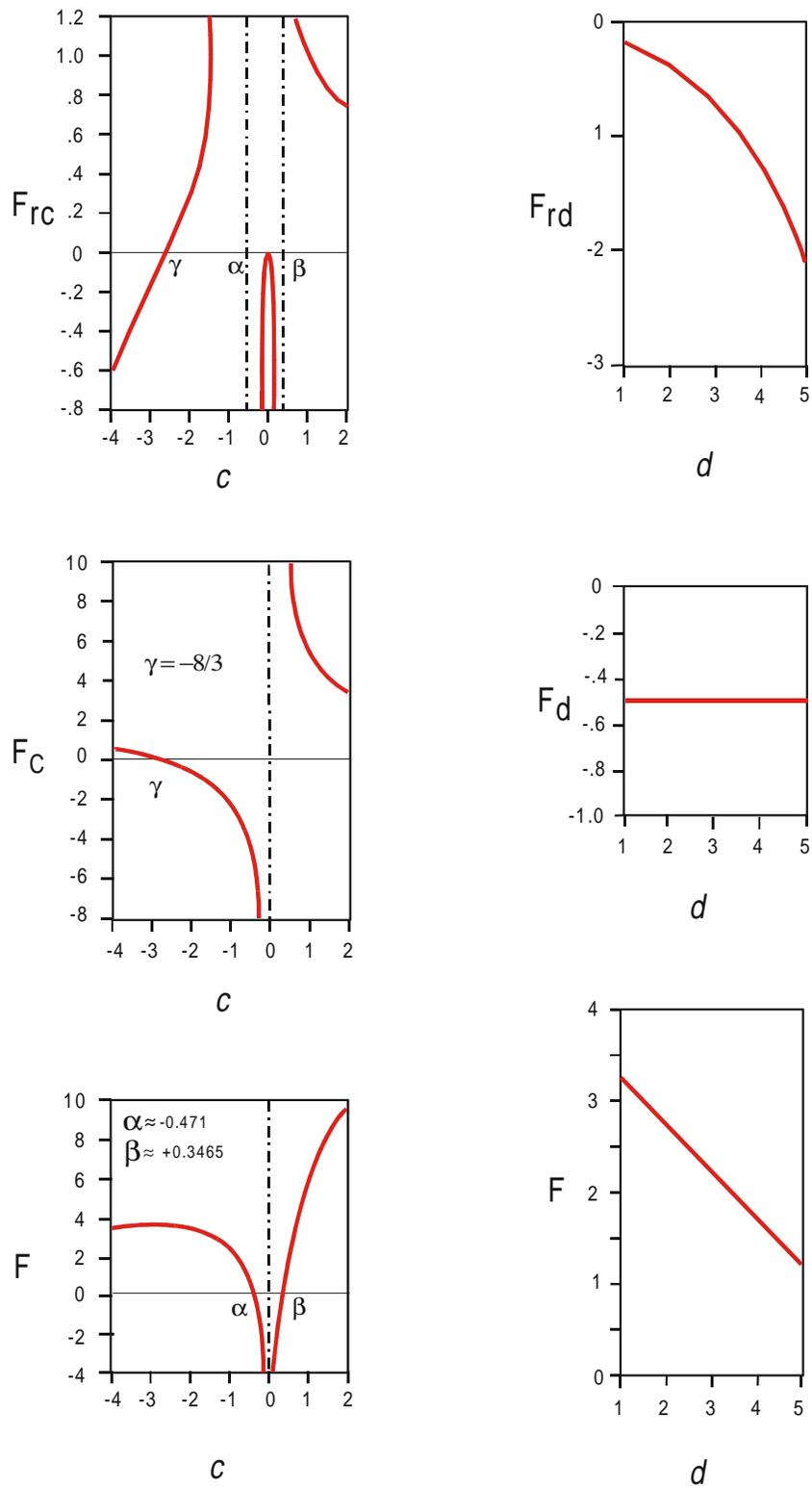
Figure 4-3. Sensitivities and relative sensitivities of F with respect to c and d, with reference to the base case in Equation (4-10).

35
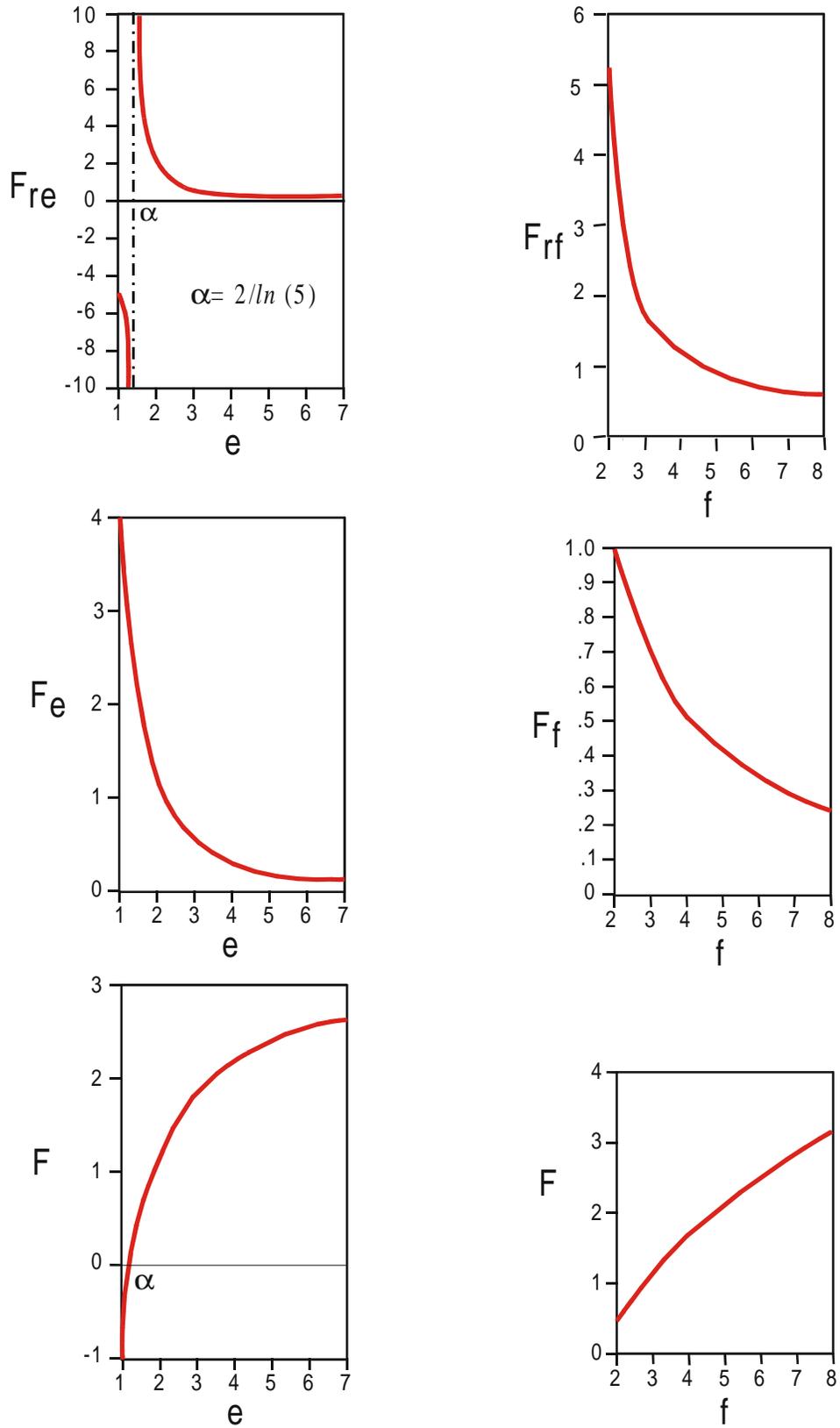
Figure 4-4. Sensitivities and relative sensitivities of F with respect to e and f, with reference to the base case in Equation (4-10).

Section 5
Parameter Sensitivity Analysis: Hypothetical Modeling Scenario

The characteristics of a representative physical site are required to realistically study the sensitivity of the five models proposed in this report for simulating the transport and fate of radionuclides in the unsaturated zone. Such a site would be used to set the standards for base parameter choices in the sensitivity tests and for parameter range determination. The ideal candidate site should have well characterized soil properties, and should have sufficient chemical transport and fate data and climatological information for running the pertinent simulations. Once a site is chosen, a conceptual model of that site is required so that the site data, the five proposed modeling codes, and the intended application of the models are all consistent with one another. In what follows, we consider the site selection process, selection of the candidate site, characteristics of the Las Cruces Trench Site in New Mexico, development of a conceptual model, and the base parameter selection.

5.1 Site Selection Process

The sensitivity studies reported in this document are part of an overall evaluation of the general applicability of each model (i.e., HYDRUS, CHAIN 2D, FECTUZ, MULTIMED-DP 1.0, and CHAIN) for simulating the fate and transport of radionuclides. The radionuclides of interest are the following five elements/isotopes (U.S. EPA, 2000b):

Element/Isotope	K_d _Default Values in ml/g_
Plutonium (^{238}Pu)	5
Strontium (^{90}Sr)	1
Technetium (^{99}Tc)	0.007
Tritium (^{3}H)	0
Uranium (^{238}U)	0.4 ,

where K_d is the soil/water partition coefficient for the linear Freundlich isotherm. These five elements/isotopes are taken to be the parent species in the decay chains and the major segments of the chains are shown in Figure 5-1 along with the corresponding half-lives of the species.

The quantity, K_d, in all five models being studied, is a lumped parameter representing known and unknown phenomena. It tends to lose some of its meaning in the modeling world, while retaining its full meaning in the laboratory. In the laboratory K_d is determined under carefully controlled conditions, but the real world cannot be completely controlled or measured. Thus, the conditions surrounding the sorption phenomenon must be estimated, and these estimates will only represent localized conditions in the vicinity of the sampling. Consequently, the large heterogeneities of most, if not all, subsurface systems make it difficult to identify a single K_d value for the system. Further, unless the model has a geochemical component, K_d will also represent everything one does not know about the site's geochemistry. The relationships between K_d values, the chemical species, and a site's geochemistry are discussed in U.S. EPA (1999ab, 2000b). However, in the current report, the default K_d values, given above, are taken as the base values for the sensitivity analyses combined with an interval domain about these values, to partially represent the heterogeneity found in the vadose zone.

Based on the above radionuclides, the site selection process consisted of identifying three features: site listing, data availability, and existing field and modeling studies. By reviewing existing literature and databases, a ***list of candidate sites*** was developed, see Table 5-1. These candidate sites, in general, were either contaminated with radionuclides, or were current or future radioactive waste disposal sites. For example, Superfund sites with soil contaminated by one or more of the above five radionuclides were identified in the U.S. EPA's ***VISITT*** database (i.e., the Vendor Information System for Innovative Treatment Technologies, Version 6.0). Many of these radionuclide
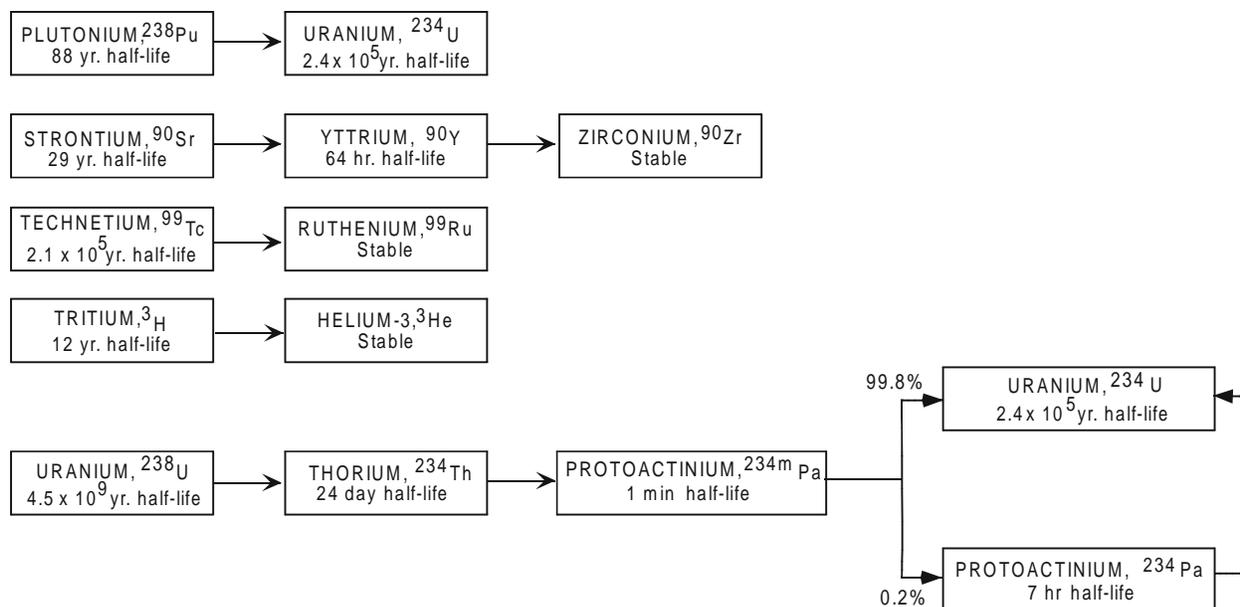
Figure 5-1.   The major segments of the decay chains for the five elements/isotopes considered to be parents in these analyses (U.S. EPA, 2000b).

contaminated sites were a result of past nuclear production and related activities, and are currently under the environmental restoration program operated by the U.S. Department of Energy. With reference to low-level radioactive waste storage sites, the most attractive areas were those having low annual precipitation, high evapotranspiration, and thick unsaturated soils/sediments. An example of such a site is the Mojave Desert Waste-Burial Site near Beatty, NV. In addition, the Nevada Test Site is a radionuclide contaminated site from nuclear testing as well as an on-site/off-site low-level waste disposal facility. The only non-nuclear contaminated site and non-nuclear storage site considered in this evaluation was the Las Cruces Trench Research Site in New Mexico. The field studies at this site have been used to provide data to test deterministic and stochastic models for water flow and solute transport, Wierenga, et al. (1991), Hills, et al. (1991, 1994), and Rockhold, et al. (1996). The Las Cruces Trench Site was included in the list of candidate sites because it fit the above physical characteristics for waste disposal facilities and because many detailed site characterization studies and field experiments have been conducted at this location.

The *availability of soil data and climatological records* are essential for the proper simulation of water flow and radionuclide transport in unsaturated soils. From the twenty-some sites in the original candidate list, four sites that had the most available data were selected for further evaluation. These were the Las Cruces Trench Site, the Beatty Waste Storage Site, Idaho Falls National Laboratory and the Hanford Washington Site. In addition, the Perdido Alabama Site was placed on the list; this was the site that was analyzed in the earlier sensitivity study of Nofziger, et al. (1994). Actually, the Perdido Site, which is a benzene contaminated site in an area of high annual precipitation, was assigned soil properties obtained from another site having the same soil series. Thus, no site-specific soil properties were available for the Perdido site. This led to the elimination of the Perdido site from further consideration. The existing *field/modeling studies* for the four remaining sites were reviewed and summarized. The studies considered were water balance, recharge and infiltration experiments; tracer and radionuclide migration studies; laboratory and field measurements of bulk density, K_s, and soil water retention curve data; and model construction, testing, and simulation runs.

5.2 Selection of the Candidate Site

For the final four sites (Las Cruces, Beatty, Idaho Falls, Hanford), additional factors and options were considered in the choice of the best candidate site. Two of the important factors were the availability of required soil data for the five pre-selected transport models in this study and the attainability of transport parameters from the

Table 5-1. Partial List of Radionuclide Contaminated and Disposal Sites in the U.S. (U.S. EPA's VISITT Database).

	SITE NAME	Location, City	State	Contaminants	Site Characteristics
1	Rocky Flats Environ-mental Technology Site	Golden	Colorado	Plutonium, Uranium	Superfund Site. On-site waste disposal
2	Idaho National Engineering & Environmental Laboratory	Idaho Falls	Idaho	Radioactive Materials, Plutonium, Tritium	Radionuclide Contaminated Site: Radioactive Waste Management Complex was used for disposal site for low-level and transuranic radioactive waste
3	Ethyl Corporation	Baton Rouge	Louisiana	Uranium	Superfund Site
4	DOE FUSRAP St. Louis Site Treatability Study	St. Louis	Missouri	Uranium	Superfund Site
5	Nevada Test Site	Mercury	Nevada	Plutonium, Tritium	Hazardous Waste Site: Radio-nuclide contaminated site from nuclear testing: Low-level waste disposal facility for both onsite and off-site generated defense low-level waste
6	Mojave Desert Waste Burial Site	Beatty	Nevada	Various Radionuclides	Low-level radioactive waste and hazardous chemical waste disposal
7	NL Industries, Inc.	Pedricktown	New Jersey	Strontium	Superfund Site
8	Los Alamos Natl. Laboratory	Los Alamos	New Mexico	Plutonium, Uranium	Superfund Site
9	Las Cruces Trench Site	Las Cruces	New Mexico	None	Experimental Site
10	Sandia Natl. Lab.	Albuquerque	New Mexico	Uranium, Plutonium	Superfund Site
11	West Valley Nuclear	West Valley	New York	Strontium	Superfund Site
12	Mound Demonstration Project	Miamisburg	Ohio	Plutonium	Superfund Site
13	Portsmouth Gaseous Diffusion Plant (DOE)	Piketon	Ohio	Uranium, Technetium	Superfund Site
14	EPA SITE Demonstration	Alliance	Ohio	Uranium	Superfund Site
15	Fernald Feed Materials Production Center	Fernald	Ohio	Uranium, Technetium	Superfund Site
16	Apollo Fuel Conversion Plant	Apollo	Pennsylvania	Uranium	Superfund Site
17	Savannah River Site	Aiken	South Carolina	Uranium	Superfund Site
18	INEL Pit 9 Pilot Project	Clemson	South Carolina	Uranium	Superfund Site
19	K-25 Site	Oak Ridge	Tennessee	Technetium, Uranium	Superfund Site
20	Hanford Site	Richland	Washington	Uranium, Strontium	Superfund Site. On-site waste disposal.
21	DOE Morgantown Energy Tech. Center	Morgantown	West Virginia	Various Radionuclides	Superfund Site

existing site modeling studies. Selection of the final candidate site was also dependent upon decision-making options. For example, when verification of modeling results is an important issue (i.e., comparison of modeling results with field and laboratory experimental data) in addition to data availability, the Las Cruces Trench Site was the best candidate. However, when reliable model input data is the only issue and model verification is less important (i.e., comparison among the SSG screening models is more important than model field verification or comparison of the screening models with more comprehensive modeling of the area), then the Beatty Waste-Burial Site is a good alternative candidate.

Four of the five proposed SSG models, HYDRUS, CHAIN 2D, MULTIMED-DP 1.0, and FECTUZ, require van Genuchten soil-water retention parameters (Table 2-1) These parameters plus dispersivities were available at the Las Cruces Site. For the Beatty Site, the van Genuchten parameters were not available and would have to be derived from the raw soil-water content/pressure head data (Andraski, 1996). Furthermore, a great amount of model testing at the Las Cruces Site has been conducted for the transport and fate of tritium, bromide and chromium in the unsaturated zone. Considering the location and climatological features of the site, and the abundance of existing field data in conjunction with significant modeling studies, the Las Cruces Trench Site was chosen as the candidate site for the model evaluation in the SSG for radionuclides.

5.3 Characteristics of the Las Cruces Trench Site in New Mexico

In the soil screening level (SSL) process, generic SSLs for radionuclides can be calculated based on a number of default assumptions chosen to be protective of human health for most site conditions. However, these are expected to be more conservative than calculated site-specific SSLs. When site-specific SSLs are of interest, a simulation using an appropriate model and site-specific data is required. Thus, in the current study, a typical physical site is required for the evaluation of the HYDRUS, CHAIN 2D, FECTUZ, MULTIMED-DP 1.0, and CHAIN Codes in the SSL process.

The Las Cruces Trench Research Site in New Mexico was chosen as the typical physical site because:

1. The site characteristics met the criteria of radioactive waste disposal areas (low annual precipitation, high annual evapotranspiration, and a deep water table);

2. The site had been subjected to extensive testing of its soil physical and chemical properties and soil-moisture distribution and movement in the unsaturated zone;

3. Results of tracer tests (chloride, bromide and tritium) and metal movement (chromium) were available.

This site lies in the Chihuahuan Desert Province of southern New Mexico (Bailey, 1980). This province is mostly desert and the Rio Grande and the Pecos River and a few of their larger tributaries are the only perennial streams. The area has undulating plains with elevations near 1200 m from which somewhat isolated mountains rise 600 m to 1500 m. There are washes which are dry most of the year that fill with water following a rain. Basins that have no outlets drain into shallow playa lakes that dry up during rainless periods. Extensive dunes of silica sand cover parts of the province, and in places, there are dunes of gypsum sand, the most notable being the White Sands National Monument near Alamogordo (a town 100 km northeast of Las Cruces).

The climate of the Chihuahuan Desert is distinctly arid and the spring and early summer are extremely dry. During July the summer rains usually begin, and they continue through October (Bailey, 1980). In general, these summer rains are local torrential storms. Average annual temperature in the province ranges from 10◦C to 18◦C. Summers are hot and long, and winters are short but may include brief periods when temperatures fall below freezing. The characteristic vegetation of the Chihuahuan Desert is a number of thorny shrubs. These shrubs frequently grow in open stands, but sometimes form low closed thickets. Short grass often grows in association with the shrubs. On deep soils, mesquite is usually the dominant plant; creosote bush covers great areas in its characteristic open stand and is especially common on gravel fans. Royo (2000) says the creosote bush is a desert plant "par excellence," a true xerophyte. It is a drought-tolerant shrub with small dark green leaves and has an extensive double root system – both radial and deep – to accumulate water from both surface and ground water. These plants can tolerate up to two years without precipitation. The leaves are coated with a varnish-like resin which reduces water loss by evaporation. The original creosote bush can live to about 100 years old, but it can produce clones of the parent as the bush ages. These clones are produced in a circular pattern of genetically-identical plants, expanding outward at the rate of about one meter every 500 years. The "King Clone" family on BLM land near Victorville, California, is estimated to be 11,700 years old.

The actual experimental site is located on the New Mexico State University college ranch some 20 or more kilometers due north of the city of Las Cruces, New Mexico. The site is on a basin slope of Mount Summerford at the north end of the Dona Ana Mountains (Wierenga, et al., 1991; Defense Mapping Agency, 1987). Geologically, these mountains are a domal uplift complex composed of younger rhyolitic and the older andesitic volcanics which were intruded by monzonite. The covered trench that provides horizontal access to the experimental plots and is used to provide soil samples for these plots is an evacuated earthen box with dimensions 26.4 m long, 4.8 m wide, and 6.0 m deep.

The published soil hydraulic properties for this site, given by Wierenga, et al. (1991), are listed in Table 5-2. Some pertinent site characteristics obtained by Gee et al (1994) are given on Table 5-3. Table 5-2 shows that the estimates for the hydraulic parameters were obtained for a uniform soil model and for a nine-layered soil model. The layers in the layered soil model correspond to the nine soil layers identified at the site. The saturated hydraulic conductivity for each soil layer was estimated by taking the geometric mean of the 50 laboratory-measured saturated hydraulic conductivities obtained from each soil layer. Likewise, the water retention data from all 50 samples from a given layer were used to estimate α, β, θ_r, and θ_s for a single water retention curve for that layer. For the uniform soil model, the geometric mean of 450 laboratory measured saturated hydraulic conductivities (nine layers with 50 per layer) was used to estimate a uniform soil saturated hydraulic conductivity value. Likewise, the water retention data for all 450 sample locations were simultaneously used to estimate single values for each of the parameters α, β, θ_r, and θ_s in a least squares sense (Wierenga, et al., 1991).

In Porro and Wierenga (1993), the solute transport dispersivity (cm) was determined for six layers ranging over $0 < z < 500$ cm. The values varied from 2.20 cm to 7.80 cm with an arithmetic average of 4.53 cm for the combined layer of 500 cm. Minor adaptations of some of these data have been made in the conceptual model developed for the sensitivity analyses. The details are given in the following subsection. Finally, Figure 5-2 shows the daily precipitation and potential evapotranspiration (PET) at the Las Cruces Site. The PET is calculated from daily climatic data using Penman's general equation for a well-watered grass reference crop (Jensen, et al., 1990):

$$\lambda E_{t0} = \Gamma \bullet (R_n - G) + 6.43 (1 - \Gamma) W(e_0 - e) , \tag{5-1}$$

where the terms in Equation (5-1) are defined as:

λ	=	latent heat of vaporization in mega-joules per kilogram,
E_{t0}	=	evapotranspiration rate (E_t) from a well-watered grass reference crop, in kilograms per meter squared per day,
λE_{t0}	=	latent heat flux density in mega-joules per meter squared per day,
Γ	=	dimensionless parameter dependent upon surface elevation and air temperature, Table 6-1 of Jensen, et al., 1990,
R_n	=	net radiation at the surface in mega-joules per meter squared per day,
G	=	heat flux density to the ground in mega-joules per meter squared per day,
W	=	$a + b\, u_2$ = wind function in meters per second,
a,b	=	positive constants,
u_2	=	wind speed at 2m above surface in meters per second,
e_0	=	saturated vapor pressure of air at some height z in kPa,
e	=	water vapor pressure in air at height z in kPa,
PET	=	potential evapotranspiration rate in mm/d, given by $E_{t0} \div$ water density in kilograms per meter squared per millimeter.

For the eighteen year period (1983-2000) shown in Figure 5-2, the annual precipitation ranged over the values from 11.5 cm/yr to 30.8 cm/yr, with an annual average of 22.5 cm/yr. For this same period, 28% of the precipitation came in the January to June period, and 72% came in the July to December period. This is consistent with the climatological description given by Bailey (1980).

5.4. Development of a Conceptual Model

The conceptual model for SSLs using detailed site-specific data is developed in a manner which is theoretically and operationally consistent with the simplified methodology described in Section 2 of the Soil Screening Guidance

Table 5-2. Soil Hydraulic Properties at the Las Cruces Trench Site for SSG Model Evaluation Study (reprinted from *Water Resources Research*, 1991, by P.J. Wierenga, R.G. Hills, and D.B. Hudson with the permission of the American Geophysical Union, Washington, DC).

Layers	Depth (cm)	Saturated Water Content (cm³/cm³)	Residual Water Content (cm³/cm³)	van Genuchten Alpha Coefficient, α, (cm⁻¹)	van Genuchten Beta Coefficient, β, (—)	Saturated Hydraulic Conductivity, K_s, (cm/d)
			Uniform Soil Model			
all	0 - 600	0.321	0.083	0.055	1.509	270.1
			Layered Soil Model			
1	0 - 15	0.348	0.095	0.042	1.903	539
2	15 - 140	0.343	0.091	0.062	1.528	250
3	140 - 205	0.336	0.085	0.060	1.574	267
4	205 - 250	0.313	0.071	0.068	1.537	300
5	250 - 305	0.302	0.072	0.040	1.550	250
6	305 - 370	0.294	0.090	0.070	1.711	334
7	370 - 460	0.310	0.073	0.027	1.418	221
8	460 - 540	0.325	0.083	0.041	1.383	172
9	540 - 600	0.306	0.078	0.047	1.432	226

Table 5-3. Characteristics of the Las Cruces Trench Site for SSG Model Evaluation Study (reprinted from *Soil Sci. Soc. Am. J.*, 1994, by G.W. Gee, P.J. Wierenca, B.J. Andraski, M.H. Young, M.J. Fayer, and M.L. Rockhold with the permission of *Soil Sci. Soc. Am. J.*, Madison, WI).

Annual Precipi-tation (cm/yr)	Annual Potential (Pan) Evapora-tion (cm/yr)	Annual Potential Recharge (cm/yr)	Average Daily Max. Air Temper-ature (°C)	Average Daily Min Air Temper-ature (°C)	Elevation (m)	Depth to Water Table (m)	Geology	Typical Soil Type	Typical Vegeta-tion
23	239	8.7	28	13	1357	60	Alluvial	Berino fine loamy sand	Creosote bush
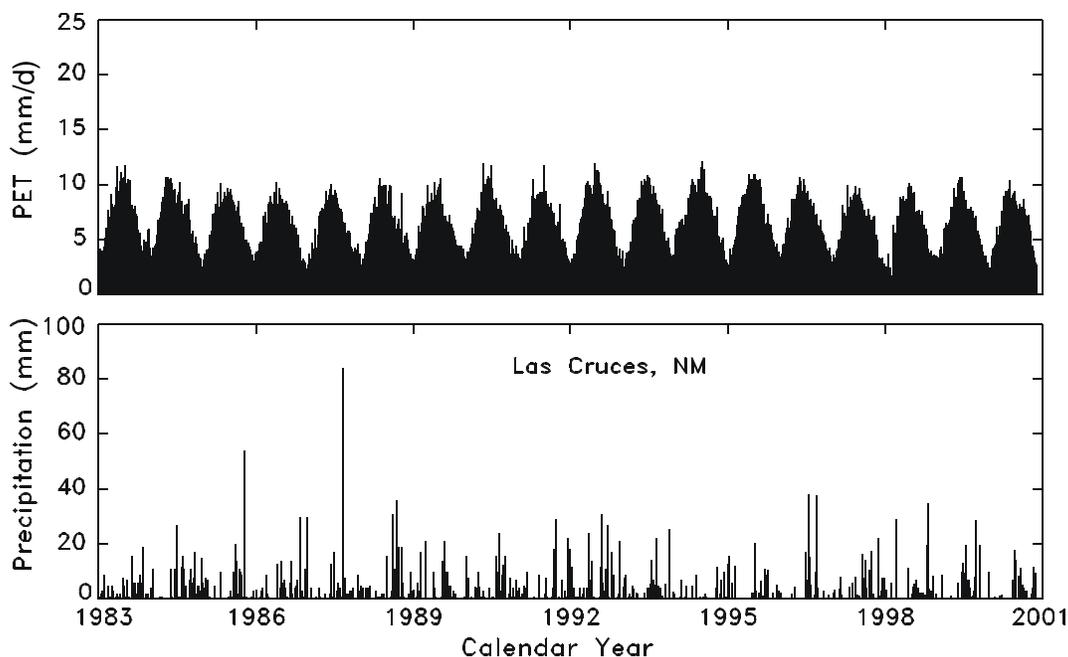
Figure 5-2.   Daily precipitation and potential evapotranspiration (PET) at Las Cruces Site, NM. PET is calculated from daily climate data using Penman's equation (Jensen et al., 1990).

for Radionuclides: Technical Background Document (U.S. EPA, 2000b). In so doing, it is assumed that the Las Cruces Trench Site in New Mexico has been used as a waste disposal/storage facility where radionuclides from tank leaks or improper waste disposal were released to the soil surface for a period of time with a specified total amount of release set for each radionuclide (e.g., 10 mg/cm^2 of ^{238}U was released). Thus, a finite radionuclide contaminated source is assumed. The driving force to send this material on a downward migration to the water table is the infiltrated rainfall which produces a net annual recharge rate of 87 mm/yr. (Table 5-3). The site-specific soil hydraulic properties given in the "all-layer" row of Table 5-2 and the mean layer dispersivity of 4.53 cm, obtained for tritium transport through Berino fine loamy sand, are also used in the current analyses.

Further assumptions are:

- The unsaturated zone is homogeneous although HYDRUS, CHAIN 2D, FECTUZ and MULTIMED-DP 1.0 are capable of simulating layered soils and the hydraulic properties for layered soils are available at the site.
- There is no significant vapor pressure for most radionuclides (except for radon, which is not considered in this study) and the dimensionless Henry's Law constant is assumed to be zero.
- Only vertical flow and transport are considered; horizontal flow and transport are ignored, even though CHAIN 2D is capable of simulating two-dimensional flow and transport.
- There is no chemical or biological degradation in the unsaturated zone.
- There is radioactive decay (Figure 5-1) in the unsaturated zone; however, since the published data on decay rates (or half-lives) for radionuclides are reasonably accurate and precise, no sensitivity analysis will be made on decay rates.
- Complexation, oxidation-reduction, dissolution and precipitation, and ion-exchange are not considered because these processes are not implemented in the five models being evaluated.
- There is no facilitated transport (e.g., colloidal transport, preferential flow in fractures or root channels, fingering pathways) of the radionuclides in the unsaturated zone.
- The aquifer lying below the unsaturated zone is unconsolidated and unconfined. However, flow and transport of the radionuclides in the saturated zone are not considered and only leachate contributions to the ground water at the center of the disposal area are of interest.
- Initial concentrations of radionuclides in the soil are zero.

In order to specify a total amount of radionuclide and a reasonable level of a radionuclide concentration release from the waste source, a literature survey of radionuclide contamination in soils was conducted. Based on the survey information, the radionuclide concentration released from the hypothesized waste source and the duration of radionuclide release were determined. Thus, the total amount of radionuclide release can be obtained from the product of the recharge rate, source concentration, and the duration time of waste release. The depth of radioactive contaminated soil at the termination point of waste release from the source can be determined from the product of the pore velocity times the duration time of waste release.

The decay series of the radionuclides in the sensitivity analyses in this report are based on the chain segments given in Figure 5-1. The chain segments for plutonium-238 and uranium-238 are not complete but are sufficient for current purposes because of the long half-life of uranium-234. Further, due to the time discretization in the five models and the relatively short half-lives of the intermediate species in the strontium-90 and uranium-238 chains, the following parent-daughter chains are only of importance in this report:

$$^{238}Pu \longrightarrow {}^{234}U \qquad\qquad {}^{90}Sr \longrightarrow {}^{90}Zr$$

$$^{99}Tc \longrightarrow {}^{99}Ru \qquad\qquad {}^{3}H \longrightarrow {}^{3}He$$

$$^{238}U \longrightarrow {}^{234}U$$
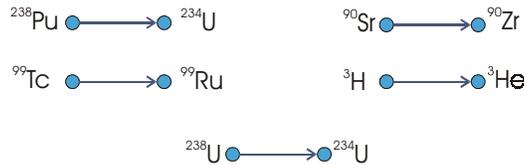
5.5 Base Parameter Selection

Table 5-4 provides the base values of selected input parameters to be used in the sensitivity analyses given in later sections. These values are those that are basically used in the analyses of HYDRUS and CHAIN 2D. Subsets of these values will be used in the analyses of FECTUZ, MULTIMED-DP 1.0 and CHAIN. Justification and rationale for the use of these specific base parameters are presented in the following paragraphs.

The area of the *disposal facility* is arbitrarily taken as 400 m^2, whose length and width are both 20 m. The one-dimensional vertical models are assumed to be located at the center of the square, thus eliminating edge effects in the unsaturated zone simulation. The *total duration* of the release of the radionuclide mass was arbitrarily chosen to be 1000 days; however, this value was reasonably consistent with the survey information mentioned in the previous subsection.

The *potential evapotranspiration (PET)* from the surface of well-watered short grass was calculated from Las Cruces climatic data using Penman's equation (Jensen, et al. 1990). The weather/climatic data required for this equation are temperature, relative humidity, wind speed, and solar radiation, along with the estimated albedo coefficient of 0.21 and the 1357 m elevation of the site. Using the daily climatic data for the years 1983 to 2000, the estimated value of PET is 204 cm/yr and the average precipitation at the site is 22.5 cm/yr. These values are consistent with those reported by Gee, et al. (1994), see Table 5-3; thus, we use the *annual potential recharge* of 8.7 cm/yr given by Gee, et al. In Table 5-2, the all-layer *residual moisture content* is given as 0.083 and the all-layer *saturated moisture content* is given as 0.321. It is expected that the "uniform" annual recharge of 8.7 cm/yr will produce a soil moisture somewhere between θ_r and θ_s. Thus, we arbitrarily chose an *initial water content*, θ, equal to the geometric mean of θ_r and θ_s, $(\theta_r\theta_s)^{1/2}$. This value to two significant figures is $\theta = 0.16$.

As stated in the previous subsection, the total mass of the individual radionuclides released from the hypothetical Las Cruces disposal/storage site was chosen to be consistent with radionuclide releases from real sites throughout the country. The relationship between the *mass released* and the *concentration of the radionuclide in the recharge water* from the waste source is given by:

$$\text{Mass (mg/cm}^2) = \text{Recharge (cm/yr)} \cdot \frac{\text{Duration (d)}}{365 \text{ (d/yr)}} \cdot \frac{1}{1000 \text{ (cm}^3\text{/L)}} \cdot \text{Concentration (mg/L)} ,$$

$$= (8.7)\left(\tfrac{1000}{365}\right)\left(\tfrac{1}{1000}\right)\text{Concentration (mg/L)} , \tag{5-2}$$

$$= 0.024 \,(\text{Concentration, mg/L}) ,$$

Table 5-4.   Base Values of Input Parameters for Unsaturated Zone Radionuclide Models (from Wierenga, et al., 1991; Gee, et al., 1994; U.S. EPA, 2000ab; and U.S. EPA VISITT Database).

Parameters	*Values*
Source-Specific Parameters	
Area of disposal facility (m^2)	400
Width of disposal facility (m)	20
Length of disposal facility (m)	20
Mass release of Radionuclide ^{238}U (mg/cm^2)	10
Concentration of ^{238}U in recharge water from waste source (mg/L)	417
Mass Release of Radionuclide ^{99}Tc (mg/cm^2)	3×10^{-4}
Concentration of ^{99}Tc in Recharge Water from Waste Source (mg/L)	1.25×10^{-2}
Mass Release of Radionuclide ^{90}Sr (mg/cm^2)	4.8×10^{-3}
Concentration of ^{90}Sr in Recharge Water from Waste Source (mg/L)	0.2
Mass Release of Radionuclide ^{238}Pu (mg/cm^2)	2.4×10^{-9}
Concentration of ^{238}Pu in Recharge Water from Waste Source (mg/L)	1.0×10^{-7}
Mass Release of Radionuclide ^3H (mg/cm^2)	2.6×10^{-9}
Concentration of ^3H in Recharge Water from Waste Source (mg/L)	1.1×10^{-7}
Duration of Waste Source Being Completely Released (days)	1000
Potential Recharge Rate (mm/yr)	87
Initial Water Content (cm^3/cm^3)	0.16
Soil Properties in Unsaturated Zone	
Saturated Hydraulic Conductivity, K_s, (cm/d)	270.1
Porosity (–)	0.358
Residual Water Content (cm^3/cm^3)	0.083
Saturated Water Content (cm^3/cm^3)	0.321
Bulk Density (g/cm^3)	1.70
van Genuchten Alpha Coefficient, α, (cm^{-1})	0.055
van Genuchten Beta Coefficient, β, (–)	1.509
Depth to Water Table (m)	6
Solute Transport Parameters	
Decay Coefficient for Parent Product ^{99}Tc (1/d)	9×10^{-9}
Decay Coefficient for Daughter Product ^{99}Ru (1/d)	Stable
Distribution Coefficient for ^{99}Tc (ml/g)	0.007
Distribution Coefficient for ^{99}Ru (ml/g)	5.0
Dispersivity (cm)	4.53
Diffusion Coefficient in Free Water (cm^2/d)	1.73
Apparent Molecular Dispersion Coefficient (cm^2/d)	0.33
Dispersion Coefficient (cm^2/d)	1.01

or

$$\text{Concentration (mg/L)} = 41.7 \text{ (Mass, } mg/cm^2). \tag{5-3}$$

Using Equation (5-3) and the mass releases of ^{238}U, ^{99}Tc, ^{90}Sr, ^{238}Pu and ^3H in Table 5-4 results in the corresponding concentrations of these species given in the table.

In order to keep the initial concentration and the total amount of the radionuclide entering the soil fixed for varying recharge rates, q, in the sensitivity analyses, the duration of the source emissions in Equation (5.2) was

allowed to vary. That is, the following product in Equation (5-2) was held fixed at its base value as the time duration of the source varied with the recharge rate, q:

$$\text{(Duration) x (Recharge Rate)} = 8700 \text{ cm-d/yr} . \tag{5-4}$$

For the range of q used in the sensitivity analyses, 5.11 cm/yr $\leq$ q $\leq$ 10.95 cm/yr, the source duration ranges over the interval 795 d $\leq$ duration $\leq$ 1703 d. However, for the species considered in this report, the differences in source time duration have a negligible effect on the output values of concern in this report. That is, since the total mass of a radionuclide and its initial concentration are held fixed, the differences produced by the total release times (i.e., the pulse width of release) have sufficient time to smooth out in the soil column before the major parts of the breakthrough curves (BTCs) are seen at the bottom, the 6 m depth, of the soil columns.

Table 5-3 lists the depth to water table at the Las Cruces Test Site as 60 m. However, the detailed soil moisture data are given only for the first 6 m, as listed in Table 5-2. Thus, for the hypothetical modeling scenario of this report, we chose the 6 m depth to be the top of the water table in our sensitivity analyses. It is felt that this assumption will meet the project's objectives. As stated in the previous subsection, this 6 m layer is taken to be homogeneous with the **soil properties** listed in the all-layer row of Table 5-2, namely: $\theta_s = 0.321$, $\theta_r = 0.083$, VG-α = 0.055 cm^{-1}, VG-β = 1.509, and K_s = 270.1 cm/d.

Wierenga, et al. (1991) found that the **bulk densities** of the nine soil layers in Table 5-2 range in values from 1.66 to 1.74 g/cm^3, thus giving a geometric mean of the end points of 1.70 g/cm^3. In Table 5-3, Gee et al. (1994) stated that the typical soil type at the Las Cruces Trench Site is a Berino fine loamy sand. With these two pieces of information and two "rules of thumb" used by Eagleson (1970), we can roughly determine the **porosity** (n) and the **effective porosity** (n_e) at the site. The following "rules of thumb" were used by Eagleson to analyze the properties of a Touchet silt loam ($\rho_s = 2.60$ g/cm^3), a Columbia sandy loam ($\rho_s = 2.67$ g/cm^3), and an unconsolidated sand ($\rho_s = 2.71$ g/cm^3), where ρ_s is the density of the solid matrix and ρ is the bulk density:

$$n = 1 - \rho/\rho_s , \tag{5-5}$$

$$n_e = n - \theta_r . \tag{5-6}$$

Thus, using a density, ρ_s, of 2.65 g/cm^3 for Berino fine loamy sand and a bulk density of 1.70 g/cm^3 gives a porosity of 0.358 and an effective porosity of 0.275 for the all-layer soil column in Table 5-2.

The radionuclide used in the sensitivity analyses reported in Section 6 and 7 is technetium (^{99}Tc). This species possesses a rather long half-life and is highly mobile in the soil column, as seen by its default value for K_d (0.007 ml/g, as given in U.S. EPA 2000b). The decay coefficient for ^{99}Tc in Table 5-4 is derived from the radionuclide half-life given in Figure 5-1 The daughter product of ^{99}Tc (i.e., ruthenium, ^{99}Ru) is stable, and its decay coefficient is zero. The default values of K_d for ^{99}Ru is 5 ml/g, which indicates that this radionuclide is not very mobile in the soil column. Because of ^{99}Tc's high mobility and long half-life, it possesses many of the characteristics of a conservative species as it moves through the soil column. Conversely, a species such as plutonium (^{238}Pu), with a shorter half-life and a low mobility, may decay before reaching a receptor if the soil column is sufficiently long and facilitated transport does not exist.

The **dispersion coefficient, D,** in the unsaturated zone is given by Hills, et al. (1991) as (also see Equations 2-22 and 2-23):

$$D = \tau_w D_w + D_L \left| q \right| / \theta , \tag{5-7}$$

where θ is taken as the initial water content of 0.16 and $\left| q \right|$ is the infiltration rate of 8.7 cm/yr. Taking the dispersivity of 4.53 cm given for tritium transport at the Las Cruces Site by Porro and Wierenga (1993), and the above values of θ and $\left| q \right|$, gives a value of 0.68 cm^2/d for $D_L \left| q \right| \theta^{-1}$. The **diffusion coefficient in free water** is assumed to be 1.73 cm^2/d and the tortuosity factor τ_w is taken as 0.19 (Tomasko, et al., 1989). Thus, the value of $\tau_w D_w$ in Equation (5-7) is given as 0.33 cm^2/d. Consequently, the sum of the two terms in Equation (5-7) is given as 1.01 cm^2/d, the value of the dispersion coefficient in Table 5-4.

The HYDRUS and CHAIN 2D Codes have the capacity for accounting for water uptake by plant roots, while the other three models do not have this feature (see Table 2-1). Therefore, **root water uptake** was only considered in Appendix F to show its impact on radionuclide movement using the HYDRUS Code. As we have

previously stated, the creosote bush (Larrea tridentata) is the dominant plant at the Las Cruces Site. Gile, et al. (1998) indicated that the root depth system of this plant varies with the soil environment and the slope of the terrain; the depth of roots can extend 5 m, or so. Jenkins, et al. (1988) reported that the creosote bush roots at the Las Cruces Site have a vertical distribution over a range of 0.5 m to 3 m. Thus, for demonstration purposes, a ***root distribution*** of 0.5 m to 2.5 m was used in the current study (see Appendix F).

Section 6
Parameter Sensitivity Analysis: Implementation and Results

The basic elements of the parameter sensitivity analysis for the five models considered in this report are illustrated in Section 4 through the use of a simple model, $y = F(a,b,c,d,e,f)$. In the current section, these procedures will be implemented for the HYDRUS Code as applied to the hypothetical modeling scenario described in Section 5. In what follows, we consider the general procedures for parameter sensitivity analysis as applied to the five models under investigation, the input parameters for constant recharge rate and constant water content, the input parameters for constant recharge rate and variable water content, the output variables of interest to SSL application, and the sensitivity analysis results for the HYDRUS Code.

6.1 General Procedures for Parameter Sensitivity Analysis

The procedures for conducting the parameter sensitivity analysis reported in this section and in Section 7 are analogous to those given in Section 4.2 (Equations 4-9 to 4-13) for the simple model, $y = F(a,b,c,d,e,f)$. For the current case, the input/output relationships are represented by expressions of the following form:

$$Q_{ij} = F_{ij}(P_{b1}, P_{b2},...,P_p, ..., P_{bn}),\tag{6-1}$$

where Q_{ij} represents the jth output for the ith model, P_{bk} is the base value of the kth parameter, P_p is the variable p^{th} parameter, and $F_{ij}(\cdot,\cdot,...,\cdot)$ is the functional relationship between the n-1 base parameters and the one variable parameter determined by the ith model for the jth output. This functional relationship represents empirical physical laws (e.g., Darcy's Law), conservation laws (e.g., the continuity equations) and constitutive equations (e.g., van Genuchten soil parameter model).

The specific procedures for conducting a parameter sensitivity analysis for the current SSL application are as follows:

1. Select a radionuclide from the list: ^{3}H, ^{99}Tc, ^{238}U, ^{90}Sr, ^{238}Pu;
2. Select a model for analysis from the list: CHAIN (i = 1), MULTIMED-DP 1.0 (i = 2), FECTUZ (i = 3), CHAIN 2D (i = 4), HYDRUS (i = 5);
3. Choose the set of input parameters for the specific model selected in Step 2;
4. Select the model outputs of interest, j = 1,2,...,k;
5. Select a particular variable input parameter P_p and select its domain of variation,

$$A_p \leq P_p \leq B_p;\tag{6-2}$$

6. Run model simulations using the n - 1 base input parameter values and the one variable input parameter P_p, thus giving the functional relationships given in Equation (6-1);
7. Calculate the sensitivity S and the relative sensitivity S_r of the model outputs to the various input parameters following the approach described in Equations (4-1) to (4-8);
8. Repeat the procedure given in Steps 1 to 7 for each pertinent input parameter and for each model and radionuclide.

6.2 Input Parameters for Constant Recharge Rate and Constant Water Content

There is no flow module in the CHAIN Code, and the recharge rate, q, and the water content, θ, are specified, constant, input parameters for given homogeneous layers. Thus, the governing differential equation for the ***parent species*** is defined as follows:

$$\frac{\partial c}{\partial t} + \frac{q}{\theta + \rho K_d} \frac{\partial c}{\partial z} = \frac{\theta D}{\theta + \rho K_d} \frac{\partial^2 c}{\partial z^2} - \mu c ,$$

(6-3)

where ρ is the bulk density of the soil (g/cm^3), c is the concentration of the liquid phase (mg/L), K_d is the distribution coefficient (ml/g), D is the dispersion coefficient (cm^2/d), and μ is the decay rate (1/d) which is assumed fixed for a given radionuclide. That is, for a given radionuclide, the decay rate, μ, is the same for the sorbed phase and the dissolved phase, and μ is sufficiently well known that no sensitivity analysis will be run on it. As in Equation (5-7), θD can be written as:

$$\theta D = \theta \tau_w D_w + D_L |q| ,$$

(6-4)

where τ_w is a dimensionless tortuosity factor taken as 0.19, D_w is the molecular diffusion coefficient in free water (cm^2/d) and D_L is the longitudinal dispersivity of the radionuclide (cm). Using the base values given in Table 5-4, $\theta \tau_w D_w$ is about one-half of the value of $D_L |q|$. The reason that the diffusion component of D is so important is because of the low annual average recharge rate represented by $|q|$.

The denominators in the second and third terms in Equation (6-3) represent the product of the soil moisture and the retardation factor R (unitless):

$$\theta R = \theta + \rho K_d .$$

(6-5)

For the default values of K_d listed in Section 5 and the base values of θ and ρ given in Table 5-4, we get the following ratios, $\rho K_d \div \theta R$, for the five radionuclides:

Radionuclides	ρK_d	θR	$[\rho K_d \div \theta R]$ 100
Tritium (^{3}H)	0.000	0.160	0.00%
Technetium (^{99}Tc)	0.012	0.172	6.98%
Uranium (^{238}U)	0.680	0.840	80.95%
Strontium (^{90}Sr)	1.700	1.860	91.40%
Plutonium (^{238}Pu)	8.500	8.660	98.15%

These ratios show the relative importance of the distribution coefficient K_d to the product θR as K_d increases. For example, ρ and K_d are relatively unimportant in the transport and fate of technetium (^{99}Tc), but very important for that of plutonium (^{238}Pu).

Equations (6-3) to (6-5) indicate how the seven input parameters (K_d,q,θ,ρ,D,D_L,D_w) influence the transport and fate of radionuclides in the unsaturated zone when q and θ are assumed to be constant input parameters. For comparison purposes, all five models were analyzed under these constant q and θ conditions for sensitivity to variations of these seven parameters. The boundary conditions for the liquid phase concentration, c, were the source term at the top of the 6m column, as described in Section 5.5, and a zero gradient at the bottom of the column. However, the models do not all possess dispersion coefficients of the type shown in Equation (6-4). In the CHAIN Code, only a constant D is specified, while MULTIMED-DP 1.0 and FECTUZ only specify D_L. CHAIN 2D and HYDRUS specify both D_L and D_w. The sensitivity analyses conducted for these five models for the seven input parameters under the constant q and θ assumptions are summarized in Table 6-1.

6.3 Input Parameters for Constant Recharge Rate, but Variable Water Content

For a constant recharge rate, q, and a variable water content, θ, in a vertical soil column, the governing equations are *Darcy's Law,*

$$q = -K \left[\frac{\partial h}{\partial z} + 1 \right] ,$$

(6-6)

and the *equation of continuity,*

Table 6-1. The Sensitivity Analyses Performed (●) for the Five Models Under the Assumption of Constant Recharge Rate and Constant Water Content.

Model Input Parameter	Sensitivity Analyses Performed				
	CHAIN	MULTIMED-DP 1.0	FECTUZ	CHAIN 2D	HYDRUS
K_d	●	●	●	●	●
q	●	●	●	●	●
θ	●	●	●	●	●
ρ	●	●	●	●	●
D	●				
D_L		●	●	●	●
D_w				●	●

$$\frac{\partial \theta}{\partial t} + \frac{\partial q}{\partial z} = \text{-}S \ , \tag{6-7}$$

where q is in units of (cm/d), K is the unsaturated hydraulic conductivity (cm/d), h is the soil water pressure head (cm), the z-coordinate is positive upward with the origin at the bottom of the layer, and S is a sink term due to plant water uptake (cm³/cm³d). Combining Equations (6-6) and (6-7) leads to the ***modified Richards Equation***:

$$\frac{\partial \theta}{\partial t} = \frac{\partial}{\partial z} \left[K \left(\frac{\partial h}{\partial z} + 1 \right) \right] - S \ . \tag{6-8}$$

The ***van Genuchten Model*** for the parameters K(h) and θ(h) is as follows (see Appendix A):

$$K(h) = K_s K_r(h)$$
$$= K_s S_e^{1/2} \left[1 - \left(1 - S_e^{1/m} \right)^m \right]^2 , \tag{6-9}$$

$$\theta(h) = \begin{cases} \theta_r + \dfrac{\theta_s - \theta_r}{\left[1 + |\alpha h|^\beta \right]^m} , & h < 0 \\ \theta_s , & h \geq 0 , \end{cases} \tag{6-10}$$

where the effective water content S_e is given by

$$S_e = \frac{\theta - \theta_r}{\theta_s - \theta_r} , \tag{6-11}$$

and where K_s is the saturated hydraulic conductivity (cm/d), K_r is the unitless relative hydraulic conductivity, θ_s is the saturated water content, θ_r is the residual water content, α is the inverse of the air-entry value or bubbling pressure head (cm⁻¹), β is the unitless pore-size distribution index, and m is defined by

$$m = 1 - 1/\beta \ . \tag{6-12}$$

For h < 0, Equation (6-10) can be rearranged to give h as a function of the effective water content S_e:

$$h = h(S_e) = -\frac{1}{\alpha}\left[S_e^{-1/m} - 1\right]^{1/\beta} \; .$$

(6-13)

For the parameter sensitivity results in this section and Section 7, it is assumed that the sink term, S, due to plant water uptake is identically zero. Thus, from the continuity equation and from the assumption of constant recharge rate, q, the water content, θ, is found to be independent of time. When θ is independent of time, the modified Richards Equation reduces to Darcy's Law in Equation (6-6), and the water content becomes a space-varying quantity, $\theta(z)$, through Equation (6-10).

As indicated in Table 2-1, the flow modules of MULTIMED-DP 1.0 and FECTUZ are based on Darcy's Law, while those for HYDRUS and CHAIN 2D are based on Richards Equation. As stated above, the parameter sensitivity analysis for the van Genuchten parameters (K_s,θ_s,θ_r,α,ß) are based on a constant recharge rate, q, and a variable water content, $\theta(z)$. The determination of $\theta(z)$ for MULTIMED-DP 1.0 and FECTUZ follows from the solution of Darcy's Law, which is a nonhomogeneous, nonlinear, first-order ordinary differential equations in the water pressure head, h(z). To solve this system, the head has to be specified at the bottom of the soil column (z = 0) and at the top of the column (z = L). These boundary conditions for h are determined from the specifications of θ at the two boundaries, namely:

(1) $\theta = \theta_s$ at z = 0, giving h = 0 at z = 0;
(2) $\theta =$ Base value in Table 5-4 at z = L, giving a value of h at z = L derived from Equations (6-11) and (6-13).

Once h(z) is known, $\theta(z)$ can be determined from Equation (6-10). Given $\theta(z)$, the influence on the liquid phase concentration, c, is experienced through Equation (2-15), of which Equation (6-3) is a simplified version. As the five input parameters (K_s,θ_s,θ_r,α,ß) are varied, one at a time, for the sensitivity analysis, different water content profiles, $\theta(z)$, are generated leading to different responses for the breakthrough curves (BTCs) of the liquid phase concentrations.

The determination of $\theta(z)$ for HYDRUS and the one-dimensional version of CHAIN 2D is realized from the steady-state solution of the Richards Equation. Using the expressions for K and θ in Equations (6-9) and (6-10), respectively, Richards Equation is a homogenous, nonlinear, partial differential equation in h, requiring both boundary conditions and an initial condition. The boundary conditions for h are obtained in the same way as those for MULTIMED-DP 1.0 and FECTUZ. The initial condition is specified as that value of h corresponding to the base value of θ given in Table 5-4, as calculated from Equation (6-13). Thus, the water content profile, $\theta(z)$, is given as the steady-state solution of this initial, boundary value system for h(z,t), or $\theta(z,t)$, as given by equation (6-10). Again, as the van Genuchten parameters (K_s,θ_s,θ_r,α,ß) are varied, one at a time, for the sensitivity analysis, different profiles, $\theta(z)$, are generated and the resultant BTCs for c are varied. Table 6-2 summarizes the sensitivity analyses performed for the four models (CHAIN is not included) under the assumption of constant recharge rates, q, and variable water content, $\theta(z)$.

Table 6-3 lists the base values of the twelve input parameters (K_d,q,θ,ρ,D,D_L,D_w,K_s,θ_s,θ_r,α,ß), along with the range of variation for each of the twelve parameters. The ranges of variation of the twelve parameters were chosen to be reasonably consistent with the variations shown over the nine-layer soil column at the Las Cruces Trench Site given in Table 5-2, the hydrologic records shown in Figures 5-2 and F-1, and the physical properties of the Berino fine loamy sand at the site. These base values and ranges were used in the parameter sensitivity analyses for all five models being analyzed in this report.

6.4 Output Parameters Evaluated

The time evolution of the radionuclide concentration in the leachate at the bottom of the unsaturated zone (i.e., at the entry point to the ground-water zone) is of interest in the Soil Screening Level (SSL) process. The curve of concentration versus time at this entry point is called the breakthrough curve (BTC). For sensitivity analysis, three characteristics of these curves are of importance:

1.   The peak concentration of the radionuclide, C_{peak},
2.   The time to reach peak concentration, T_{peak}, and
3.   The time when the concentration of radionuclide is high enough so that the resulting concentration at a receptor well will exceed the MCL (i.e., the time to reach MCL, denoted by T_{MCL}).

51

Table 6-2. The Sensitivity Analyses Performed (●) for Four of the Five Models Under the Assumption of Constant Recharge Rate and Variable Water Content, where "Base" Represents the Base Parameter Values Given in Table 5-4, and the Water Content Profile, $\theta(z)$, Varies with the Changing van Genuchten Parameters ($K_s, \theta_s, \theta_r, \alpha, \beta$).

Model Input Parameter	Sensitivity Analyses Performed				
	CHAIN	MULTIMED-DP 1.0	FECTUZ	CHAIN 2D	HYDRUS
K_d		Base	Base	Base	Base
q		Base	Base	Base	Base
θ		$\theta(z)$	$\theta(z)$	$\theta(z)$	$\theta(z)$
ρ		Base	Base	Base	Base
D					
D_L		Base	Base	Base	Base
D_w				Base	Base
K_s		●	●	●	●
θ_s		●	●	●	●
θ_r		●	●	●	●
α		●	●	●	●
β		●	●	●	●

Table 6-3. Input Parameters for Each Model and the Range of Each Variable Parameter, Along with the Base Value of the Parameter.

p	Model[a]	Parameter, P_p Symbol	Units	A_p	P_{bp}	B_p
1	1,2,3,4,5	K_d	ml/g	0.001	0.007	0.019
2	1,2,3,4,5	q	cm/d	0.016	0.024	0.030[b]
3	1,2,3,4,5	θ	cm^3/cm^3	0.10	0.16	0.22[c]
4	1,2,3,4,5	ρ	g/cm^3	1.62[d]	1.70	1.78
5	1	D	cm^2/d	0.40	1.00	2.20
6	2,3,4,5	D_L	cm	3.73	4.53	5.33
7	4,5	D_w	cm^2/d	0.93	1.73	2.53
8	2,3,4,5	K_s	cm/d	175	270	365
9	2,3,4,5	θ_s	cm^3/cm^3	0.29	0.32	0.35
10	2,3,4,5	θ_r	cm^3/cm^3	0.06	0.08	0.10
11	2,3,4,5	α	1/cm	0.051	0.055	0.059
12	2,3,4,5	β	1/1	1.43[e]	1.51	1.59[e]

[a] 1 = CHAIN, 2 = MULTIMED-DP 1.0, 3 = FECTUZ, 4 = CHAIN 2D, 5 = HYDRUS;
[b] $B_2 = 0.032$ for CHAIN;
[c] $B_3 = 0.26$ for CHAIN;
[d] $A_4 = 1.60$ for CHAIN;
[e] $A_{12} = 1.45$ and $B_{12} = 1.57$ for FECTUZ

In the SSL process, the concentration at a receptor well is assumed to exceed the MCL whenever the concentration at the ground water entry point exceeds the MCL times a dilution attenuation factor (DAF). A value of 20 for DAF is proposed in U.S. EPA(2000ab), and this is the value used in this report. Thus, the ***three output quantities*** that will be considered in the sensitivity analyses of this section and Section 7 are C_{peak}, T_{peak} and T_{MCL}.

6.5 Sensitivity Results for the HYDRUS Model

As indicated by Tables 6-1 and 6-2, parameter sensitivity analyses for the HYDRUS Model were carried out for the eleven input parameters $(K_d, q, \theta, \rho, D_L, D_w, K_s, \theta_s, \theta_r, \alpha, \text{ß})$. For the first six parameters $(K_d, q, \theta, \rho, D_L, D_w)$ the analyses were conducted under the constraints of constant recharge rates, q, and constant moisture content, θ. For the van Genuchten parameters $(K_s, \theta_s, \theta_r, \alpha, \text{ß})$, the analyses were executed under the constraints of constant recharge rate, q, and variable water content, $\theta(z)$. The BTCs for ^{99}Tc concentrations at the bottom of the homogeneous, 6 meter soil column were recorded, as given in Figure 6-1a to 6-1k. Three BTCs for each parameter were obtained, one for the base value of the parameter in question, P_p, one for the upper limit of the range in Table 6-3, B_p, and one for the lower limit, A_p. Data from these BTCs were used to calculate the sensitivities and relative sensitivities of the peak concentraitons at the depth of 6 meters to the eleven input parameters, see Figures 6-2a to 6-2k; the sensitivities and relative sensitivities of the times to reach peak concentration at the depth of 6 meters to the eleven input parameters, see Figures 6-3a to 6-3k; and the sensitivities and relative sensitivities of the time to exceed MCL to the eleven input parameters, Figures 6-4a to 6-4k. The relative sensitivity curves show the rates of increase (+) or decrease (-) of the outputs, C_{peak}, T_{peak}, and T_{MCL}, to increases in the eleven input parameters.

Table 6-4 summarizes the relative sensitivities of C_{peak}, T_{peak}, and T_{MCL} with respect to the eleven basic input parameters for HYDRUS, the relative sensitivities being measured at the base values of the input parameters. The dominant input parameters for all outputs are those which have the greatest influence on the advection term in Equation (6-3), followed by those which have the greatest influence on the diffusion term. The parameters, ρ and K_d, have a very small influence on the transport and fate of ^{99}Tc since $\theta >> \rho K_d$ in the coefficients of Equation (6-3). As one would expect from the statements about Equation (6-4), the outputs for D_L and D_W are nearly the same, as are their sensitivities. Thus, the ratios of the relative sensitivities of the outputs to D_L and D_W should be roughly in the same proportions as the ratio of their base values, $4.53 \div 1.73 = 2.62$, which is the case in Table 6-4 if one allows for round-off error. For the first six input parameters, C_{peak} is most influenced by θ and the sum of D_L and D_W, while T_{peak}, and T_{MCL} are most influenced by q and θ. The direction of these influences (increasing/ decreasing) is seen by the algebraic signs in Table 6-4 and is easily justified by referring to Equation (6-3).

The last five input parameters listed in Table 6-4 are concerned with the van Genuchten Model for $\theta(h)$ and $K(h)$, as given in Equations (6-9) to (6-13). These five parameters influence the distribution of soil moisture in the soil column, and thus influence both the advection and diffusion terms in Equation (6-3). Because of the low annual recharge rate of 87 mm/yr, the least influential parameter is K_s, followed by the soil structure parameter α. The most influential input parameter for all the outputs is the soil texture coefficient β. The next most influential parameters are the upper and lower moisture bounds of the van Genuchten Model, respectively θ_s and θ_r.

Table 6-4.   Relative Sensitivities for C_{peak}, T_{peak} and T_{MCL} with Respect to the Input Parameters for HYDRUS, Measured at the Base Values of the Input Parameters.

| Parameters | *Relative Sensitivity @ Base Values of the Input Parameters* | | |
	C_{peak}	T_{peak}	T_{MCL}
K_d	-0.06	+0.06	+0.07
q	+0.12	-1.10	-0.98
θ	-1.10	+0.80	+0.86
ρ	-0.05	+0.06	+0.07
D_L	-0.28	-0.02	-0.07
D_w	-0.10	-0.01	-0.03
K_s	+0.05	-0.04	-0.04
θ_s	-0.66	+0.57	+0.64
θ_r	-0.29	+0.22	+0.24
α	+0.13	-0.05	-0.05
β	+1.38	-1.00	-1.03
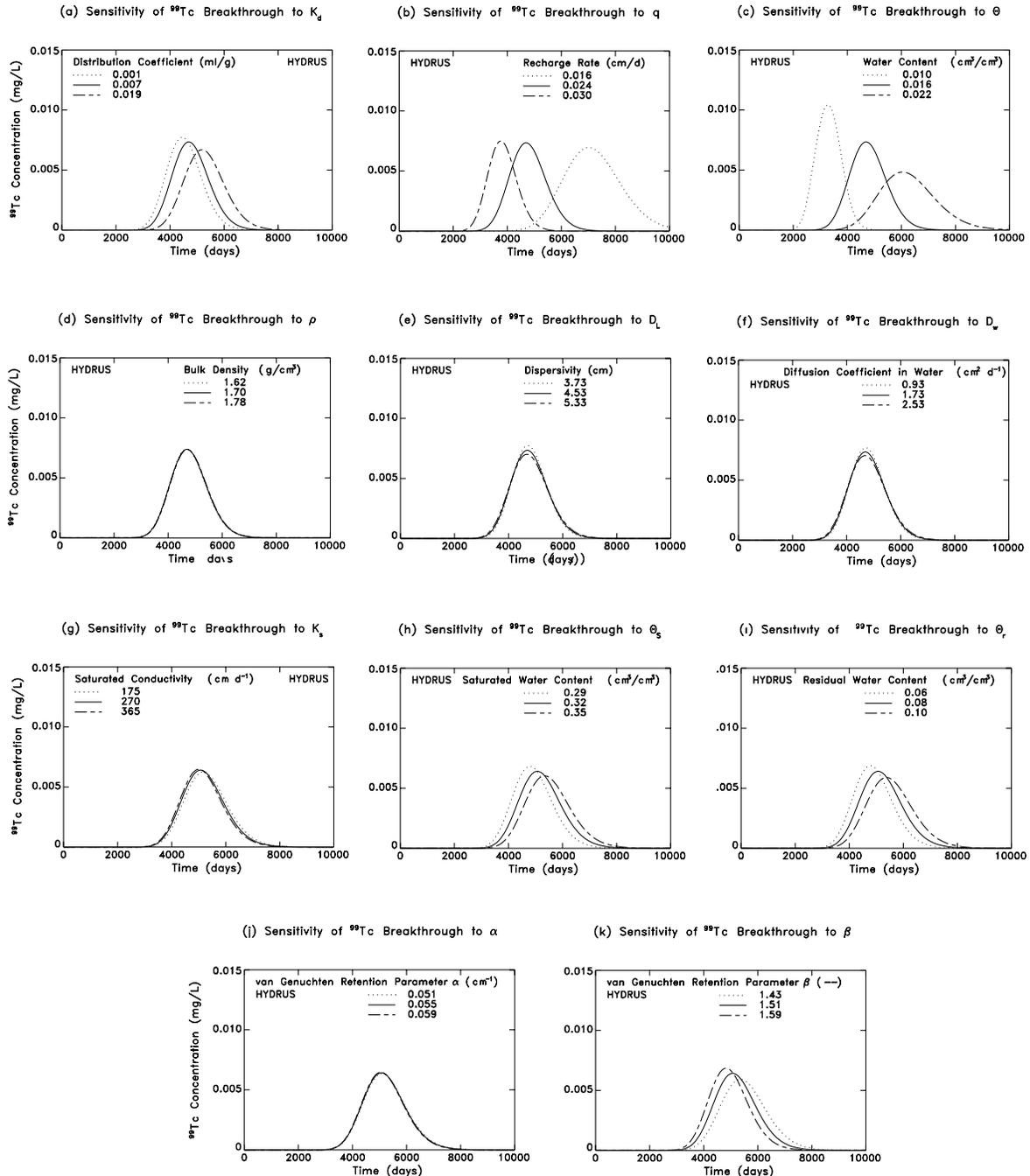
Figure 6-1. Sensitivity of ^{99}Tc breakthrough (through the 6m layer) to the system parameters using the HYDRUS Model: (a) distribution coefficient, (b) recharge rate, (c) water content, (d) bulk density, (e) dispersivity, (f) diffusion coefficient in water, (g) saturated conductivity, (h) saturated water content, (i) residual water content, (j) van Genuchten retention parameter α, (k) van Genuchten retention parameter β.

Figure 6-2. Sensitivity and relative sensitivity of peak concentrations at the depth of 6m to the system parameters using the HYDRUS Model: (a) distribution coefficient, (b) recharge rate, (c) water content, (d) bulk density.
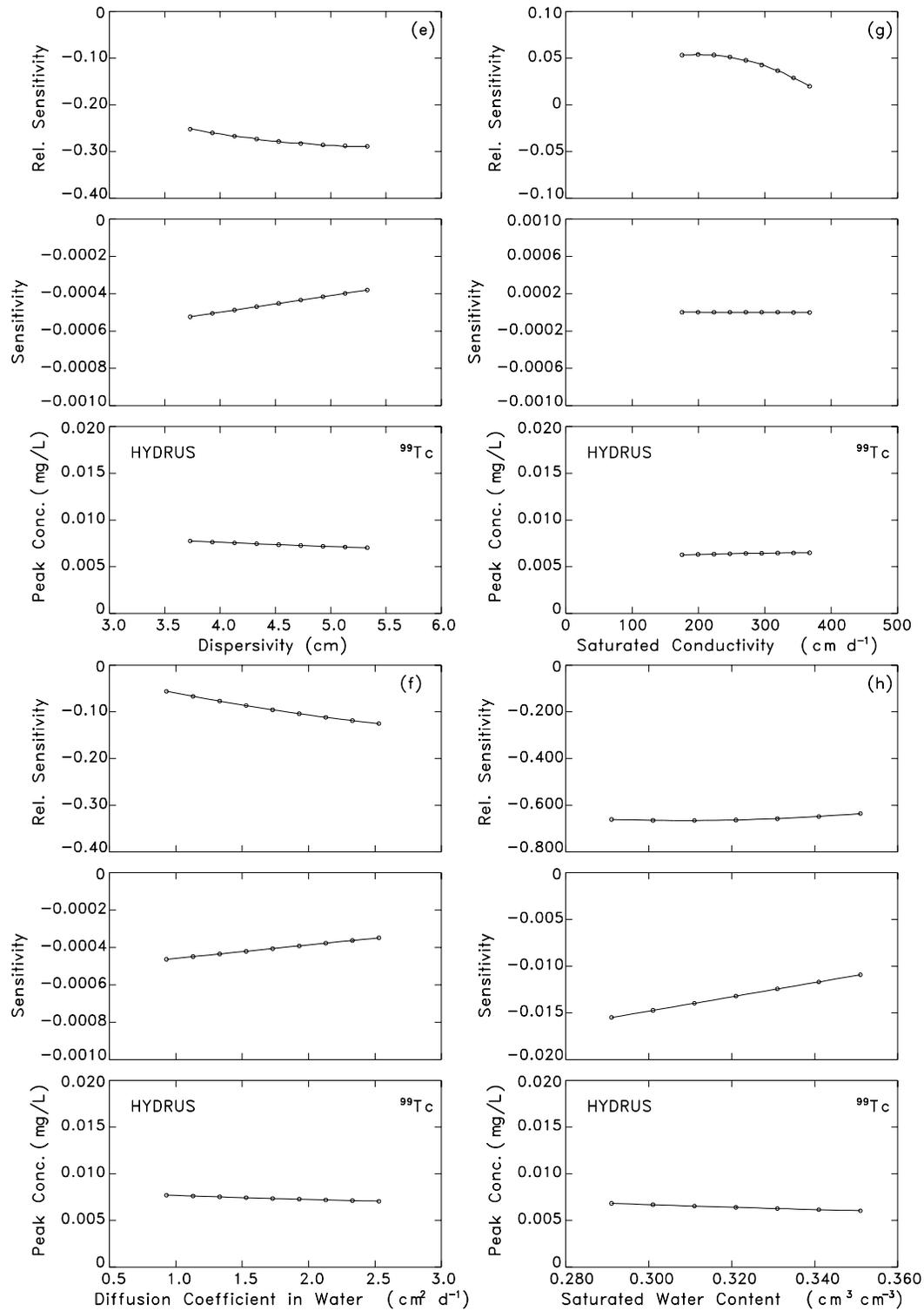
Figure 6-3. Sensitivity and relative sensitivity of peak concentrations at the depth of 6m to the system parameters using the HYDRUS Model: (e) dispersivity, (f) diffusion coefficient in water, (g) saturated conductivity, (h) saturated water content.

Figure 6-2. Sensitivity and relative sensitivity of peak concentrations at the depth of 6m to the system parameters using the HYDRUS Model: (i) residual water content, (j) van Genuchten retention parameter α, (k) van Genuchten retention parameter β.

Figure 6-3. Sensitivity and relative sensitivity of time to reach peak concentrations at the depth of 6m to the system parameters using the HYDRUS Model: (a) distribution coefficient, (b) recharge rate, (c) water content, (d) bulk density.

Figure 6-3. Sensitivity and relative sensitivity of time to reach peak concentrations at the depth of 6m to the system parameters using the HYDRUS Model: (e) dispersivity, (f) diffusion coefficient in water, (g) saturated conductivity, (h) saturated water content.

Figure 6-3. Sensitivity and relative sensitivity of time to reach peak concentrations at the depth of 6m to the system parameters using the HYDRUS Model: (i) residual water content, (j) van Genuchten retention parameter α, (k) van Genuchten retention parameter β.

60
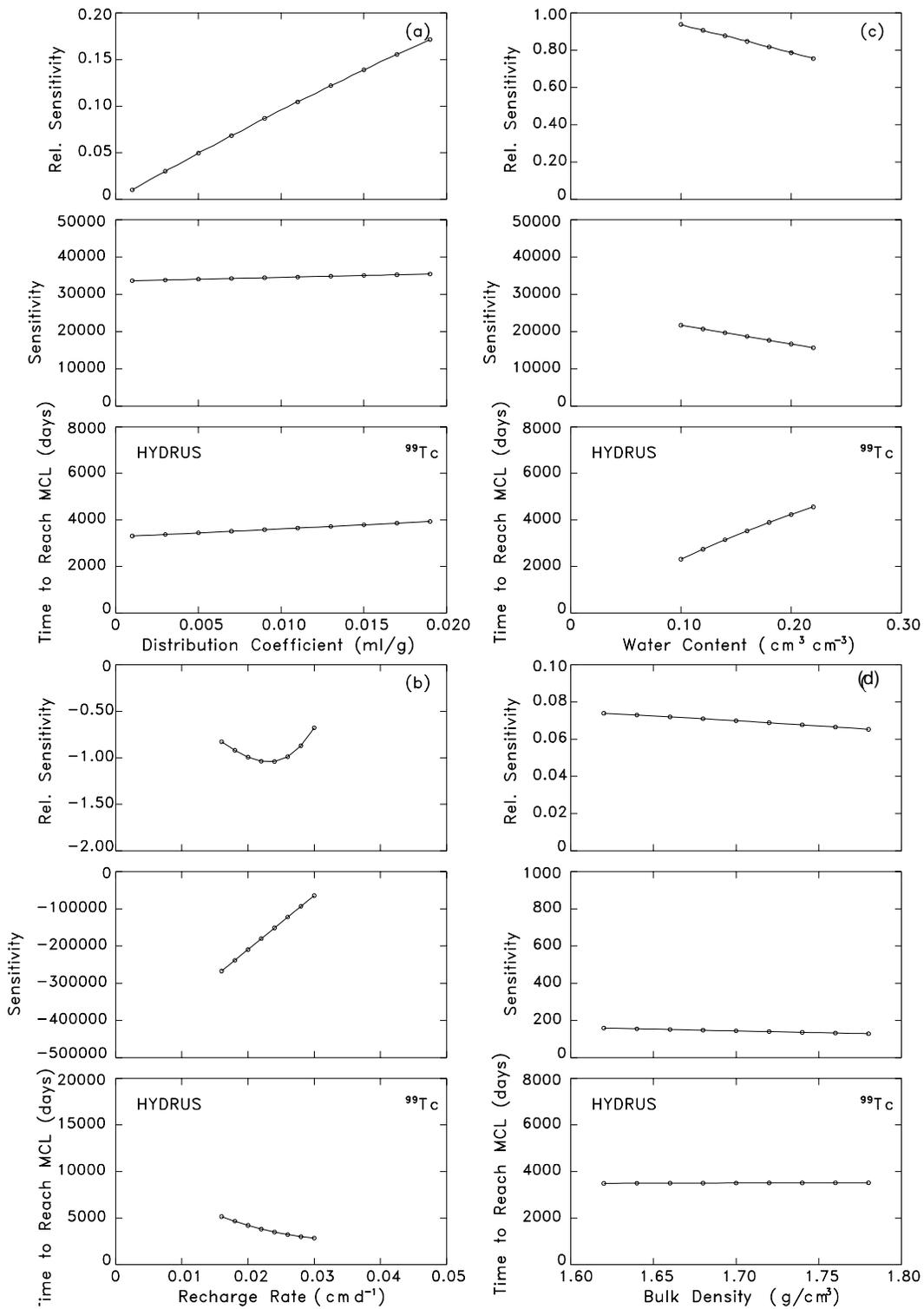
Figure 6-4. Sensitivity and relative sensitivity of time to exceed MCL to the system parameters using the HYDRUS Model: (a) distribution coefficient, (b) recharge rate, (c) water content, (d) bulk density.

Figure 6-4. Sensitivity and relative sensitivity of time to exceed MCL to the system parameters using the HYDRUS Model: (e) dispersivity, (f) diffusion coefficient in water, (g) saturated conductivity, (h) saturated water content.

Figure 6-4. Sensitivity and relative sensitivity of time to exceed MCL to the system parameters using the HYDRUS Model: (i) residual water content, (j) van Genuchten retention parameter α, (k) van Genuchten retention parameter β.

63
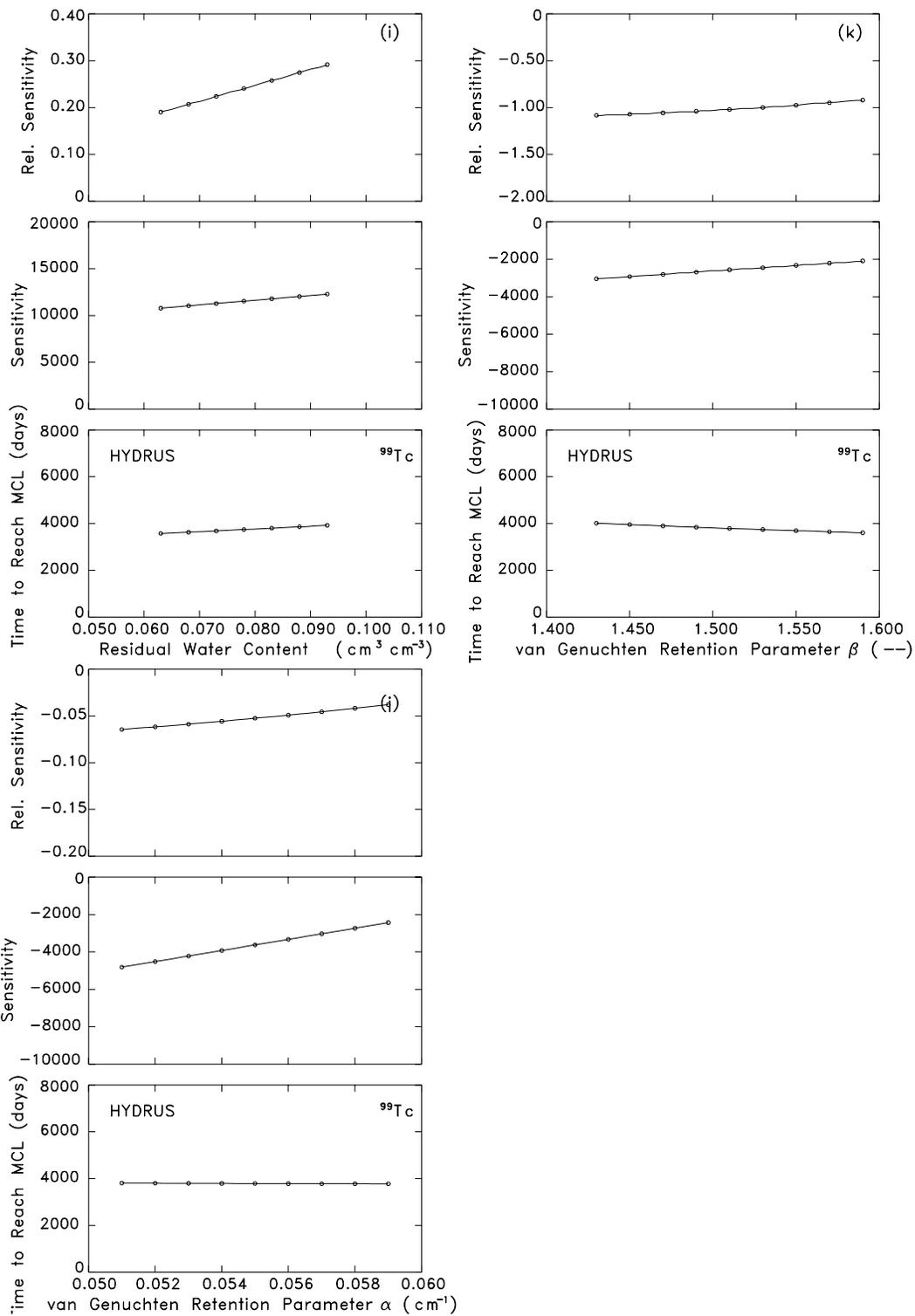
Section 7

Comparison of Sensitivity Results Between Models: Illuminating Numerical Differences

This section is concerned with the comparison of the parameter sensitivity results derived for the five models being studied in this report. The input parameters being considered form subsets of the twelve parameters $(K_d, q, \theta, \rho, D, D_L, D_w, K_s, \theta_s, \theta_r, \alpha, \beta)$ described in Sections 6.2 and 6.3 The output parameters $(C_{peak}, T_{peak}, T_{MCL})$ are those introduced in Section 6.4. In what follows, we consider the modeling codes and their differences, the parameter sensitivity results, and other results illuminating numerical differences and errors between the models.

7.1 The Modeling Codes and Their Differences

Table 2-1 lists the flow and transport modeling components, and the type of boundary conditions available to each of the five codes being tested in this report. From this table, the depth and breadth of application of each code can be determined. However, for the comparison of parameter sensitivity given in this section, we consider a constant flow (i.e., recharge rate) through a 6m, vertical homogeneous soil column, with a constant or spatially varying water content. The boundary conditions for the transport of the radionuclide, ^{99}Tc, consist of a stepwise constant source at the top of the soil column and a zero concentration gradient at the bottom of the column.

As we have previously stated, the CHAIN Code is an analytical transport model which assumes uniform flow conditions in the homogeneous soil column; that is, the soil moisture and recharge rate are both constant. Even though CHAIN possesses an analytical solution for the pollutant breakthrough curves (BTCs) at the 6m level of the soil column, numerical methods are required to generate the graphs of the BTCs from the closed-form analytical expressions. Thus, the CHAIN Code can exhibit numerical error, with reference to the exact analytical expressions, due to truncation of the series of functions representing the analytical solution in the numerical approximation method, and due to computer round-off error.

The MULTIMED-DP 1.0 and FECTUZ Codes can handle constant recharge rates with constant or spatially varying water contents. With respect to the BTCs for pollutant transport, these codes are semi-analytical models which approximate the inversion of complex analytical solutions in transform space using numerical inverse transform modules. Thus, the numerical errors most prevalent in these codes are those due to the numerical solution of Darcy's Law for the pressure head (leading to a variable water content in the soil column) and those due to the numerical inversion (i.e., a numerical Laplace inversion) of the analytical solutions for the pollutant concentration in the Laplace transform space. If these two codes use the same differencing scheme or one of comparable accuracy for solving Darcy's Law and the same or comparable numerical inversion schemes for the pollutant BTCs, then one would expect that the BTCs for a given boundary-initial value problem would be nearly the same for both codes.

The CHAIN 2D (the one-dimensional, vertical version) and the HYDRUS Codes handle constant recharge rates with constant, spatially varying, or temporally and spatially varying water contents. With respect to pollutant transport, these codes solve the advection-dispersion-decay partial differential equations using finite-difference or finite-element methods. Thus, the numerical errors most prevalent in these two codes are those due to the numerical schemes used to solve the Richards Equation for the temporally and spatially varying pressure head (leading to a temporally and spatially varying water content), those due to deriving a spatially varying water content from the numerically obtained steady-state solution of the Richards Equation, and those due to the numerical schemes used to obtain the BTCs for pollutant transport from the advection-dispersion-decay partial differential equations. If CHAIN 2D and HYDRUS use the same numerical solution schemes or ones of comparable accuracy for the Richards Equation and the advection-dispersion-decay equations, then one would expect (as with MULTIMED-DP 1.0 and FECTUZ) that the BTCs for a given boundary-initial value problem would be nearly the same for both codes.

64

From the above discussions, one would be tempted to place the derived BTCs into three categories for the current parameter sensitivity modeling scenario (the scenario as described in Sections 5, and 6.1 to 6.3). These three categories, based on the potential for numerical error, would be those BTCs derived by the CHAIN Code, those BTCs derived by the MULTIMED-DP 1.0 and FECTUZ Codes, and those BTCs derived by the CHAIN 2D and HYDRUS Codes. As pointed out in Sections 6.2 and 6.3 (see Tables 6-1 and 6-2), there are two other discriminating factors between the codes for the current modeling scenario; namely: (1) the specification of a constant or spatially varying water content in the homogeneous, 6m soil column, and (2) the construction of the dispersion factor, θD, in Equation (6-4). Table 7-1 is a composite of Tables 6-1 and 6-2, and points out the impact that these two discriminating factors have on the current parameter sensitivity analyses.

For the first seven parameters (K_d,q,θ,ρ,D,D_L,D_w) in Table 7-1, the five models were run under the constraints of a constant recharge rate, q, and a constant water content, θ, using the base input values and input ranges given in Table 6-3. As previously stated and as indicated in Table 7-1, CHAIN specifies a constant value for D and does not resolve θD into components as given in Equation (6-4). MULTIMED-DP 1.0 and FECTUZ only specify constant values for D_L in Equation 6-4, while CHAIN 2D (the one-dimensional, vertical version) and HYDRUS specify constant values for both D_L and D_w. Since the recharge rate, q, in the current sensitivity modeling scenario is so small, the quantity $\theta\tau_w D_w$ in Equation (6-4) is relatively important as compared to the dispersion term $D_L|q|$. Thus, for the base values listed in Table 6-3, one would expect less total dispersion effects (i.e., effects due to θD) on the BTCs derived by MULTIMED-DP 1.0 and FECTUZ than for those derived by CHAIN 2D and HYDRUS. The fourth row of Table 7-2 gives the numerical justification of this statement. As this row of values indicates, the base value of D in the CHAIN Code gives a value for θD which is nearly the same as those for CHAIN 2D and HYDRUS, while the value of θD for MULTIMED-DP 1.0 and FECTUZ is about 2/3 of the values for the values for

Table 7-1. The Sensitivity Analyses Performed (●) for the Five Models Under the Assumption of Constant Recharge Rate and Constant Water Content, and the Sensitivity Analyses Performed (○) for Four of the Five Models Under the Assumption of Constant Recharge Rate and Variable Water Content.

Model Input Parameter	Sensitivity Analyses Performed				
	CHAIN	MULTIMED-DP 1.0	FECTUZ	CHAIN 2D	HYDRUS
K_d	●	●	●	●	●
q	●	●	●	●	●
θ	●	●	●	●	●
ρ	●	●	●	●	●
D	●				
D_L		●	●	●	●
D_w				●	●
K_s		○	○	○	○
θ_s		○	○	○	○
θ_r		○	○	○	○
α		○	○	○	○
β		○	○	○	○

65

Table 7-2. The Values of the Dispersion Factor, θD, as Derived from Equation (6-4) and the Base Values of D, D_L, D_w, θ and q and the Ranges of D, D_L and D_w as given in Table 6-3.

					θD in cm²/d				
D cm²/d	D_L cm	D_w cm²/d	$D_L|q|$ cm²/d	$θτ_wD_w$ cm²/d	*CHAIN*	*MULTIMED-DP 1.0*	*FECTUZ*	*CHAIN 2D*	*HYDRUS*
0.40	4.53	1.73	0.109	0.053	0.064	0.109	0.109	0.162	0.162
1.00	3.73	1.73	0.090	0.053	0.160	0.090	0.090	0.143	0.143
1.00	4.53	0.93	0.109	0.028	0.160	0.109	0.109	0.137	0.137
1.00	4.53	1.73	0.109	0.053	0.160	0.109	0.109	0.162	0.162
1.00	5.33	1.73	0.128	0.053	0.160	0.128	0.128	0.181	0.181
1.00	4.53	2.53	0.109	0.077	0.160	0.109	0.109	0.186	0.186
2.20	4.53	1.73	0.109	0.053	0.352	0.109	0.109	0.162	0.162

the other three models. Thus, one would expect the BTCs for the base values of the input parameters to be nearly the same for the CHAIN, CHAIN 2D and HYDRUS Codes, and nearly the same for the MULTIMED-DP 1.0 and FECTUZ Codes, where the peak concentrations for the latter two models should be higher than those for the former three models. This is, in fact, the case as we will see in Section 7.2. The numerical values for θD in the other six rows of Table 7-2 can be used to interpret the various sensitivity results given in the next subsections.

For the last five input parameters in Table 7-1 (K_s,$θ_s$,$θ_r$,α,β), only four models (CHAIN does not allow variable θ) are evaluated for constant recharge rate, q, and variable water content, θ(z). Based on the above discussions, one would expect the BTCs for CHAIN 2D and HYRUS to be nearly the same, and those for MULTIMED-DP 1.0 and FECTUZ to be nearly the same, where the peak concentrations for the latter two models should be higher than those for the former two models. As we will see below, this is the case.

7.2 The Parameter Sensitivity Results

As indicated in Table 7-1, parameter sensitivity analyses are performed on all five models for the first four parameters (K_d,q,θ,ρ). CHAIN is the only model for which sensitivity analyses are performed for D. Sensitivity analyses are performed for the six parameters (D_L,K_s,$θ_s$,$θ_r$,α,β) on four of the five models (all except CHAIN), while only CHAIN 2D and HYDRUS consider the parameter D_w. The ^{99}Tc BTCs at the bottom of the 6m, homogeneous soil column are given in Figures 7-1 to 7-12, where the breakdown is as follows:

- Figures 7-1 to 7-4 compare the BTCs for each of the five models for the first four parameters (K_d,q,θ,ρ), respectively;

- Figure 7-5 gives the BTCs for the CHAIN Code for the parameter D; this figure is given for the purpose of completion;

- Figure 7-6 compares the BTCs for each of the four models (CHAIN being excluded) for the dispersivity, D_L;

- Figure 7-7 compares the BTCs for CHAIN 2D and HYDRUS for the diffusion coefficient in water, D_w;

- Figures 7-8 to 7-12 compare the BTCs for each of the four models (CHAIN being excluded) for the five van Genuchten parameters (K_s,$θ_s$,$θ_r$,α,β), respectively.

These twelve figures of ^{99}Tc BTCs fulfill the expectations set forth in Section 7.1. These results, or expectations, are summarized in the following list:
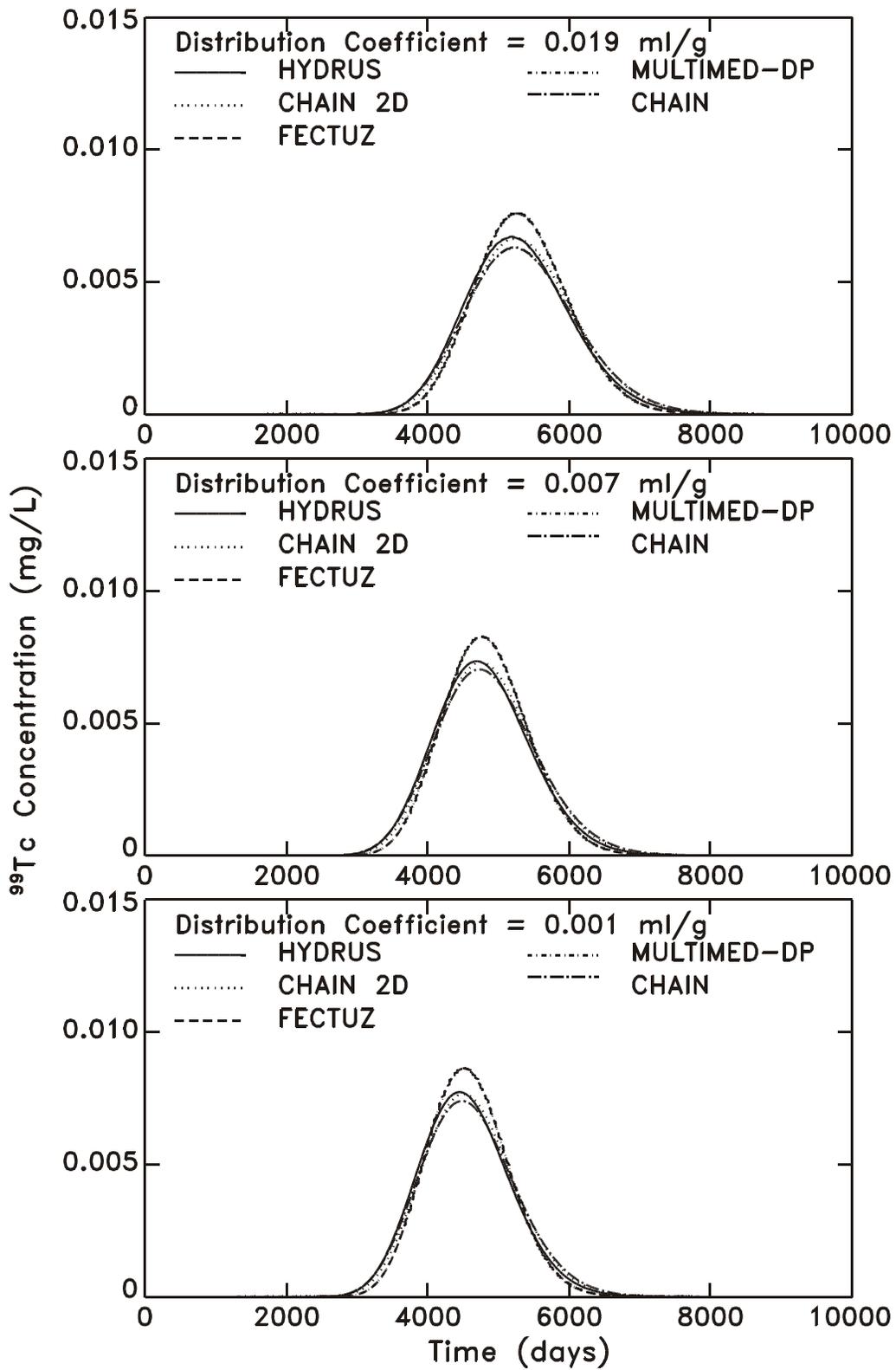
Figure 7-1. Sensitivity of ^{99}Tc breakthrough (through the 6m layer) to the distribution coefficient using the CHAIN, MULTIMED-DP 1.0, FECTUZ, CHAIN 2D, HYDRUS Models, where K_d = 0.019 ml/g, 0.007 ml/g, and 0.001 ml/g.
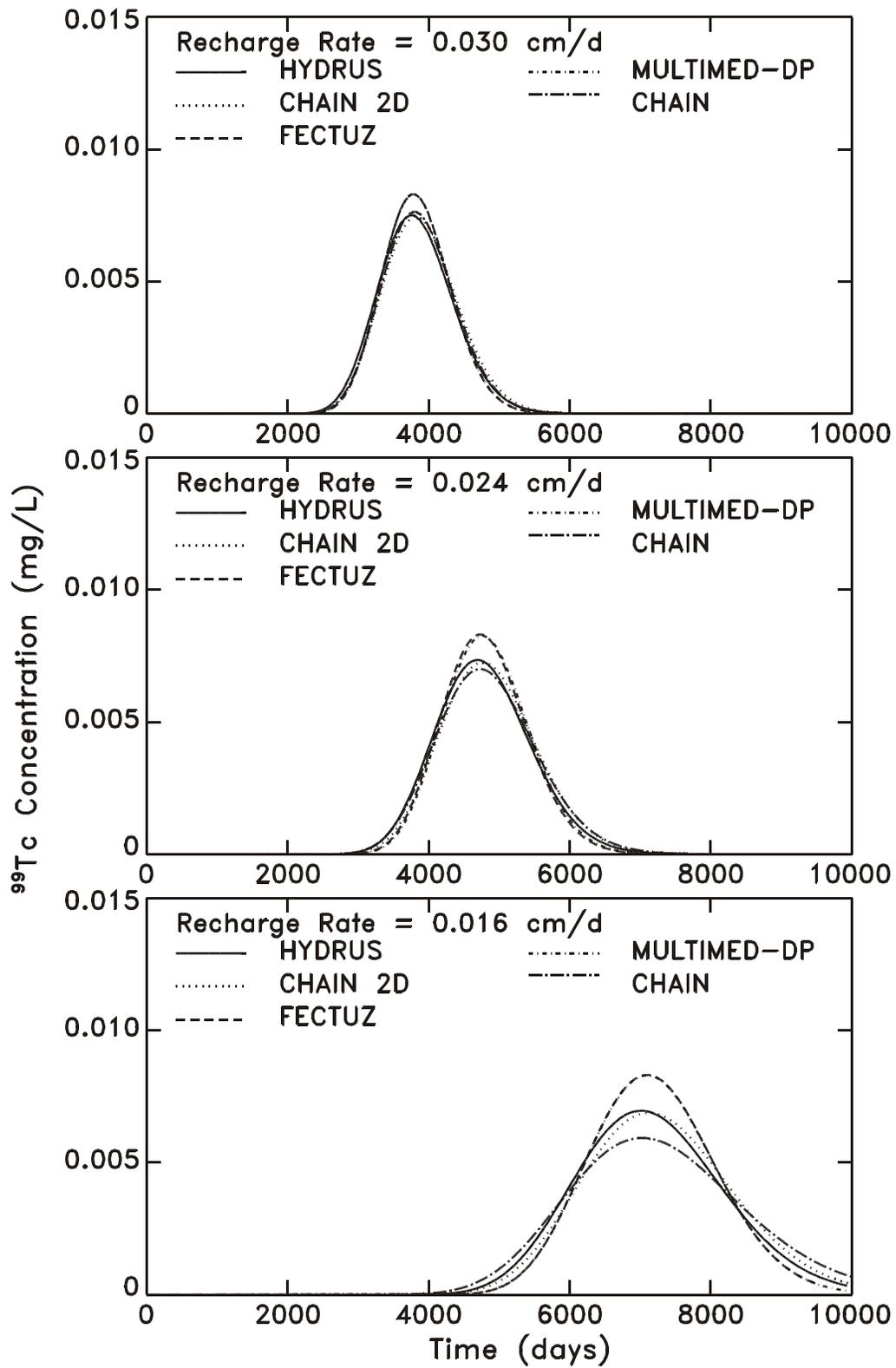
Figure 7-2. Sensitivity of ^{99}Tc breakthrough (through the 6m layer) to the recharge rate using the CHAIN, MULTIMED-DP 1.0, FECTUZ, CHAIN 2D, and HYDRUS Models, where q = 0.030 cm/d, 0.024 cm/d, and 0.016 cm/d.
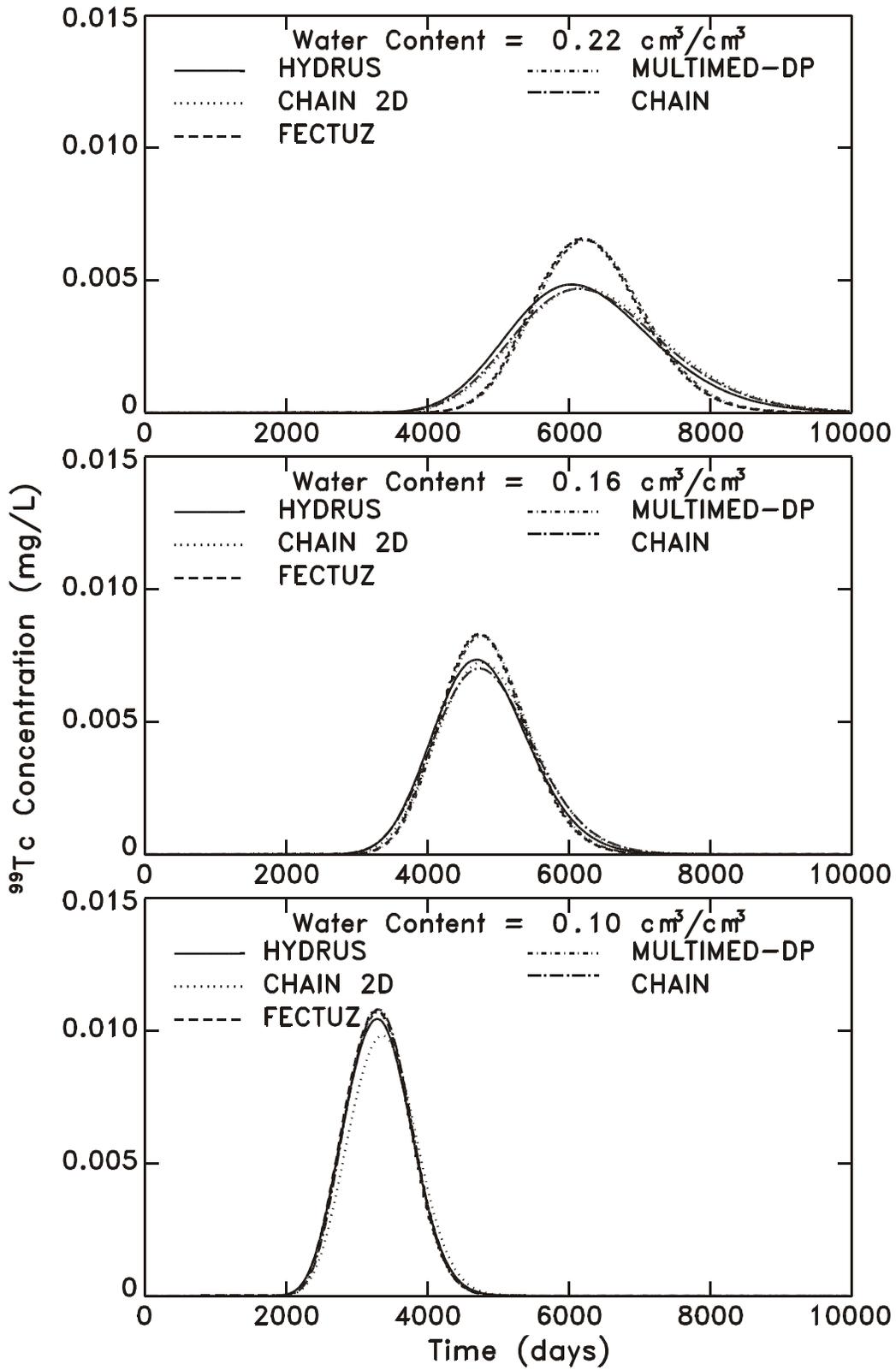
Figure 7-3. Sensitivity of ^{99}Tc breakthrough (through the 6m layer) to the water content using the CHAIN, MULTIMED-DP 1.0, FECTUZ, CHAIN 2D, and HYDRUS Models, where $\theta = 0.22$ cm^3/cm^3, 0.16 cm^3/cm^3, and 0.10 cm^3/cm^3.

69
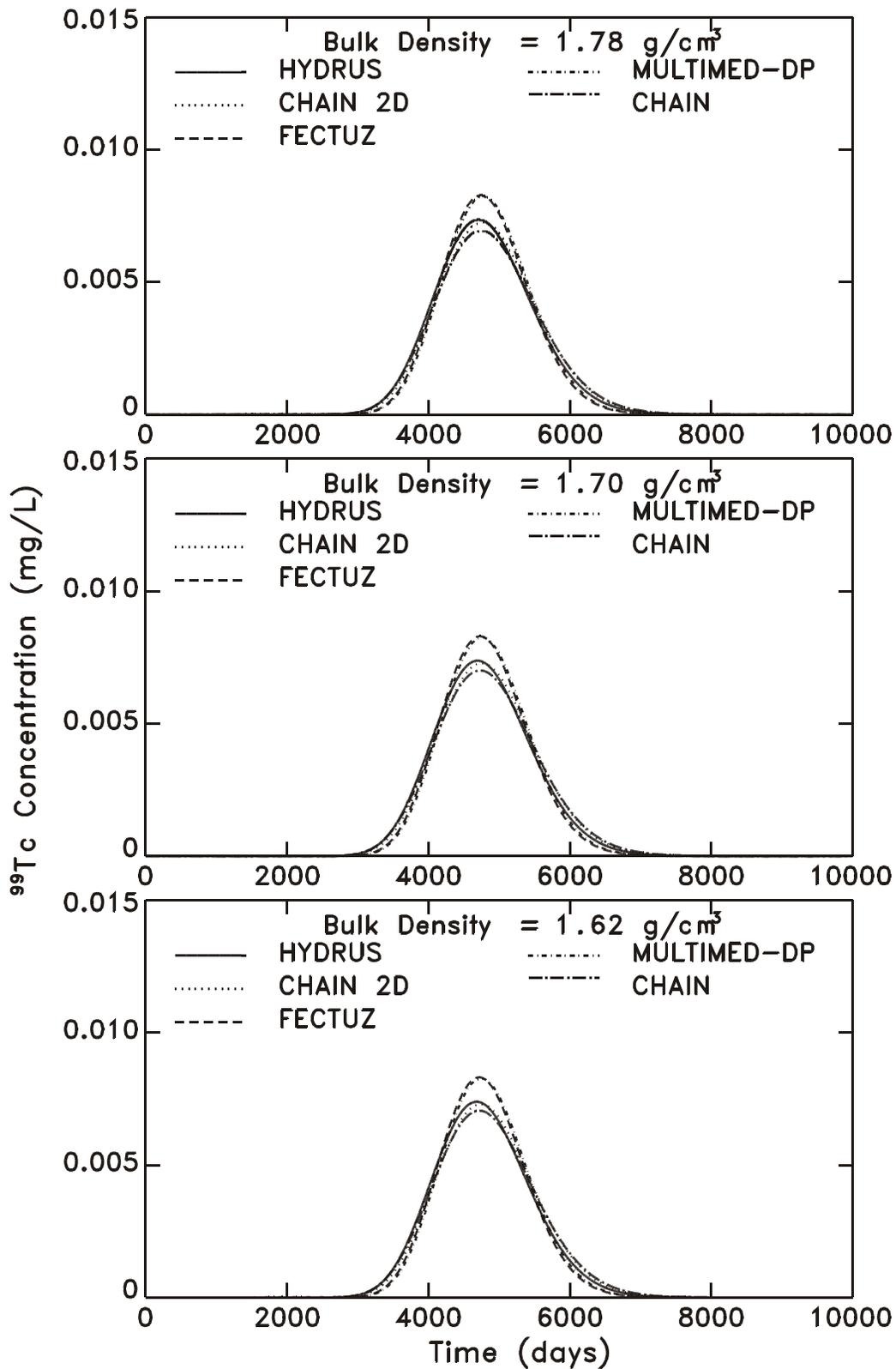
Figure 7-4. Sensitivity of ^{99}Tc breakthrough (through the 6m layer) to the bulk density using the CHAIN, MULTIMED-DP 1.0, FECTUZ, CHAIN 2D, and HYDRUS Models, where $\rho = 1.78$ g/cm^3, 1.70 g/cm^3, and 1.62 g/cm^3.
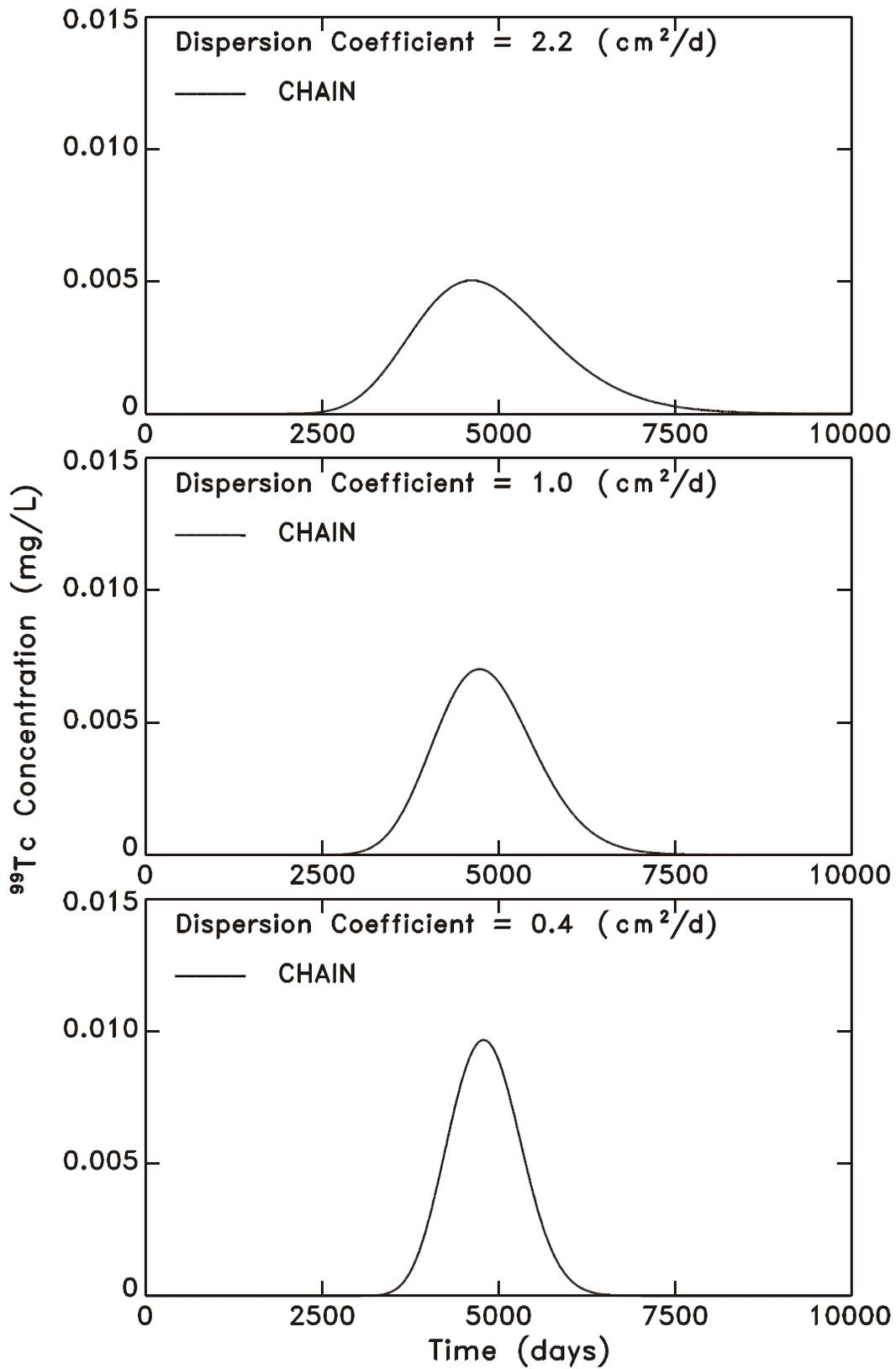
Figure 7-5. Sensitivity of ^{99}Tc breakthrough (through the 6m layer) to the dispersion coefficient using the CHAIN Model, where D = 2.20 cm^2/d, 1.00 cm^2/d, and 0.40 cm^2/d.
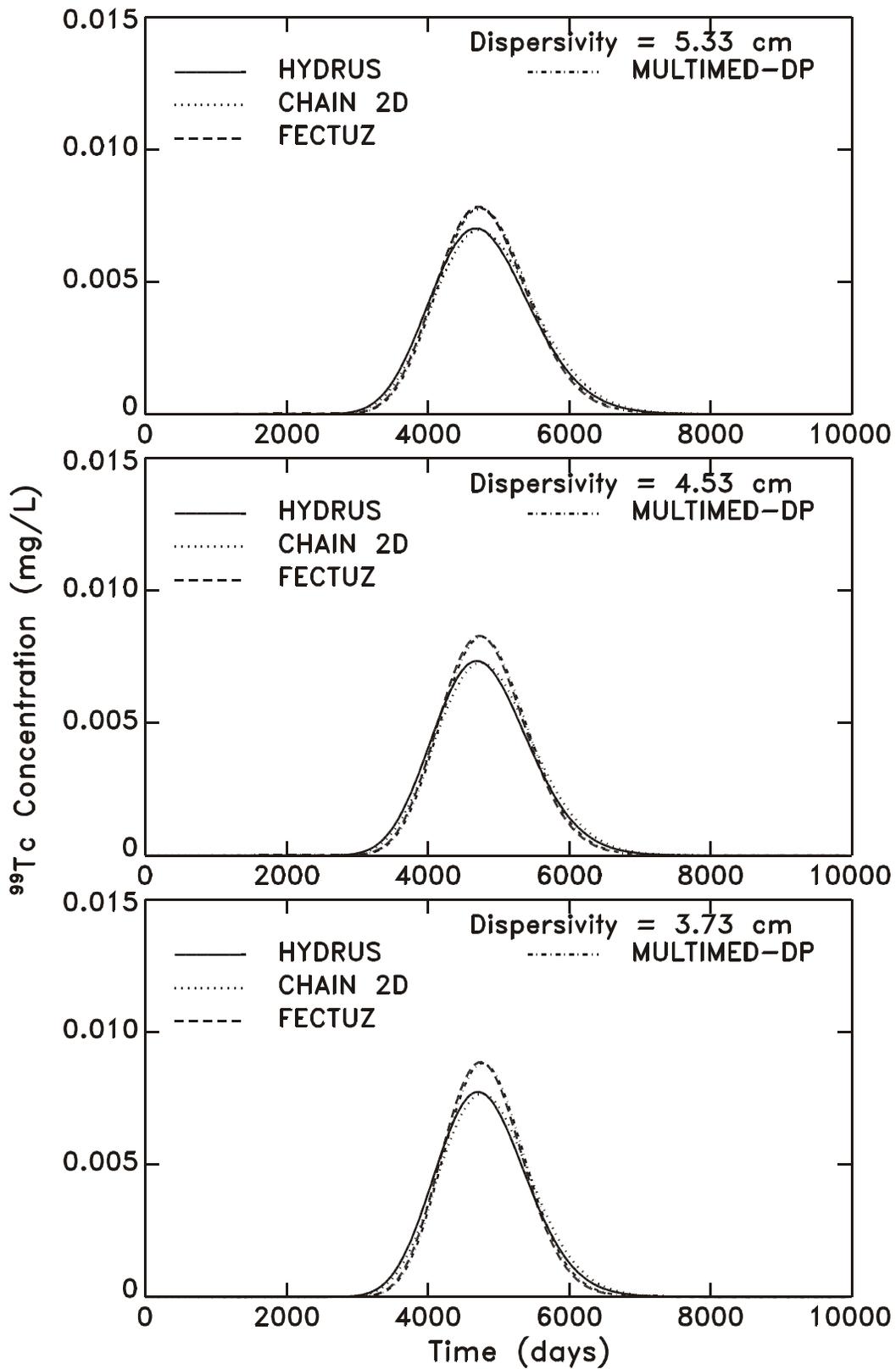
Figure 7-6. Sensitivity of ^{99}Tc breakthrough (through the 6m layer) to the dispersivity using the MULTIMED-DP 1.0, FECTUZ, CHAIN 2D, and HYDRUS Models, where D_L = 5.33 cm, 4.53 cm, and 3.73 cm.
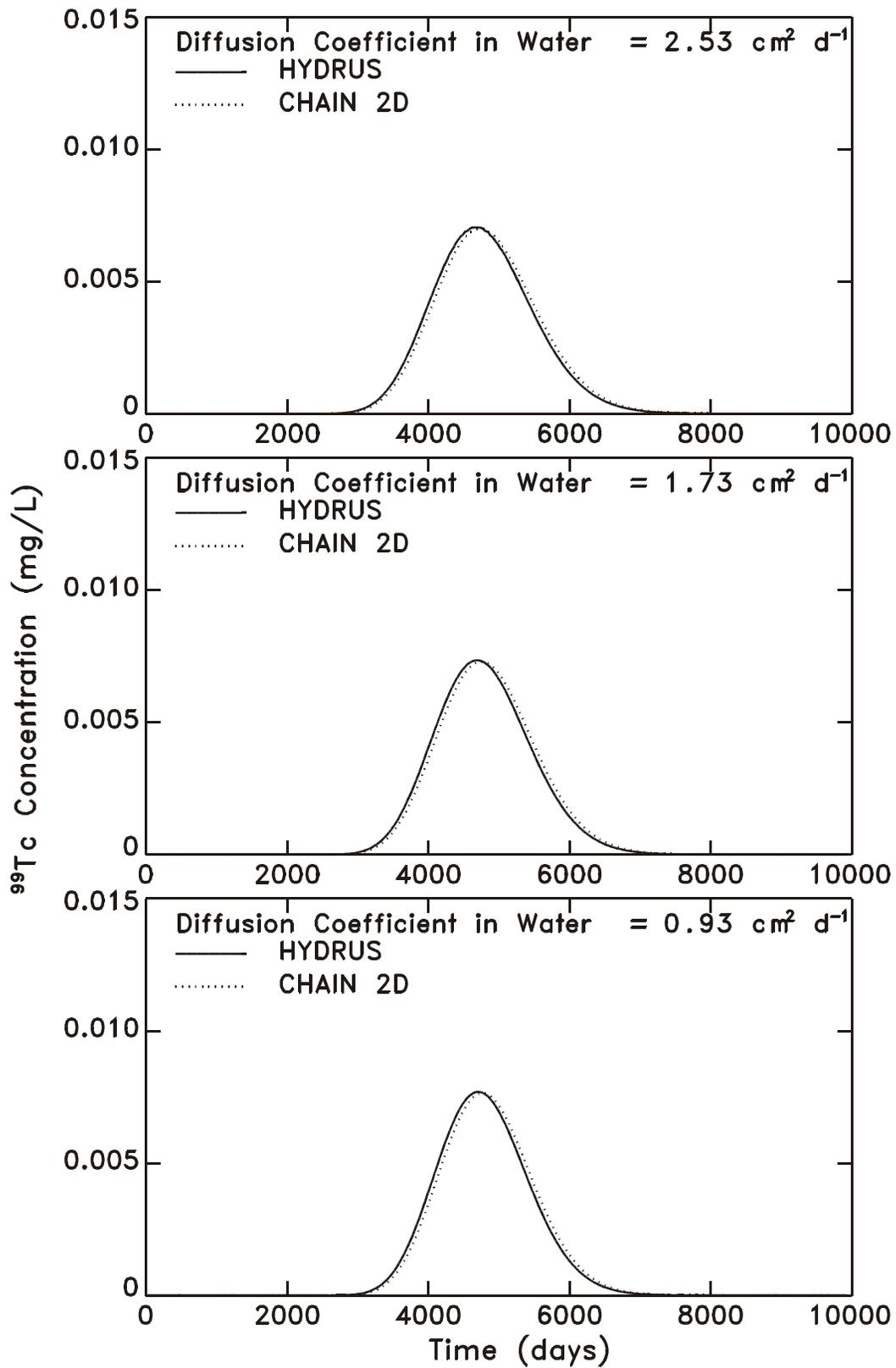
Figure 7-7. Sensitivity of ^{99}Tc breakthrough (through the 6m layer) to the diffusion coefficient in water using the CHAIN 2D and HYDRUS Models, where $D_w = 2.53$ cm^2/d, 1.73 cm^2/d, and 0.93 cm^2/d.
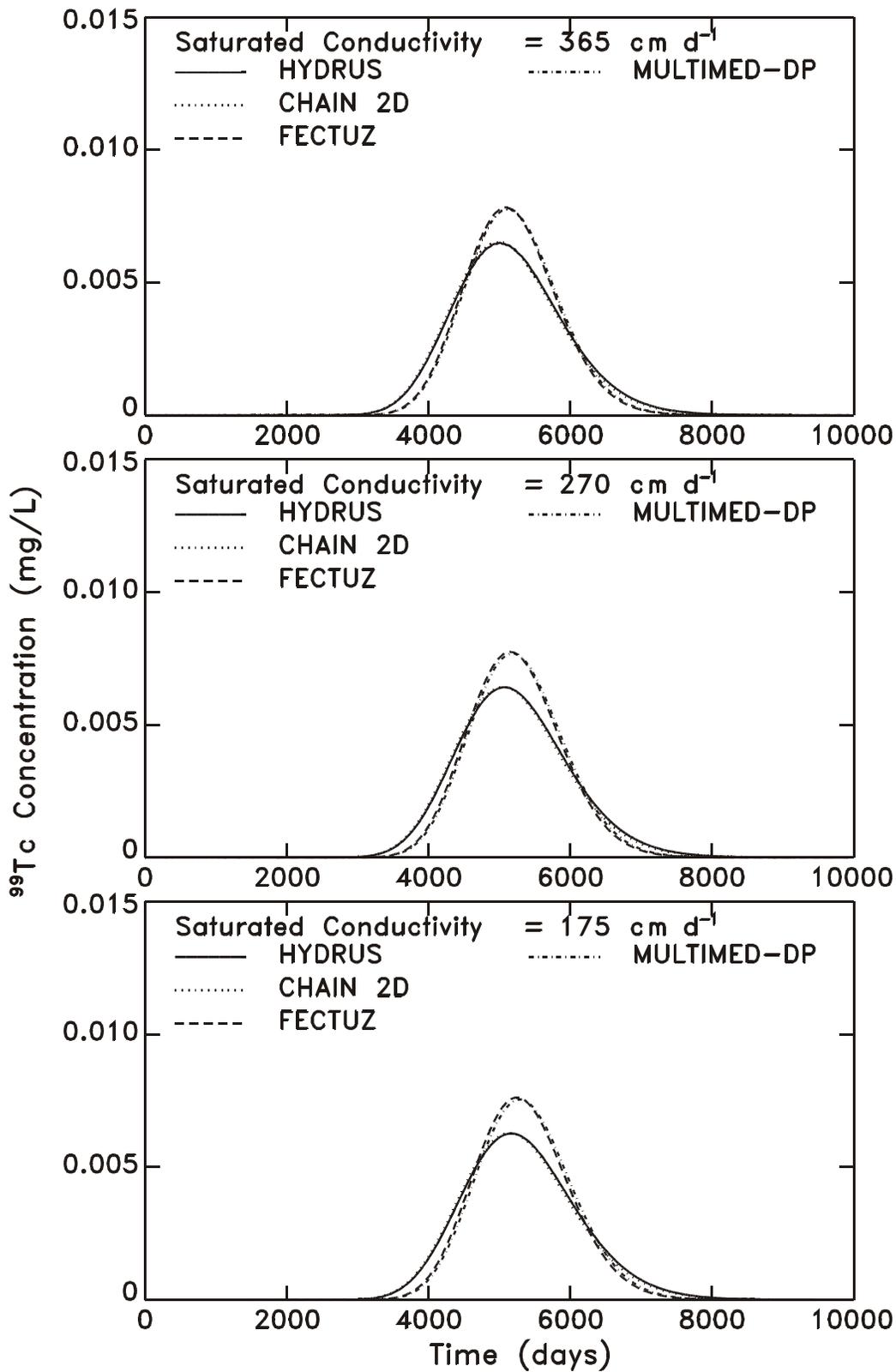
Figure 7-8. Sensitivity of ⁹⁹Tc breakthrough (through the 6m layer) to the saturated conductivity using the MULTIMED-DP 1.0, FECTUZ, CHAIN 2D and HYDRUS Models, where K_s = 365 cm/d, 270 cm/d, and 175 cm/d.
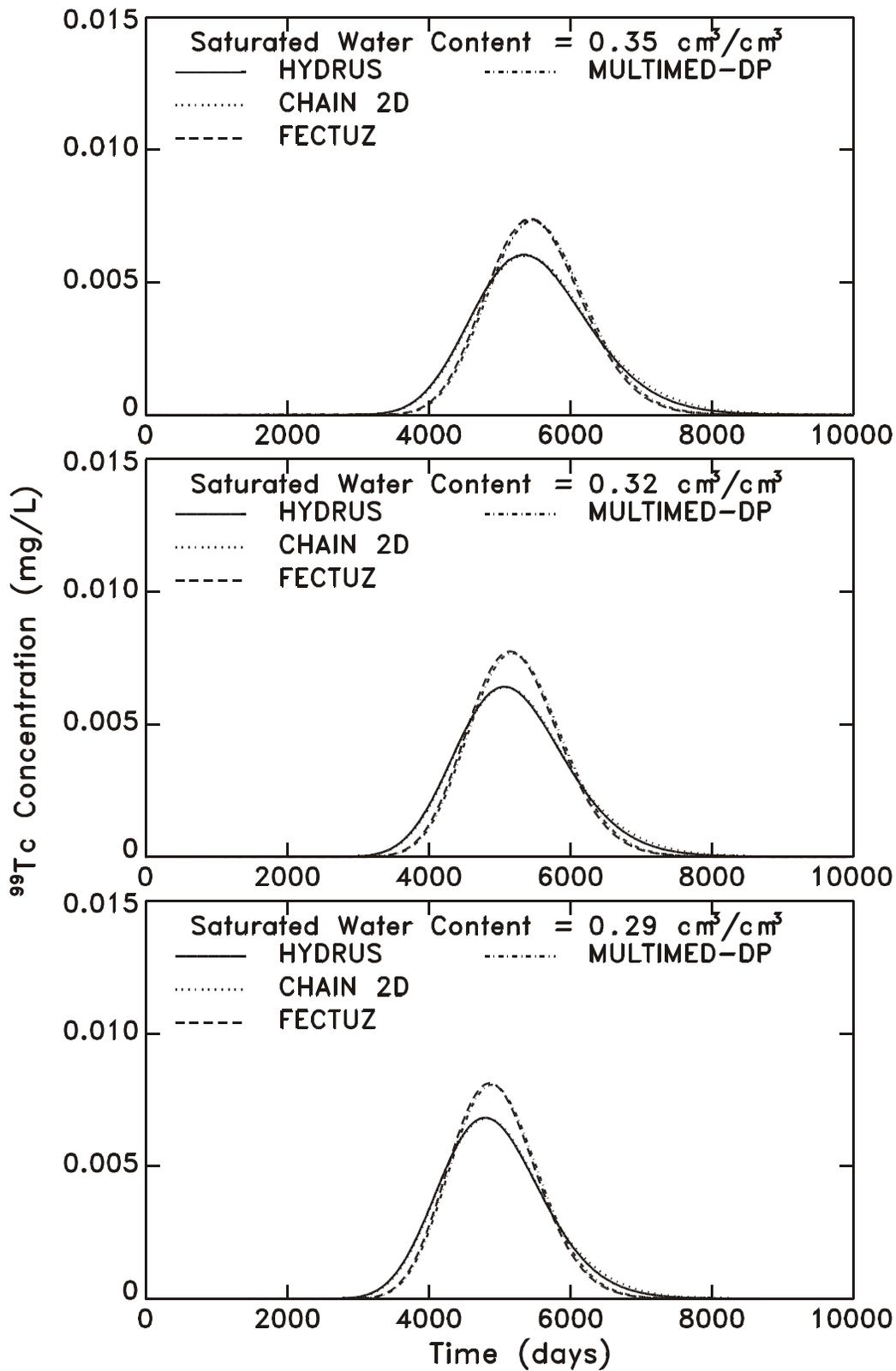
Figure 7-9. Sensitivity of ^{99}Tc breakthrough (through the 6m layer) to the saturated water content using the MULTIMED-DP 1.0, FECTUZ, CHAIN 2D and HYDRUS Models, where $\theta_s = 0.35$ cm^3/cm^3, 0.32 cm^3/cm^3, and 0.29 cm^3/cm^3.
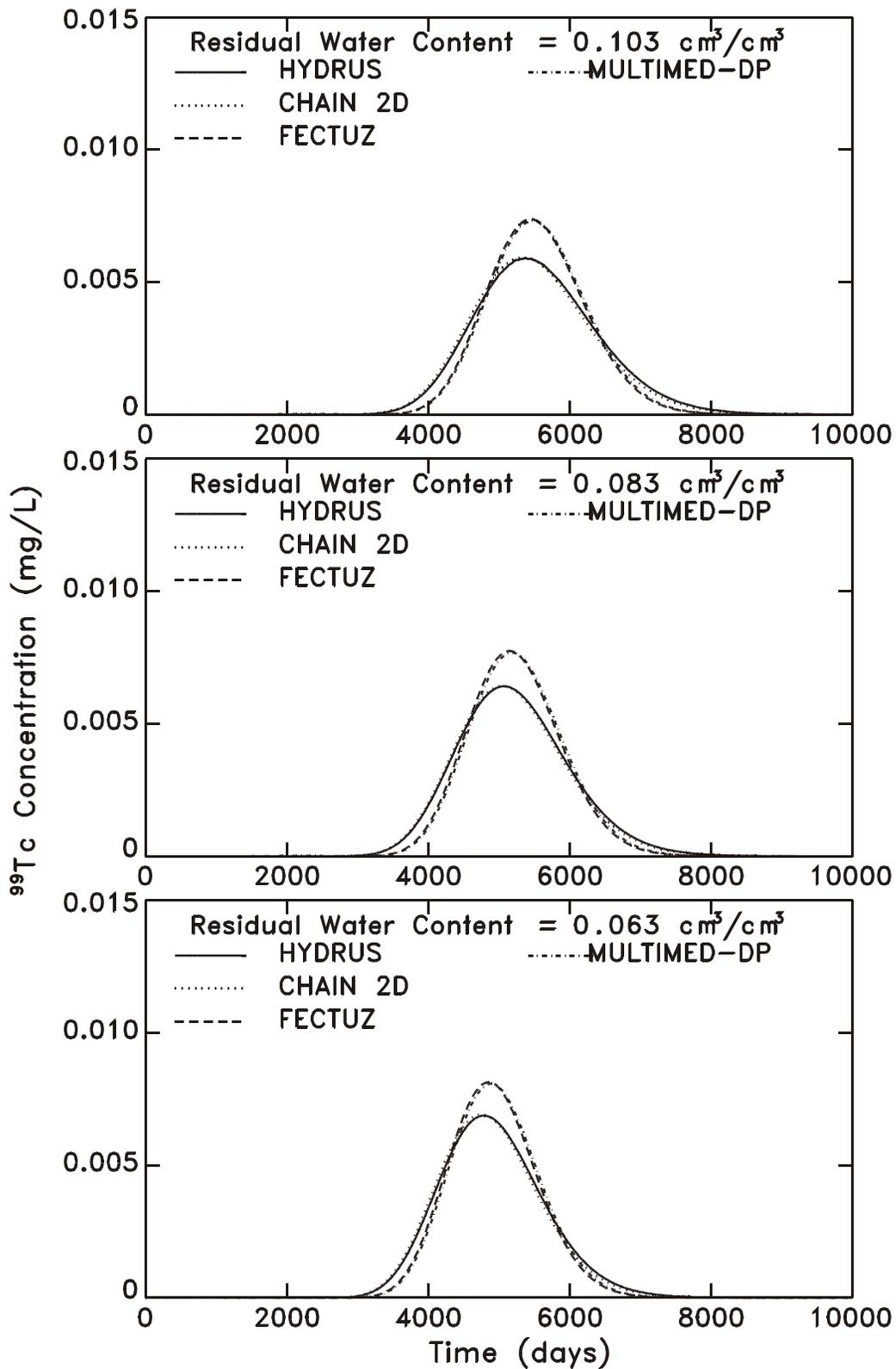
Figure 7-10. Sensitivity of ^{99}Tc breakthrough (through the 6m layer) to the residual water content using the MULTIMED-DP 1.0, FECTUZ, CHAIN 2D and HYDRUS Models, where $\theta_r = 0.103$ cm^3/cm^3, 0.083 cm^3/cm^3, and 0.063 cm^3/cm^3.
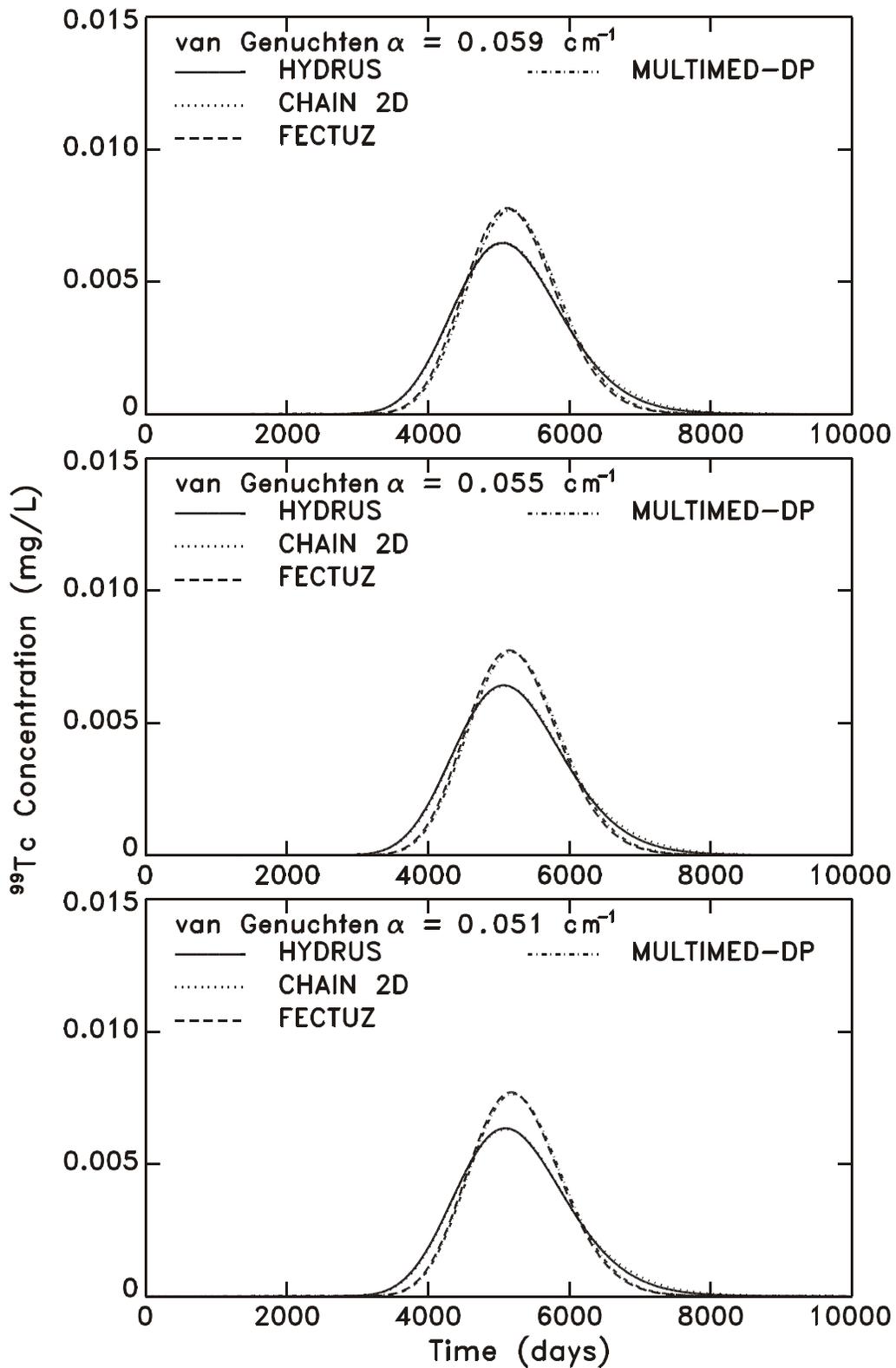
Figure 7-11. Sensitivity of ^{99}Tc breakthrough (through the 6m layer) to the van Genuchten retention parameter α using the MULTIMED-DP 1.0, FECTUZ, CHAIN 2D and HYDRUS Models, where $\alpha = 0.059$cm^{-1}, 0.055 cm^{-1}, and 0.051 cm^{-1}.
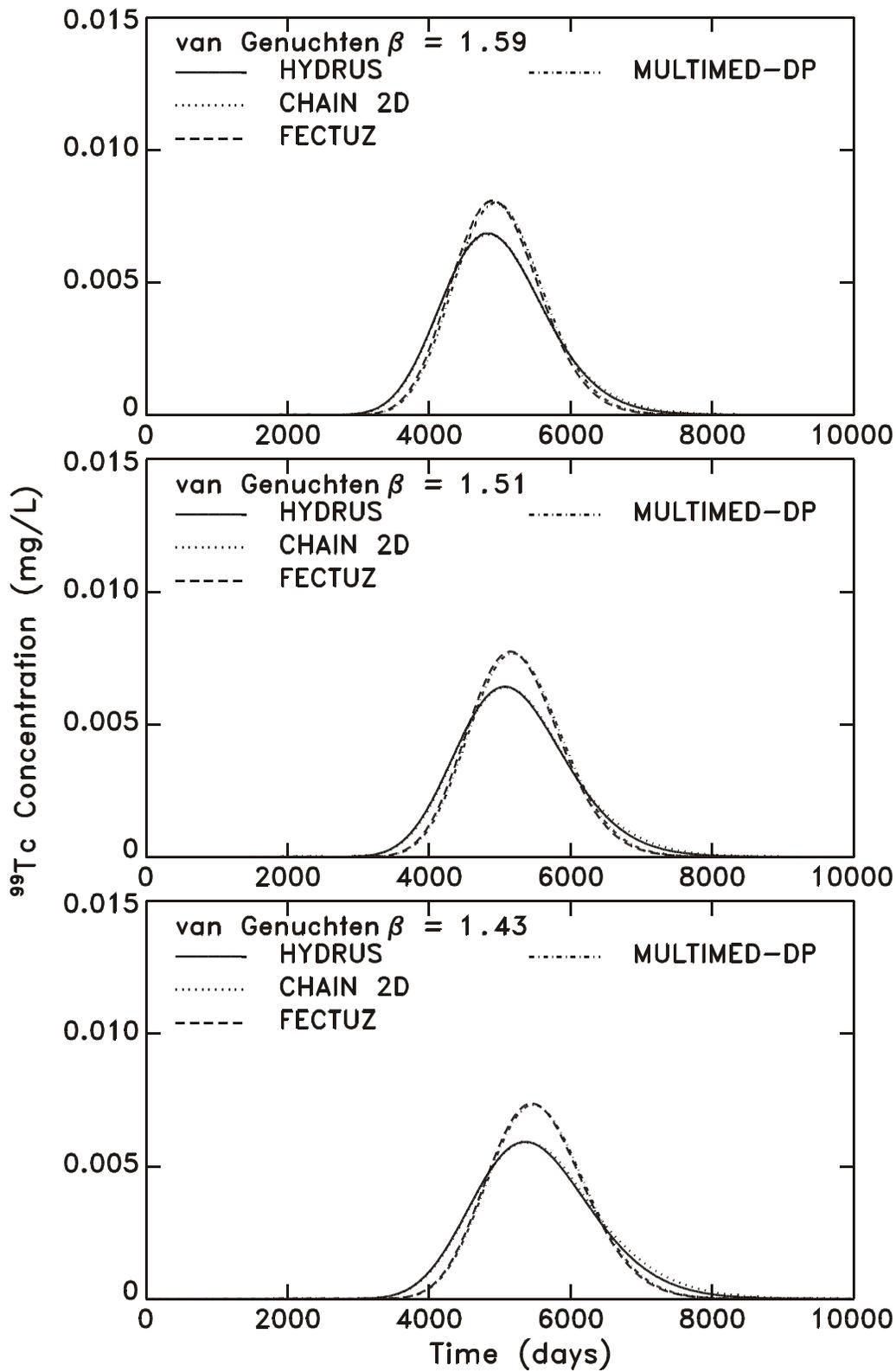
Figure 7-12. Sensitivity of ^{99}Tc breakthrough (through the 6m layer) to the van Genuchten retention parameter β using the MULTIMED-DP 1.0, FECTUZ, CHAIN 2D and HYDRUS Models, where β = 1.59, 1.51, and 1.43.

- The BTCs for the CHAIN 2D and HYDRUS Codes are nearly the same for all base parameter values and upper and lower bounds of the parameter ranges, except for $\theta = 0.10$ in Figure 7-3; but even for this exception, the peak concentration for CHAIN 2D is about 95% of that for the HYDRUS Code;

- For the first four parameters (K_d, q, θ, ρ), the CHAIN BTCs are fairly close to those for CHAIN 2D and HYDRUS, except for $q = 0.016$ cm/d in Figure 7-2; but even for this exception, the peak concentration for CHAIN is about 87% of those for the CHAIN 2D and HYDRUS Codes;

- The BTCs for the MULTIMED-DP 1.0 and FECTUZ Codes are almost identical for all values of all parameters considered.

- The peak concentrations for the MULTIMED-DP 1.0 and FECTUZ BTCs range from 5% to 35% higher than those for CHAIN 2D and HYDRUS, depending on the specific input parameter and its particular value;

- For the base values of ($K_d, q, \theta, \rho, D_L$), the concentration peaks of the MULTIMED-DP 1.0 and FECTUZ BTCs are about 14% higher than those for CHAIN 2D and HYDRUS;

- For the base values of the van Genuchten parameters ($K_s, \theta_s, \theta_r, \alpha, \beta$), the concentration peaks of the MULTIMED-DP1.0 and FECTUZ BTCs are about 21% higher than those of CHAIN 2D and HYDRUS.

The sensitivities and relative sensitivities of the output parameters (C_{peak}, T_{peak}, T_{MCL}) to the twelve input parameters ($K_d, q, \theta, \rho, D, D_L, D_w, K_s, \theta_s, \theta_r, \alpha, \beta$), corresponding to the BTCs given in Figures 7-1 to 7-12, are graphically presented in Figures 7-13 to 7-24. The breakdown of these figures is as follows:

- Figures 7-13 to 7-16 compare the output parameters and their sensitivities and relative sensitivities for each of the five models for the first four input parameters (K_d, q, θ, ρ), respectively;

- Figure 7-17 gives the output parameters and their sensitivities and relative sensitivities for the CHAIN Code for the input parameter, D; this figure is given for the purposes of completion;

- Figure 7-18 compares the output parameters and their sensitivities and relative sensitivities for each of the four models (CHAIN being excluded) for the dispersivity, D_L;

- Figure 7-19 compares the output parameters and their sensitivities and relative sensitivities for CHAIN 2D and HYDRUS for the diffusion coefficient in water, D_w;

- Figures 7-20 to 7-24 compare the output parameters and their sensitivities and relative sensitivities for each of the four models (CHAIN being excluded) for the five van Genuchten parameters ($K_s, \theta_s, \theta_r, \alpha, \beta$), respectively.

As shown in Section 4 for the simple model, $y = F(a,b,c,d,e,f)$, the relative sensitivity is a good measure for comparing output parameter sensitivity to changing input parameters. For this reason, Table 7-3 was constructed from the information contained in Figures 7-13 to 7-24. This table is a summary of the relative sensitivities for each of the three output parameters for the ^{99}Tc BTCs with respect to all the pertinent input parameters for each of the five models being tested. The relative sensitivities listed in the table are referenced to the base values of the input parameters given in Table 6-3. The results evident from Table 7-3 are as follows:

- The relative sensitivities are nearly the same for MULTIMED-DP 1.0 and FECTUZ for all output and input parameters;

- The relative sensitivities are nearly the same for CHAIN 2D and HYDRUS for all output and input parameters;

- The relative sensitivities are nearly the same for all models for the output parameters, T_{peak} and T_{MCL}, and all input parameters;
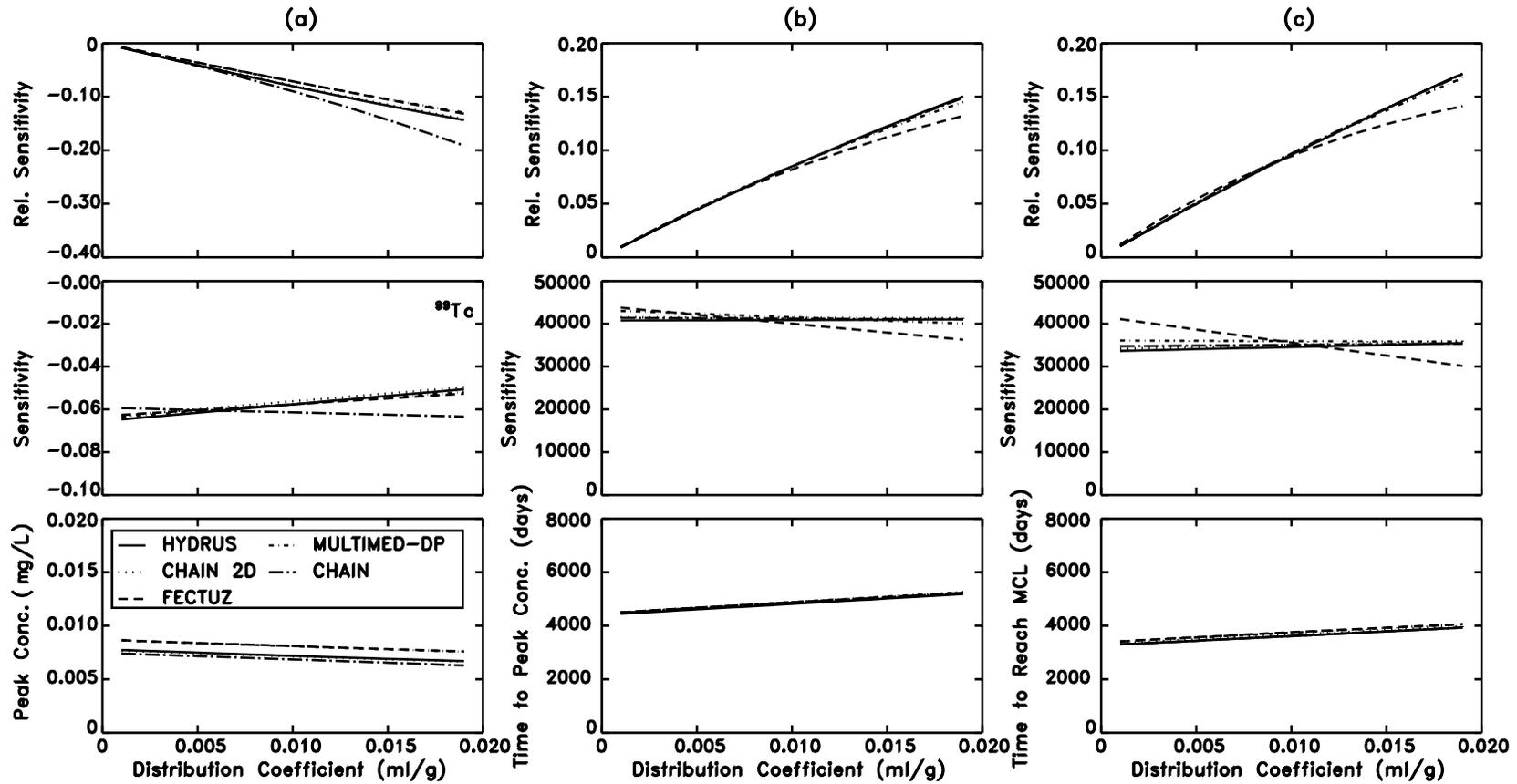
Figure 7-13. Sensitivity and relative sensitivity of (a) peak concentration at the depth of 6m, (b) time to reach peak concentration at the depth of 6m, and (c) time to exceed MCL at the receptor well to the distribution coefficient using the CHAIN, MULTIMED-DP 1.0, FECTUZ, CHAIN 2D and HYDRUS Models.
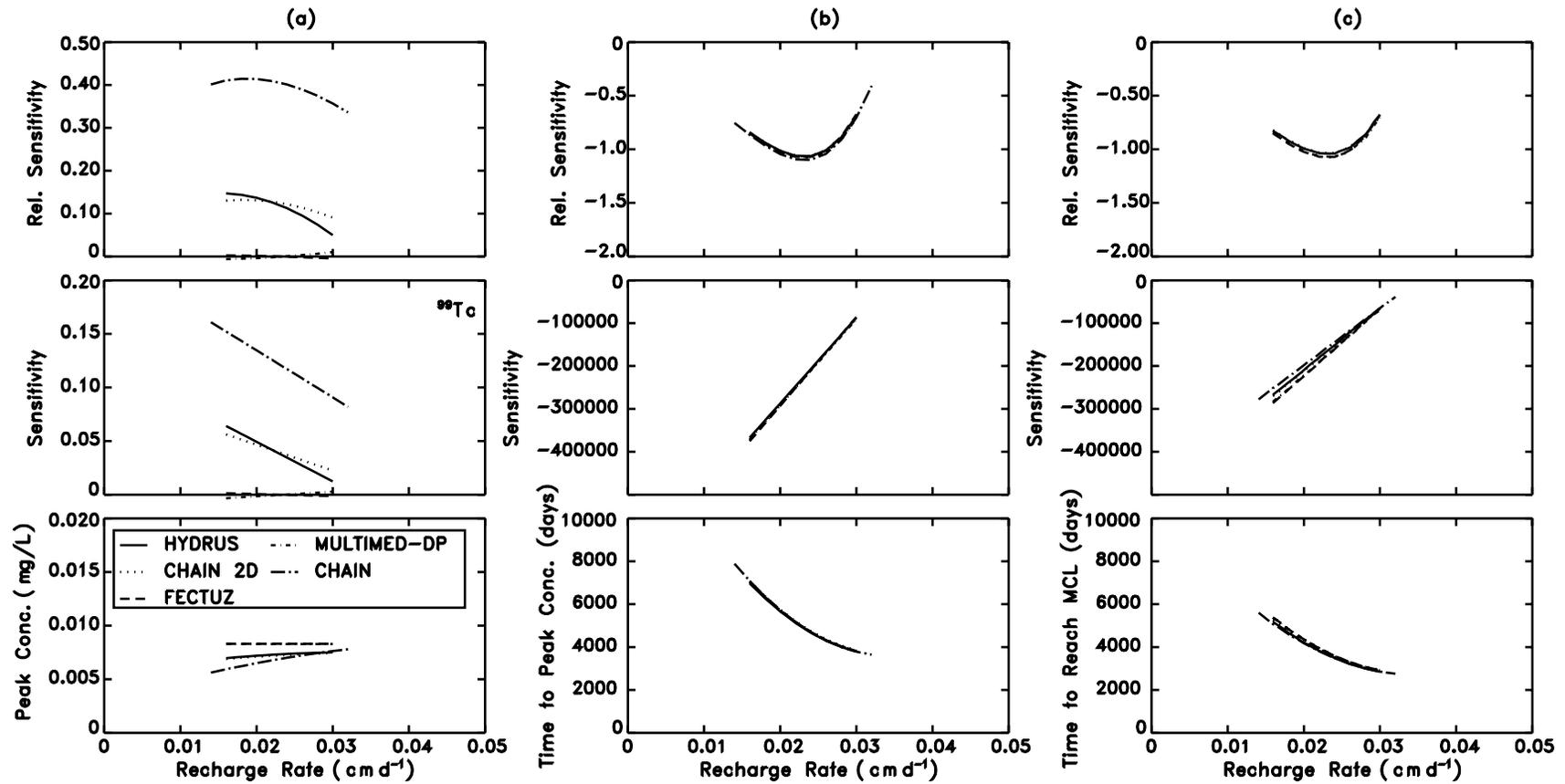
Figure 7-14. Sensitivity and relative sensitivity of (a) peak concentration at the depth of 6m, (b) time to reach peak concentration at the depth of 6m, and (c) time to exceed MCL at the receptor well to the recharge rate using the CHAIN, MULTIMED-DP 1.0, FECTUZ, CHAIN 2D and HYDRUS Models.
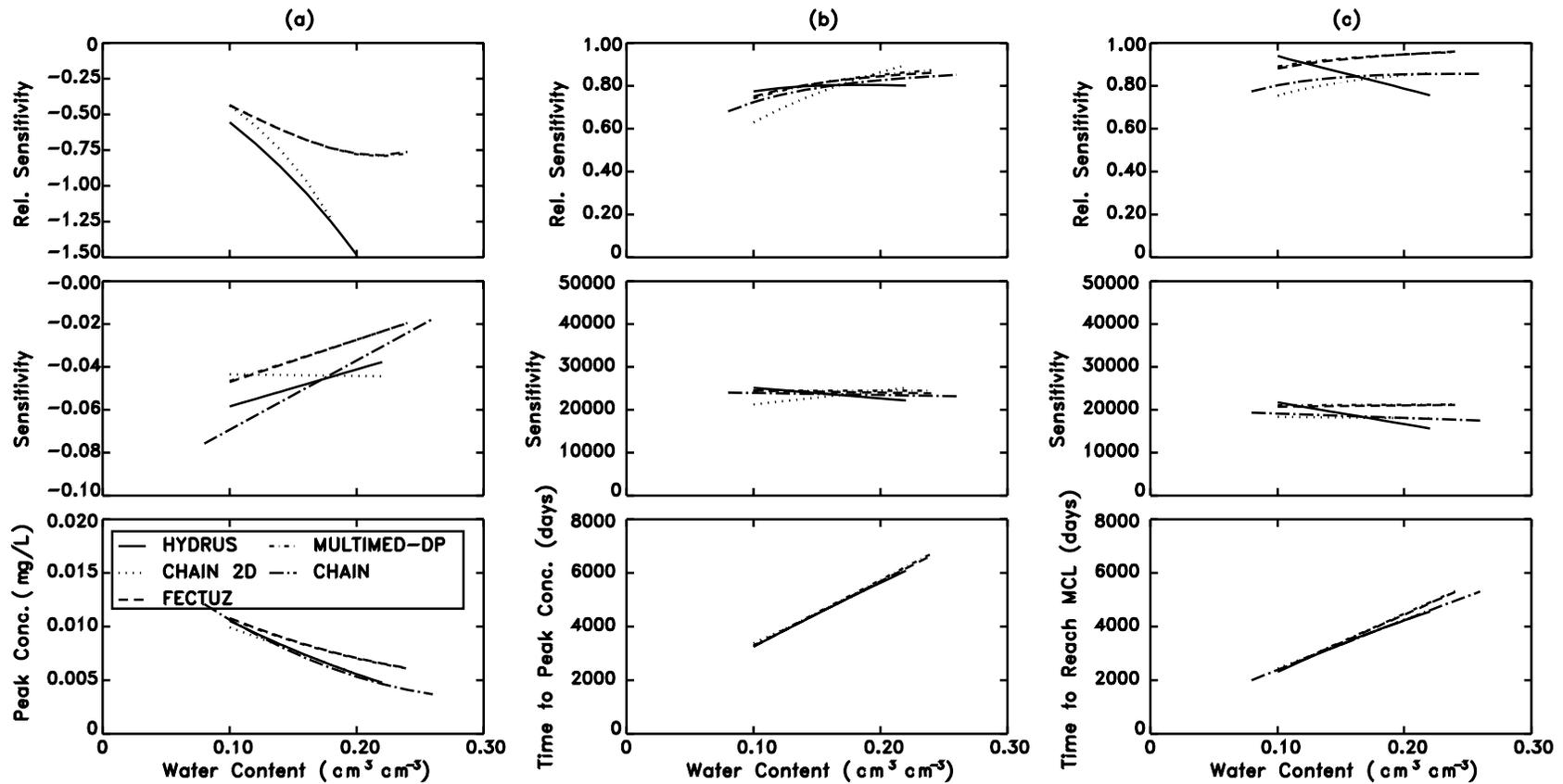
Figure 7-15. Sensitivity and relative sensitivity of (a) peak concentration at the depth of 6m, (b) time to reach peak concentration at the depth of 6m, and (c) time to exceed MCL at the receptor well to the water content using the CHAIN, MULTIMED-DP 1.0, FECTUZ, CHAIN 2D and HYDRUS Models.
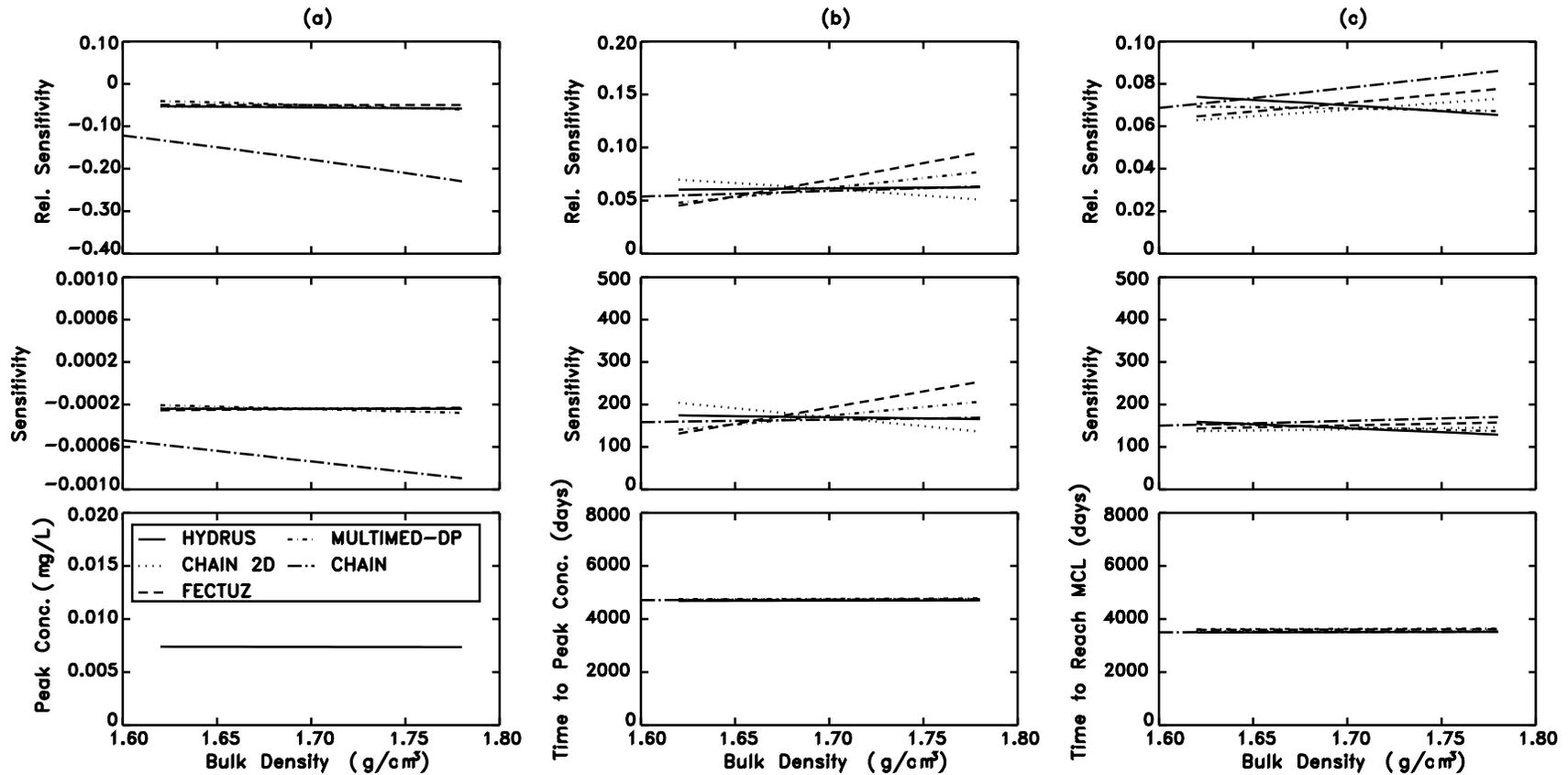
Figure 7-16. Sensitivity and relative sensitivity of (a) peak concentration at the depth of 6m, (b) time to reach peak concentration at the depth of 6m, and (c) time to exceed MCL at the receptor well to the bulk density using the CHAIN, MULTIMED-DP 1.0, FECTUZ, CHAIN 2D and HYDRUS Models.
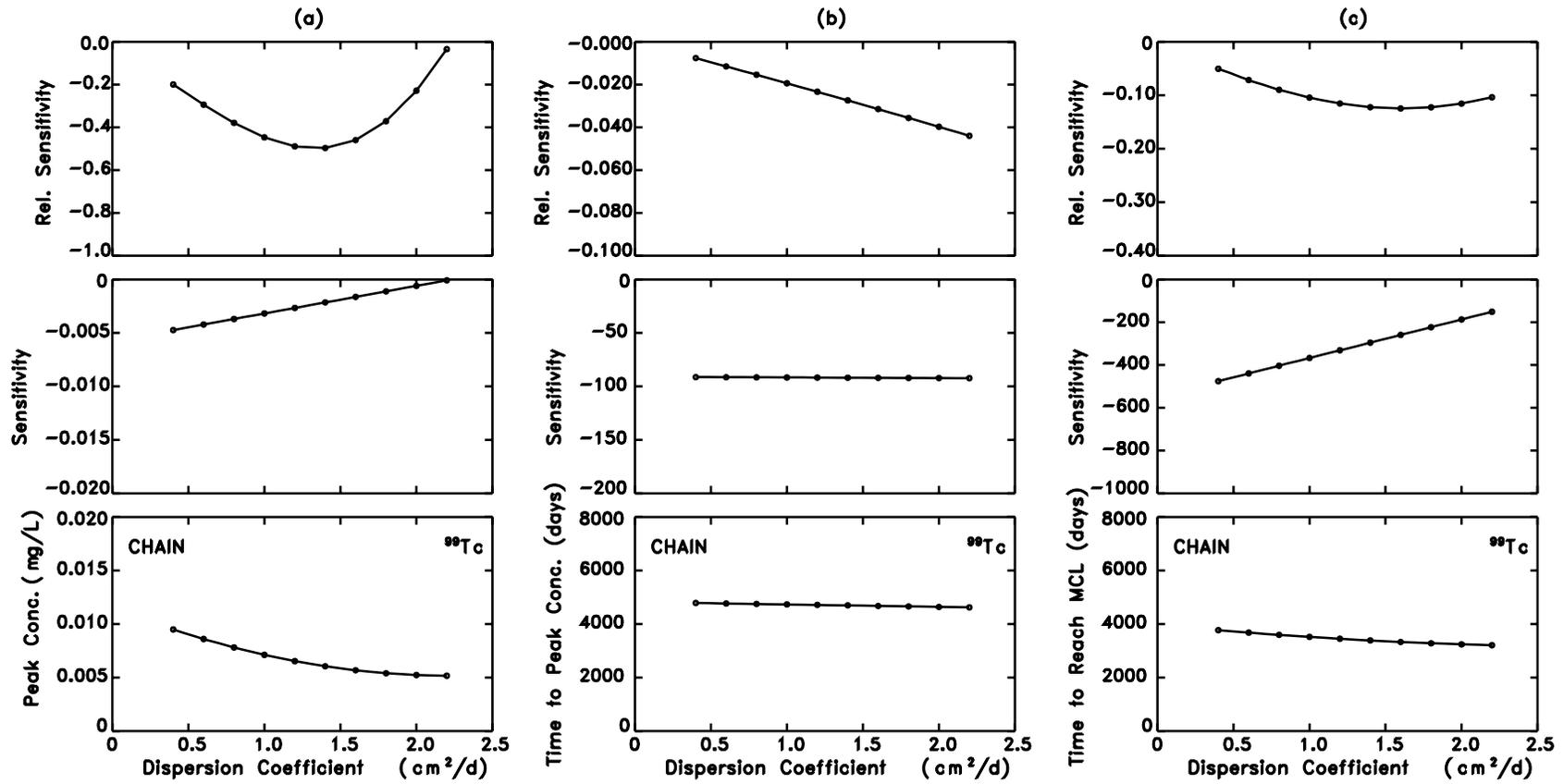
Figure 7-17. Sensitivity and relative sensitivity of (a) peak concentration at the depth of 6m, (b) time to reach peak concentration at the depth of 6m, and (c) time to exceed MCL at the receptor well to the dispersion coefficient using the CHAIN Model.
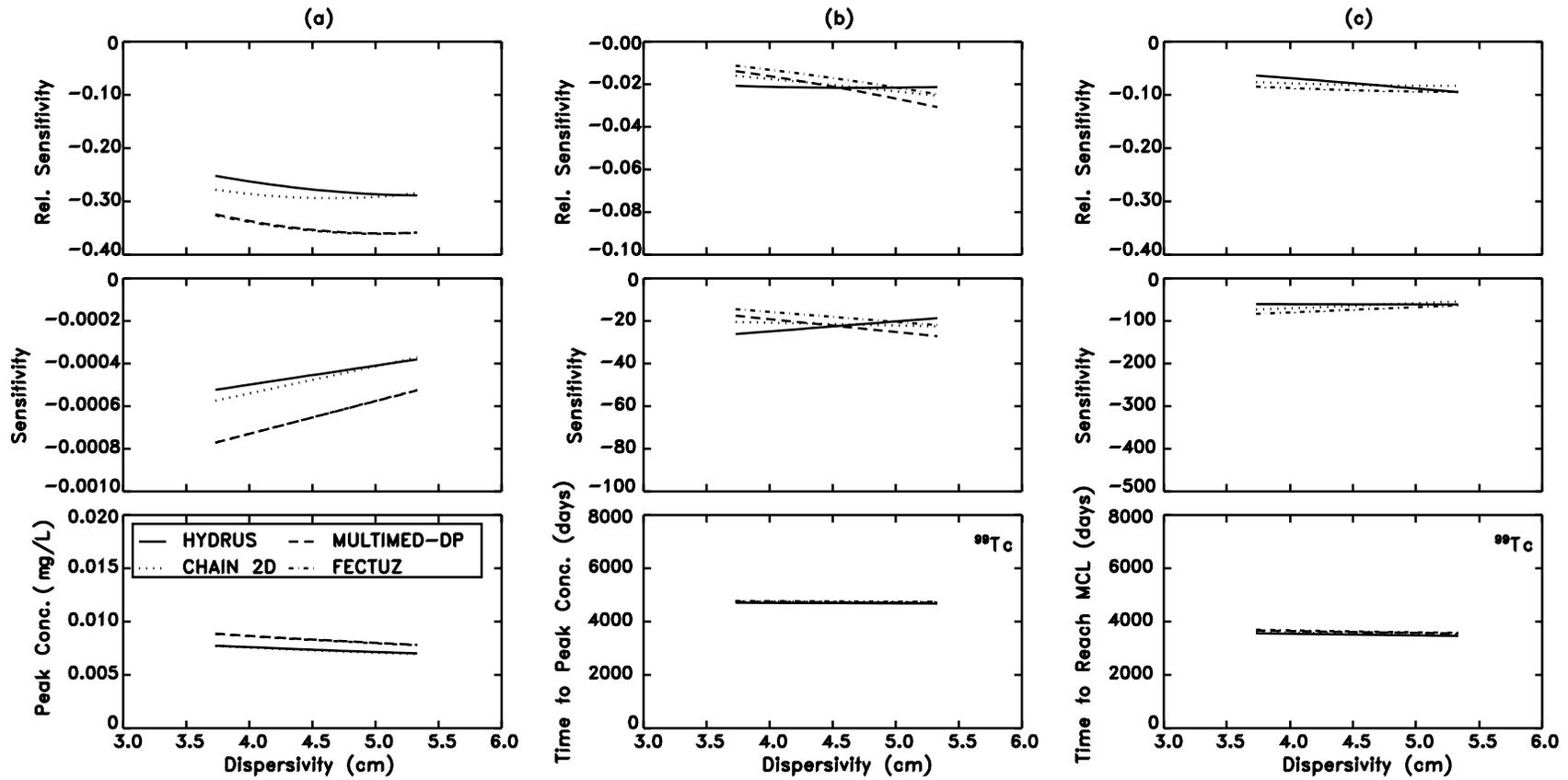
Figure 7-18. Sensitivity and relative sensitivity of (a) peak concentration at the depth of 6m, (b) time to reach peak concentration at the depth of 6m, and (c) time to exceed MCL at the receptor well to the dispersivity using the MULTIMED-DP 1.0, FECTUZ, CHAIN 2D, and HYDRUS Models.
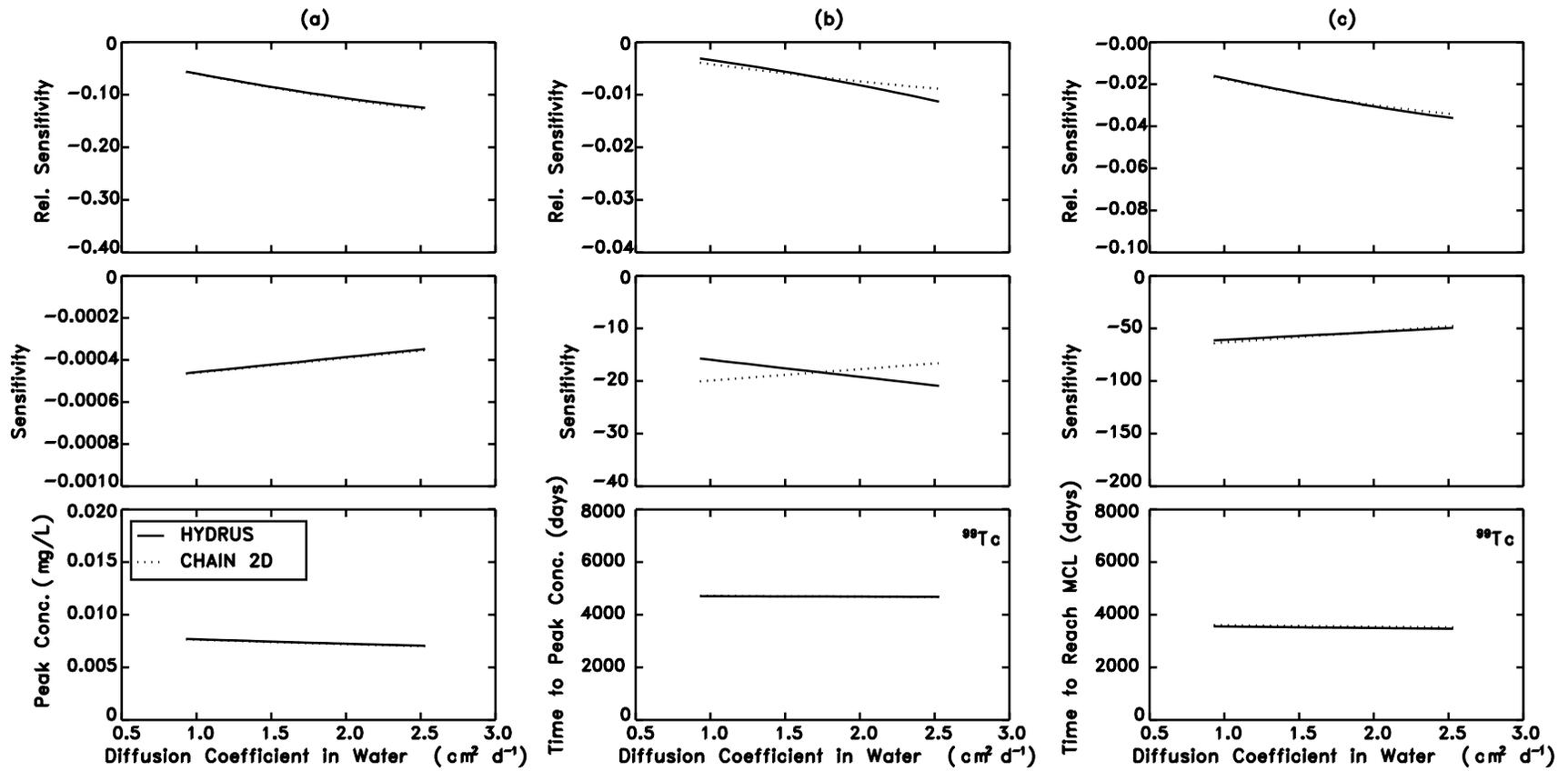
Figure 7-19. Sensitivity and relative sensitivity of (a) peak concentration at the depth of 6m, (b) time to reach peak concentration at the depth of 6m, and (c) time to exceed MCL at the receptor well to the diffusion coefficient in water using the CHAIN 2D and HYDRUS Models.
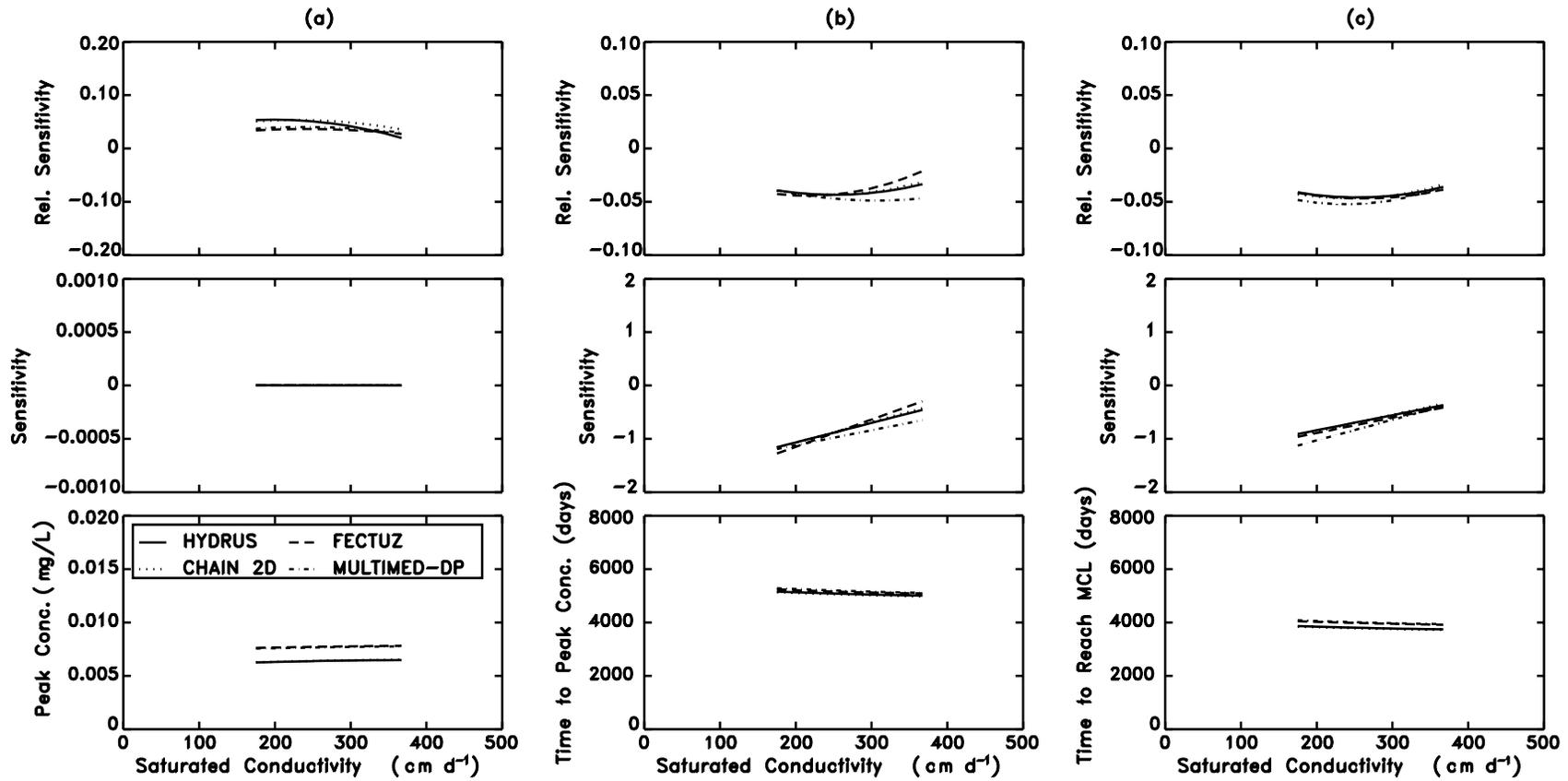
Figure 7-20. Sensitivity and relative sensitivity of (a) peak concentration at the depth of 6m, (b) time to reach peak concentration at the depth of 6m, and (c) time to exceed MCL at the receptor well to the saturated conductivity using the MULTIMED-DP 1.0, FECTUZ, CHAIN 2D, and HYDRUS Models.
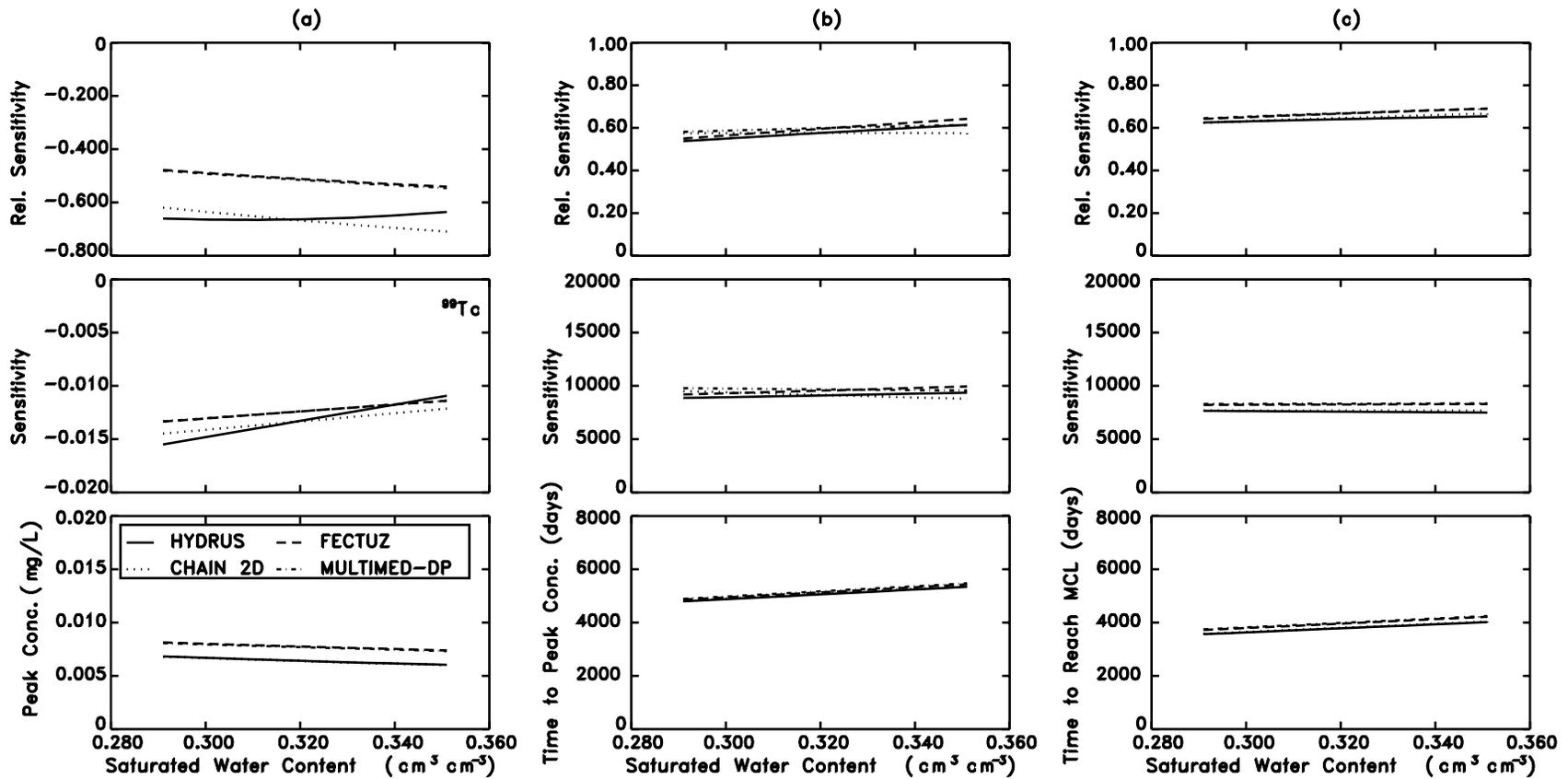
Figure 7-21. Sensitivity and relative sensitivity of (a) peak concentration at the depth of 6m, (b) time to reach peak concentration at the depth of 6m, and (c) time to exceed MCL at the receptor well to the saturated water content using the MULTIMED-DP 1.0, FECTUZ, CHAIN 2D, and HYDRUS Models.
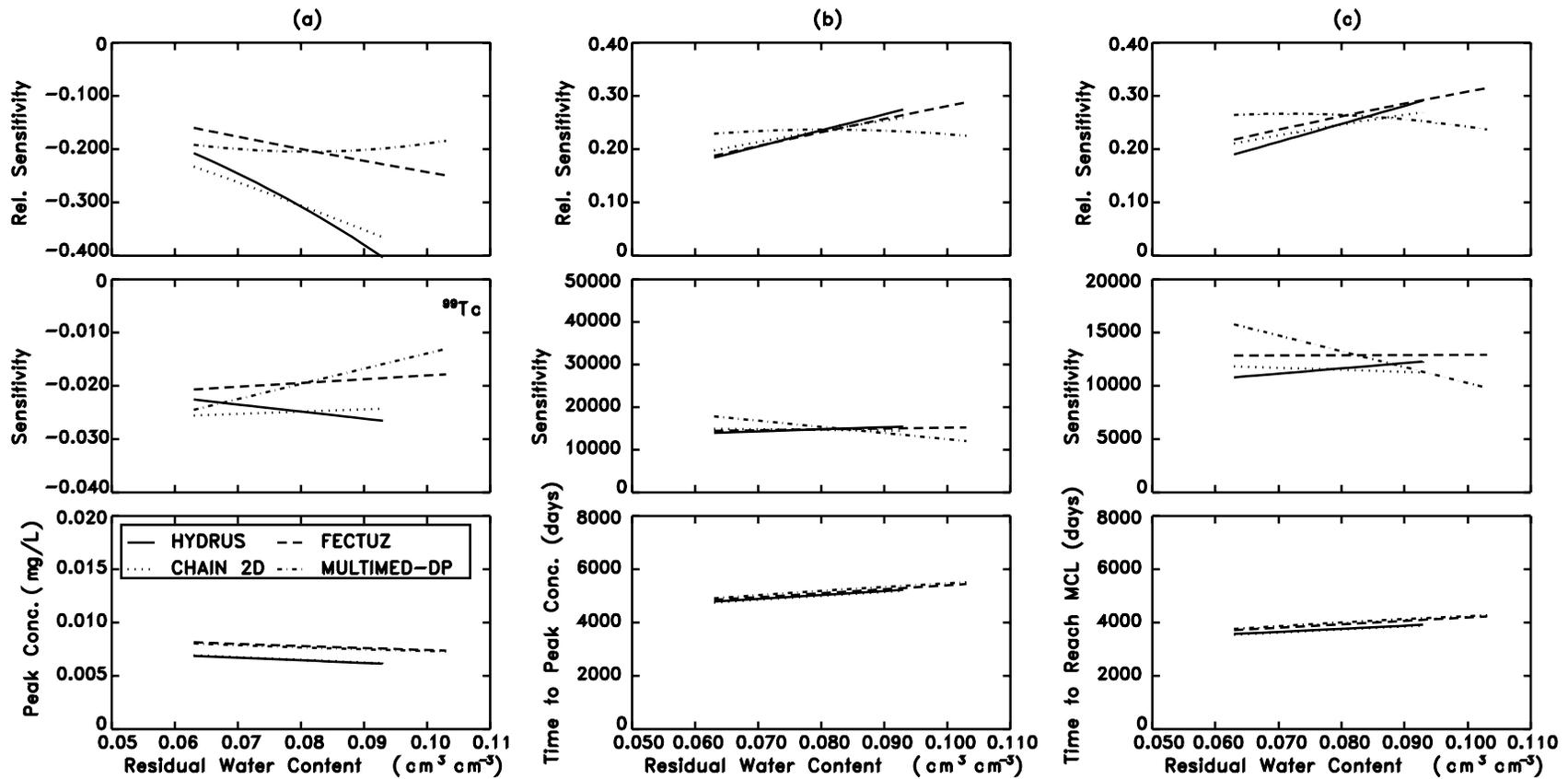
Figure 7-22. Sensitivity and relative sensitivity of (a) peak concentration at the depth of 6m, (b) time to reach peak concentration at the depth of 6m, and (c) time to exceed MCL at the receptor well to the residual water content using the MULTIMED-DP 1.0, FECTUZ, CHAIN 2D, and HYDRUS Models.
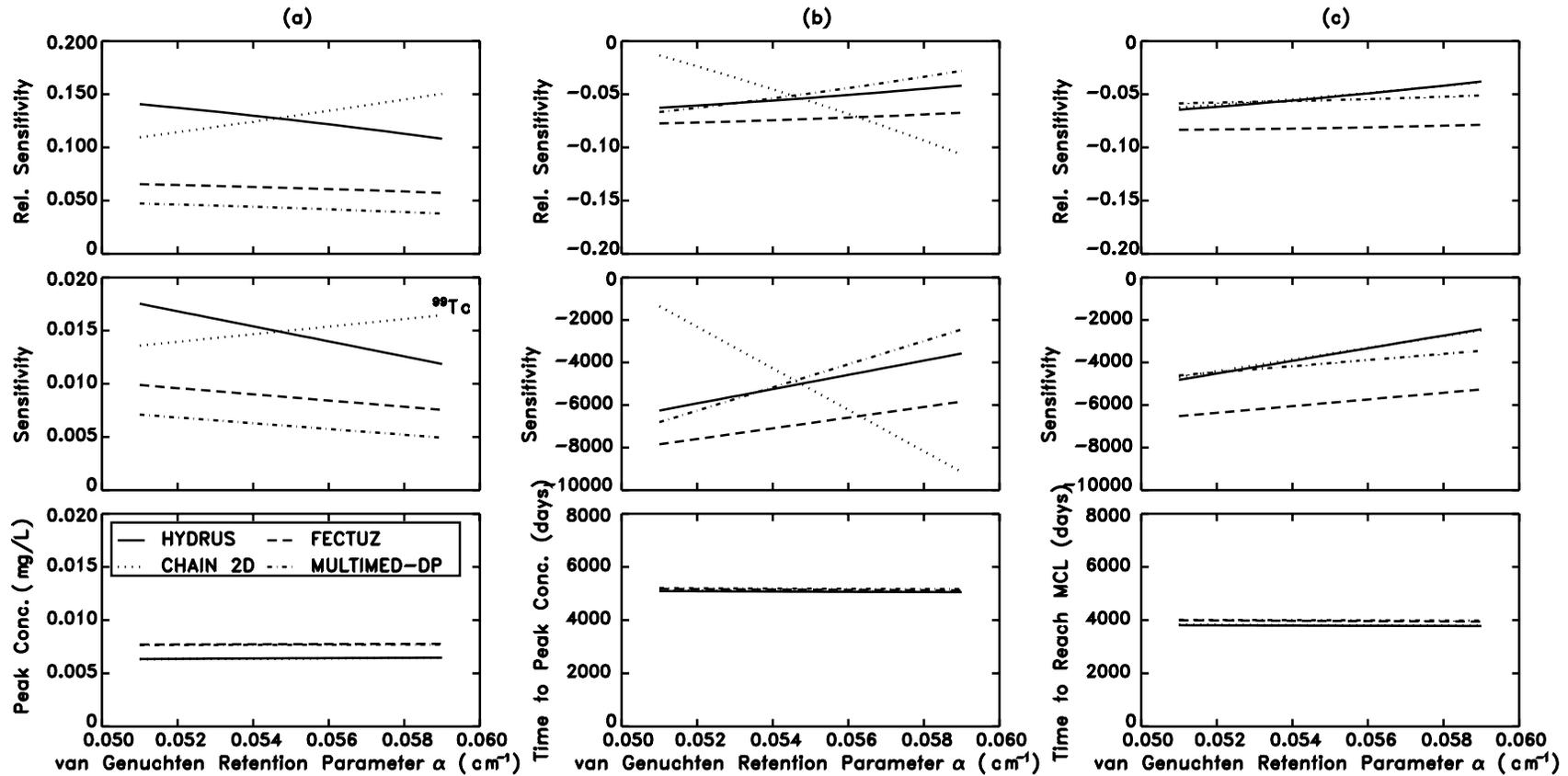
Figure 7-23. Sensitivity and relative sensitivity of (a) peak concentration at the depth of 6m, (b) time to reach peak concentration at the depth of 6m, and (c) time to exceed MCL at the receptor well to the van Genuchten retention parameter α using the MULTIMED-DP 1.0, FECTUZ, CHAIN 2D, and HYDRUS Models.
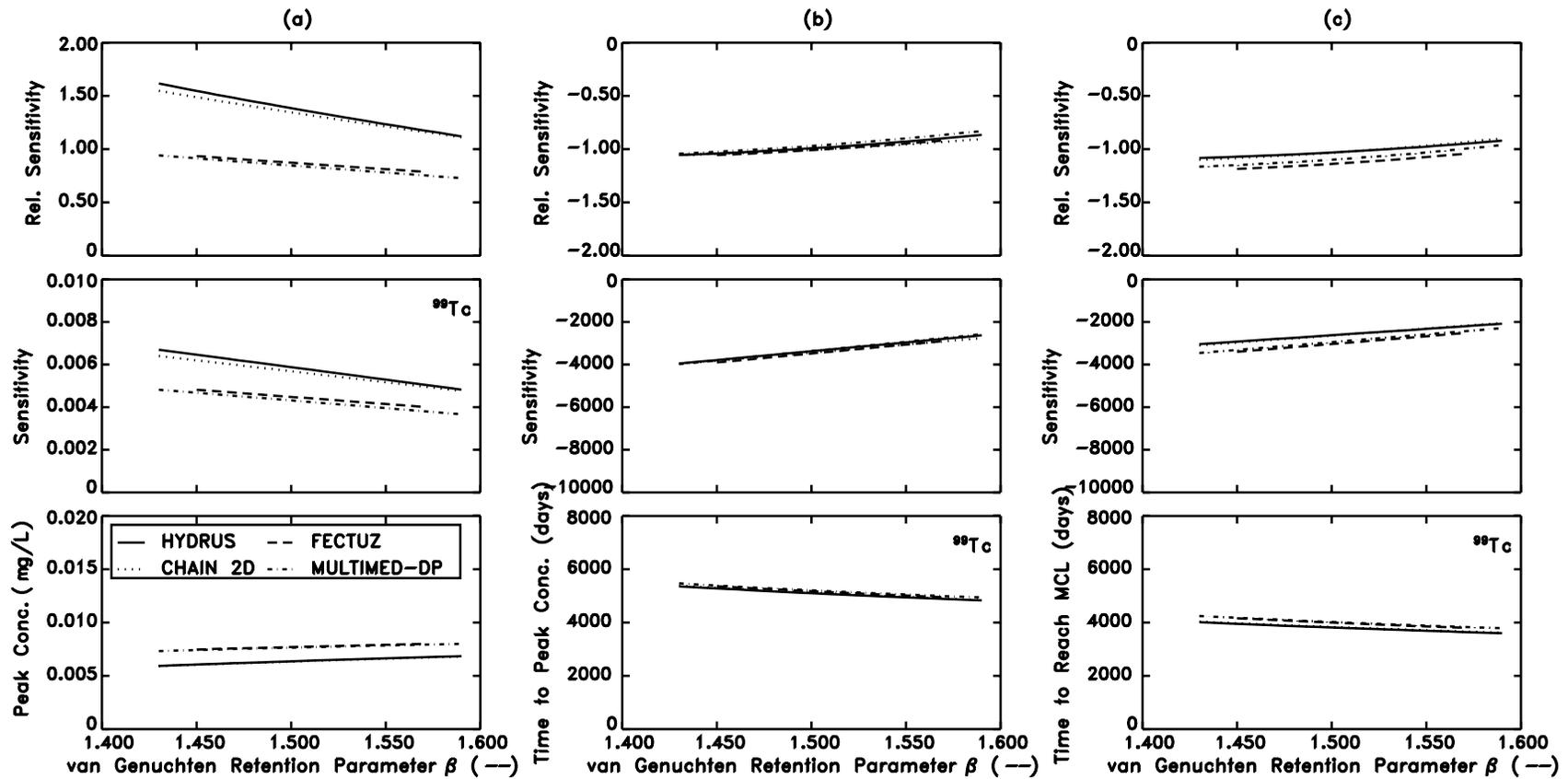
Figure 7-24. Sensitivity and relative sensitivity of (a) peak concentration at the depth of 6m, (b) time to reach peak concentration at the depth of 6m, and (c) time to exceed MCL at the receptor well to the van Genuchten retention parameter β using the MULTIMED-DP 1.0, FECTUZ, CHAIN 2D, and HYDRUS Models.

Table 7-3. Summary of Relative Sensitivities for the Outputs Obtained from the ^{99}Tc Breakthrough Curves with Respect to All the Pertinent Input Parameters for All Models, Referenced to the Base Values of the Input Parameters.

Model Input Parameter	C_{peak}					T_{peak}					T_{MCL}				
	CHAIN	MULTIMED-DP 1.0	FECTUZ	CHAIN 2D	HYDRUS	CHAIN	MULTIMED-DP 1.0	FECTUZ	CHAIN 2D	HYDRUS	CHAIN	MULTIMED-DP 1.0	FECTUZ	CHAIN 2D	HYDRUS
K_d	-0.06	-0.05	-0.05	-0.06	-0.06	+0.06	+0.06	+0.06	+0.06	+0.06	+0.07	+0.07	+0.07	+0.07	+0.07
q	+0.40	+0.00	+0.00	+0.12	+0.12	-1.10	-1.10	-1.10	-1.10	-1.10	-0.98	-1.00	-1.00	-0.98	-0.98
θ	-1.10	-0.62	-0.62	-0.90	-1.10	+0.80	+0.80	+0.81	+0.78	+0.80	+0.85	+0.92	+0.92	+0.84	+0.86
ρ	-0.17	-0.05	-0.05	-0.05	-0.05	+0.06	+0.06	+0.07	+0.06	+0.06	+0.08	+0.07	+0.07	+0.07	+0.07
D	-0.45	—	—	—	—	-0.02	—	—	—	—	-0.10	—	—	—	—
D_L	—	-0.36	-0.36	-0.29	-0.28	—	-0.02	-0.02	-0.02	-0.02	—	-0.09	-0.09	-0.07	-0.07
D_w	—	—	—	-0.10	-0.10	—	—	—	-0.01	-0.01	—	—	—	-0.03	-0.03
K_s	—	+0.04	+0.04	+0.05	+0.05	—	-0.05	-0.04	-0.04	-0.04	—	-0.05	-0.04	-0.04	-0.04
θ_s	—	-0.51	-0.51	-0.66	-0.66	—	+0.60	+0.60	+0.57	+0.57	—	+0.66	+0.66	+0.64	+0.64
θ_r	—	-0.20	-0.20	-0.29	-0.29	—	+0.22	+0.22	+0.22	+0.22	—	+0.26	+0.26	+0.24	+0.24
α	—	+0.05	+0.06	+0.13	+0.13	—	-0.05	-0.08	-0.05	-0.05	—	-0.06	-0.09	-0.05	-0.05
β	—	+0.86	+0.86	+1.30	+1.38	—	-1.00	-1.00	-1.00	-1.00	—	-1.13	-1.15	-1.03	-1.03

- For the output C_{peak}, there are some differences in the relative sensitivities between the CHAIN Model, the MULTIMED-DP 1.0 and FECTUZ Models, and the CHAIN 2D and HYDRUS Models;

- All output parameters for all models are rather insensitive to K_d and ρ, as one would expect for the ^{99}Tc BTCs as discussed in Section 6-2 (i.e., $\theta \gg \rho K_d$);

- Conversely, all output parameters for all models are rather sensitive to θ;

- The output parameters, T_{peak} and T_{MCL}, for all models are also rather sensitive to q, while output C_{peak} is much less sensitive to q, the sensitivity being model-dependent;

- For the van Genuchten parameters, the model output parameters are most sensitive to β, followed by θ_s, while the output parameters are least sensitive to K_s and α.

7.3 Other Results Illuminating Numerical Differences/Errors Between the Models

For the sensitivity modeling scenario employed in this report, the major differences between the models arose due to an error in coding, the use of different numerical inversion schemes (inversion from Laplace space to physical space), and the treatment of the dispersion factor, θD, in Equation (6-4).

7.3.1   *Correction of the MULTIMED-DP 1.0 Code*

When the van Genuchten Model for the water retention parameters $(K_s, \theta_s, \theta_r, \alpha, \beta)$ was considered in the sensitivity analysis depicted in Table 7-1, an error in the originally distributed MULTIMED-DP 1.0 Code was detected. This error arose from the solution of Darcy's Law for the pressure head, which gives the water content in the soil column through the use of the van Genuchten Model. Figure 7-25 shows the water content profiles in the 6m soil column derived from Darcy's Law for the MULTIMED-DP 1.0 and FECTUZ Codes, and from the steady-state solution of Richards Equation for the CHAIN 2D and HYDRUS Codes. The water contents obtained through the use of the originally distributed MULTIMED-DP 1.0 Code are inconsistent with respect to those obtained from the other three codes. The reason for the inconsistency was found to be the incorrect use of the residual water content, θ_r, in the van Genuchten Module. When this error was corrected, the new water content results became consistent with those of the other three models, as shown in Figure 7-25. Figure 7-25 also shows that the steady-state solution of the Richards Equation gives the same results as the solution of Darcy's Law, as we know it should from our discussion in Section 6-3.
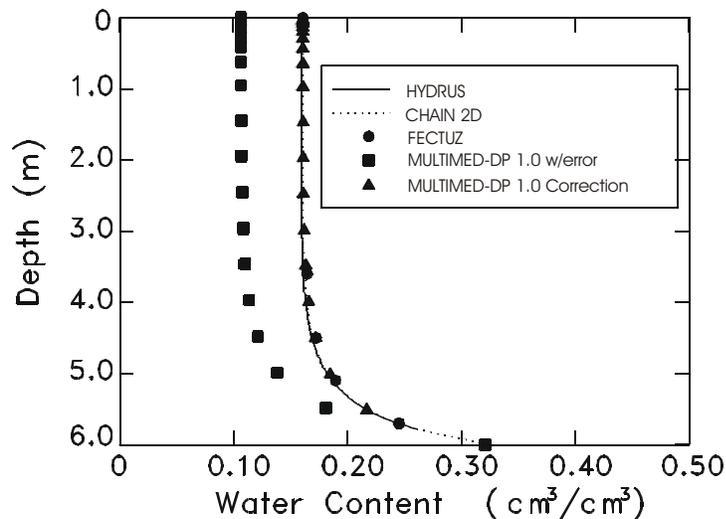
Figure 7-25.   Water content distributions predicted by the HYDRUS, CHAIN 2D, FECTUZ, and MULTIMED-DP 1.0 models. Note that the water contents (■) obtained from the originally distributed MULTIMED-DP 1.0 code are in error. The corrected code gives a consistent water content distribution (▲) with the other three models.

7.3.2 Comparison of the Stehfest and DeHoog Inversion Algorithms

All the major modules of the MULTIMED-DP 1.0 and FECTUZ Codes are the same (or nearly the same), except the MULTIMED-DP 1.0 Code has four alternate inverse transform modules (analytical, convolution, Stehfest, DeHoog), while the FECTUZ only uses the DeHoog Module. For the current uses of these codes, the analytical and convolution modules are not applicable. Thus, one may ask: Are there any differences between the Stehfest and DeHoog Algorithms? We found that the answer is **YES** to this question for the generation of ^{99}Tc BTCs using the MULTIMED-DP 1.0 Code.

The Stehfest Algorithm (Stehfest, 1970) produced non-realistic oscillations in the ^{99}Tc BTCs for most of the parameters studied in this report. The DeHoog Algorithm (DeHoog et al., 1982) is an improved inversion scheme which was developed to eliminate errors in the use of the analytical and convolution algorithms and to reduce the oscillatory conditions often produced by the Stehfest Algorithm. We compared the ^{99}Tc BTCs produced by the Stehfest and DeHoog Algorithms in the MULTIMED-DP 1.0 Code for several different input parameters. The following results were evident from this study:

- For all input parameters tested, the Stehfest Algorithm produced oscillatory behavior and peak concentrations lower than those produced by the DeHoog Algorithm;

- For all input parameters tested, the DeHoog Algorithm produced ^{99}Tc BTCs almost identical to those produced by the FECTUZ Code;

- As an example of this comparison, Figure 7-26 shows the ^{99}Tc BTCs for θ = 0.08, 0.16, 0.22, where (a) illustrates the oscillatory behavior of the Stehfest Algorithm in MULTIMED-DP 1.0, (b) illustrates the corrective behavior of the DeHoog Algorithm in MULTIMED-DP 1.0, and (c) indicates the near perfect comparison between the FECTUZ and MULTIMED-DP 1.0 Codes, when the DeHoog Algorithm is used.

7.3.3. Increasing the Base Value of Dispersivity in the FECTUZ Code

As we have previously discussed, CHAIN only specifies the value for D in the dispersion factor, θD, in Equation (6-4), while MULTIMED-DP 1.0 and FECTUZ only specify the value for D_L. CHAIN 2D and HYDRUS specify both D_L and D_w. Since the recharge rate, q, is so small in our sensitivity modeling scenario, there is a significant difference between the base value of θD for MULTIMED-DP 1.0 and FECTUZ, and that for CHAIN 2D and HYDRUS (see the fourth row of Table 7-2). This effect was evident in the ^{99}Tc BTC curves shown in Figures 7-1 to 7-12, where the peak concentrations from MULTIMED-DP 1.0 and FECTUZ were higher than those of CHAIN 2D and HYDRUS. To see if this difference was primarily due to θD, we increased the base value of D_L in FECTUZ to 6.53 cm. This gives a value of θD for FECTUZ of 0.157 cm^2/d, versus that of 0.160 cm^2/d for CHAIN and 0.162 cm^2/d for CHAIN 2D and HYDRUS. Figure 7-27 compares the ^{99}Tc BTCs for the base parameters for the HYDRUS, CHAIN 2D and CHAIN Models versus the ^{99}Tc BTC for the FECTUZ Model with the base value of D_L = 4.53 cm replaced by the value D_L = 6.53 cm. This comparison proves that the major differences between the model BTCs in Figures 7-1 to 7-12 are due to the formulation of the dispersion factor, θD, and **not to other factors**.
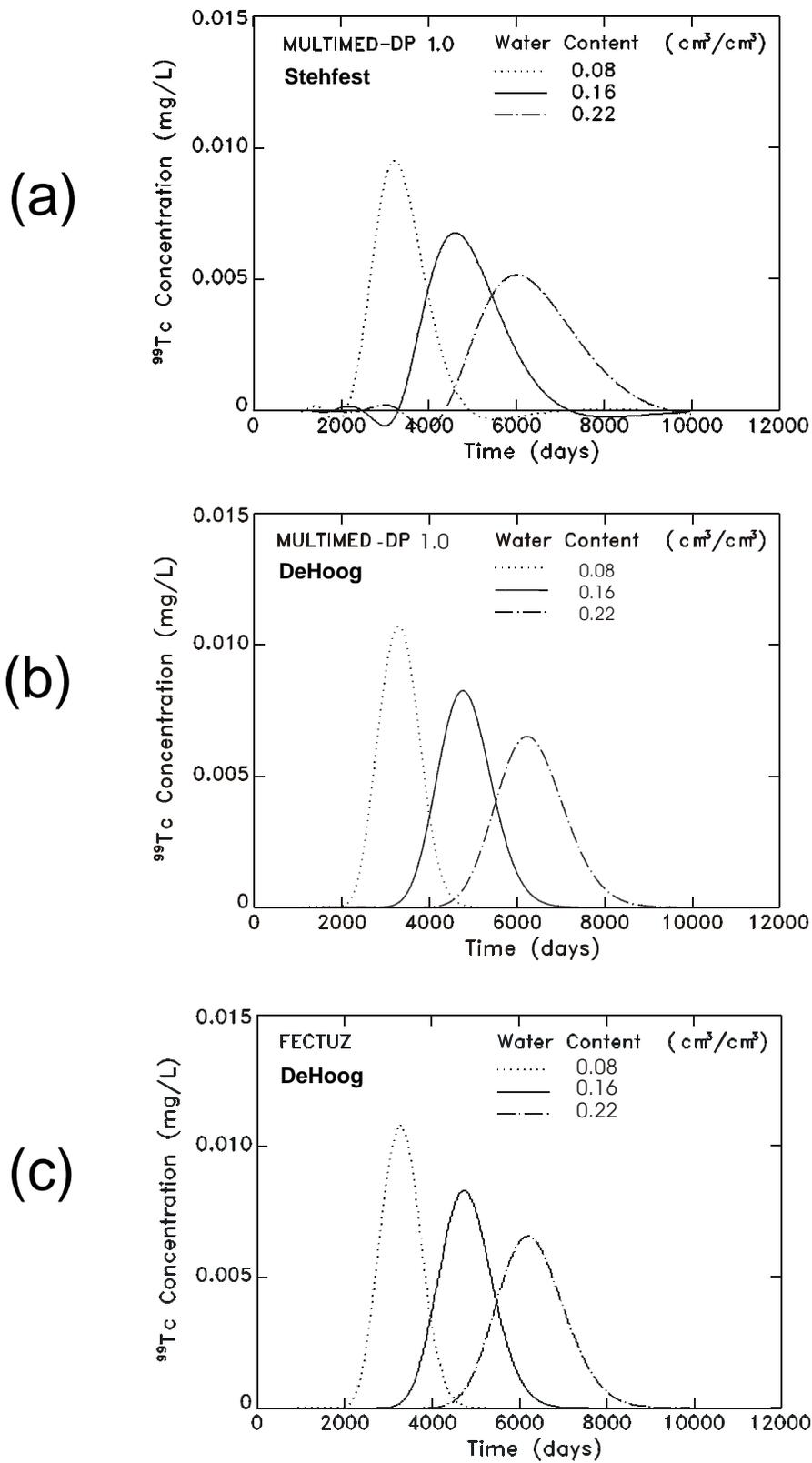
Figure 7-26. Sensitivity of ^{99}Tc BTCs at 6m depth to water content, where (a) uses Stehfest Algorithm of MULTIMED-DP 1.0, (b) uses DeHoog Algorithm of MULTIMED-DP 1.0, and (c) uses DeHoog Algorithm of FECTUZ Code.
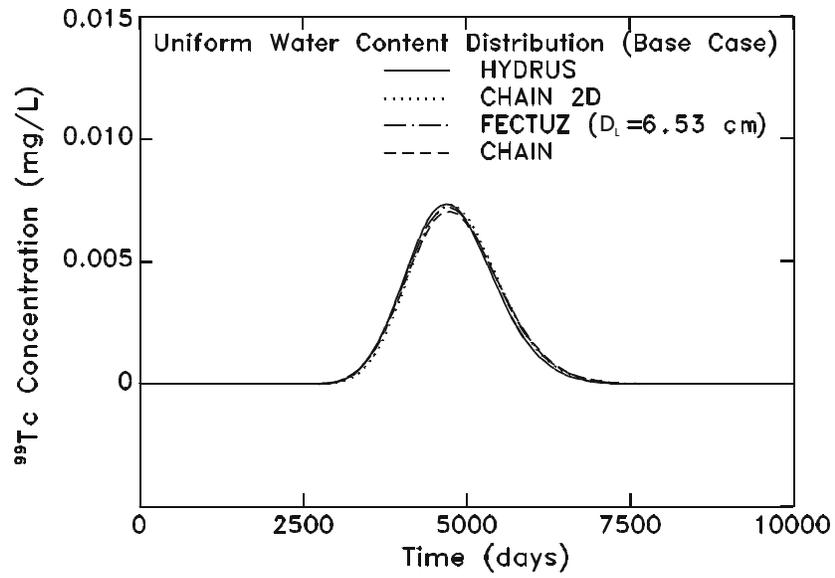
Figure 7-27. Comparison of the ^{99}Tc BTCs for the HYDRUS, CHAIN 2D and CHAIN Models for the base values of the input parameters with the BTC for the FECTUZ Model with the base value of $D_L = 4.53$ cm replaced by the value $D_L = 6.53$ cm.

Section 8
Summary and Conclusions

The *purpose of this report* was to evaluate and perform sensitivity analyses on select computer models for simulating radionuclide fate and transport in the unsaturated zone. The work reported here was performed in support of the U.S. Environmental Protection Agency's (EPA's) project on Soil Screening Guidance (SSG) for Radionuclides (U.S. EPA, 2000ab). The U.S. EPA developed the SSG as a tool to help standardize and accelerate the evaluation and cleanup of soil contaminated with radioactive materials at sites on the National Priority List (NPL) with future residential land use. This guidance is intended for the appropriate environmental professionals to be able to calculate risk-based, site-specific, soil screening levels (SSLs) for radionuclides in soil, thus allowing them to identify areas needing further investigation and possible remediation at NPL sites. The models reviewed and evaluated in the current report form a small subset of the models available to the public, and those which are considered here have not met U.S. EPA approval for exclusive use in the SSL process. Other models may be applicable to the SSL effort, depending on pollutant- and site-specific circumstances.

The *model selection process* for the radionuclide SSL effort is briefly described in Section 2.1, and resulted in the following five models being chosen for evaluation and sensitivity analysis:

- One-dimensional CHAIN Code (van Genuchten, 1985),
- One-dimensional MULTIMED-DP 1.0 Code (Liu et al., 1995; Sharp-Hansen et al., 1995; Salhotra et al., 1995)
- One-dimensional FECTUZ Code (U.S. EPA, 1995ab),
- One-dimensional HYDRUS Code (Šimúnek et al., 1998),
- Two-dimensional CHAIN 2D Code (Šimúnek and van Genuchten, 1994).

The CHAIN Code is an analytical model which requires the assumption of uniform flow conditions. The MULTIMED-DP 1.0 and FECTUZ Codes are semi-analytic models which approximate complex analytical solutions using numerical methods such as numerical inverse transform modules. Transient and steady-state conditions can be accommodated in both the analytical and semi-analytical models, while layered media are usually only accommodated by the semi-analytical codes. The HYDRUS and CHAIN 2D Codes solve the pertinent sets of partial differential equations using finite-difference or finite-element methods. The resolution in space and time of these numerical models depends on the physical characteristics of the site in question, the computational resources available to the modeler, and the purposes of the simulation. Numerical codes are used when simulating time-dependent scenarios under spatially varying soil conditions and unsteady flow fields. Table 2-1 lists, in a comparative manner, the flow and transport model components of each of the five models. Further explanation of the model components is given in Appendices A to D.

Computer model predictions are uncertain and erroneous because of *uncertainties and errors* that can occur at various points in the modeling process and in the model's structure. Errors can occur in conceptualization or model structure when processes and the assumptions represented by the model fail to represent the intended reality of the physical problem at hand. Errors in experimental measurements of model input parameters and model output parameters used for calibration and testing can also lead to uncertainties. For numerical computer codes, the discretization in space and time introduces error; the computer, itself, introduces roundoff error; and truncation errors are produced whenever analytical expressions are replaced by truncated series of elementary functions. Other errors and uncertainties result from the imprecise specification of boundary and initial conditions, poor model parameterization, and incorrect spatial scale transitions (see Section 1.3). These uncertainties and errors lead to a three-tier sensitivity analysis:

- Sensitivity of simulated results to conceptual model selection (Section 3),
- Model output parameter sensitivity to varying model input parameters (Sections 4 to 6),
- Comparison of sensitivity results due to numerical differences and errors (Section 7).

The breadth and depth of the ***variability and heterogeneity of the phenomena*** that can occur in the fate and transport of radionuclides in the unsaturated zone are briefly considered in Section 3 of this report. Phenomena considered include the following: the selection of a physical problem's time/space domain, the choice of boundary and initial conditions for the flow and transport variables, the potential impacts of hysteretic effects and density and thermal gradients, the importance of preferential pathways and facilitated transport, the form of the transport dispersion processes, the impacts of non-ideal sorption and reaction processes, the importance of decay processes and the evolution of decay products, the influence of multicomponent and multiphase systems, and the effects of highly heterogeneous media. Against this backdrop, the five selected models were compared (see Table 2-1). All of the models are deterministic, and thus, are incapable of stochastic simulation, except for Monte Carlo simulations for certain input parameter or boundary condition distributions. Four of the five models are one-dimensional and only CHAIN 2D is two-dimensional. Thus, truly three dimensional features cannot be easily, or even correctly, simulated, except for idealistic features such as those presented in Figure 3-1. Density gradient problems cannot be addressed by these models, nor can facilitated transport and preferential pathways. The scale dependency of hydraulic conductivity and dispersivity due to soil heterogeneities is not considered by these models. Other processes and features that are not addressed by these models are nonlinear reactions, nonlinear nonequilibrium sorption, nonequilibrium site heterogeneity, and variable decay processes. To address precipitation/evapotranspiration/infiltration processes on a storm event basis for the several-year periods required for some radionuclides will require extensive computational resources for the models in this group which are capable of performing such simulations. Appendices E to I present the sensitivity results of the various models to the following conceptualizations, given respectively as: nonuniform moisture distribution versus uniform moisture distribution, daily variation of precipitation/evaporation/infiltration versus annual recharge rate, layered soil column versus homogeneous soil column, nonequilibrium sorption of pollutants versus equilibrium sorption of pollutants, and variations in fate and transport of radionuclides with different distribution coefficients and half-lives.

The ***basic elements of parameter sensitivity analysis*** are defined and illustrated in Section 4. To carry out this analysis for radionuclides in the unsaturated zone realistically requires the characteristics and properties from a representative physical site. The site selection process and the choice of the candidate site are given in Sections 5.1 and 5.2, respectively. The candidate site, located in the semi-arid West, is the Las Cruces Trench Research Site in New Mexico. Some of the soil hydraulic properties at this site and other site characteristics are given in Tables 5-2 and 5-3 and Figure 5-2. The hypothetical modeling scenario for this site assumed a step-wise constant source of radionuclides at the top of a 6m, vertical, homogeneous soil column with a zero concentration gradient at the bottom of the column. The input parameters (the base values given in Table 5-4) and the output parameters used in the sensitivity analyses are as follows:

Input Parameters

K_d	=	Distribution Coefficient	D_w	=	Diffusion Coefficient in Water
q	=	Recharge Rate	K_s	=	Saturated Hydraulic Conductivity
θ	=	Soil Water Content	θ_s	=	Saturated Water Content
ρ	=	Bulk Density	θ_r	=	Residual Water Content
D	=	Dispersion Coefficient	α	=	van Genuchten Retention Parameter
D_L	=	Dispersivity	β	=	van Genuchten Retention Parameter

Output Parameters

C_{peak} = Peak Concentration of Radionuclide BTC at 6m.
T_{peak} = Time to Reach Peak Concentration at 6m.
T_{MCL} = Time When Radionuclide Concentration at 6m is High Enough to Exceed MCL at Receptor Well

Section 6 presents the parameter sensitivity analysis results for the ^{99}Tc breakthrough curves (BTCs) at the bottom of the 6m, vertical, homogeneous soil column, where the BTCs were generated by the HYDRUS Code. The BTCs for the eleven input parameters ($K_d,q,\theta,\rho,D_L,D_w,K_s,\theta_s,\theta_r,\alpha,\beta$) are given in Figure 6-1, where the BTCs for the first six input parameters ($K_d,q,\theta,\rho,D_L,D_w$) were obtained under the constraints of constant recharge rate, q, and

constant moisture content, θ, while those for the last five parameters ($K_s,\theta_s,\theta_r,\alpha,\beta$) were obtained under the constraints of constant recharge rate, q, and variable soil water content, $\theta(z)$, see Sections 6.2 and 6.3, respectively. The sensitivity and relative sensitivity results for these BTCs are given in the following figures:

- Figures 6-2a to 6-2k; for C_{peak};
- Figures 6-3a to 6-3k; for T_{peak};
- Figures 6-4a to 6-4k; for T_{MCL}.

Table 6-4 summarizes the relative sensitivities of (C_{peak}, T_{peak}, T_{MCL}) to the eleven input parameters for the HYDRUS Code, the sensitivities being measured at the base values of the input parameters. The dominant input parameters for all three output parameters are those which have the greatest influence on the advection term in the transport equations, followed by those which have the greatest influence on the dispersion term. The parameters, ρ and K_d, have a very small influence on the transport and fate of ^{99}Tc since $\theta \gg \rho K_d$ in the coefficients of the transport equations. For the first six input parameters ($K_d,q,\theta,\rho,D_L,D_w$), C_{peak} is most influenced by θ, while T_{peak} and T_{MCL} are most influenced by both θ and q. For the last five input parameters (from the van Genuchten Model, $K_s,\theta_s,\theta_r,\alpha,\beta$), the most influential input parameter for all three output parameters is β, followed by θ_s, then followed by θ_r, α, and K_s.

Section 7 compares the ***sensitivity results between the five models***, illuminating numerical differences and errors. The numerical differences and errors separating the five models are summarized in Table 8-1. Each set of sensitivity results are derived for the 6m, vertical, homogeneous soil column; and the first seven input parameters ($K_d,q,\theta,\rho,D,D_L,D_w$) are compared under the constraints of constant recharge rate, q, and constant water content, θ. The last five input parameters ($K_s,\theta_s,\theta_r,\alpha,\beta$) are compared under the constraints of constant recharge rate, q, and variable water content, $\theta(z)$. Figures 7-1 to 7-12 compare the ^{99}Tc BTCs at the bottom of the 6m soil column for the various models and input parameters, while Figures 7-13 to 7-24 compare the sensitivities and relative sensitivities of (C_{peak}, T_{peak}, T_{MCL}) to the twelve input parameters for the various models. The breakdown of these various figures with reference to input parameters and models is given in Table 8-2. The results derived from these figures and calculations are as follows:

- The BTCs for the CHAIN 2D and HYDRUS Codes are nearly the same for all input parameter values considered.
- For the input parameters (K_d,q,θ,ρ), the CHAIN BTCs are fairly close to those for CHAIN 2D and HYDRUS.
- The BTCs for the MULTIMED-DP 1.0 and FECTUZ Codes are almost identical for all values of the input parameters considered.
- For the base values of (K_d,q,θ,ρ,D_L), the concentration peaks of the MULTIMED-DP 1.0 and FECTUZ BTCs are about 14% higher than those for CHAIN 2D and HYDRUS, because of the differences in the dispersion factor, θD, as given in Table 8-1.
- For the base values of the van Genuchten parameters ($K_s,\theta_s,\theta_r,\alpha,\beta$), the concentration peaks of the MULTIMED-DP 1.0 and FECTUZ BTCs are about 21% higher than those of CHAIN 2D and HYDRUS, for the reason given above.
- When the base value of D_L is increased to compensate for the absence of $\theta\tau_w D_w$ in θD (see Table 8-1), FECTUZ and MULTIMED-DP 1.0 peak concentrations of the BTCs closely approach those of CHAIN 2D and HYDRUS (see Figure 7-27).
- The relative sensitivities are nearly the same for MULTIMED-DP 1.0 and FECTUZ for all output parameters and all input parameters.
- The relative sensitivities are nearly the same for CHAIN 2D and HYDRUS for all output parameters and all input parameters.
- The relative sensitivities are nearly the same for outputs (T_{peak}, T_{MCL}) for all models and all input parameters.
- For the output (C_{peak}), there are some differences in the relative sensitivities for the three groups of models: CHAIN, MULTIMED-DP 1.0 and FECTUZ, CHAIN 2D and HYDRUS.
- All output parameters for all models are rather insensitive to K_d and ρ, as one would expect for the ^{99}Tc BTCs since $\theta \gg \rho K_d$ in the coefficients of the transport equations. This will not be the case for higher K_d radionuclides.
- Conversely, all output parameters for ^{99}Tc BTCs are rather sensitive to θ for all models.
- The output parameters (T_{peak}, T_{MCL}) for all models are also rather sensitive to q, while C_{peak} is much less sensitive to q, the sensitivity being model-dependent.

Table 8-1. The Possible Numerical Differences and Errors (●) Separating the Five Models Tested for Water Flow and Radionuclide Transport through the 6m, Vertical, Homogeneous Soil Column.

Numerical Differences and Errors	Models Tested in Report				
	CHAIN	MULTIMED-DP 1.0	FECTUZ	CHAIN 2D	HYDRUS
Computer Roundoff Errors	●	●	●	●	●
Analytical Solution Truncation Errors for Transport Equations	●				
Inverse Transform Scheme Errors for Laplace Space Analytical Solutions of Transport Equations		●	●		
Finite Difference/Finite Element Solution Errors for Transport Equations				●	●
Constant Recharge Rate, q, and Constant Water Content, θ	●	●	●	●	●
Constant Recharge Rate, q, and Variable Water Content, $\theta(z)$		●	●	●	●
Numerical Integration Errors of Darcy's Law		●	●		
Numerical Integration Errors of Richards Equation				●	●
Numerical Errors in Deriving the Steady State Solution of Richards Equation				●	●
Specification of $\theta D = \theta \tau_w D_w + D_L \lvert q \rvert$ in the Transport Equations	Specifies only D	Specifies only D_L	Specifies only D_L	Specifies both D_L and D_w	Specifies both D_L and D_w
Possible Numerical Diffusion in the Transport Equations				●	●

- For the van Genuchten parameters ($K_s, \theta_s, \theta_r, \alpha, \beta$), the model output parameters are most sensitive to β, followed by θ_s, while the output parameters are least sensitive to K_s and α.
- Numerical diffusion for the current modeling scenario is rather insignificant (see Figure 7-27) since the D_L-adjusted FECTUZ BTCs (a model with no numerical diffusion) correspond closely to those for CHAIN 2D and HYDRUS, models which may have numerical diffusion.
- The strongest discriminating differences (see Table 8-1) between the five models are those due to the form of θD, and those due to the uniform/nonuniform water content. Other numerical differences/errors appear to be of lower order effect for the current modeling scenario.
- Of the five models tested in this report and for the given modeling scenario, there are basically three groupings: CHAIN, MULTIMED-DP 1.0 and FECTUZ, CHAIN 2D and HYDRUS.

Table 8-2. The Figures in Section 7 Comparing ^{99}Tc BTCs and Output Sensitivities with Respect to Model Input Parameters and Modeling Codes.

Model Input Parameter	*Figures Comparing BTCs*					*Figures Comparing Sensitivities*				
	CHAIN	MULTIMED-DP 1.0	FECTUZ	CHAIN 2D	HYDRUS	CHAIN	MULTIMED-DP 1.0	FECTUZ	CHAIN 2D	HYDRUS
K_d	7-1	7-1	7-1	7-1	7-1	7-13	7-13	7-13	7-13	7-13
q	7-2	7-2	7-2	7-2	7-2	7-14	7-14	7-14	7-14	7-14
θ	7-3	7-3	7-3	7-3	7-3	7-15	7-15	7-15	7-15	7-15
ρ	7-4	7-4	7-4	7-4	7-4	7-16	7-16	7-16	7-16	7-16
D	7-5					7-17				
D_L		7-6	7-6	7-6	7-6		7-18	7-18	7-18	7-18
D_w				7-7	7-7				7-19	7-19
K_s		7-8	7-8	7-8	7-8		7-20	7-20	7-20	7-20
θ_s		7-9	7-9	7-9	7-9		7-21	7-21	7-21	7-21
θ_r		7-10	7-10	7-10	7-10		7-22	7-22	7-22	7-22
α		7-11	7-11	7-11	7-11		7-23	7-23	7-23	7-23
β		7-12	7-12	7-12	7-12		7-24	7-24	7-24	7-24

Section 9
References

Adler, P.M. and J.-F. Thovert. 1993. "Fractal porous media." Transport in Porous Media. 13, 41-78

Andraski, B.J. 1996. "Properties and variability of soil and trench fill at an arid waste-burial site." Soil Sci. Soc. Am. J. 60, 54-66.

Andraski, B.J. 1997. "Soil-water movement under natural-site and waste-site conditions: A multiple year field study in the Mojave Desert, Nevada." Water Resour. Res.. 33(8), 1901-1916.

Assouline, S.D., D. Tessier, and A. Bruand. 1998. "A conceptual model of the soil water retention curve." Water Resour. Res. 34(2), 223-231.

Ayyub, B.M. 1998. Uncertainty Modeling and Analysis in Civil Engineering. CRC Press, Boca Raton, FL. 506 pp.

Bai, M., D. Elsworth, H.I. Inyang and J.-C. Roegiers. 1997. "Modeling contaminant migration with linear sorption in strongly heterogeneous media." Journal of Environ. Eng. 123 (11), 1116-1125.

Bailey, R.G. 1980. Description of the Ecoregions of the United States. United States Department of Agriculture. Forest Service. Misc. Publ. 1391. Washington, DC. 77 pp.

Bear, J. 1993. "Modeling flow and contaminant transport in fractured rocks." Flow and Contaminant Tranport in Fractured Rock. Academic Press, Inc. New York, NY. 1-37.

Bear, J. and J.J. Nitao. 1995. "On equilibrium and primary variables in transport in porous media." Transport in Porous Media. 18, 151-184.

Bear, J. and A. Verruijt. 1987. Modeling Groundwater Flow and Pollution. D. Reidel Publishing Company. Boston, MA. 414 pp.

Beckie, R., A.A. Aldama and E.F. Wood. 1994. "The universal structure of the groundwater flow equations." Water Resour. Res. 30(5), 1407-1419.

Bedient, P.B., H.S. Rifai and C.J. Newell. 1999. Ground Water Contaminant: Transport and Remediation, Second Edition. Prentice Hall PTR. Upper Saddle River, NJ. 604 pp.

Berglund, S. and V. Cvetkovic. 1996. "Contaminant displacement in aquifers: Coupled effects of flow heterogeneity and nonlinear sorption." Water Resour. Res. 32(1) 23-32.

Boek, E.S. and P. van der Schoot. 1998. "Resolution effects in dissipative particle dynamics simulations." Inter. J. of Modern Physics C. 9(8), 1307-1318.

Brewer, K.E. and S.W. Wheatcraft. 1994. "Including multi-scale information in the characterization of hydraulic conductivity distributions." Wavelets in Geophysics. Academic Press, Inc. New York, NY. 213-248.

Brokate, M. and J. Sprekels. 1996. Hysteresis and Phase Transitions. Springer-Verlag, Inc. New York, NY. 357 pp.

Brooks, R.H. and A.T. Corey. 1964. <u>Hydraulic Properties of Porous Media.</u> Hydrology Paper No. 3. Colorado State University. Fort Collins, CO.

Brusseau, M.L. and P.S.C. Rao. 1989. "Sorption nonideality during organic contaminant transport in porous media." <u>CRC Crit. Rev. Environ. Control.</u> 19, 33-99.

Carerra, J. 1993. "An overview of uncertainties in modelling groundwater solute transport." <u>Journal of Contam. Hydrology.</u> 13, 23-48.

Charbeneau, R.J. 2000. <u>Groundwater Hydraulics and Pollutant Transport.</u> Prentice Hall. Upper Saddle River, NJ. 593 pp.

Chen, W. and R.J. Wagenet. 1995. "Solute transport in porous media with sorption-site heterogeneity." <u>Environ. Sci. Technol.</u> 29, 2725-2734.

Chilès, J-P. and G. de Marsily. 1993. "Stochastic models of fractured systems and their use in flow and transport modeling." <u>Flow and Contaminant Transport in Fractured Rock.</u> Academic Press, Inc. 169-236.

Clemo, T. and L. Smith. 1997. "A hierarchical model for solute transport in fractured media." <u>Water Resour. Res.</u>33(8), 1763-1783.

Corapcioglu, M.Y. and H. Choi. 1996. "Modeling colloid transport in unsaturated porous media and validation with laboratory column data." <u>Water Resour. Res.</u> 32(12), 3437-3449.

Corwin, D.L., K. Loague, and T.R. Ellsworth. Editors. 1999. <u>Assessment of Non-Point Source Pollution in the Vadose Zone.</u> Geophysical Monograph 108. American Geophysical Union. Washington, D.C. 369 pp.

Coveney, P.V. and K.E. Novik. 1996. "Computer simulations of domain growth and phase separation of two-dimensional binary immiscible fluids using dissipative particle dynamics." <u>Physical Review E.</u> 54(5), 5134-5141.

Crawford, J.W., P. Baveye, P. Grindrod and C. Rappoldt. 1999. "Application of fractals to soil properties, landscape patterns, and solute transport in porous media." <u>Assessment of Non-Point Source Pollution in the Vadose Zone.</u> Geophysical Monograph 108. American Geophysical Union, Washington, DC. 151-164.

Dagan, G. 1989. <u>Flow and Transport in Porous Formations.</u> Springer-Verlag. New York, NY. 465 pp.

Defence Mapping Agency. 1987. <u>Official Road Map: U.S. Army White Sands Missile Range, New Mexico.</u> Defence Mapping Agency. Hydrographic/Topographic Center. White Sand Missile Range, NM.

De Hoog, F.R., J.H. Knight and A.N. Stokes. 1982. "An improved method for numerical inversion of Laplace Transforms". <u>SIAM J. SCI. STAT. COMPUT.</u> 3(3), 357-366.

Domenico, P.A. and F.W. Schwartz. 1990. <u>Physical and Chemical Hydrogeology.</u> John Wiley and Sons. New York, NY. 824 pp.

Drew, D.A. and S.L. Passman. 1999. <u>Theory of Multicomponent Fluids.</u> Springer-Verlag. New York, NY. 308 pp.

Eagleson, P.S. 1970. <u>Dynamic Hydrology.</u> McGraw-Hill Book Co. New York, NY. 462 pp.

Eeckhout, E.V. 1997. <u>Use of Data Fusion to Optimize Contaminant Transport Predictions.</u> LA- UR-98-845. U.S. DOE, Los Alamos National Laboratory. Los Alamos, NM. 16 pp.

Faybishenko, B., P.A. Witherspoon and S.M. Benson. Editors. 2000. <u>Dynamaics of Fluids in Fractured Rock.</u>. Geophysical Monograph 122. American Geophysical Union. Washington, DC. 400 pp.

Fetter, C.W. 1999. <u>Contaminant Hdyrogeology</u>, Second Edition. Prentice Hall. Upper Saddle River, NJ. 500 pp.

Flury, M. and H. Flühler. 1995. "Modeling solute leaching soils by diffusion-limited aggregation: Basic concepts and application to conservative solutes." Water Resour. Res. 31(10), 2443-2452.

Gao, Y. and M.M. Sharma. 1994. "A LGA model for fluid flow in heterogeneous porous media." Transport in Porous Media 17, 1-17.

Gee, G.W.., C.T. Kincaid, R.J. Lenhard and C.S. Simmons. 1991. "Recent studies of flow and transport in the vadose zone." U.S. National Report to International Union of Geodesy and Geophysics, 1987-1990. American Geophysical Union, Washington, DC. 227-239.

Gee, G.W., P.J. Wierenga, B.J. Andraski, M.H. Young, M.J. Fayer, and M.L. Rockhold. 1994. "Variations in water balance and recharge potential at three western desert sites." Soil Sci. Soc. Am. J. 58(1), 63-72.

Gelhar, L.W. 1993. Stochastic Subsurface Hydrology. Prentice-Hall. Englewood Cliffs, NJ.

Gile, L.H., R.P. Gibbens, and J.M. Lenz. 1998. "Soil-induced variability in root systems of creosotebush (Larrea tridentata) and tarbush (Flourensia cernua)." J. Arid Environ. 39(1), 57-78.

Gouyet, J-F. 1996. Physics and Fractal Structures. Springer-Verlag, Inc. New York, NY. 234 pp.

Gray, W.G., A. Leijnse, R.L. Kolar and C.A. Blain. 1993. Mathematical Tools for Changing Spatial Scales in the Analysis of Physical Systems. CRC Press, Boca Raton, FL. 232 pp.

Groot, R.D. and P.B. Warren. 1997. "Dissipative particle dynamics: Bridging the gap between atomistic and mesoscopic simulation. J. Chem. Phys. 107(11), 4423-4435.

Guymon, G.L. 1994. Unsaturated Zone Hydrology. PTR Prentice Hall. Englewood Cliffs, New Jersey. 210 pp.

Hamed, M.M. and P.B. Bedient. 1999. Reliably-Based Uncertainty Analysis of Groundwater Contaminant Transport and Remediation. EPA/600/R-99/028. National Risk Management Research Laboratory, ORD, US. EPA. Cincinnati, OH.

Helton, J.C. 1993. "Uncertainty and sensitivity analysis techniques for use in performance assessment for radioactive waste disposal" Reliability Eng. and System Safety 42, 327-367.

Hills, R.G., P.J. Wierenga, D.B. Hudson, and M.R. Kirkland. 1991. "The second Las Cruces trench experiment: experimental results and two-dimensional flow predictions." Water Resour. Res. 27(10), 2707-2718.

Hills, R.G., K.A. Fisher, M.R. Kirkland, and P.J. Wierenga. 1994. "Application of flux-corrected transport to the Las Cruces trench site." Water Resour. Res. 30(8), 2377-2385.

Hornung, U. 1997. Homogenization and Porous Media. Springer-Verlag, Inc. New York, NY. 279 pp.

Huyakorn, P.S., and J.E. Buckley. 1987. Finite Element Code for Simulating One-Dimensional Flow and Solute Transport in the Vadose Zone. Technical Report prepared for U.S. EPA, Athens, GA.

Jang, Y-S, N. Sitar and A. der Kiureghian. 1994. "Reliability analysis of contaminant transport in saturated porous media." Water Resour. Res. 30(8), 2435-2448.

Jenkins, M.B., R.A. Virgina, and W.M. Jarrell. 1988. "Depth distribution and seasonal populations of mesquite-nodulating rhizobia in warm desert ecosystem." Soil Sci. Soc. Am. J. 52(6), 1644-1650.

Jensen, M.E., R.D. Burman, and R.G. Allen. 1990. "Evapotranspiration and irrigation water requirements." ASCE Manuals and Reports on Engineering Practice. No. 70. American Society of Civil Engineers, NY. 332 pp.

Jury, W.A. and R.L. Valentine. 1986. "Transport mechanisms and loss pathways for chemicals in soil." In: S.C. Hern and S.M. Melancon (eds.), Vadose Zone Modeling of Organic Pollutants, Lewis Publishers, Inc., Chelsea, Michigan, pp. 37-60.

Kaiser, C. 1997. "A directed percolation model for clogging in a porous medium with small inhomogeneities." Transport in Porous Media 26, 133-146.

Knox, R.C., D.A. Sabatini, and L.W. Canter. 1993. Subsurface Transport and Fate Processes. Lewis Publishers. Boca Raton, FL. 430 pp.

Kretzschmar, R., K. Barmettler, D. Grolimund, Y-d. Yan, M. Borkovec and H. Stécher. 1997. "Experimental determination of colloid deposition rates and collision efficiencies in natural porous media." Water Resour. Res. 33(5), 1129-1137.

Litaor, M.I., G. Barth, E.M. Zika, G. Litus, J. Moffitt and H. Daniels. 1998. "The behavior of radionuclides in the soils of Rocky Flats, Colorado." J. Environ. Radioactivity. 38(1), 17-46.

Liu, S., W.B. Mills, and B. Baena. 1995. Multimedia Exposure Assessment Modeling Including Fate and Tranformation Products (MULTIMED_DP 1.0): Implementation, Tests and User's Manual. Technical Report prepared by U.S. EPA, Athens, GA.

Logan, J.D. 1996. "Solute transport in porous media with scale-dependent dispersion and periodic boundary conditions." Journal of Hydrology. 184, 261-276.

Logan, J.D. 2001. Transport Modeling in Hydrochemical Systems. Springer-Verlag. New York, NY. 223 pp.

Luckner, L., and W.M. Schestakow. 1991. Migration Processes in the Soil and Groundwater Zone. Lewis Publishers. Chelsea, MI. 485 pp.

Mackay, D. 2001. Mulimedia Environmental Models: The Fugacity Approach, Second Edition. Lewis Publishers. Boca Raton, FL. 261 pp.

Mayer, S., T.R. Ellsworth, D.L. Corwin and K. Loague. 1999. "Identifying effective parameters for solute transport models in heterogeneous environments." Assessment of Non-Point Source Pollution in the Vadose Zone. Geophysical Monograph 108. American Geophysical Union. Washington, DC. 119-133.

McCarthy, J.F. 1995. "Comparison of fast algorithms for estimating large-scale permeabilities of heterogeneous media." Transport in Porous Media. 19, 123-1137.

McCarthy, J.F. and J.M. Zachara. 1989. "Subsurface transport of contaminants: Mobile colloids in the subsurface environment may alter the transport of contaminants." Environ. Sci. Technol. 23(5), 496-502.

McCord, J.T., C.A. Gotway and S.H. Conrad. 1997. "Impact of geologic heterogeneity on recharge estimation using environmental tracers: Numerical modeling investigation." Water Resour. Res. 33(6), 1229-1240.

Mehl, S. and M.C. Hill. 2001. "A comparison of solute-transport solution techniques and their effect on sensitivity analysis and inverse modeling results." Ground Water. 39(2), 300-307.

Meyer, P.D., M.L. Rockhold and G.W. Gee. 1997. Uncertainty Analysis of Infiltration and Subsurface Flow and Transport for SDMP Sites. NUREG/CR-6565. PNNL-11705. United States Nuclear Regulatory Commission. Division of Regulatory Applications. Washington, DC.

Miller, E.E. and R.D. Miller. 1956. "Physical theory for capillary flow phenomena." J. App. Phys. 27, 324-332.

Miralles-Wilhelm, F. and L.W. Gelhar. 1996. "Stochastic analysis of transport and decay of a solute in heterogeneous aquifers." Water Resour. Res. 32(12), 3451-3459.

Miyazaki, T., S. Hasegawa and T. Kasubuchi. 1993. Water Flow in Soils. Marcel Dekker, Inc. New York, NY. 296 pp.

Morel-Seytoux, H.J., P.D. Meyer, M. Nachabe, J. Touma, M. Th. Van Genuchten and R.J. Lenhard. 1996. "Parameter equivalence for Brooks-Corey and van Genuchten soil characteristics: preserving the effective capillary drive." Water Resour. Res. 32(5), 1251-1258.

Mulla, D.J. and T.M. Addiscott. 1999. "Validation approach for field-, basin-, and regional-scale water quality models." Assessment of Non-Point Source Pollution in the Vadose Zone. Geophysical Monograph 108. American Geophysical Union. Washington, DC. 63-78.

Murray, J.D. 1989. Mathematical Biology. Springer-Verlag. New York, NY. 767 pp.

Nachabe, M.H. 1996. "Macroscopic capillary length, sorptivity, and shaping factor in modeling the infiltration rate." Soil Sci. Soc. Am. J. 60, 957-962.

Neuman, S.P. and V.D. Federico. 1998. "Correlation, flow, and transport in multiscale permeability fields." In Scale Dependence and Scale Invariance in Hydrology. Cambridge University Press. New York, NY. 354-397.

Nirmalakhandan, N. 2002. Modeling Tools for Environmental Engineers and Scientists. CRC Press. Boca Raton, FL. 312 pp.

Nofziger, D.L., J-S. Chen, and C.R. Haan. 1994. Evaluation of Unsaturated/Vadose Zone Models for Superfund Sites. EPA/600/R-93/184. U.S. EPA. R.S. Kerr Environmental Research Laboratory, Ada, OK. 188 pp.

Oldenburg, C.M. and K. Pruess. 1996. "Mixing with first-order decay in variable-velocity porous media flow." Transport in Porous Media. 22, 161-180.

Porro, I., and P.J. Wierenga. 1993. "Transient and steady state solute transport through a large unsaturated soil column." Ground Water. 31(2), 193-200.

Preuss, K., B. Faybishenko and G.S. Bodcarsson. 1999. "Alternative concepts and approaches for modeling flow and transport in thick unsaturated zones of fractured rocks." Journal of Contam. Hydrology. 38, 281-322.

Probstein, R.F. 1994. Physicochemical Hydrodynamics: An Introduction. Second Edition. John Wiley and Sons, Inc. New York, NY. 400 pp.

Ravi, V. and J. Williams. 1998. Estimation of Infiltration Rate in the Vadose Zone: Compilation of Simple Mathematical Models. Volume I. EPA/600/R-97/128a. National Risk Management Research Laboratory. U.S. EPA Cincinnati, OH.

Renard, Ph., and G. de Marsily. 1997. "Calculating equivalent permeability: a review." Advances in Water Resources. 20 (5-6), 253-278.

Richards, L.A. 1931. "Capillary conduction of liquids through porous mediums." Physics. 1, 318-331.

Rockhold, M.L. 1999. "Parameterizing flow and transport models for field-scale applications in heterogeneous, unsaturated soils." Assessment of Non-Point Source Pollution in the Vadose Zone. Geophysical Monograph 108. American Geophysical Union. Washington, DC. 243-260.

Rockhold, M.L., R.E. Rossi, and R.G. Hills. 1996. "Application of similar media scaling and conditional simulation for modeling water flow and tritium transport at the Las Cruces trench site." Water Resour. Res. 32(3), 595-609.

Rockhold, M.L., C.S. Simmons and M.F. Fayer. 1997. "An analytical solution technique for one-dimensional, steady vertical water flow in layered soils." Water Resour. Res. 33(4), 897-902.

Royo, A.R. 2000. "Desert Plant Survival." DesertUSA Newsletter. Http://www.desertusa.com/du_plantsurv.html. 5 pp.

Sachdev, P.L. 2000. Self-Similarity and Beyond: Exact Solutions of Nonlinear Problems. Chapman and Hall/CRC. Boca Raton, FL. 319 pp.

Salhotra, A.M., P. Mineart, S. Sharp-Hansen, T. Allison, R. Johns, and W.B. Mills. 1995. Mulimedia Exposure Assessment Model (MULIMED 2.0) for Evaluating the Land Disposal of Waste-Model Theory. Final Report prepared for U.S. EPA. Athens, GA.

Sharp-Hansen, S., C. Travers, P. Hummel, T. Allison, R. Johns, and W. Mills. 1995. <u>A Subtitle D Landfill Application Manual for the Multimedia Exposure Assessment Model (MULTIMED 2.0).</u> Technical Report prepared for U.S. EPA. Athens, GA.

Shurbaji, A.-R. and A.R. Campbell. 1997. "Study of evaporation and recharge in desert soil using environmental tracers, New Mexico, USA." <u>Environ. Geology.</u> 29 (3/4), 147-151.

Simon, W., P. Reichert and C. Hinz. 1997. "Properties of exact and approximate traveling wave solutions for transport with nonlinear and nonequilibrium sorption." <u>Water Resour. Res.</u> 33(5), 1139-1147.

Šimúnek, J. and M.Th. van Genuchten. 1994. <u>The CHAIN_2D Code for Simulating Two- Dimensional Movement of Water, Heat, and Muliple Solutes.</u> Research Report No. 136. U.S. Salinity Laboratory. USDA, ARS. Riverside, CA.

Šimúnek, J., K. Huang, and M.Rh. van Genuchten. 1998. <u>The HYDRUS Code for Simulating the One-Dimensional Movement of Water, Heat, and Multiple Solutes in Variable-Saturated Media.</u> Research Report No. 144. U.S. Salinity Laboratory. USDA, ARS. Riverside, CA.

Spanos, T.J.T. 2002. <u>The Thermophysics of Porous Media.</u> Chapman & Hall/CRC. Boca Raton, FL. 220 pp.

Sposito, G. (Ed.). 1998. <u>Scale Dependence and Scale Invariance in Hydrology.</u> Cambridge University Press. New York, NY. 423 pp.

Stehfest, H. (1970). "Numerical inversion of Laplace Transforms." <u>Commun. ACM.</u> 13(1), 47-49.

Stockman, H.W. 1997. "A lattice gas study of retardation and dispersion in fractures: Assessment of errors from desorption kinetics and buoyancy." <u>Water Resour. Res.</u> 33(8), 1823-1831.

Thibodeaux, L.J. 1996. <u>Environmental Chemodynamics: Movement of Chemicals in Air, Water, and Soil.</u> 2nd Edition. John Wiley & Sons, Inc. New York, NY. 593 pp.

Tomaski, D., M. Reeves, B.A. Kelley, and J.F. Pickens. 1989. "Parameter sensitivity and importance for radionuclide transport in double-porosity systems." In: B.E. Buxton (ed.) <u>Proceedings of the Conference on Geostatistical, Sensitivity, and Uncertainty Methods for Ground-Water Flow and Radionuclide Transport Modeling.</u> San Fransisco, CA. September 15-17, 1987. Battelle Press. Columbus, OH. pp. 297-321.

Toride, N., F.J. Leij, and M.T. van Genuchten. 1993. "A comprehensive set of analytical solutions for nonequilibrium solute transport with first-order decay and zero-order production." <u>Water Resour. Res.</u> 29(7), 2167-2182.

Turcotte, D.L. 1992. <u>Fractals and Chaos in Geology and Geophysics.</u> Cambridge University Press. New York, NY. 221 pp.

U.S. EPA. 1995a. <u>EPA's Composite Model for Leachate Migration with Transformation Products, EPACMTP.</u> Background Document. Office of Solid Waste, U.S. EPA, Washington, DC.

U.S. EPA. 1995b. <u>EPA's Composite Model for Leachate Migration with Transformation Products, EPACMTP.</u> User's Guide. Office of Solid Waste, U.S. EPA, Washington, DC.

U.S. EPA. 1996. <u>Summary Report for the Workshop on Monte Carlo Analysis.</u> EPA/630/R-96/010. Risk Assessment Forum, U.S. EPA, Washington, D.C.

U.S. EPA. 1999a. <u>Understanding Variations in Partition Coefficients, K_d, Values: The K_d Model, Methods of Measurement, and Application of Chemical Reaction Codes.</u> Volume I. EPA 402-R-99-004A. Office of Radiation and Indoor Air & Office of Solid Waste and Emergency Response. U.S. EPA. Washington, D.C.

U.S. EPA. 1999b. <u>Understanding Variation in Partition Coefficient, K_d, Values: Review of Geochemistry and Available K_d Values for Cadmium, Cesium, Chromium, Lead, Plutonium, Radon, Strontium, Thorium, Tritium, (^{3}H), and Uranium.</u> Volume II. EPA 402-R-99-004B. Office of Radiation and Indoor Air & Office of Solid Waste and Emergency Response. U.S. EPA. Washington, D.C.

U.S. EPA. 2000a. <u>Soil Screening Guidance for Radionuclides: User's Guide.</u> EPA/540-R-00-007. Office of Radiation and Indoor Air and Office of Solid Waste and Emergency Response, U.S. EPA, Washington, D.C.

U.S. EPA. 2000b. <u>Soil Screening Gudiance for Radionuclides: Technical Background Document.</u> EPA/540-R-00-006. Office of Radiation and Indoor Air and Office of Solid Waste and Emergency Response, U.S. EPA, Washington, D.C.

Van de Ven, T.G.M. 1989. <u>Colloidal Hydrodynamics.</u> Academic Press. New York, NY. 582 pp.

Van der Heijde, P.K.M. 1994. <u>Identification and Compilation of Unsaturated/Vadose Zone Models.</u> EPA/600/R-94/028. R.S. Kerr Environmental Research Laboratory, U.S. EPA, Ada, OK.

Van der Heijde, P.K.M. and O.A. Elnawawy. 1993. <u>Compilation of Ground-Water Models.</u> EPA/600/R-93/118. R.S. Kerr Environmental Research Laboratory, U.S. EPA, Ada, OK.

Van der Heijde, P.K.M. and D.A. Kanzer. 1995. <u>Ground-Water Model Testing: Systematic Evaluation and Testing of Code Functionality, Performance, and Applicability to Practical Problems.</u> IGWMC-GWMI 95-01. International Ground Water Modeling Center,Colorado School of Mines, Golden, CO.

Van Genuchten, M. Th. 1980. "A closed-form equation for predicting the hydraulic conductivity of unsaturated soils." <u>Soil Sci. Soc. Am. J.</u> 44, 892-898.

Van Genuchten, M. Th. 1985. "Convective-dispersive transport of solutes involved in sequential first-order decay reactions." <u>Computer & Geosciences,</u> 11(2), 129-147.

Van Genuchten, M. Th., and R.J. Wagenet. 1989. "Two-site/two-region models for pesticide transport and degradation: theoretical development and analytical solutions." <u>Soil Sci. Soc. Am. J.</u> 53, 1303-1310.

Visintin, A. 1994. <u>Differential Models of Hysteresis.</u> Springer-Verlag. New York, NY. 407 pp.

Vogel, T., and M. Cislerová. 1988. "On the reliability of unsaturated hydraulic conductivity calculated from the moisture retention curve." <u>Transport in Porous Media.</u> 3, 1-15.

Vogel, T., M. Cislerová, and J.W. Hopmans. 1991. "Porous media with linearly variable hydraulic properties." <u>Water Resour. Res.</u> 27(10), 2735-2741.

Vollmayr, H., F. Kleint and G. Schüürmann. 1997. "Discrete modeling of water and pesticide movement in soil." <u>Water Resour. Res.</u> 33(7), 1743-1747.

Wang, Z., J. Feyen, D.R. Nielson, and M.T. van Genuchten. 1997. "Two-phase flow infiltration equations accounting for air entrapment effects." <u>Water Resour. Res.</u> 33(12), 2759-2767.

Wang, Z., J. Feyen and D.E. Elrick. 1998. "Prediction of fingering in porous media." <u>Water Resour. Res.</u> 34(9), 2183-2190.

Wang, Z., J. Feyen and C.J. Ritsema. 1998. "Susceptibility and predictability of conditions for preferential flow." <u>Water Resour. Res.</u> 34(9), 2169-2182.

Wang, Z., J. Feyen, M.T. van Genuchten, and D.R. Nielsen. 1998. "Air entrapment effects on infiltration rate and flow instability." <u>Water Resour. Res.</u> 34(2), 213-222.

Wang, Z., L. Wu, and Q.J. Wu. 2000. "Water-entry value as an alternative indicator of soil water-repellency on infiltration rate and flow instability." <u>J. Hydrol.</u> 231-232, 76-83.

Wang, Z., Q.J. Wu, L. Wu, C.J. Ritsema, L.W. Dekker and J. Feyen. 2000. "Effects of soil water-repellency on infiltration rate and flow instability." <u>J. Hydrol.</u> 231-232, 265-276.

Warrick, A.W., G.J. Mullen and D.R. Nielsen. 1977. "Scaling field-measured soil hydraulic properties using a similar media concept." <u>Water Resour. Res.</u> 13, 355-362.

Weber, W.J., Jr., P.M. McGinley, and L.E. Katz. 1991. "Sorption phenomena in subsurface systems: concepts, models and effects on contaminant fate and transport." <u>Water Res.</u> 25, 499-528.

Wierenga, P.J., R.G. Hills, and D.B. Hudson. 1991. "The Las Cruces trench site: characterization, experimental results, and one-dimensional flow predictions." <u>Water Resour. Res.</u> 27(1), 2695-2705.

Williams, J.R., Y. Ouyang, J.-S. Chen, and V. Ravi. 1998. <u>Estimation of Infiltration Rate in Vadose Zone: Application of Selected Mathematical Models.</u> Volume II. EPA/600/R-97/128b. National Risk Management Research Laboratory. U.S. EPA. Cincinnati, OH.

Yao, T-M. and J.M.H. Hendrickx. 1996. "Stability of wetting fronts in dry homogeneous soils under low infiltration rates." <u>Soil Sci. Soc. Am. J.</u> 60, 20-28.

Yortsos, Y.C. and K. Shing. 1999. <u>Evaluation and Analysis of Microscale Flow and Transport During Remediation.</u> EPA/600/R-99/022. National Risk Management Research Laboratory, Office of Research and Development, U.S. EPA, Cincinnati, OH. 160 pp.

Zheng, C., and G.D. Bennett. 1995. <u>Applied Contaminant Transport Modeling: Theory and Practice.</u> Van Nostrand Reinhold. New York, NY. 440 pp.

Appendix A
Empirical Models of the Unsaturated Soil Hydraulic Properties
Which Are Used in the Various Models

One-dimensional soil-water movement in a partially saturated rigid porous medium is described in the HYDRUS Code (Šimůnek et al, 1998) by a modified form of the Richards Equation:

$$\frac{\partial \theta}{\partial t} = \frac{\partial}{\partial z}\left[K\left(\frac{\partial h}{\partial z} + 1\right)\right] - S \, ,$$

(A-1)

where θ is the soil-water volumetric content (L^3L^{-3}), h is the soil-water pressure head (L), a negative quantity for unsaturated conditions, K is the unsaturated hydraulic conductivity function (LT^{-1}), t is time (T), z is the vertical coordinate (L), positive upward with an origin at some finite depth in the soil, and S(h,z) is a sink term defined as the volume of water removed from a unit volume of soil per unit time due to plant water uptake ($L^3L^{-3}T^{-1}$). The formulation of Equation (A-1) assumes that the air phase plays an insignificant role in the liquid flow process and that water flow due to thermal gradients can be neglected. The general form of K is given by:

$$K \equiv K(h,z) = K_s(z)\, K_r(h,z) \, ,$$

(A-2)

where K_s is the saturated hydraulic conductivity (LT^{-1}) and K_r is the relative hydraulic conductivity (1).

The HYDRUS Code features three models for the unsaturated soil hydraulic properties, θ and K. In homogeneous media, these properties can be expressed as nonlinear functions of the soil-water pressure head, $\theta(h)$ and K(h). The three models are analytical expressions denoted by BC, VG, and VC, respectively given by Brooks and Corey (1964), van Genuchten (1980), and Vogel and Cislerová (1988).

The BC-Model is defined by the following equations:

$$S_e = \frac{\theta - \theta_r}{\theta_s - \theta_r} = \begin{cases} |\alpha h|^{-n} \, , & h < -1/\alpha \\ 1 & , \ h \geq -1/\alpha \end{cases} \, ,$$

(A-3)

$$K = K_s S_e^{2/n + c + 2} \, ,$$

(A-4)

where S_e is the effective water content, θ_s is the saturated water content, θ_r is the residual water content, α is the inverse of the air-entry value or bubbling pressure, n is a pore-size distribution index, and c is a pore-connectivity parameter (c was assumed to be 2.0 in the original Brooks-Corey study). Thus, this model consists of six free parameters (θ_r, θ_s, K_s, n, c, α). The quantities (θ_r, θ_s, K_s) can be measured in the laboratory or in the field, while the parameters (n,c,α) are considered to be empirical coefficients affecting the shapes of the hydraulic functions.

The VG-Model is defined by the analytical expressions given below:

$$\theta(h) = \begin{cases} \theta_r + \dfrac{\theta_s - \theta_r}{\left[1 + |\alpha h|^n\right]^m}, & h < 0 \\ \theta_s, & h \geq 0 \end{cases}, \tag{A-5}$$

$$K(h) = K_s S_e^c \left[1 - \left(1 - S_e^{1/m}\right)^m\right]^2, \tag{A-6}$$

where

$$m = 1 - 1/n, \quad n > 1. \tag{A-7}$$

In some of the codes, other than that of HYDRUS, the parameter m is denoted by γ, and the parameter n is denoted by β. The pore-connectivity parameter, c, has been estimated to be about 0.5 as an average for many soils (Mualem, 1976). As in the BC-Model, this model contains the six parameters $(\theta_r, \theta_s, K_s, n, c, \alpha)$.

The third set of hydraulic equations implemented in HYDRUS are the defining equations of the VC-Model, which are modifications of the VG-Equations to add flexibility in the description of the hydraulic properties near saturation. These modified equations are as follows:

$$\theta(h) = \begin{cases} \theta_a + \dfrac{\theta_m - \theta_a}{\left[1 + |\alpha h|^n\right]^m}, & h < h_s \\ \theta_s, & h \geq h_s \end{cases}, \tag{A-8}$$

$$K(h) = \begin{cases} K_s K_r(h), & h \leq h_k \\ K_k + \dfrac{(h - h_k)(K_s - K_k)}{h_s - h_k}, & h_k < h < h_s \\ K_s, & h \geq h_s \end{cases}, \tag{A-9}$$

where

$$K_r = \dfrac{K_k}{K_s}\left[\dfrac{S_e}{S_{ek}}\right]^c \left[\dfrac{F(\theta_r) - F(\theta)}{F(\theta_r) - F(\theta_k)}\right]^2, \tag{A-10}$$

$$F(\theta) = \left[1 - \left(\dfrac{\theta - \theta_a}{\theta_m - \theta_a}\right)^{1/m}\right]^m, \tag{A-11}$$

$$S_{ek} = \dfrac{\theta_k - \theta_r}{\theta_s - \theta_r}. \tag{A-12}$$

This model allows for a nonzero minimum capillary height, h_s, by replacing θ_s in the VG-Model by an extrapolated parameter, θ_m, which is slightly more than θ_s (Figure A-1a). In general, this change from θ_s to θ_m has little to no effect on the soil-water retention curve; but its effect on the shape and value of K may be considerable, especially for fine-textured soils when n is small (i.e., $1.0 < n < 1.3$). A further increase in the flexibility of the analytical expressions of the VC-Model is experienced by replacing θ_r in the equation for $\theta(h)$ by another extrapolated parameter $\theta_a \leq \theta_r$.
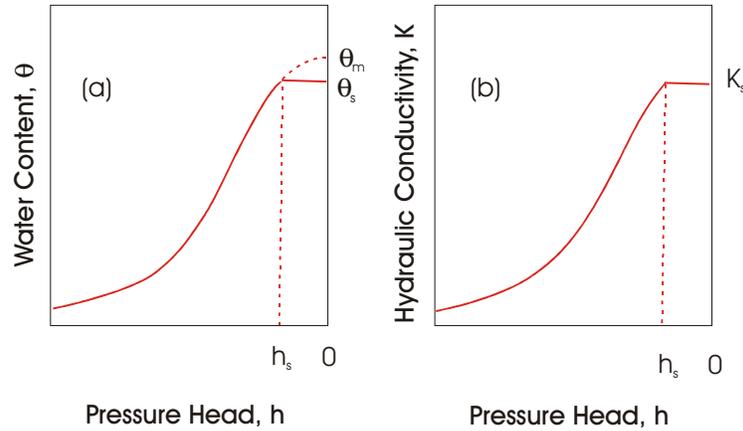
Figure A-1. Schematics of the soil-water retention curve (a) and the hydraulic conductivity function (b) for the VC-Model (from Šimůnek et al., 1998).

This model retains the physical meaning of θ_r and θ_s as measurable quantities while adding two new fitting parameters, θ_a and θ_m. Equation (A-10) assumes that the predicted hydraulic conductivity function is matched to a measured value of the function, $K_k = K(\theta_k)$, at some water content θ_k satisfying

$$\theta_k \le \theta_s, \quad K_k \le K_s .$$ (A-13)

The VC-Model contains 10 unknown parameters: θ_r, θ_s, θ_a, θ_m, α, c, n, K_s, K_k and θ_k. However, as in the VG-Model, c is often assumed to be 0.5. When

$$\theta_a = \theta_r, \quad \theta_m = \theta_k = \theta_s, \quad K_k = K_s$$ (A-14)

the VC-Model reduces to the VG-Model.

The question arises, "Which model should a user employ?" The claim is that the VC-Model is more versatile than the VG-Model, but three more unknown parameters are required to use the VC-Model. Of the BC- and VG-Models, which is the best to use? Morel-Seytoux et al. (1996) defined an equivalence which provides a simple way to convert BC-parameters into VG-parameters, and vice versa, when one set of parameters is known and preservation of the maximum value of a physical characteristic called the "effective capillary drive" is guaranteed. This quantity is defined by:

$$H_{cm} = \int_o^\infty k_{rw} dh_c ,$$ (A-15)

where k_{rw} is the relative permeability (or conductivity) to water and h_c is the capillary pressure head, a positive quantity equal to minus h. This equivalence makes infiltration capacity calculations insensitive to the model used (BC or VG) to represent the soil hydraulic properties. It is strictly a matter of convenience for the user which expressions are used. As one would expect, this equivalence only applies for situations which lead to high water contents in some part of the domain of interest. However, because of the equivalence criterion which preserves the asymptotic behavior of capillary pressure at low water contents and thus preserves the hydraulic gradient, the authors claim there are at least plausible grounds that the parameter equivalence will be reasonably satisfactory for situations involving drainage and evapotranspiration. But, the application of this paper to these latter processes should be further tested.

Further support for the equivalence relationship of Morel-Seytoux et al. (1996) is given by the work of Nachabe (1996). The work of this author was based on the fact that infiltration tests in the field routinely involve measurements of sorptivity and macroscopic capillary length, the latter being related to the effective capillary drive defined in Equation A-15. In addition, these two factors are strongly related through a shape factor b, which is a measure of the nonlinearity of the soil water hydraulic diffusivity $D(\theta)$, (L^2T^{-1}):

$$D(\theta) = K(\theta)\ \frac{dh}{d\theta}\ .\tag{A-16}$$

The macroscopic capillary length λ_s, which is equivalent to the wetting front suction head, is defined by

$$\lambda_s = \frac{1}{K(\theta_o) - K(\theta_n)} \int_{\theta_n}^{\theta_o} D(\theta)\ d\theta\ ,\tag{A-17}$$

where θ_o is the supply water content applied at the surface and θ_n is the dry, antecedent water content in the soil, ahead of the wetting front. The sorptivity, $\overline{S}$, is well approximated by

$$\overline{S}^2 = \int_{\theta_n}^{\theta_o} \left(\theta_o + \theta - 2\theta_n \right) D(\theta)\ d\theta\ ,\tag{A-18}$$

where $\overline{S}$, ($LT^{-1/2}$), is defined by the early stages of an infiltration test. In Nachabe's study, relationships were developed between λ_s, $\overline{S}$, and shape factor b, and the parameters of the BC- and VG-Models for $K(\theta)$ and $D(\theta)$. Numerical simulations using a dimensionless form of Richards Equation showed that the predicted infiltration rate is not very sensitive to small variations in the shape factor, b, provided λ_s is the same in all the simulations. This result is important because b is difficult to determine accurately in the field. Thus, this similarity of the dimensional infiltration solutions under small variations in b shows that λ_s is a *scale-factor* (see Appendix B) because:

(1) λ_s renders predictions of infiltration rates fairly insensitive to the models used for $K(\theta)$ and $D(\theta)$; and

(2) λ_s reduces the number of parameters needed to characterize infiltration.

Therefore, given the generalized infiltration solution from this scale analysis, an infiltration curve into a particular soil at a particular location and time can be deduced by choosing the proper units in time and space (i.e., scaling) of this generalized solution, thus minimizing the computations for obtaining infiltration curves over spatially varying domains. Further, the small range of variation of the shape factor, b, and the insensitivity to this variation by λ_s-scaled infiltration rates based on the BC- and VG-Models used in the Richards Equation supports the use of linear scaling in the HYDRUS Code, see Appendix B.

In spite of the results obtained by the two previous investigations, researchers are still looking for better soil-water retention curve (WRC) models. Assouline et al. (1998) introduced a new conceptual model for WRC's. Before introducing this new concept, the authors gave a brief, but comprehensive, survey of WRC construction from the work of Brooks and Corey (1964) to recent studies based on fractal and multifractal soil structures. The proposed concept and model for the WRC given by Assouline et al. (1998) are based on two assumptions:

(1) A soil structure resulting from a uniform random fragmentation process where the probability of fragmentation of an aggregate of soil material is proportional to its size; and

(2) A power function describing a relationship between the volume of the aggregates and the corresponding pore volumes.

This new model WRC was tested on 12 different soil types that presented a wide range of textures and mechanical analysis. The model accurately reproduced the very different shapes of the respective WRC's, from the step-function shape of a sand to the sigmoidal almost linear shape of a clay. Also, the new model accurately reproduced measured data over the whole range of water contents, from saturation conditions to water contents at the wilting point. Compared with the VG-Model and another popular WRC-Model, the new model of Assouline et al. exhibited increased flexibility and reproduced the measured data in the high and low water content ranges better than the two other models. Thus, the authors claim two major benefits for the new WRC-Model:

(1) For this new two fitting parameter model, there is a gain in accuracy and flexibility over competing two fitting parameter models, such as the BC- and VG-Models.

(2) The conceptual basis on which the WRC-Model is constructed forms a basis for further research toward a more physically based relationship between soil structure and its corresponding hydraulic properties.

References

Assouline, S, D.Tessier and A. Bruand. 1998. "A conceptual model of the soil water retention curve." Water Resour, Res., 34 (2), 223-231.

Brooks, R. H. and A.T. Corey. 1964. Hydraulic Properties of Porous Media. Hydrology Paper No.3. Colorado State University. Fort Collins, CO.

Morel-Seytoux, H.J., P.D. Meyer, M. Nachabe, J. Touma, M. Th. van Genuchten and R.J. Lenhard. 1996. "Parameter equivalence for Brooks-Corey and van Genuchten soil characteristics: Preserving the effective capillary drive." Water Resour. Res., 32 (5), 1251-1258.

Mualem, Y. 1976. "A new model for predicting the hydraulic conductivity of unsaturated porous media." Water Resour. Res., 12(3), 513–522.

Nachabe, M. H. 1996. "Macroscopic capillary length, sorptivity, and shape factor in modeling the infiltration rate." Soil Sci. Soc. Am. J. 60, 957-962.

Šimùnek, J., K. Huang and M. Th. van Genuchten. 1998. The HYDRUS Code for Simulating the One-Dimensional Movement of Water, Heat, and Multiple Solutes in Variably-Saturated Media. Version 6.0. Res. Rep. No. 144. U.S. Salinity Laboratory, Ag. Res. Ser., USDA, Riverside, CA.

van Genuchten, M. Th. 1980. "A closed-form equation for predicting the hydraulic conductivity of unsaturated soils." Soil Sci. Soc. Am. J., 44, 892–898.

Vogel, T. and M. Cislerová. 1988. "On the reliability of unsaturated hydraulic conductivity calculated from the moisture retention curve." Transport in Porous Media. 3, 1-15.

Appendix B
A Discussion on the Scaling of Field Soil-Water Behavior

The scaling features for soil-water behavior found in the HYDRUS and CHAIN 2D Codes are part of a bigger picture in science which includes the concepts of symmetry, invariance, and conservation. Further, it is difficult to meaningfully discuss scaling without involving some of these more fundamental concepts. For example, Skoglund (1967) defines **scaling** as a technique for relating the variables of a "prototype" to those of a "model" at corresponding points and times in the two systems. Further, he says that scaling often requires that the ratios of the corresponding dimensional variables of the "prototype" and the "model" at corresponding points and times be constant. These constants are called **scaling factors** and are commonly used in the design and interpretation of physical and mathematical models. But Skoglund says that this often obscures the more fundamental process of **searching for symmetry in nature**. In what follows, the roles between scaling, symmetry, invariance, and conservation are explained.

B.1 Symmetry in Nature

Rosen (1995) says a symmetric situation is one which possesses the possibility of change; and if such a change occurs, some aspect of the situation remains unchanged. Thus, the situation is said to be symmetric under the change, or **transformation**, with respect to that aspect. Consequently, there are two essential components of symmetry in nature (Rosen, 1995):

1. **Possibility of change** – it must be possible to perform the change, although the change does not actually have to be performed.

2. **Immunity** – some aspect of the natural situation remains unchanged if the change is actually performed.

If a change is possible but some aspect of the situation is not immune to it, **asymmetry** exists. If there is no possibility of change, with reference to the physical reality of the situation, then the concepts of symmetry and asymmetry are inapplicable.

In the geophysical sciences, as opposed to several situations in fundamental particle physics, pure mathematical symmetry is not the rule; but **approximate symmetry** does exist. That is, in natural situations there are aspects which are approximately immune to possible transformations. There is no approximation in the transformation or in its possibility; it must indeed be possible to perform the transformation. The approximation is in the immunity; that is, some aspect of the natural situation must change by only a "little" when some transformation is performed (Rosen, 1995). The concept of "little" is based on the variations of the aspect in question being much less in magnitude than some characteristic length, time, mass, velocity, or what have you. Thus, the situation is said to be approximately symmetric under the transformation with respect to that aspect. In spite of the lack of perfect symmetry in the biological and geophysical sciences, the search for symmetry is a fruitful undertaking as it has been and is in the more fundamental areas of physics (Rosen, 1995).

As a science matures its reproductive and predictive features lead to the formulation of fundamental laws which are usually expressed in mathematical statements and equations given in some system of coordinates (i.e., a reference frame). Hence, Rosen (1995) states that the search for symmetry in nature consists of transformations, immunity from these changes, frames of reference, and non-immunity from the changes (or asymmetry). This search requires a general formalism of symmetry. Rosen shows that this formalism is couched in the mathematical language of transformations and symmetry, which is known as **group theory**. As geometry is the appropriate mathematics for investigating space, and calculus is the appropriate mathematics for investigating motion, group theory is the mathematics of symmetry. It is essential for the search of symmetry in all fields of science, including investigations in soil science and subsurface geology.

B.2 Similitude, Transformation Groups, Inspectional Analysis, Self-Similarity

The search for symmetry in physical systems invokes the use of concepts such as similitude, dimensional analysis, similar physical systems, inspectional analysis, transformations, groups, and self similarity. Skoglund (1967) says that *similitude* includes both the concepts of dimensional analysis and similar physical systems. *Dimensional analysis* is the special mathematics of units. All scientific measurements are referred to four internationally recognized fundamental or primary units of measurement: the kilogram, meter, second, and degree Kelvin. The fundamental or primary concepts of physical things and systems are mass M, length L, time T, and temperature Θ. These units of measurement and the primary concepts, although somewhat arbitrarily chosen, are the minimum number required for all macroscopic measurements of physical phenomena. From a microscopic point of view (i.e., individual molecules, atoms and subatomic particles), the fundamental units are the kilogram, meter and second. Thus, both viewpoints, macroscopic and microscopic, can be treated as one with respect to similitude concerns.

Dimensions comprise a class of units for the same variable, where the primary dimensions are M, L, T and Θ. For example, the universal gas constant in units of cal/degree K has the physical dimensions of $ML^2/T^2\Theta$. The fundamental principle of *dimensional substitution* (Skoglund, 1967) states that any "complete equation of physics" is satisfied when the units or dimensions of the variables are substituted for the variables themselves. Thus, any "complete equation" can be converted to a nondimensional form by dividing by a variable or group of variables with the same units as each of the sides of the equation. This forms a corollary of the principle of dimensional substitution, namely, that any "complete equation" can be converted into a nondimensional form. Therefore, any "complete equation" is independent of units, or *unit free*. "Complete equations" are also said to be *dimensionally homogeneous*. In essence, the above properties of a *complete physical equation* form a set of equivalent definitions for such an entity.

Birkhoff (1955) states that it is often claimed that "only dimensional homogeneous equations can be regarded as having fundamental physical significance." However, not all physically significant equations are true in all units! In fact, there exist no known fundamental units with respect to which all known physical laws are unit free. Birkhoff says no "Swift's Lilliput" can exist, for to do so would require changing some of the fundamental physical constants, such as the speed of light and Planck's constant in quantum mechanics. Nevertheless, for the current applications we are not limited in this regard. Birkhoff shows that for normal velocity distributions and temperature variations, the Newtonian mechanics of fluids possess as independent, fundamental units the quantities of mass, length, time and temperature. Thus, the above concepts of complete physical equations and dimensional substitution are valid for our current applications.

Two physical systems are said to be *similar* to each other if their pertinent, corresponding variables (e.g., velocity, acceleration, mass distribution, force fields and temperature fields) are proportional at corresponding locations and times. For example, we have previously introduced the terms prototype and model. A *prototype* of a given problem is the physical system itself. A *model* of the problem is *any* system that is similar to it. Mathematically speaking, and this is the only way that similarity can be precisely stated, the first requirement for the similarity of two systems is that their nondimensional governing equations be the same. Further, to guarantee that two similar systems possess the same nondimensional solutions it is required that both systems be well-formulated or well-posed (Flavin and Rionero, 1996) and that their nondimensional initial and boundary conditions be equivalent at corresponding points and times in their respective geometric domains. Thus, the complete establishment of similarity, its existence and its properties, dictates that these requirements be met. Anything less than this leads to a similarity between systems that is less than whole.

The various levels of similarity of importance in continuum mechanics are described in Skoglund (1967). A model is *geometrically similar* to a prototype if all the geometric features of the model can be related to those of the prototype by a single scale factor, as illustrated in Figure B-1. *Kinematic similarity* is concerned with similar "particles" (solid or fluid particles) possessing similar velocities and accelerations at corresponding points and times in similar geometries. *Dynamic similarity* is similarly defined for systems involving masses, forces, velocities, accelerations, geometries, and time. Finally, the *thermodynamic similarity* of a prototype continuum and its continuum model is based on the requirements and results derived from the principles of the conservation of mass, momentum and energy, along with pertinent initial and boundary conditions for the dependent variables.

Mathematically speaking (obviously, there is also a very strong experimental component of the search), the search for symmetry in the fields of continuum mechanics, which includes subsurface processes, first consists of writing down the governing equations and initial and boundary conditions on which the area of continuum mechanics in question is based. Then this system is tested for its *invariance* (i.e., similarity) under groups of
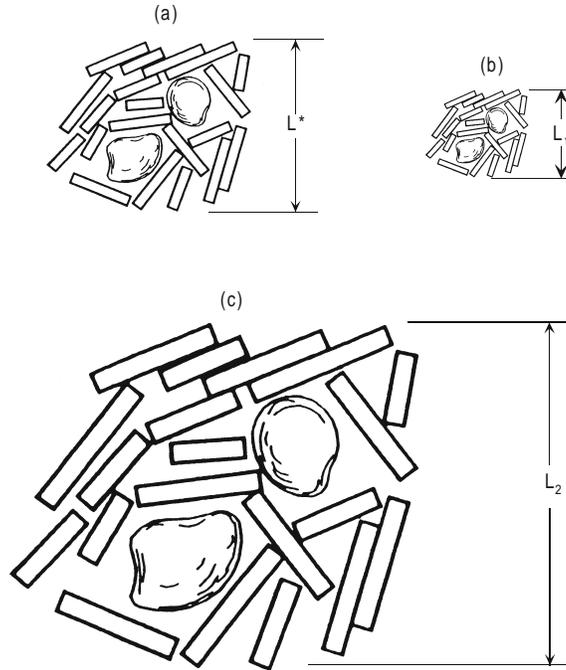
Figure B-1. Geometrically similar figures, where (a) is the reference figure with characteristic length L*, (b) is a similar figure with characteristic length L_1, $L^* = \alpha_1 L_1$, with scale factor $\alpha_1 = 2$, and (c) is a similar figure with $\alpha_2 L_2 = L^*$, $\alpha_2 = \frac{1}{2}$ (reprinted from *Unsaturated Zone Hydrology*, 1994, by Gary L. Guymon, with permission of Pearson Education, Inc., Upper Saddle River, NJ).

transformations of interest. This procedure is called ***inspectional analysis*** by Birkhoff (1955). For example, two fluid motions denoted by Φ and Φ' are dynamically similar if they can be described by Newtonian coordinate systems (i.e., systems in which Newton's laws of motion are valid) which are related by the transformation of space, time, and mass of the form:

$$x' = \alpha x, y' = \alpha y, z' = \alpha z, t' = \beta t, m' = \gamma m, \qquad (B-1)$$

where (α, β, γ) are constant scale factors, and x, y, z, t, m have their usual meanings of length, time and mass. If T, $T(\Phi) = \Phi'$, represents the transformation in Equation (B-1) with scale factors (α, β, γ), then T^{-1}, $T^{-1}(\Phi') = \Phi$, represents its inverse transformation with scale factors $(\alpha^{-1}, \beta^{-1}, \gamma^{-1})$. The successive application of T and T^{-1}, or T^{-1} and T, leads back to the original fluid motion. Thus, the product $T^{-1}T$ or TT^{-1} defines the identity transformation I with scale factors (1,1,1). Suppose we have two transformations of the type given in Equation (B-1): T_1 with scale factors $(\alpha_1, \beta_1, \gamma_1)$ and T_2 with scale factors $(\alpha_2, \beta_2, \gamma_2)$. The product of T_1 and T_2, apply T_1 to Φ and T_2 to Φ_1, is defined by: $T_2(T_1 \Phi) = T_2 \Phi_1 = \Phi_2$, where the scale factors of $T_2 T_1$ are given by $(\alpha_2 \alpha_1, \beta_2 \beta_1, \gamma_2 \gamma_1)$. Transformations which satisfy the above properties form a ***group***. Thus, as stated above, Newton's three laws of motion (for speeds much less than the speed of light) are invariant under this group of transformations. And in general, if the hypotheses of a given physical theory (e.g., governing equations and initial and boundary conditions) are invariant under a given group G of transformations, then the conclusions (e.g., system's solutions) are invariant under G; and these invariances are related to the system's symmetries.

Another important group of transformations in continuum mechanics is the ten parameter Galilei-Newton Group defined by Birkhoff (1955):

1. The space translation subgroup,

$$x_1' = x_1 + c_1, \quad x_2' = x_2 + c_2, \quad x_3' = x_3 + c_3 ; \qquad (B-2)$$

2. The time translation subgroup,

$$t' = t + c \; ; \tag{B-3}$$

3. The three parameter subgroup of rigid motions,

$$x'_i = \sum_{k=1}^{3} a_{ik} x_k \; , \tag{B-4}$$

$\|a_{ik}\| =$ most general 3x3 orthogonal matrix;

4. The three parameter subgroup of moving axes translated with constant velocity,

$$x'_i = x_i - b_i t \; . \tag{B-5}$$

Newton's three laws of motion, for speeds much less than the speed of light, are also invariant under the Galilei-Newton Group as they are under the group in Equation (B-1). Under these transformations, the definitions of the material constants (density, viscosity, etc.) are left unchanged for constant mass in the original and primed systems.

In Birkhoff's classical work of 1955, he concluded that because there are no general uniqueness theorems for the combined system of Navier-Stokes Equations, the continuity equation, the equation of state, and general initial and boundary conditions, *complete inspectional analysis* of hydrodynamic modeling is not possible. Such analysis awaits fundamentally new theorems about partial differential equations. Although much advancement has taken place since 1955, this is still the case in many areas of hydrodynamics, especially in some areas of interest to subsurface scientists, such as hysteresis (Visintin, 1994) and phase transitions (Brokate and Sprekels, 1996).

Self-similarity is a special condition of a single system (Skoglund, 1967). A system is self-similar if there exist a separable variable of the governing equation and the initial and boundary conditions of the system. This separable variable is called the similarity variable, and it permits one to reduce the number of variables/parameters which need to be considered in the system. Such variables are very valuable in the search for symmetric solutions of special partial differential and integral equations which satisfy special initial and boundary conditions. Classical examples of the application of self-similarity variables are the solutions of certain diffusion systems, the Prandll boundary-layer equations of viscous fluids, and the coagulation equation describing interacting liquid and solid particles. Whether or not a system is self-similar is not obvious, and the discovery of similarity variables may be a tedious process. However, the use of group-theoretic techniques and other mathematical tools reduces some of this tedium as evidenced by the work of Rogers and Ames (1989), Hill (1992), and Sachdev (2000). Several examples of interest to the subsurface scientist are detailed in these three books.

B.3 Scale Dependence and Scale Invariance in Hydrology

Sposito (1998a) has edited a recent survey concerned with symmetry and asymmetry in the field of hydrology. The symmetric features identified in the field are related to the concept of *scale invariance*, while the asymmetric features are related to *scale dependence.* If a system's features are symmetric, then there are no intrinsic scales for these features, be they length scales, time scales, velocity scales, or what have you. The symmetric features are similar for "any positive numerical values" of the scale factors in question. Of course, the use of the word "any" is only mathematical; based on realistic physical considerations, there are both upper and lower limits on the values of the pertinent scale factors. If some feature is asymmetric or becomes asymmetric for some reason, we say that this feature's symmetry is *broken* and the feature becomes scale dependent. An intrinsic scale exists for the feature. Thus, as the pertinent scales vary, the feature of the system changes in a nonsimilar manner.

The review of Sposito (1998a) is concerned with a variety of topics such as: scale analyses for land-surface hydrology, scaling of river networks, spatial variability and scale invariance in hydrologic regionalization, scaling of field soil-water behavior, scaling invariance of Richards Equation and its application to watershed modeling, scale issues of heterogeneity and stochastic modeling of scale-dependent macrodispersion in vadose-zone hydrology, dilution of nonreactive solutes in heterogeneous porous media and scale effects in large-scale solute-transport models, and scale effects in fluid flow through fractured geologic media and transport in multiscale permeability fields. Many of these topics are of direct concern to investigators of soil-moisture distribution and solute transport in the unsaturated, subsurface media. In what follows, we will briefly consider some of the topics in this review and show how they are related to the scaling features found in the HYDRUS and CHAIN-2D Codes.

One of the first papers on the similarity of soil-water behavior in unsaturated porous media and a paper related to the subject at hand is that of Miller and Miller (1956). Their work is based on the principle of *geometric similitude* in the microscopic arrangement of pores and solid particles, as illustrated in Figure B-1. Such similar porous media will have the same porosities and the same volumetric water content θ. Thus, these similarity assumptions resulted in the following scaling relationships:

Soil-Water Property	*Symbol and Dimensions*	*Scaling Relationships*
Volumetric Water Content	$\theta[1]$	$\theta^* = \theta$
Soil-Water Pressure Head	$h[L]$	$h^* = \alpha\, h$
Hydraulic Conductivity	$K[LT^{-1}]$	$K^* = \alpha^{-2}K$

where the asterisk denotes the referenced quantities, or the scaled properties that are the same for all the Miller-Miller similar porous media. The quantity α denotes the scale factor for the pores and solid particles combined (as shown in Figure B-1). The Miller-Miller similitude has been successfully applied to laboratory studies of sandy soils but has not been as successful in the analysis of field soils. The reason for this is that the saturated soil moisture content θ_s usually varies from place to place in a field such as shown in Figure B-2. In this figure, θ_s will usually vary (and thus, the θ-distribution) as one moves from vertical profile to vertical profile. That is to say, the soil profile p_i has a different internal geometry than that of soil profile p_j, $i \neq j$. Geometric similitude is not satisfied.

Warrick, et al. (1977) accounted for the fact that total porosity of a field soil is highly variable even within a given soil mapping unit by replacing θ in the Miller-Miller similitude by $S_{eo} = \theta/\theta_s$, where the residual soil moisture content θ_r in the effective water content S_e is taken to be zero. In essence, these authors introduced another scale factor into the Miller-Miller system, namely the saturated soil moisture content θ_s which accounts for the different internal geometries in field soils. The resulting scaling relationships for this new system are as follows:

Soil-Water Property	*Symbol and Dimensions*	*Scaling Relationships*
Relative Saturation	$S_{eo}[1]$	$S_{eo}^* = S_{eo}$
Soil-Water Pressure Head	$h[L]$	$h^* = \alpha_h h$
Hydraulic Conductivity	$K[LT^{-1}]$	$K^* = \alpha_k^{-2}K$
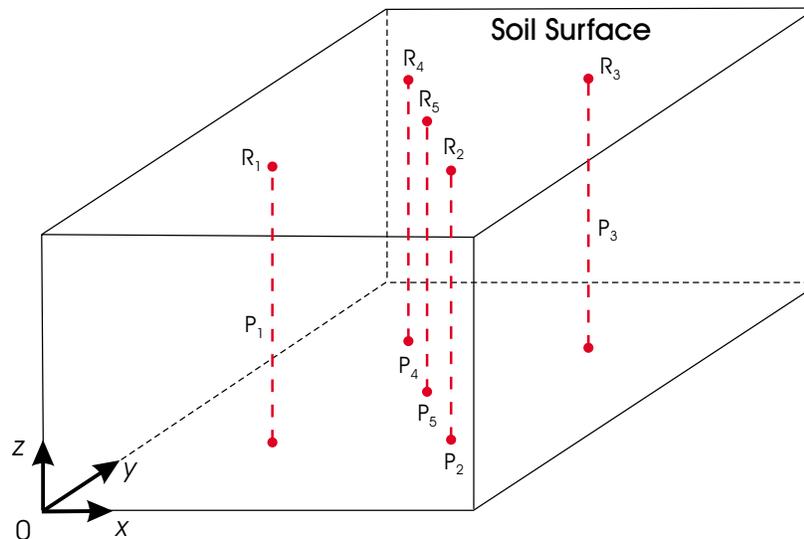
Figure B-2. The depiction of a set of vertical soil profiles $p_1, p_2, \ldots$ distributed over a field mapping unit, where z represents the local variable within a soil profile and R_i ($i = 1, 2, \ldots$) represent the horizontal vectors in the xy-plane giving the global positioning of the vertical profiles, $p_1, p_2, \ldots$.

where the asterisk denotes the referenced quantities which may be fieldwide averages, whereas the un-asterisked quantities denote field-plot-specific profiles of the quantities in question. The scale factors α_h and α_k are, in general, not equal as in the Miller-Miller similitude case.

Warrick, et al. (1977) avoided a search for a microscopic physical length, as required by geometric similarity, by merely deriving values of α_r that minimized the sum of squares

$$SS = \sum_{r=1}^{N} \sum_{i=1}^{M} (h^* - \alpha_r h_i)^2 \ , \tag{B-6}$$

where N represents the number of macroscopic locations within a field soil and M and number of observations of h as a function of S_{eo}. Figures B-3abcd illustrate this procedure for observations taken over an agriculture field consisting of panoche soil. Figure B-3a shows 840 measurements of (θ,h) plotted as h vs S_{eo}, where the soil samples were taken at six soil depths at 20 sites within the field, giving an N = 120. Each of these 120 soil samples were analyzed in the laboratory with seven values of h, giving various values of S_{eo} for each h, thus M is equal to 7. The result of minimizing SS in Equation (B-6) was the coalescing of the data in Figure B-3a into the single curve $h^*(S_{eo})$ shown in Figure B-3b, the h*-curve being a low order rational function in S_{eo}. Similarly, the 2640 values of (K,θ) in Figure B-3c, plotted as S_{eo} vs K, were coalesced and described by the regression curve indicated in Figure B-3d. This regression relationship is a cubic polynomial in S_{eo} for the logarithm to the base e of K*. Warrick, et al. found that the scale factors for α_h were not equal to those for scaling K,α_k. Further, it should be noted that the values of $h(\theta)$ scaled in Figure B-3ab were those measured in the laboratory on soil cores removed from the field, and the values of $K(\theta)$ scaled in Figures B-3cd relied on the laboratory results for $h(\theta)$ to obtain estimates of $\theta(t)$ based on field tensiometric measurements.
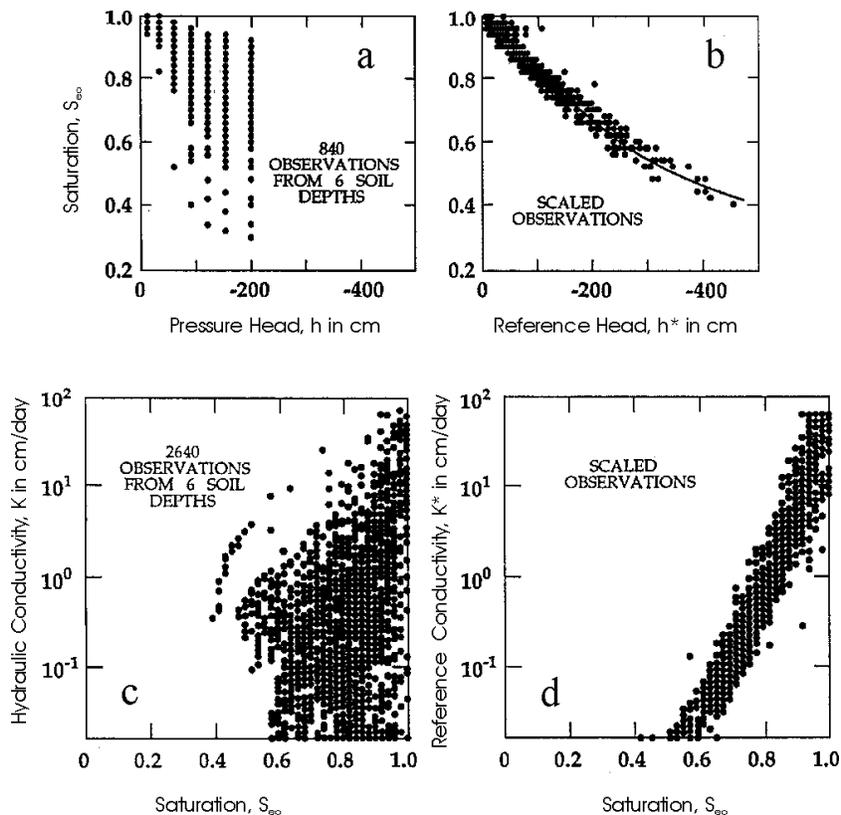
Figure B-3. (a) Unscaled observations of $S_{eo}(h)$, (b) Scaled observations of $S_{eo}(h^*)$, showing the reference relationship as a solid curve, (c) unscaled observations of $K(S_{eo})$, and (d) scaled observations of $K^*(S_{eo})$ (reprinted from *Water Resources Research,* 1977, by A.W. Warrick, G.J. Mullen and D.R. Nielsen with the permission of the American Geophysical Union, Washington, DC).

Based on the early work of Miller and Miller (1956) and Warrick, et al. (1977), as well as the principles of similitude and invariance, Vogel, et al. (1991) introduced and studied the system of transformations that form the foundation of the scaling relationships in the HYDRUS and CHAIN 2D Codes. These **_linear transformations_** account for the linear variability in the soil moisture parameters and are defined by the following:

$$h = \alpha_h h^* ,$$ (B-7)

$$\theta(h) - \theta_r = \alpha_\theta \left[\theta^*(h^*) - \theta_r^* \right],$$ (B-8)

$$K(h) = \alpha_k K^*(h^*) ,$$ (B-9)

where once again the asterisk denotes reference quantities and the three scale factors $\left(\alpha_h, \alpha_\theta, \alpha_k \right)$ are assumed to be independent of one another.

Vogel, et al. (1991) claim that these linear transformations will explain the variability due to soil structure within a given soil textural class, but will not account for the nonlinear phenomena expressed by different soil textural classes. For example, if the soil-water behavior is represented by one of the models considered in Appendix A, say the VG-Model, then the α fitting parameter in the model relates to the linear scaling factors and is dominated by the soil structure. The shape factors in the quantities $\theta(h)$ and $K(h)$ of the VG-Model are expressed by the n fitting parameter which is highly correlated with soil texture and represents phenomena not accounted for in Equations (B-7) to (B-9). Thus, the scaling laws in Equations (B-7) to (B-9), with their scale factors $\left(\alpha_h, \alpha_\theta, \alpha_k \right)$, reference hydraulic characteristics (h*, θ*, K*), and the parameters of the reference quantities derived from analytical expressions (e.g., the BC-, VG-, or VC-Models), identify a set of **_similar soil classes_** where each member of the set corresponds to a given textural class. Hence, this linear transformation allows an investigator to resolve a set of soil measurements (from one field mapping unit, or a set of field mapping units) into a set of similar soil classes where the similar class distinction is given by the various soil textural classes found in the data. Within a given similarity class, the soils are linearly related by the transformations in Equations (B-7) to (B-9), and this relationship is dominated by varying soil structure within the given textural class. These variations in soil structure may be due to certain linearly changing, heterogeneous layers in a vertical profile and/or due to global changes in soil structure as one changes horizontal location within field mapping units (Figure B-2). Figure B-4 is a schematic which summarizes the similarity classification process.

Other features of the Vogel, et al. (1991) similarity system include the resolution of the scaling factors $\left(\alpha_h, \alpha_\theta, \alpha_k \right)$ into products of two subfactors. One subfactor accounts for the local variation within a given profile (the z-variation of profiles $p_1, p_2, \ldots$ in Figure B-2) and the other subfactor accounts for the global variation between profiles (the $R_1, R_2, \ldots$ locations in Figure B-2). However, the reference quantities (h*, θ*, K*) are constructed to be independent of global variations, while being locally dependent on some type of mean-field profile. Further, the authors consider the invariance of Richards Equation (Appendix A and the main text) for a set of soil profiles with respect to the transformations in Equations (B-7) to (B-9), supplemented by linear transformations in the variable, z, time, t, infiltration rate, v, cumulative infiltration, I, and cumulative outflow, Q. Richards Equation was shown to be invariant under these transformations, thus giving invariant solutions to the system, provided certain restrictions were met. These restrictions were placed on the local and global subfactors of the scaling factors, and on the initial and boundary conditions of the system. The results of the derived invariances led to simple relationships between the soil-moisture scaling factors $\left(\alpha_h, \alpha_\theta, \alpha_k \right)$ and the dynamic scaling factors ($\alpha_t, \alpha_z, \alpha_v, \alpha_I, \alpha_Q$). Because of the restrictions placed on the system's auxiliary conditions, these invariances were shown to hold only for the following situations:

1. Constant head infiltration into a stratified soil profile.

2. Water redistribution within a soil-water system with zero flux boundaries.

3. Drainage flow with constant suction head boundary conditions, such as in laboratory outflow experiments.

Finally, Vogel, et al. (1991) outline the procedures for identifying the $\left(\alpha_h, \alpha_\theta, \alpha_k \right)$ scaling factors and reference quantities (h*, θ*, K*) from measured soil hydraulic data, as well as the indirect identification procedures of these quantities from measured dynamic characteristics of soil-water systems, such as those obtained from field infiltration tests and laboratory outflow studies. The authors conclude that these linear transformation procedures and their resultant dynamical similarities produce the following advantages in the analyses of soil-moisture processes:

Nonlinear Variability in Soils | Linear Variability in Soils

Shape Parameters Correlate with Soil Texture | Scaling Parameters Dominated by Soil Structure

S_{11}

Texture 1 S_{12} Class 1

S_{1n}

SOIL

S_{21}

Soil Observa-tions   Texture 2 S_{22} Class 2

S_{2p}

STRUCTURES

S_{m1}

Texture m S_{m2} Class m

S_{mq}
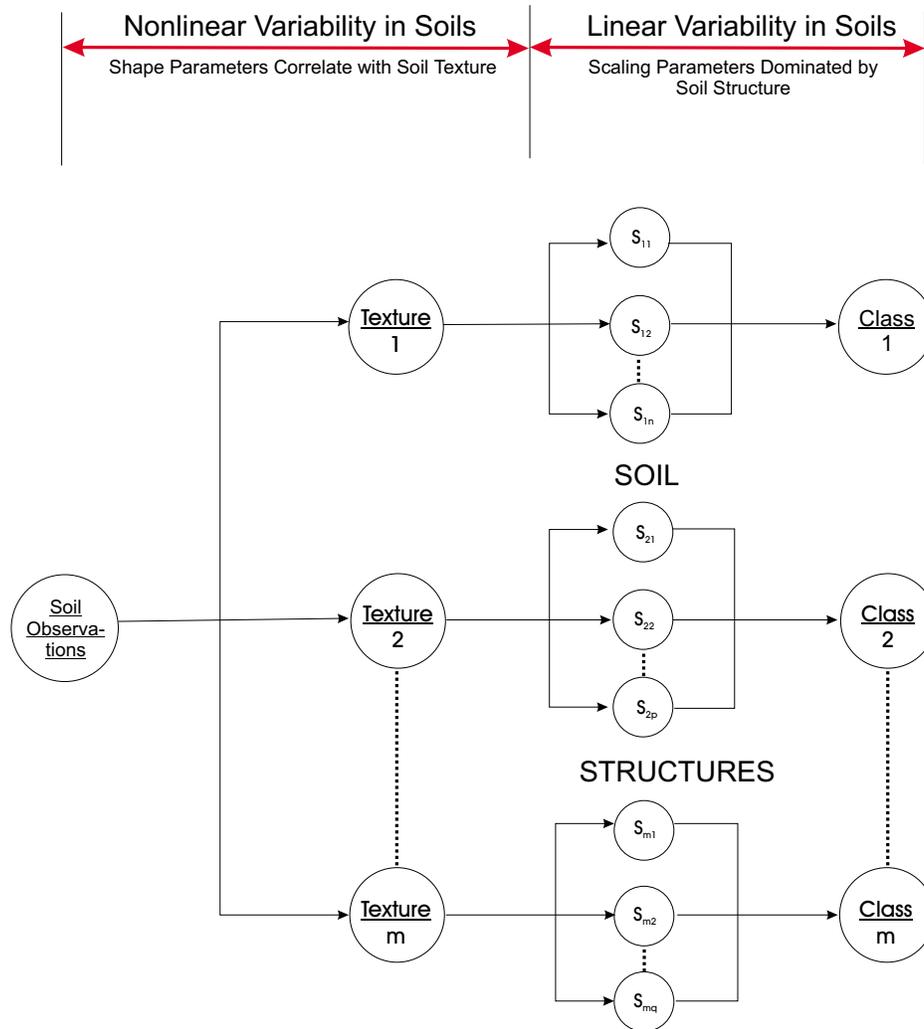
Figure B-4. The application of linear scaling to a set of soil-moisture observations, resulting in a set of m similar soil classes. The mth class of similar soils accounts for the soil structures s_{m1}, s_{m2}, ..., s_{mq} within the soil textural class m. The number of similar soil classes corresponds to the number of soil textural classes.

1. There exists savings in the experimental and computing efforts required in the analyses of heterogeneous soils;

2. There exists simplifications in the analyses of certain phenomena, such as the derivation of θ and K distributions from outflow experiments and infiltration tests; and

3. There exists efficient and viable methods of relating laboratory scale results to field scale results.

Rockhold, et al. (1996) applied the basic principles found in the previous three studies to simulate the water flow and the transport of tritium measured at an initially unsampled domain of the Las Cruces Trench Site. The hydraulic parameters in this simulation were obtained in the following manner. From water-retention data for core samples collected at the site (but not from the domain in question), the scale factors α_h in $h^* = \alpha_h h$ were determined from a scale-mean BC-Model (Appendix A) and the measured moisture data. Parameters for the soil-water retention were then used in the Burdine (1953) relative-permeability model to estimate $K(\theta)$. Saturated values for the hydraulic conductivity K_s were measured in the field at nearly 600 locations. The K_s data were scaled according to

$K(\theta) = \alpha_k^2 K^*(\theta)$. The probability distribution for α_h and α_k was found to be lognormal. The geostatistical horizontal variograms for the log-transformed scale factors (α_h, α_k) show similar spatial structures to lags of 4 to 6 meters, which is an indication of a Miller-Miller similitude structure. Thus, Rockhold, et al. (1996) found that it was not necessary to invoke three independent factors $(\alpha_h, \alpha_\theta, \alpha_k)$ to condition the hydraulic properties of the field to run their simulations. Rather they used a constant value for θ_s, constant values for the slopes of $S_{eo}(h)$ and $K(S_{eo})$, and the same distribution for α_h and α_k to condition the hydraulic properties of the field in their simulations. Simulations of water flow adequately agreed with those measured without any further "calibration" of the model. Hence, the authors showed the power of scaling analyses in the simulation of unsaturated flow and transport processes.

In the Sposito (1998a) review, which was previously mentioned, there are six sections that are of particular interest to the subject at hand. These are Sections 5 to 10. In **Section 5**, Nielsen, et al. (1998) gives a detailed survey of the scaling of field soil-water behavior, from the work of Miller and Miller, to the use of fractal and multifractal concepts for representing soil structures. In addition, they review the work which combines linear-variability scaling with the inverse solution of the Richards Equation to estimate in situ hydraulic properties of the soil. Although many of the techniques surveyed have been successfully applied in various problems, the authors conclude that there exists **no generalized theory** at this time for the **comprehensive scaling** of the behavior of field soil-water regimes.

In **Section 6**, Sposito (1998b) considers the relationship between scaling invariance and Richards Equation (the Richards Equation which is free of sources and sinks). Using group analysis (Lie Groups in particular), Sposito shows that the invariance of the pore size distribution under scaling leads to the result that similar media will show mathematical identical forms of $S_e(\alpha h)$ but not for $\theta(\alpha h)$. This invariance is compatible with a broad range of particle sizes and the nonuniform porosity of field soils. Further, the scale invariance is a more general concept than fractal self-similarity. The Lie Group analysis of the Richards Equation, using the transformation

$$(\theta', t', z') = (\mu\theta, \delta t, \alpha z), \tag{B-10}$$

where (μ, δ, α) are independent scale factors, requires that the parameters $D(\theta)$, $K(\theta)$, and $h(\theta)$ must be **power** or **exponential functions** if the Richards Equation is scale invariant. For the derivation of invariant solutions of the transformed Richards Equation, compatible (invariant) initial and boundary conditions are also required. The scale invariance of the Richards Equation implies the scale invariance of S_e, implies that the BC-Function can be a model for $h(\theta)$, and also implies that $h(\theta)$ can be represented by a generic fractal model Perrier, et al. (1996). In addition, Sposito (1998b) considers the effects of broken symmetries, for example the effects of time being unscaled, and the effects of length being unscaled.

In **Section 7,** Haverkamp, et al. (1998) consider the scaling of Richards Equation and its application to watershed modeling. They make a strong plea for the use of dimensional analysis and inspectional analysis (i.e., dynamic similarity) as opposed to just the scaling of a soil's static hydraulic characteristics. This latter procedure fails to scale vadose-zone behavior in a general way. With this in mind, this section is concerned with cumulative-infiltration curves I(t) analyzed for different surface boundary conditions and for subsurface water movement governed by the Richards Equation. They found that for general field soils, there is **no unique dynamic similarity** for the behavior of soil-water movement in the vadose zone (see Figure B-4). Only for two soils (Green and Ampt, 1911; and Gardner, 1958) does unique dynamic similarity exist. However, these two soils define the limits of the envelope for all possible similarity classes that exist for general field soils. For the description of general infiltration, three scaling parameters are required, while only two are required for the two limiting cases. Further, because of these two limiting cases, in practical applications such as watershed modeling, one can assume that there exists a unique dynamic similarity, thus simplifying certain hydrologic analyses.

In **Section 8**, Yeh (1998) investigates the key scale issues of heterogeneity in vadose-zone hydrology. He defines a field scale representative elementary volume (FSREV) and considers the effects on specifying the hydraulic parameters when our domain of interest is greater than FSREV and when it is less. He considers the use of stochastic methods to give better estimates of these parameters, but dogmatically states that only large amounts of data can lessen the uncertainties in vadose-zone parameters and can make the stochastic results statistically meaningful.

In **Section 9,** Russo (1998) considers the problem of solute transport through partially saturated heterogeneous porous formations, while in **Section 10,** Kapoor and Kitanidis (1998) are concerned with the dilution of nonreactive solutes in heterogeneous porous media. The key results of these papers show that solute plumes may not spread as much in the longitudinal direction as expected in homogeneous cases, that the travel distances required for the longitudinal component of the macrodispersion tensor to approach its asymptotic value (i.e., Fickian behavior) can be

exceedingly large, and that current standard approaches of estimating plume concentrations can severely overestimate dilution in heterogeneous media.

References

Birkhoff, G. 1955. <u>Hydrodynamics: A Study in Logic, Fact and Similitude</u>. Dover Publications, Inc. New York, NY. 186 pp.

Brokate, M. and J. Sprekels. 1996. <u>Hysteresis and Phase Transitions</u>. Springer-Verlag, Inc. New York, NY, 357 pp.

Burdine, N.T. 1953. "Relative permeability calculations from size distribution data." <u>Am. Inst. Min. Metal. Pet. Eng</u>. 198, 71–77.

Flavin, J.N. and S. Rionero. 1996. <u>Qualitative Estimates for Partial Differential Equations: An Introduction</u>. CRC Press. Boca Raton, FL. 368 pp.

Gardner, W.R. 1958. "Some steady-state solutions of the unsaturated moisture flow equation with application to evaporation from a water table." <u>Soil Sci</u>. 85. 228–232.

Green, W.H. and G.A. Ampt. 1911. "Studies in soil physics: I. The flow of air and water through soils." <u>J. Agric. Sci.</u> 4, 1–24.

Guymon, G.L. 1994. <u>Unsaturated Zone Hydrology</u>. PTR Prentice Hall. Englewood Cliffs, NJ. 210 pp.

Haverkamp, R., J.-Y. Parlange, R. Cuenca, P.J. Ross and T.S. Steenhuis. 1998. "Scaling of the Richards equation and its application to watershed modeling." In <u>Scale Dependence and Scale Invariance in Hydrology</u>, Edited by G. Sposito. Cambridge University Press. New York, NY. 190–223.

Hill, J.M. 1992. <u>Differential Equations and Group Methods for Scientists and Engineers</u>. CRC Press. Boca Raton, FL 201 pp.

Kapoor, V. and P. Kitanidis. 1998. "Dilution of nonreactive solutes in heterogeneous porous media." In <u>Scale Dependence and Scale Invariance in Hydrology</u>. Edited by G. Sposito. Cambridge University Press. New York, NY, 291–313.

Miller, E.E. and R.D. Miller. 1956. "Physical theory for capillary flow phenomena." <u>J. Appl. Phys</u>. 27. 324–332.

Nielson, D.R., J.W. Hopmans and K. Reichardt. 1998. " An emerging technology for scaling field soil-water behavior." In <u>Scale Dependence and Scale Invariance in Hydrology</u>. Edited by G. Sposito. Cambridge University Press. New York, NY. 136–166.

Perrier, E., M. Rieu, G. Sposito and G. de Marsily. 1996. "Models of the water retention curve for soils with a fractal pore size distribution." <u>Water Resour. Res.</u> 32(10). 3025–3031.

Rockhold, M.L., R.E. Rossi and R.G. Hills. 1996. "Application of similar media scaling and conditional simulation for modeling water flow and tritium transport at the Las Cruses Trench Site." <u>Water Resour. Res</u>. 32(3). 595-609.

Rogers, C. and W.F. Ames. 1989. <u>Nonlinear Boundary Value Problems in Science and Engineering</u>. Academic Press, Inc. New York, NY. 416 pp.

Rosen, J. 1995. <u>Symmetry in Science: An Introduction to the General Theory</u>. Springer-Verlag. New York, NY. 213 pp.

Russo, D. 1998. "Stochastic modeling of scale-dependent macrodispersion in the vadose zone." In <u>Scale Dependence and Scale Invariance in Hydrology</u>. Edited by G. Sposito. Cambridge University Press. New York, NY. 266-290.

Sachdev, P.L. 2000. <u>Self-Similarity and Beyond: Exact Solutions of Nonlinear Problems</u>. Chapman & Hall/CRC. Boca Raton, FL. 319 pp.

Skoglund, V.J. 1967. <u>Similitude: Theory and Applications</u>. International Textbook Company. Scranton, PA 320 pp.

Sposito, G. 1998a. Editor of <u>Scale Dependence and Scale Invariance in Hydrology</u>. Cambridge University Press. New York, NY 423 pp.

Sposito, G. 1998b. "Scaling invariance and the Richards equation." In <u>Scale Dependence and Scale Invariance in Hydrology</u> . Edited by G. Sposito. Cambridge University Press. New York, NY. 167–189.

Visintin, A. 1994. <u>Differential Models of Hysteresis</u>. Springer-Verlag. New York, NY. 407 pp.

Vogel, T., M. Cislerova and J.W. Hopmans. 1991. "Porous media with linearly variable hydraulic properties." <u>Water Resour. Res</u>. 27(10). 2735–2741.

Warwick, A.W., G.W. Mullen and D.R. Nielsen. 1977. "Scaling field-measured soil hydraulic properties using a similar media concept." <u>Water Resour. Res</u>. 13. 355–362.

Yeh, T. – C.J. 1998. "Scale issues of heterogeneity in vadose-zone hydrology: In <u>Scale Dependence and Scale Invariance in Hydrology</u>. Edited by G. Sposito. Cambridge University Press. New York, NY. 224–265.

Appendix C
An Explanation of the Hysteretic
Characteristics of Soil-Water Properties

The HYDRUS Code is the only code of the five considered in this report to introduce the phenomenological concept of hysteresis in the formulation of the soil-water properties, $\theta(h)$ and $K(h)$. This phenomenon is certainly not unique to the field of soil physics, for it has a long history in many engineering and scientific systems such as mechanical, electrical, chemical, biological, physical, and geophysical systems, and even in psychological systems. The presence of hysteretic components in a system tends to make the system highly nonlinear, may produce instabilities and discontinuities, and certainly introduces memory dependent processes. Thus, hysteresis will make easy problems complex, and complex problems even more complicated. But hysteresis is a natural phenomenon that does exist and must be dealt with in many areas of soil physics, as well as in other scientific areas.

There are two sets of inquiries which one is concerned with when dealing with such a phenomenon. One set consists of the following questions: In what physical systems does it occur? Under what conditions is the phenomenon important? And, how does one formulate the phenomenological component in mathematical terms and incorporate it into the governing equations of the system in question? The other set of inquiries deals with the well-posedness of the formulated systems containing the phenomenon. The questions in this set of inquiries include: Does a solution exist for the formulated system? Is the solution obtained unique for the given governing equation and initial and boundary conditions? And, is the solution continuous with respect to the system parameters, the form of the phenomenological component, and the initial and boundary conditions?

With reference to the first set of inquiries for the phenomenon of hysteresis, one runs across such concepts as hysteresis loops, hysteresis operators, hysteretic models, partial differential equations with memory, and discontinuous hysteresis, as well as ideas from catastrophe theory. Because of the complexity introduced by hysteresis operators and the memory components, it is necessary to analyze the resultant systems with respect to the concepts of well-posedness, our second set of inquiries. The tools used to answer this set of inquiries are highly mathematical and involve such fields as functional analysis, semigroups, variational inequalities, and differential inclusions. In the following subsections we will only briefly cover some of the key points in the first set of inquiries and will not discuss any of the mathematical tools used in the second set of inquiries. The subsections that follow are designated as:

(1) The Origins and Application of Hysteretic Phenomena,
(2) Hysteresis Loops, Operators and Models,
(3) Hysteresis in Soil-Moisture Parameters.

Although this appendix does not cover the mathematical aspects of hysteretic phenomena, we list several pertinent references for the mathematically-inclined reader:

(1) For the origins and applications of hysteresis, the formulation of hysteresis operators and models, and the investigations of the well-posedness of the systems see Visintin (1994), and Brokate and Sprekels (1996).
(2) For the theory and application of functional analysis see Rudin (1991) and Edwards (1995).
(3) For the formulation and applications of catastrophe theory see Gilmore (1981), and Castrigiano and Hayes (1993).
(4) For the application of variational inequalities in porous media and other mechanical systems see Chipot (1984), and Hlaváček et al. (1988).
(5) For the theory and applications of semigroups in linear and nonlinear systems see Goldstein (1985) and Miyadera (1992).
(6) For the definition, use, and solution of differential inclusions see Aubin and Cellina (1984) and Visintin (1994).

C.1 The Origins and Applications of Hysteretic Phenomena

Hysteresis is a phenomenon that occurs in rather different situations. It can be a byproduct of fundamental physical mechanisms, such as phase transitions; or a consequence of a degradation or imperfection, like the play in a mechanical system; or a deliberate construct of a system in order to monitor the system's behavior, as in the case of heat control via thermostats (Brokate and Sprekels, 1996). In physics, we encounter hysteresis in plasticity, friction, ferromagnetism, ferroelectricity, superconductivity, adsorption and desorption, and other processes. Recently, shape memory effects have been observed and exploited in some new materials. Hysteresis also occurs in the engineering disciplines, such as in porous media filtration, granular motion, semiconductors, spin glasses, and mechanical damage and fatigue. In addition, the phenomenon appears in chemical, economical, psychological, and biological processes (Visintin, 1994).

As indicated above, hysteresis effects are often caused by ***phase transitions*** which are accompanied by abrupt changes of some of the involved physical quantities, as well as the absorption or release of energy in the form of latent heat. The area of the hysteresis loop (Figure C-1) gives a measure of the amount of energy that has been dissipated or absorbed during the phase transformation. For example, phase transitions possess hysteresis effects when there is undercooling prior to nucleation and superheating prior to vaporization. Other phase transitions possessing hysteresis effects are as follows (Visintin, 1994):

Phase Transition	*Order Parameter*	*External Field*
ferromagnetic	magnetization	magnetic field
ferroelectric	polarization	electric field
liquid-vapor	reduced density	pressure
martinsite	strain	stress
phase separation	concentration	chemical potential differences

C.2 Hysteresis Loops, Operators and Models

Figure C-1 shows a typical ***continuous, closed hysteresis loop*** for a system whose state is defined by the two scalar variables (u, v). The variable u represents the input to the system (i.e., the independent variable) and v represents the output (i.e., the dependent variable). Both u and v depend on time t, and evolve as time increases in a

CONTINUOUS HYSTERESIS LOOP
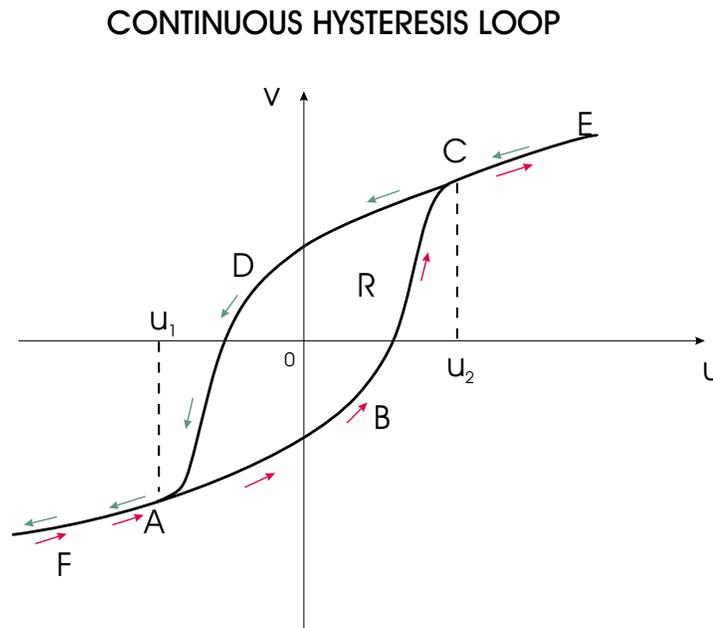
Figure C-1.   A continuous hysteresis loop for a system whose state is given by the couple (u,v), where u is the input and v is the output (reprinted from *Differential Models of Hysteresis*, 1994, by Augusto Visintin, with permission of Springer-Verlag, GmbH & Co. KG, Heidelberg, Germany).

manner dictated by the system in question. When u increases from u_1 to u_2, then the state of the system (u, v) evolves along the lower curve of the loop, ABC. If u increases beyond u_2, then the state (u, v) follows the curve from C to E. If u now decreases from its value at point E, then the state (u, v) moves along the curve from E to C. As u decreases from u_2 to u_1, the state (u, v) follows the upper curve of the loop CDA. If u decreases beyond u_1, then (u, v) follows the curve from A to F. Now, if u begins to increase from the u at point F, the cycle begins to repeat itself.

If u is between u_1 and u_2 and the evolution of the state (u, v) is inverted, (u, v) will move into the interior of the region bounded by ABCDA, (i.e., region R). In standard examples, the couple (u, v) can attain any interior point of R by a suitable choice of the input function u. These last two properties follow from the memory aspect of hysteresis. As early as (1905), Madelung attempted to formalize these memory attributes into a set of rules governing the experimentally observed branchings and loopings of ferromagnetic hysteresis. The rules which were developed are as follows (see Figure C-2):

(1) As the state of the system (u, v) moves down curve Γ from point C, it arrives at turning point A, where the state (u, v) now moves up curve Γ_1. **Rule 1** states that Γ_1 is uniquely determined by the coordinates of A.

(2) Point B is now taken as any point on curve Γ_1 where the motion of the state (u, v) is inverted, point B becomes a new turning point. **Rule 2** says that the evolution of the state is now along curve Γ_2 and that curve starts at B and terminates at A.

(3) If the input value u decreases beyond its value for point A, **Rule 3** says the state (u, v) follows along curve Γ from A to D.

These rules of Madelung can be applied at any point on the loop ABCDA in Figure C-1, and at any point in its interior R if previous state evolutions have reached that interior point.

We assume that the evolution of v is uniquely determined by that of u, and such a result is made precise by formulating the concept of a ***hysteresis operator,*** $W: u \rightarrow v$. However, we know from above, that whenever
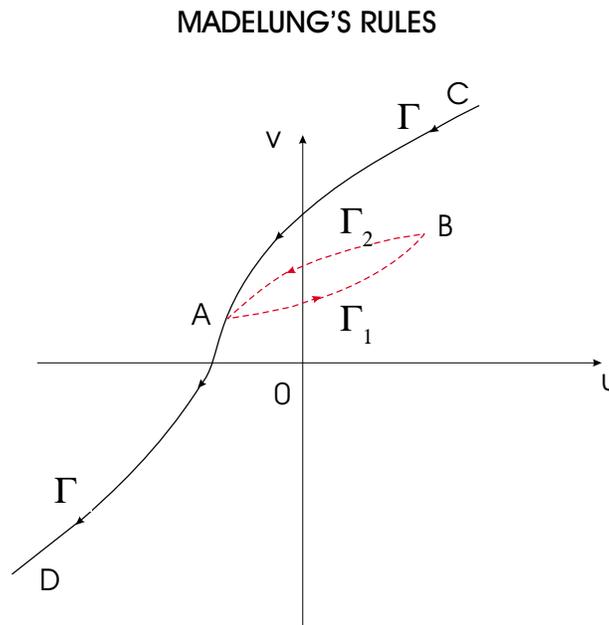
MADELUNG'S RULES

Figure C-2.   A defining sketch of Madelung's Rules for the memory attributes of ferromagnetic hysteresis (reprinted from *Hysteresis and Phase Transitions*, 1996 by Martin Brokate, Jürgen Sprekels, with permission of Springer-Verlag, GmbH & Co. KG, Heidelberg, Germany).

$u_1 < u(t) < u_2$, v(t) is not determined by the value of u(t) at the same instant, but also depends upon the previous evolution of u *(the memory effect)* and possibly on the initial state of the system. Therefore, the operator W should be written as:

$$v(t) = W[u] \equiv W[u(t), H(u), u_0, v_0],$$
(C-1)

where H(u) represents the pertinent history of u and (u_0, v_0) is the initial state.

For hysteresis, we also require that the path of the couple [u(t), v(t)] be invariant with respect to any increasing time homeomorphism (Visintin, 1994). This means that at any instant of time t, v(t) only depends on the range of the restriction on u (i.e., the values of u(t') over the time interval $o \leq t' \leq t$) , and on the order in which the values are attained as t' increases from o to t. There is no dependence upon the time derivatives of u: du/dt, d^2u/dt^2, etc. In fact, these time derivatives (du/dt, d^2u/dt^2, ...) may not exist in general, or at least not exist at some points. This condition is essential for the existence of Figure C-1; for if it did not hold, the path of the state (u, v) would depend on (du/dt, dv/dt)and Figure C-1 would be invalid. This condition is commonly called *rate independence,* and means that the output is invariant with respect to changes of the time scale. Thus, hysteresis is characterized by two features: memory and rate independence. Rate independent memory is persistent and thus scale invariant, while rate dependent memory is typically fading and thus scale dependent (Visintin, 1994).

The above restrictions on hysteretic phenomena excludes any viscous type memory such as those represented by time convolution. Typical hysteretic phenomena such as ferromagnetism, ferroelectricity and plasticity possess memory effects that are not purely rate independent since the hysteresis is coupled with viscous-type effects. But if the evolving state is not too fast, (du/dt, dv/dt) is relatively small in magnitude, and the rate independent component prevails. Thus, hysteresis is more evident in slow regimes, and rate dependent effects get larger as rates increase and vanish as (du/dt, dv/dt) approaches zero. Finally, hysteresis loops as shown in Figure C-1 need not appear in the physical systems listed in the above paragraphs. Some regions which are surrounded by hysteresis curves may be unbounded, some regions may be bounded but the hysteresis curves are discontinuous at various points, and some systems may possess rate dependent loops (e.g., electric losses in ferromagnetism due to eddy currents), see Visintin (1994).

Visintin (1994) states that maybe the most powerful *hysteresis model* among those available for analysis is the *Preisach Model*. This model is the superposition of a continuous family of elementary discontinuous hysteresis models, called *delayed relays*. The Preisach Model was originally proposed for scalar ferromagnetism and offers a good qualitative description of several phenomena in that field. Since then, it has been regarded by engineers and physicists as a fundamental tool in several areas. In fact, it has been applied to hysteretic phenomena in the field of *unsaturated flow through porous media*.

The underlying idea of the Preisach Model is quite simple and relies on the delayed relay shown in Figure C-3a. This relay with hysteresis can be defined by the four parameters shown in the figure: width a, height b, center point (u_c, v_c). Thus, we denote this relay by the expression R(a, b, u_c, v_c). The linear combination of a finite family of such delayed functions R(a_i, b_i, u_{ci}, v_{ci}), i = 1, 2, ..., n, yields a hysteresis loop as shown in Figure C-3b, whose enclosed region is denoted by R_f. This construction, in the limit, allows one to approximate a fairly large class of continuous hysteresis laws (including those for soil-moisture parameters) and yields an operator which acts in the space of continuous time functions. With reference to Figure C-3b, this limiting procedure is such that the discontinuous hysteresis loop approaches the continuous loop which is the envelope of the finite combination of delayed relays. Further, the region R_f of the discontinuous loop approaches the region R of the continuous loop as shown in Figure C-1. Finally, the limiting operator, or Preisach Model, is denoted by

$$v = P(u) .$$
(C-2)

The formal mathematical definition of the Preisach Model is given in Visintin (1994) and in Brokate and Sprekels (1996).

Visintin (1994) considers the effects of incorporating the Preisach Model, as well as other hysteretic models, into systems governed by ordinary and partial differential equations. For example, the coupling of rate independent hysteretic nonlinearities with ordinary differential equations leads to interesting and complicated problems in the theory of nonlinear oscillations, such as the oscillator with a hysteretic restoring force:

$$\frac{d^2u(t)}{dt^2} + P(u) = f(t) ,$$
(C-3)
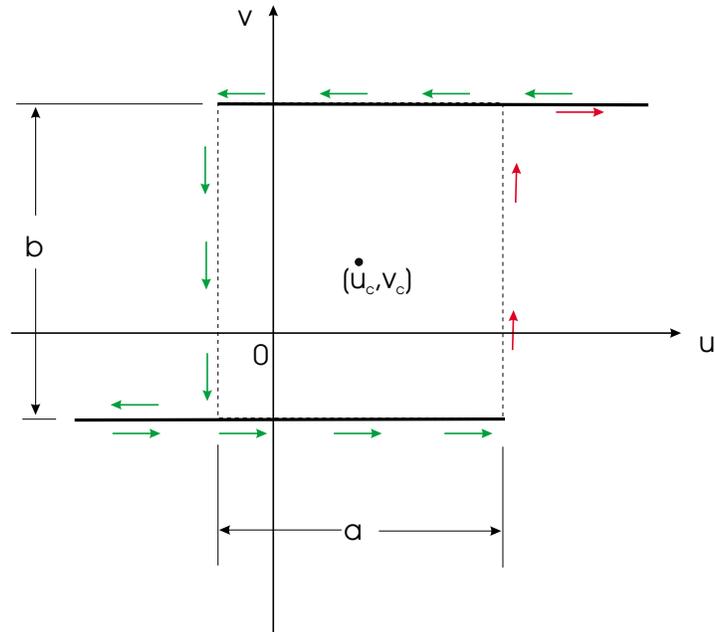
Figure C-3a. A relay with hysteresis, or a delayed relay, defined by the parameters (a, b, u $_c$, v$_c$) with repect to the system defined by states (u,v) (reprinted from *Differential Models of Hysteresis*, 1994, by Augusto Visintin, with permission of Springer-Verlag, GmbH & Co. KG, Heidelberg, Germany).
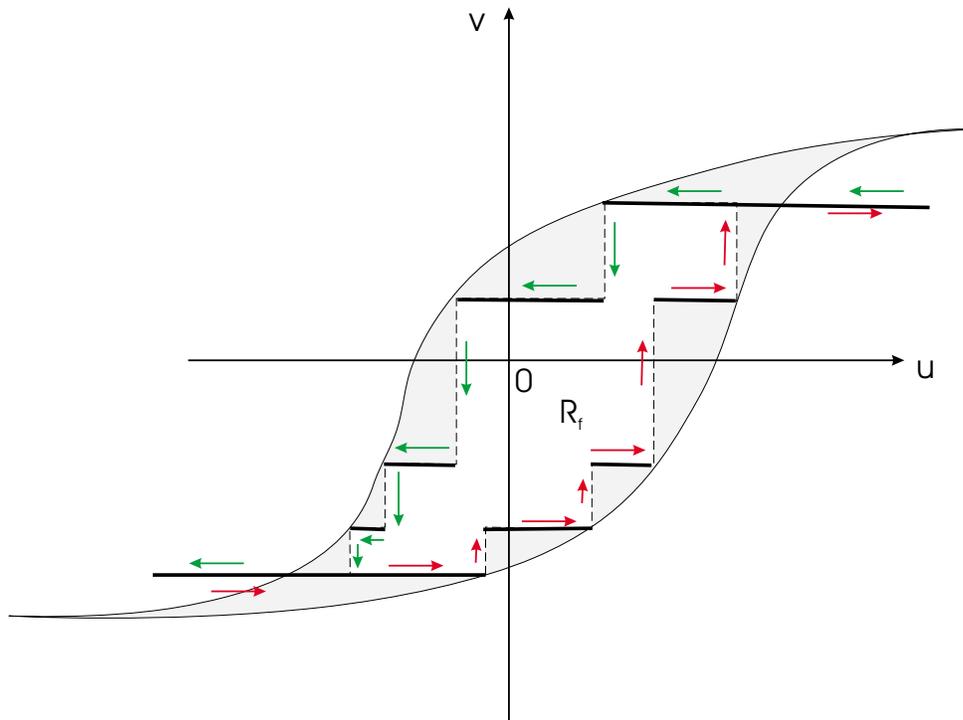
Figure C-3b. An approximation to a continuous hysteresis loop by a linear combination of a finite family of delayed relays. The quantity R_f is the region inside the discontinuous loop formed by the finite family of relays (reprinted from *Differential Models of Hysteresis*, 1994, by Augusto Visintin, with permission of Springer-Verlag, GmbH & Co. KG, Heidelberg, Germany).

complemented with pertinent initial conditions. Optimal control problems for ordinary differential equations with hysteresis require specific attention since, even though hysteresis operators are in some sense continuous, they are usually not differentiable. Understanding such systems cannot be accomplished by merely setting up a "numerical solution" scheme, programming it, and generating computer output. Mathematical analyses are required for these complex problems.

Constitutive laws in continuum mechanics formulated in terms of hysteresis operators lead in a natural way to the partial differential equations of the conservation of mass, momentum and interval energy being coupled with hysteresis operators. Mathematically speaking, the most interesting and complicated situations are those where the hysteresis operators appear in the ***principal part*** of the partial differential equations. For these systems, basic existence and uniqueness results are strongly linked in non-obvious ways to the properties of the hysteresis diagrams and of the memory structure. For such situations, Visintin (1994) considers two model problems: the ***heat equation*** (comparable to the concentration equation) ***with hysteresis***,

$$\frac{\partial u}{\partial t} + \frac{\partial}{\partial t}\left[P(u)\right] - \frac{\partial^2 u}{\partial x^2} - \frac{\partial^2 u}{\partial z^2} = f(x,z,t) \ , \tag{C-4a}$$

and the ***wave equation with hysteresis***,

$$\frac{\partial^2 u}{\partial t^2} - \frac{\partial}{\partial x}\left[P\left(\frac{\partial u}{\partial x}\right)\right] = 0 \ , \tag{C-4b}$$

where $P(\bullet)$ is the Preisach Model of hysteresis or some other hysteresis model. Although not studied in detail, Visintin (1994) introduced two systems of prime interest to the subsurface investigator. One of these systems is the partial differential equation model describing the growth of bacteria in the presence of nutrients. This phenomenon exhibits a pattern of growing rings in response to nutrient diffusion. The constitutive relation between the concentrations of nutrients and the activity of the bacteria leads to a bistability region in the "nutrient space", which in turn leads to the occurrence of hysteresis in the evolution of the concentration of the bacteria. The other system considered by Visintin is of direct interest to the problem at hand. This problem is the study of ***unsaturated water flow through porous media*** whose constitutive laws, $\theta(h)$ and $K(h)$, account for compressibility, and the history of drainage/wetting, thus leading to hysteretic effects. In a ***simplified setting***, the "Richards Equation" is written as:

$$\frac{\partial}{\partial t}\left[\theta + P(\theta)\right] - \frac{\partial^2 \theta}{\partial z^2} - \frac{\partial}{\partial z}\left[P(\theta)\right] = -S \ , \tag{C-5}$$

where $P(\theta)$ is the hysteretic constitutive equation. Suitable initial and boundary conditions must be specified for Equation (C-5), and S and the starting point of $P(\theta)$ must be given.

C.3 Hysteresis in Soil-Moisture Parameters

In Volume 2 of the Annual Review of Fluid Mechanics, Philip (1970) says that the usual state of the unsaturated zone is that wetting and drying are simultaneously occurring in different regions of the zone, and that this leads to the occurrence and the importance of the phenomenon of hysteresis. This phenomenon is most pronounced for media and moisture ranges where ***capillarity*** is dominant. Philip says that the study of this problem started in the late 1800's with the investigation of interfacial stability. However, it was not until the late 1920's that these ideas were systematically applied to subsurface phenomenon. During this period, it was recognized that many of the possible equilibrium interface configurations in capillary-porous media are unstable and that the configuration changes are often spontaneous and uncontrollable. Such changes involve irreversibility and produce hysteretic effects in the soil-moisture parameters. In addition, Philip says that there is another source of the discontinuities seen in stable interface configurations, that source is due to the noncontinuous lines of solid-liquid-gas contact which exist due to the geometrical impossibility of contact lines on some parts of the solid surface. The significance of this latter effect was illustrated by Philip by making interface configuration calculations in a tube with a radius varying periodically with the axial coordinate. Following up on the interfacial stability discussions of Philip are discussions given by Luckner and Schestakow (1991) in their book on subsurface processes. These discussions are concerned with

interfacial tension, contact angles between gaseous-liquid interfaces and surface of the solid phase (i.e., a measure of wettability), and the differential between contact angles at the advancing front of the wetting liquid phase and that at the receding front (i.e., there exists a hysteresis of contact angles).

In some respects the above comments of Philip can be thought of as the more theoretical aspects of hysteresis in soil-moisture parameters, while the more phenomenological aspects of the problem are framed in the language of soil water potential and pressure head. This latter approach is more in line with the hysteresis components considered in the HYDRUS Code. *Water potential*, symbolized by ψ, is the free energy of water, or its capacity to do work (Miller and Donahue, 1995; Mauseth, 1998). When $\psi > 0$, the water is capable of doing positive work, while $\psi < 0$ means that work must be done on the water to remove it from its given location and move it to a reference pool (e.g., moving adsorbed water on soil particles to a free pool of water). The free energy of water can be increased by heating it, putting it under pressure, and by elevating it. Conversely, the energy of water is reduced by cooling it, reducing its pressure, and lowering it with respect to gravity. Water's capacity to do work can also be decreased by its adherence to a solid substance due to hydrogen bonding between the water molecules and the material.

Soil water potential is a combination of the following effects (Miller and Donahue, 1995):

1. The surface area of soil particles and small soil pores that adsorb water – *matrix potential* ψ_m;

2. The effects of dissolved substances – *solute or osmotic potential* ψ_s;

3. The atmospheric or gas pressure effects – *pressure potential* ψ_p;

4. The position of the water with respect to a reference state, a state usually taken as zero – *gravitational potential* ψ_g.

In summary, the water potential for soils independent of a reference state is given by

$$\psi_w = \psi_m + \psi_s + \psi_p, \tag{C-6}$$

and the total water potential is defined by

$$\psi_t = \psi_w + \psi_g. \tag{C-7}$$

Water moves whenever there is a difference of water potential within a specific mass of water; this is true in subsurface soils, within plants, and between soils and living cells. However, if the water potentials of two regions are equal, the regions are in equilibrium and there is no net movement of water. Temperature differences are usually not a factor in the subsurface because the solutions being compared are assumed to be at nearly the same temperatures. Even the temperature differences between leaves and roots in a plant are usually not of significance for water movement.

With reference to the components in Equations (C-6) and (C-7), the quantity ψ_s is zero for pure water and is always negative for solutions. The quantity ψ_p can either be positive or negative and the matrix potential ψ_m is a measure of water's adhesion to nondissolved structures such as soil particles, cell walls and membranes. Since adhesion can only decrease water's free energy, ψ_m is always negative. In soils ψ_m is very important because so much soil water is tightly bound to soil particles; while in living cells, ψ_m is usually much less important than ψ_s and ψ_p. Miller and Donahue (1995) state that most productive soils do not have a depth of water standing on them (i.e., $|\psi_p|$ is small) and most soils have few salts (i.e., $|\psi_s|$ is small), thus

$$\psi_t \cong \psi_w \cong \psi_m. \tag{C-8}$$

So for most situations, ψ_m is the dominant component of ψ_t and represents about 95% or more of ψ_t. For living cells, the cell potential ψ_c is fairly well approximated by

$$\psi_c \cong \psi_s + \psi_p \leq 0. \tag{C-9}$$

The description of hysteresis given by Guymon (1994) starts with how water is distributed in a pore and how ψ_m varies through the cross section of that pore. An example of such a pore is given in Figure C-4. In this figure are shown areas which are drained by the pull of gravity, areas where water is held by capillary forces, and areas where
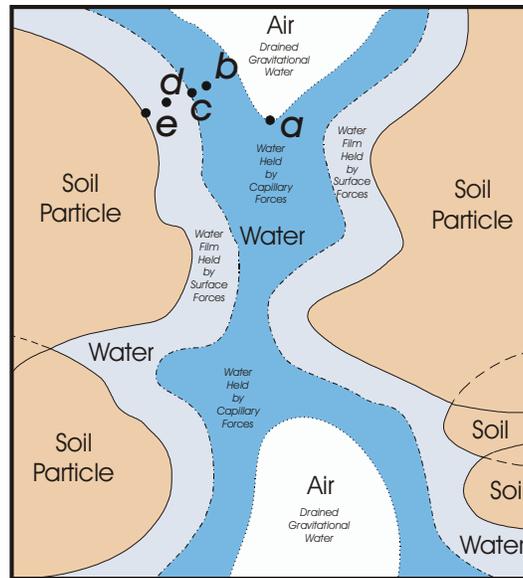
Figure C-4. A cross section of a soil pore and the solid soil particles that make up its walls, showing areas drained by the pull of gravity, areas where water is held by capillary forces, and areas where water is held by surface forces (e.g., van der Waals forces) (reprinted from *Soils in Our Environment*, 1995, 7th Ed., by R.W. Miller and R.L. Donahue, with permission of Pearson Education, Inc., Upper Saddle River, NJ).

water is held by surface forces. Point a in the figure represents a point where air begins to enter the pore; for fine grained soils, the air entry pore water pressure head is about -0.1 atm. Point b is located in the area of water being held under the influence of capillary forces and may be represented by a water pressure head on the order of -3 to -5 atm. The concept of field capacity is defined as the pore water pressure at which gravity drainage is negligible and for agriculture soils it occurs at about -2 to -3 atm. Capillary forces dominate surface forces over the range of pressures from the air entry pressure to -1 atm and beyond in the negative direction down to a pressure as low as possibly -5 atm. The permanent wilting point is the point at which plants can no longer extract water from the soil; this may occur at from -5 to -15 atm and is indicated by Point c in Figure C-4. Point d, within the area where the water film is held by surface forces, may represent a location where the pressure head is as low as -60 atm. Within a few water molecules of the surface of the soil particles, Point e in Figure C-4, the water pressure may be as low as -8000 atm. With reference to hysteresis, Guymon (1994) states that the soil-water hysteretic memory of soils is predominantly a capillary effect (as was also stated by Philip, 1970). In the ranges of soil water pressures where chemical and other surface forces predominate, hysteresis is not evident. In addition, soil memory also ceases when and where the pressure head is zero or greater. Thus, Guymon says that hysteretic memory effects commonly occur in the pore pressure range from -5 atm to 0. Of course, the lower limit is dependent upon the soil structure and texture.

The main cause of hysteresis advanced by Guymon is what is called the "ink bottle" effect as illustrated in Figure C-5. This figure (Figure C-5a) illustrates that during a drying cycle starting from saturated conditions ($h_0 = 0$), water is drained from the soil. However, because of the presence of narrow necks, the capillary forces at a given negative pressure head, $h_1 < h_0 = 0$, will tend to keep some of the lower large pores filled or partially filled with water as shown in Figure C-5a. Prior to the initiation of a wetting cycle, it is assumed in Figure C-5b that the soil has reached the residual moisture content with a soil pressure head, $h_2 << h_1 < h_0 = 0$. When the wetting cycle begins, the soil moisture increases and $h_2 \rightarrow h_1$. Since the larger pores are starting from the "empty position" with respect to capillary forces, the water retained in them is due to the lower narrow necks as $h_2 \rightarrow h_1$ and is not due to the upper narrow necks. Therefore, at the given soil-water pressure head h_1, the water content during drying is higher than that during wetting. A secondary cause of hysteresis identified by Guymon is that due to wettability, or the so-called "rain drop" effect. This effect is described as follows: a wetted soil while drying retains more sorbed water than a dry soil while being wetted. Thus, the tendency for a higher water content during drying than during wetting is enhanced.

THE INK BOTTLE EFFECT

(a) A Draining Pore	(b) A Wetting Pore
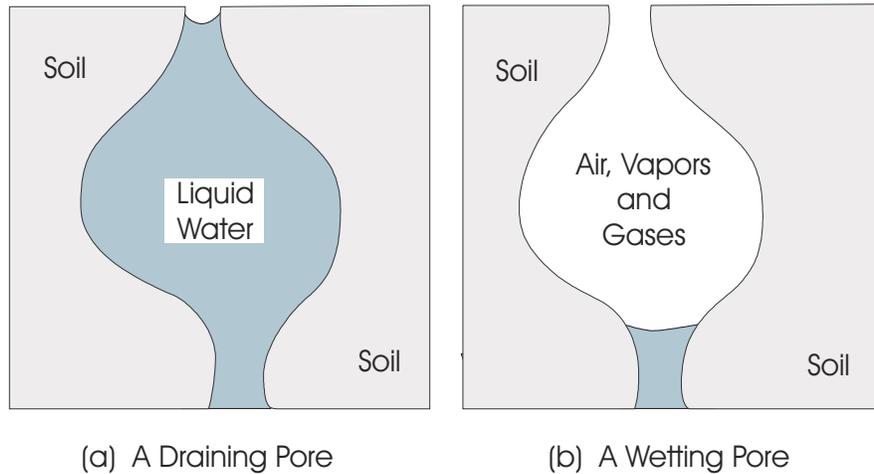
Figure C-5. The "ink bottle" effect demonstrating that draining/drying soils under the influence of capillary forces retain more water at a given soil-water pressure than a wetting soil at the same water pressure (reprinted from *Unsaturated Zone Hydrology,* 1994, by Gary L. Guymon, with permission of Pearson Education, Inc., Upper Saddle River, NJ).

Guymon (1994), as well as Luckner and Schestakow (1991), claims that significant effects of hysteresis have been observed in the soil retention curves, $\theta(h)$, while only minor hysteresis effects have been observed in the unsaturated hydraulic conductivity function, $K(h)$. These authors believe that for most practical problems the hysteretic effects experienced by $K(h)$ may be ignored, especially since there is such a large error associated with determining $K(h)$. In spite of these conclusions, the HYDRUS Code does consider hysteresis in both $\theta(h)$ and $K(h)$.

A hypothetical soil-moisture hysteresis loop with a discontinuity as the pressure head approaches zero is illustrated in Figure C-6. The discontinuity is displayed by the positive difference between the saturated moisture content for the main drying curve and that for the main wetting curve:

$$\theta_s^d - \theta_s^w > 0. \tag{C-10}$$

The reason for this difference is entrapped air in some of the soil pores, a condition that may be removed with time as the moisture redistributes. Mathematically speaking, the varying discontinuity violates the time invariance of the hysteresis loop and presents a time-varying condition that is most difficult to verify and document in the field, and to simulate by modeling.

Also shown in Figure C-6 are sets of primary and secondary scanning curves for wetting and drying cycles. These scanning curves follow the rules of Madelung depicted in Figure C-2. Knowing the time history of the wetting and drying cycles throughout a soil column allows an investigator to know at each time and space location where he/she is at with respect to the moisture state (θ,h) on the main drying and wetting curves or the moisture state (θ,h) on scanning curves within the main loop's interior. However, this is much easier to say than to precisely formulate (as indicated by the previous subsection), and much easier to say than to verify and document in the field. As indicated by the HYDRUS Code, one can set up numerical procedures which seem to parrot the soil-moisture memory effects in a soil column; but one should be cautious of the simulated outputs with respect to their verification, or lack thereof, and their field documentation.

The main drying curve shown in Figure C-6 may be experimentally determined, but is more often expressed in terms of one of the analytical forms found in Appendix A. The parameters occurring in the analytical model are evaluated from field or laboratory data. Given the main drying curve, the main wetting curve is obtained by changing (according to experimental results) one or more of the parameters in the main drying curve. The primary and secondary scanning curves are usually obtained by a scaling procedure applied to the main drying and wetting
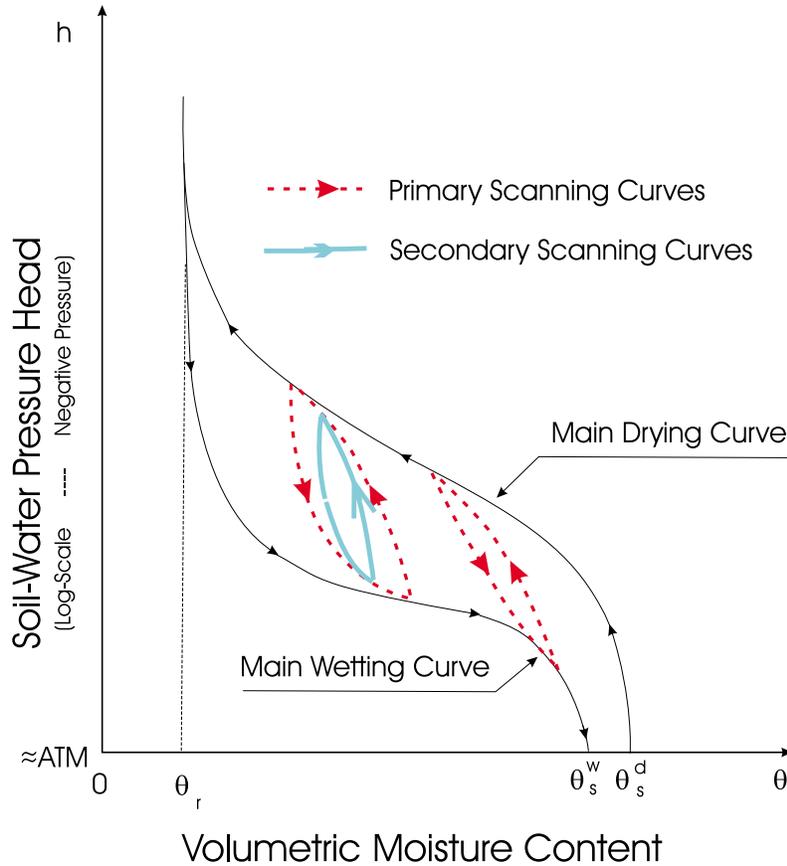
Figure C-6. A hypothetical soil-moisture hysteresis loop which is discontinuous for pressure heads near zero, showing the main drying and main wetting curves, and example primary and secondary scanning curves (reprinted from *Subsurface Transport and Fate Processes*, 1993, by R.C. Knox, D.A. Sabatini, and LW. Canter, with permission of CRC Press, Inc., Boca Raton, FL).

curves (Luckner and Schestakow, 1991). In the case of the HYDRUS Code, the analytical VG- or VC-Model of Appendix A is used to give the main drying curve with experimentally derived parameters. Allowance is made in the code for θ_s^d being equal to θ_s^w, or θ_s^d being greater than θ_s^w. Usually, the following relationships for the main curves are assumed:

$$\theta_r^d = \theta_r^w = \theta_r, \quad n^d = n^w = n, \quad \alpha^d < \alpha^w. \quad \text{(C-11)}$$

Thus, the main wetting curve is primarily differentiated from the main drying curve by the choice of $\alpha^d < \alpha^w$, and possibly by the saturated moisture contents if $\theta_s^w < \theta_s^d$. If $\theta_s^w = \theta_s^d$, the loop of the main curves closes as the pressure head approaches zero.

In the HYDRUS Code, the drying scanning curves are scaled from the main drying curve, while those for wetting are scaled from the main wetting curve. The scale factor for the pressure head in this process is unity, $\alpha_h = 1$. As previously mentioned, this code does introduce hysteretic effects into the relationship K versus h. As with soil moisture, allowance is made for differences between dry and wet saturated hydraulic conductivities:

$$K_s^w \leq K_s^d. \quad \text{(C-12)}$$

The construction of the hysteresis loop for K(h) is similar to that of the moisture hysteresis loop.

References

Aubin, J.-P. and A. Cellina. 1984. <u>Differential Inclusions: Set-Valued Maps and Viability Theory</u>. Springer-Verlag. New York, NY. 342 pp.

Brokate, M. and J. Sprekels. 1996. <u>Hysteresis and Phase Transitions</u>. Springer-Verlag. New York, NY. 357 pp.

Castrigiano, D.P.L. and S.A. Hayes. 1993. <u>Catastrophe Theory</u>. Addison-Wesley Publ. Co., Reading, MA. 250 pp.

Chipot, M. 1984. <u>Variational Inequalities and Flow in Porous Media</u>. Springer-Verlag. New York, NY. 118 pp.

Edwards, R.E. 1995. <u>Functional Analysis: Theory and Applications</u>. Dover Publ., Inc., New York, NY. 783 pp.

Gilmore, R. 1981. <u>Catastrophe Theory for Scientists and Engineers</u>. John Wiley & Sons. New York, NY. 666 pp.

Goldstein, J.A. 1985. <u>Semigroups of Linear Operators and Applications</u>. Oxford University Press. New York, NY. 241 pp.

Guymon, G.L. 1994. <u>Unsaturated Zone Hydrology.</u> PTR Prentice Hall. Englewood Cliffs, NJ. 210 pp.

Hlavaček, I., J. Haslinger, J. Nečas and J. Lovišek. 1988. <u>Solution of Variational Inequalities in Mechanics</u>. Springer-Verlag. New York, NY. 275 pp.

Knox, R.C., D.A. Sabatini and L.W. Canter. 1993. <u>Subsurface Transport and Fate Processes</u>. Lewis Publ., Boca Raton, FL. 430 pp.

Luckner, L. and W.M. Schestakow. 1991. <u>Migration Processes in the Soil and Groundwater Zone</u>. Lewis Publ. Chelsea, MI. 485 pp.

Madelung, E. 1905. " Űber Magnetisierung durch schnell verlaufende Strőme and die Wirkungsweise des Rutherford-Marconi-schen Magnetdetektors." <u>Ann. Phys</u>. 17. 861-890

Mauseth, J.D. 1998. <u>Botany: An Introduction to Plant Biology</u>, 2/e. Multimedia Enhanced Edition. Jones and Bartlett Publ. Boston, MA. 837 pp.

Miller, R.W. and R.L. Donahue. 1995. <u>Soils in Our Environment</u>. 7th Edition. Prentice Hall, Englewood Cliffs, NJ. 649 pp.

Miyadera, I. 1992. <u>Nonlinear Semigroups</u>. Translations of Mathematical Monographs. Vol. 109. Amer. Math Soc. Providence, RI. 230 pp.

Philip, J.R. 1970. "Flow in porous media." In: <u>Annual Review of Fluid Mechanics</u>. Vol. 2. Annual Reviews, Inc. Palo Alto, CA. 177-204.

Rubin. W. 1991. <u>Functional Analysis</u>. 2nd Edition. McGraw-Hill, Inc. New York, NY. 424 pp.

Visintin, A. 1994. <u>Differential Models of Hysteresis</u>. Springer-Verlag. New York, NY. 407 pp.

Appendix D
The First-Order Decay Chains Used in the Various Models

The one-dimensional version of the transport equations for solutes involved in sequential first-order decay reactions consists of the following:

$$\theta R_1 \frac{\partial c_1}{\partial t} + q \frac{\partial c_1}{\partial z} = \frac{\partial}{\partial z}\left[\theta D_1 \frac{\partial c_1}{\partial z}\right] + F_1(c_1)c_1 + G_1(s_1^*) ,$$
(D-1)

$$\theta R_2 \frac{\partial c_2}{\partial t} + q \frac{\partial c_2}{\partial z} = \frac{\partial}{\partial z}\left[\theta D_2 \frac{\partial c_2}{\partial z}\right] + F_2(c_2)c_2 + G_2(c_1,s_1^*,s_2^*) ,$$
(D-2)

$$\frac{\partial s_i^*}{\partial t} = H(c_i,s_i^*) - (\mu_i + \mu_i')s_i^* + \gamma_i, \quad i = 1,2 ,$$
(D-3)

where θ is the soil moisture content, "1" is the index for the parent species, "2" is the index for the daughter species, R is the retardation accounting for gaseous and liquid solute phases and the equilibrium solid phase, c is the concentration of the liquid phase, q is the Darcian fluid flux density, D is the dispersion coefficient, s* represents the nonequilibrium solid phase of the solute, μ is the degradation rate of s*, μ' is the rate of transfer of material from parent to daughter, and γ is the production of s*. The function F(c) represents degradation of the solute from gaseous, liquid and solid phases, transfer losses from parent passed on to daughter for the three phases, losses due to plant uptake, and changes due to the temperature variations in the system. The function G_1 (s_1^*) accounts for production of the solute in all three phases, losses due to plant uptake, and the amount of solid phase at the nonequilibrium sorption sites. The function $G_2(c_1,s_1^*,s_2^*)$ accounts for the daughter material transferred from the parent in the gaseous, liquid, equilibrium solid and nonequilibrium solid phases, accounts for the production of the daughter species in all phases, and accounts for root uptake losses. Finally, the function $H(c_i,s_i^*)$ could be thought of as the first-order sorption rate of s_1^* due to the difference between equilibrium concentrations and nonequilibrium concentrations.

The system given in Equations (D-1) to (D-3) is basically that which is presented in the HYDRUS Model. The CHAIN 2D version of these equations replaces the vertical coordinate (z) by the vertical slab coordinates (x, z), the quantity q by components in the x and z directions, and the dispersion coefficient D by a 2 x 2 matrix of dispersion coefficients. The FECTUZ Code considers the one-dimensional version of the above system, but without nonequilibrium sorption, zero-order production teams, root uptake and accounting for temperature variations. The MULTIMED-DP 1.0 Code is similar to FECTUZ but it only accounts for linear equilibrium sorption; it can also change rate constants to account for temperature. Finally, the CHAIN Code is similar to that of MULTIMED-DP 1.0 but no account is made of temperature variations and the first-order decay of the parent becomes the zero-order production of the daughter.

In the following paragraphs, we list the type of reaction chains that are considered in the various codes. Specific species and products are not identified in this discussion, only the types of chains that can be formulated in the system in question. Both **HYDRUS** and **CHAIN 2D** will allow the user to specify six solutes, either coupled in an unidirectional chain; or totally uncoupled, where each species is independent of the other. Examples that have been run have had the following forms:

Radionuclides

Nitrogen Compounds
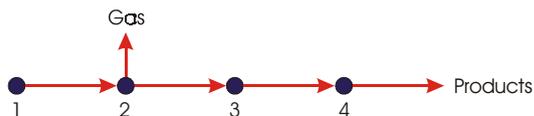
Uninterrupted Chain --
One Reaction Path for Pesticides
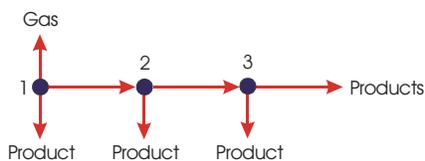
Interrupted Chain--
Two Independent Reaction Paths for Pesticides
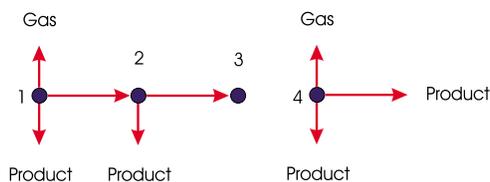
The **FECTUZ** Code can handle up to seven different chemical species, either in straight, unidirectional chains, or in branched chains. Systems for which solutions have been obtained include the following:

Straight Chains

$N \leq 7$

Simple Splitting Chains
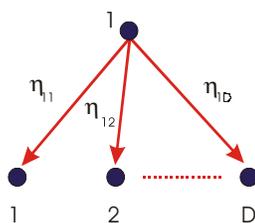
$D = $ Number of Daughters ≤ 6

$\eta_{lj} = $ Splitting Factors

$$\sum_{j=1}^{D} \eta_{lj} = 1$$

Simple Converging Chains

$N \leq 7$
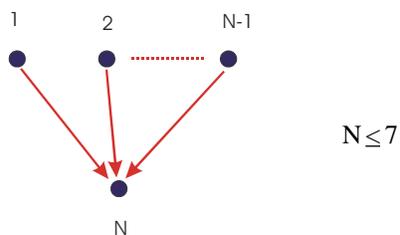
Seven-Member Branching Chain

$$\eta_{12} + \eta_{13} \;=\; \eta_{24} + \eta_{25} \;=\; \eta_{36} + \eta_{37} \;=\; 1 \,.$$
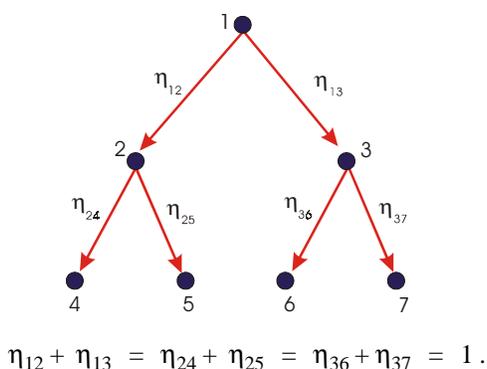
The **MULTIMED-DP 1.0** Code only considers parents, daughters and granddaughters; and within each subgroup, the code only considers 3, 4, and 4 variables (species), respectively. Pathways that have been considered in hydrolysis transformations include those given below:

Hydrolysis Pathways
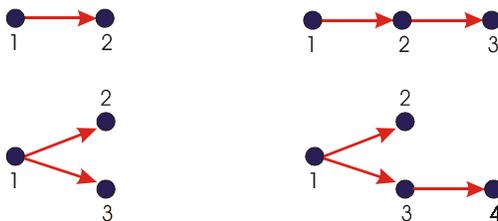
The **CHAIN** Code, as reported in van Genuchten (1985), considers four species in a straight chain. The radioactive decay chain example problem given in this paper consists of the following radionuclides:

$$^{238}Pu \longrightarrow\; ^{234}U \longrightarrow\; ^{230}Th \longrightarrow\; ^{226}Ra \;.$$

The author states that the most critical species is the last one in the chain, ^{226}Ra. This species is a high biological hazard and is highly mobile, the retardation factor R_4 is rather low.

References

van Genuchten, M.Th. 1985. "Convective-dispersive transport of solutes involved in sequential first-order decay reactions." Computers and Geosciences. 11(2):129-147.

Appendix E
The Impact of Using a Nonuniform Moisture Distribution versus a Uniform Distribution

Constant values of q, θ, and h were assumed for all models in the sensitivity analyses for the input parameters K_d, q, θ, ρ, D, D_L and D_w. On the other hand, a nonuniform water content distribution was employed by MULTIMED-DP 1.0, FECTUZ, CHAIN 2D and HYDRUS for the analyses involving K_s, $θ_r$, $θ_s$, α, and β. One should assume that the nonuniform distribution is the "standard" and the uniform distribution is the "approximation." However, when the van Genuchten Model for the water retention parameters (K_s, $θ_s$, $θ_r$, α, β) was considered in the sensitivity analyses reported in Sections 6 and 7, an error in the originally distributed MULTIMED-DP 1.0 Code was detected. The error arose from the solution of the governing equations for the pressure head, h, and the moisture content, θ. When corrected, all systems were defined for a constant recharge rate, q, and boundary conditions resulting in the following conditions for θ: θ = base value = 0.16, at the surface; and at 6 m, θ = saturated value = 0.32. Figure E-1 shows the results of solving Darcy's Law for MULTIMED-DP 1.0 and FECTUZ, and solving the Richards Equation for CHAIN 2D and HYDRUS.

The water contents obtained from using the originally distributed MULTIMED-DP 1.0 Code are inconsistent with respect to those obtained from the other three codes. The reason for the inconsistency was found to be the incorrect use of the residual water content in the van Genuchten Module. When this error was corrected, the new water content results became consistent with the results of the FECTUZ Code, as one would expect, and also became consistent with the steady state (remember q and the boundary conditions are fixed) solutions for HYDRUS and CHAIN 2D. For the simulations conducted in this report (i.e., time durations up to 10,000 days, and times to peak concentrations of from 3000 to 8000 days), the approach to steady state moisture distributions for both HYDRUS and CHAIN 2D is very fast. For the purposes of this report, the variable moisture content obtained from the van Genuchten Model and Richards Equation is a steady state distribution as shown in Figure E-1. Further, one would expect that all four models should give the same distribution (as the figure indicates) if the MULTIMED-DP 1.0 Code is properly given. The revised code for MULTIMED-DP 1.0 is the one that was used in all of the sensitivity analyses and any other subsequent calculations using this code.

Before comparing the breakthrough curves (BTCs) of ^{99}Tc for a uniform moisture content (θ = 0.16) with those for a nonuniform distribution (Figure E-1), one should note the degree of nonlinearity in the distribution shown in Figure E-1. Because of the *homogeneity of the 6m layer*, one notes that the steady state distribution is nearly uniform (θ ≈ 0.16) for the first 4m of depth. At about 4m, the distribution begins to break away from this uniform value. However, even at a depth of 5.5m, the distribution has only deviated about 33% of the total difference (0.32 - 0.16). Thus, about 67% of the total deviation of the distribution takes place in the last 0.5m of the layer. Consequently, one would assume that changes from going from a uniform water content to a nonuniform water content (of the type in Figure E-1) would not be too great.

This comparison between uniform and nonuniform distributions of water content is illustrated in Figure E-2 using the breakthrough curves (BTCs) of ^{99}Tc predicted by the four models: MULTIMED-DP 1.0, FECTUZ, CHAIN 2D and HYDRUS. The bottom graph in this figure gives the BTCs predicted by all five models, including the CHAIN Model, for the base values of the parameters given in Section 6. In the top graph, all input parameters are kept at their base values except for θ which is replaced by the distribution given in Figure E-1. No CHAIN results are given in the top graph since θ can only be a constant in this model.

In comparing the BTCs for uniform water content versus the nonuniform values, one sees that the nonuniform θ reduces the C_{peak} and increases the T_{peak} and T_{MCL} for each model. This is reasonable if we remember that the nonuniform θ-distribution increases the overall moisture in the soil column versus that for θ = 0.16 throughout the column. Increasing moisture reduces the advection term in the transport equation and increases the diffusion term.
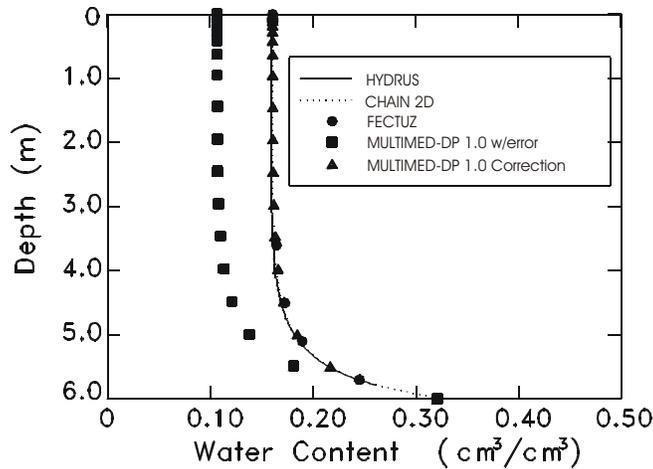
Figure E-1.   Water content distributions predicted by the HYDRUS, CHAIN 2D, FECTUZ, and MULTIMED-DP 1.0 Models. Note that the water contents (■) obtained from the originally distributed MULTIMED-DP 1.0 Code are in error. The corrected code gives a consistent water content distribution (▲) with the other three models.

This results in lower C_{peak} values for the nonuniform BTCs, produces delays in the T_{peak} values and T_{MCL} values with respect to those for the uniform case, and produces an increase in diffusive spread of the BTCs for the nonuniform case over that of the uniform case, although this spread is only about 1.08 times that for the uniform case.

To get a better quantitative effect of the impact of using the uniform approximation for the sensitivity analyses of the first seven input parameters (K_d, q, θ, ρ, D, D_L, D_w), we used the CHAIN 2D Model to derive the BTCs and sensitivities for the parameters K_d and D_L for both the uniform and nonuniform water contents. These comparative BTCs are given in Figure E-3 (K_d comparison) and Figure E-4 (D_L comparison). As in Figure E-2, the C_{peak} values for the nonuniform water content BTCs have been uniformly reduced over the ranges of the input parameters compared to those for a constant θ, while the T_{peak} values and T_{MCL} values have been increased uniformly over the input ranges. Table E-1 lists the output values for the uniform and nonuniform water content cases, values which are measured at the base values of the input parameters K_d and D_L. In addition, the table gives the relative sensitivities of these three outputs to the inputs K_d and D_L, again referenced to the base values of K_d and D_L. As one can see, the relative sensitivities for the uniform and nonuniform cases are basically the same. The percent differences of the output values, based on the nonuniform case as the standard, are as follows:

	Percent Differences	
Output	*K_d*	*D_L*
C_{peak}	15.5% Decrease	12.1% Decrease
T_{peak}	6.7% Increase	5.9% Increase
T_{MCL}	6.4% Increase	6.1% Increase

Based upon these results and the BTCs in Figures E-2 to E-4, we believe that the use of the uniform approximation for θ for the analysis of the sensitivity of the three outputs to the input parameters K_d, q, θ, ρ, D, D_L and D_w is both valid and representative of the sensitivities that would be obtained from the nonuniform water content distribution. Further, using this uniform approximation allows us to directly compare the results of the CHAIN Model with the other four models, as illustrated in the bottom graphs shown in Figure E-2. However, it should be emphasized that these results are for a ***homogeneous layer under steady state conditions***.
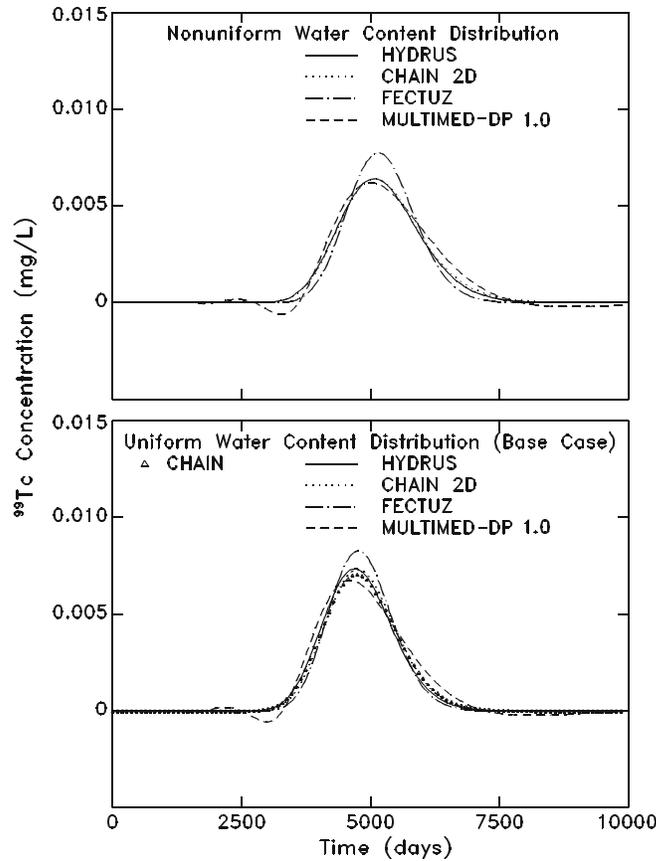
Figure E-2. Comparison of the breakthrough curves predicted by the CHAIN, HYDRUS, CHAIN 2D, FECTUZ, and MULTIIMED-DP 1.0 Models for the base case given in Section 6. The top curves are for a nonuniform water content and the bottom curves are for $\theta = 0.16$ throughout the soil column. There are no CHAIN results in the top graph because θ can only be constant in this model.

Table E-1 Comparison of Results Derived from Figures E-3 and E-4 for the Distribution Coefficient K_d and the Dispersivity D_L, respectively. The Values of C_{peak}, T_{peak} and T_{MCL} are Given for the Base Values of K_d and D_L, and the Relative Sensitivities of These Output Quantities to K_d and D_L are Given, These Values Also Being Taken at the Base Values of K_d and D_L.

Output	*Property*	*K_d in ml/g*		*D_L in cm*	
		Uniform Water Content	*Nonuniform Water Content*	*Uniform WaterContent*	*Nonuniform WaterContent*
C_{peak}	Base Value (mg/l)	0.00732	0.00634	0.00725	0.00647
	Relative Sensitivity	-0.06	-0.05	-0.28	-0.25
T_{peak}	Base Value (d)	4766	5108	4737	5036
	RelativeSensitivity	+0.06	+0.06	-0.02	-0.02
T_{MCL}	Base Value (d)	3554	3799	3552	3783
	Relative Sensitivity	+0.07	+0.07	-0.08	-0.07

E-3
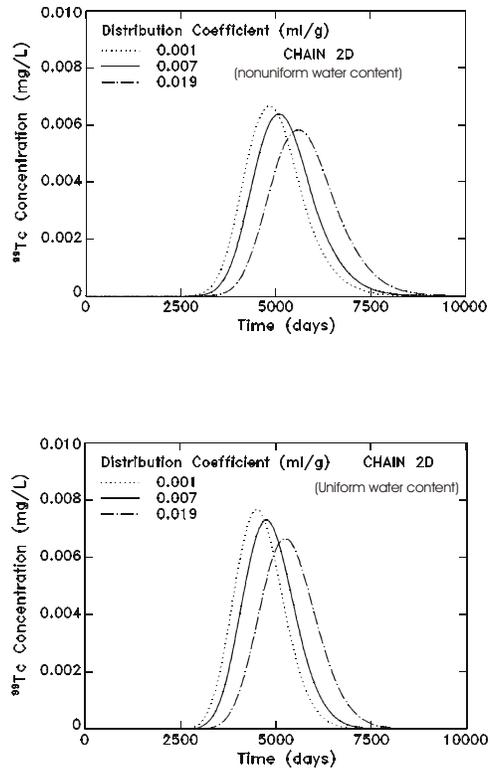
Figure E-3.   Sensitivity of ^{99}Tc breakthrough (through the 6 m layer) to the distribution coefficient using the CHAIN 2D Model, for a nonuniform water content (top) and for a uniform water content (bottom).
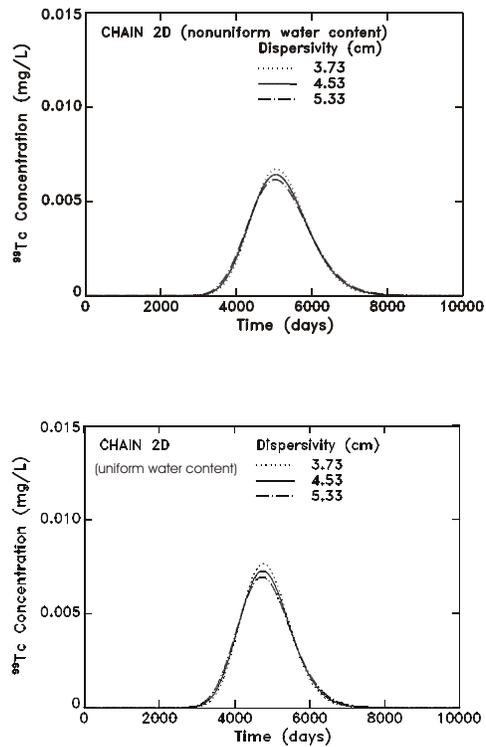
Figure E-4.   Sensitivity of ^{99}Tc breakthrough (through the 6 m layer) to the dispersivity using the CHAIN 2D Model, for a nonuniform water content (top) and for a uniform water content (bottom).

Appendix F
The Impacts of Using Daily Precipitation Rates and Daily Evapotranspiration Rates versus an Annual Average Recharge Rate

In the sensitivity analyses of Sections 6 and 7, the impact of the "natural cycles" of precipitation/runoff/ infiltration/evapotranspiration was assumed to be a constant mean annual recharge rate, q, which is applied year-after-year for a total simulation time of 25 to 40 years. It is the constant rate, q, which carries the radionuclides down through the homogeneous 6 m layer to the hypothetical water table at its lower boundary. The result of this ideal hydrologic mechanism is the classical "bell-shaped" breakthrough curve (BTC) shown throughout this report. These "bell-shaped" BTCs are probably sufficient to demonstrate the sensitivities of the three output quantities to the twelve input parameters given in Section 6. However, this "ideal mechanism" is at most a very crude approximation of the real mechanisms which produce ground-water contamination from radionuclides passing through the unsaturated zone.

The attributes of radionuclide movement through the vadose zone depend on the details of the time and space variations of the "cycles" of precipitation/runoff/infiltration/ evapotranspiration. Closely linked to these cycles are the mechanisms of flow hysteresis and flow through preferential pathways. In fact, Yao and Hendrickx (1996) state that worldwide it is thought that a major mechanism for ground-water contamination is the passage of pollutants through *preferential flow paths*, which is an event type phenomenon not currently well parameterized for large time-step simulations. These preferential flow paths can be produced by macropores such as soil cracks, old root channels or animal paths; by spatial variability of hydraulic conductivity; or by unstable wetting fronts. The occurrence of unstable wetting fronts is especially important since this mechanism can produce preferential pathways in homogeneous layers which do not contain macropores and significant changes in hydraulic conductivity, such as the 6 m layer used in the current report. In several of the mechanisms which produce wetting front instabilities, *flow hysteresis* (Appendix C) plays a major role, see Section 3.4.

An example of the impact of flow hysteresis on the results of single storm events is given in Eagleson (1970). He reported the results of a numerical experiment on the redistribution of moisture in a soil profile after the cessation of infiltration. In this simulation it was found that percolation with hysteresis was much slower than percolation without hysteresis. This simulation occurred over a two hour period and the percolation was through sandy soil. Such a result applied to a soil with vegetation would allow a longer time for evapotranspiration to act under hysteretic flow than under nonhysteretic flow, thus producing a greater loss of subsurface moisture under flow hysteresis.

Modeling codes required to simulate the above phenomena which lead to flow fingering and preferential pathways for moisture and pollutant transport through the vadose zone to the ground water should be two-dimensional in character and preferably three-dimensional, have the ability to handle event precipitation/runoff/ infiltration/evapotranspiration, have the ability to simulate air compressibility and flow hysteresis, and the ability to vary soil properties in a significant manner. In addition, such simulations would require time steps on the order of an hour or less, and space increments fine enough to simulate a two-dimensional pattern of flow fingers in the horizontal field of interest. Such simulations are beyond the objectives of the current report and beyond the capabilities of the five models under consideration, although the one-dimensional HYDRUS Code considers most of the pertinent hydrologic processes required for such simulations. Thus, even though the above preferential pathway phenomena are potentially very important for the transport and fate of radionuclides through the vadose zone, they will not and cannot be considered further in this appendix. Further, the time and space increments required for an analyses of such phenomena would be prohibitive for the current applications, where our simulations run from 10,000 days to 15,000 days.

To compromise, the simulations considered in this appendix are based on daily precipitation amounts without allowance for runoff, and on daily evapotranspiration rates based on two different root water uptake stress response distributions (Equations 2-3 and 2-6). Considering the 18 years of daily precipitation amounts shown in Figure 5-2, one notes that there is only one peak above 80 mm/d, two peaks above 40 mm/d, and about 30 peaks above 20 mm/d. These three categories, respectively, convert to 0.33 cm/hr, 0.17 cm/hr, and 0.08 cm/hr. However, one should keep in mind that these hourly rates are lower, and probably much lower, than storm event rates. Further the frequency of occurrence of the higher rates is greater when one uses storm events as opposed to using the daily precipitation rates.

In the work of Yao and Hendrickx (1996), for New Mexico type soils and hydrologic conditions, it was found that wetting front instabilities and fingering occurred for infiltration rates between 0.3 and 12 cm/hr, incomplete wetting without distinct development of fingering occurred for infiltration rates between 0.12 and 0.3 cm/hr, and stable wetting front migration occurred for infiltration rates below 0.12 cm/hr. Assuming these laboratory results are convertible to the homogeneous 6 m layer used in the current simulations, one would expect wetting front instability to occur on many days throughout the total record of 6570 days. Thus, the complexities of wetting front instability for storm events may be inconsistent with the assessment of the impacts of daily precipitation/evapotranspiration on the transport of radionuclides in the unsaturated zone. However, such complexities, as stated above, require finer time and space scale simulations than those used in the current study.

The precipitation record used in the current study, as mentioned above, is the one shown in Figure 5-2. Figure F-1 shows this same record in terms of annual precipitation amounts and monthly average amounts for the 18 years of record at the Las Cruces Site. As one can see from Figure F-1a, nine of the first ten years of record are above the annual average of 22.5 cm; the last eight years of the record are equal to or less than the mean annual average. For the monthly averages, each of the first five months has a monthly value less than 1 cm. The monthly averages begin to rise sharply in June; and from July to October, the monthly averages are greater than 2 cm per month. November's average drops below 2 cm, while December returns to just over 2 cm.

As given in Equations (2-3) and (2-6), the sink term S in the modified Richards Equation for the soil moisture distribution in the soil profile is expressed as the product of a water stress response function $\alpha(h)$ times a potential water uptake rate $S_p(z, t)$. In turn, the quantity $S_p(z, t)$ is a product of the normalized water uptake distribution function $b(z, t)$ and the potential transpiration rate $T_p(t)$. The quantity $b(z, t)$ is related to the root distribution function and in the current study was taken as uniform over an interval from 50 cm below the surface to 250 cm below the surface. This type of root distribution is probably reasonable for mesquite tree and creosote bush vegetative cover over semi-dry regions, such as the Las Cruces Site (see Royo, 2000; and Miller and Donahue, 1995). The potential transpiration rate was calculated from the site's climate data using Penman's Equation (Jensen et al, 1990). The water stress response function $\alpha(h)$ used in the current simulation was the Feddes Module of the HYDRUS Code (Šimůnek, et al, 1998). This function is the simple trapezoid shown in Figure F-2. The quantity h_1 is the value of the pressure head below which roots start to extract water from the soil (a value of -20 to -50 cm); h_2 is the pressure head below which roots start to extract water at the maximum possible rate, $\alpha(h_2) = 1$; h_3 is the pressure head below which roots can no longer extract water at the maximum rate; and finally h_4 is the pressure head below which root water uptake ceases, this being usually equal to the wilting point. Water uptake by roots can be easily varied by changing one or more of the values of the triplet (h_1, h_2, h_3). In the current simulations, two sets of this triplet were used to give two different scenarios of root water uptake. Two modifications that were not considered in these simulations were root growth and decline, and the characteristics that desert plants use to reduce water uptake and evapotranspiration rates, such as leaf coatings and root shrinkage which produces root-soil air gaps that are highly resistant to moisture transfer (Nobel, 1994). Such modifications are probably important in the first five months of the year (Figure F-1b) and during the dry years (Figure F-1a). Thus, the results that follow may be giving higher actual evapotranspiration (ET) rates than occur in nature, and lower recharge rates.

Figure F-3 summarizes the results of the two root water uptake scenarios run on the daily precipitation and PET data for the Las Cruces Site. These two sets of curves give the cumulative amounts of precipitation, actual ET and net recharge (precipitation minus actual ET, no allowance for runoff) in centimeters. The HYDRUS Model was used to calculate the actual ET values, and thus the recharge rates. The chief characteristics of these two sets of curves are given in the following notes:

- The records for both sets of curves consist of three pieces, *0 to a, a to b,* and *b to c,* covering a total of 14,140 days.
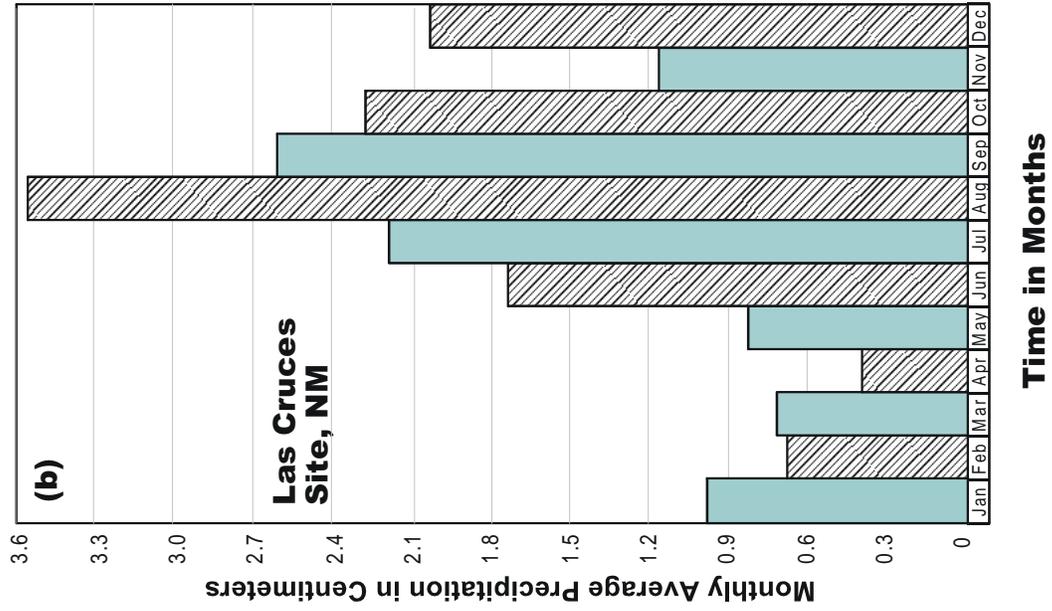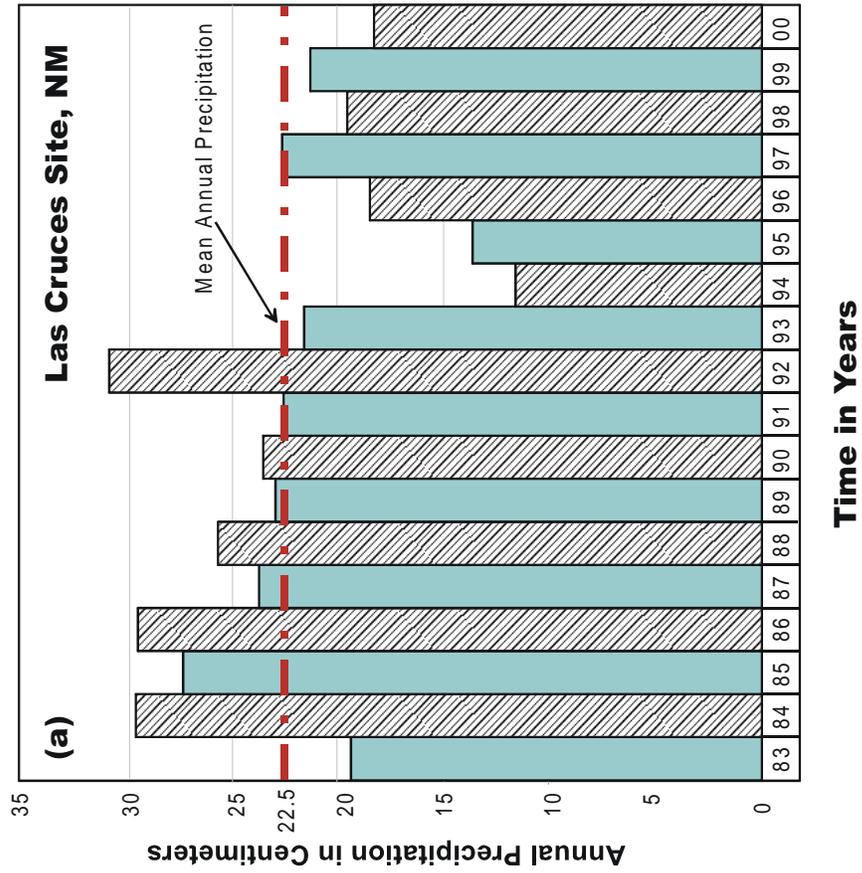
Figure F-1. The annual precipitation amounts and the monthly average amounts in centimeters for the Las Cruces, NM Site, corresponding to the daily record in Figure 5.2
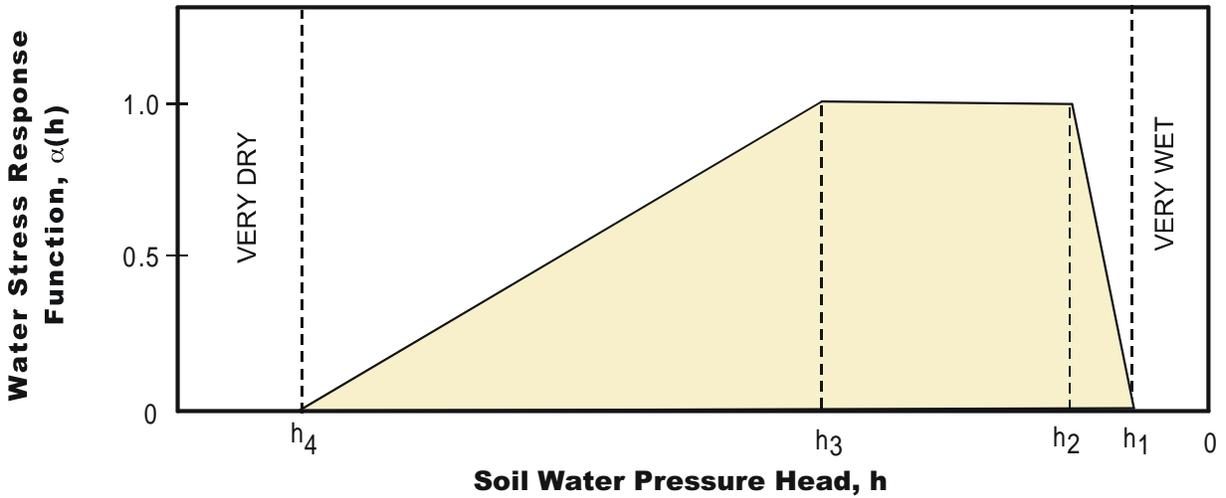
Figure F-2. The water stress response function for the Feddes Module of the HYDRUS Code (Šimúnek, et al., 1998).
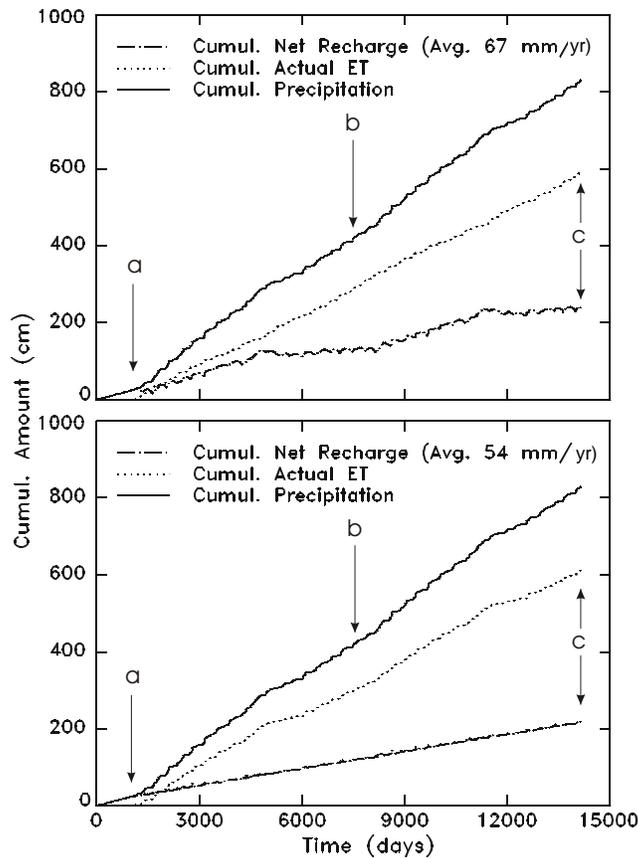
Figure F-3. Cumulative amounts in centimeters of precipitation, actual evapotranspiration (ET), and net recharge (precipitation minus actual ET) during a HYDRUS Model simulation using daily variable precipitation and potential ET rates at the surface. Cumulative net recharge and ET vary between the two figures because of differences in the root water uptake scenarios, (h_1, h_2, h_3). The precipitation/PET segment from "a to b" is repeated from "b to c."

- The records for the interval *0 to a* cover 1000 days and represent a constant recharge rate and precipitation rate (no ET taking place) of 0.024 cm/hr. This period was used to let the radionuclides distribute throughout the "upper layers" of the 6 m vadose zone under the action of the base values given in Section 6.

- Once the source of radionuclides quit emitting material at 1000 days, the daily precipitation and PET records in Figure 5-2 were applied to the system for the transport and fate of the radionuclides contained in the "upper layers" of the 6 m zone. Thus, the *second piece* of the records in Figure F-3 runs from a = 1000d to b = 7570d.

- When the simulation reached 7570 days, the daily precipitation and PET records in Figure F-2 were repeated, giving the *third piece* of the records in Figure F-3, which runs from b = 7570d to c = 14,140d.

- The average recharge rates, 67 mm/yr for the top set of curves in Figure F-3 and 54 mm/yr for the bottom set, were obtained from the graphs by taking the cumulative recharge values at 12,000 days and converting these values to mm/yr.

- Considering the wettest part of the 18 year record, the first ten years, the mean annual recharge rate for the top set of curves in Figure F-3 over the first 4650 days (10 years plus 1000 days) is about 84 mm/yr and that for the bottom set is 59 mm/yr.

- The high frequency "oscillations" in all the cumulative curves shown in Figure F-3 are due to daily and weekly variations in the precipitation and PET records.

- Ignoring these oscillations in the cumulative precipitation curves (which, of course, are the same in both sets of curves), one sees a curve made up of five line segments:

  1. 0 to 1000d, 87 mm/yr recharge rate for initial spreading of pollutants,
  2. 1000d to 5015d, first eleven years of record, the wettest period,
  3. 5015d to 7570d, last seven years of record, the driest period,
  4. 7570d to 11,585d, repeat of the wettest period,
  5. 11,585d to 14,140d, repeat of driest period.

- Ignoring the daily and weekly "oscillations" in the bottom set of curves in Figure F-3, one sees that the root water uptake scenario is such that the divergence between the cumulative precipitation and cumulative actual ET in each of the four segments from 1000d to 14,140d is roughly constant from segment to segment. This result produces a net recharge cumulative curve which is roughly a straight line, which means that after the first 1000 days the pollutants are being transported by a constant recharge rate of about 52 mm/yr.

- Once again ignoring the daily and weekly "oscillations" in the top set of curves in Figure F-3, one sees that the root water uptake scenario is such that the divergence between the cumulative precipitation and cumulative actual ET in the segment from 1000d to 5015d is greater than that for the bottom set of curves, giving a greater recharge rate of about 83 mm/yr. In the next segment, 5015d to 7570d, the cumulative precipitation curve is approximately parallel to the cumulative actual ET, giving a recharge rate which is relatively small at 20 mm/yr. The last two segments, 7570d to 11,585d and 11,585d to 14,140d, are a repeat of the previous two segments.

The impacts that the variable recharge rates in Figure F-3 have on the transport and fate of radionuclides through the 6 m of the vadose zone are shown by the ^{99}Tc breakthrough curves (BTCs) given in Figure F-4. The solid BTCs in this figure corresponds to the daily computed recharge rates, while the dashed BTCs correspond to calculations based on constant recharge rates (67 mm/yr and 54 mm/yr) for the entire time duration of the simulations. For both sets of BTCs, the moisture distribution throughout the soil column is nonuniform (i.e., the modified Richards Equation was solved). Observations that one can make about these results are as follows:

- The solid curve in the bottom set of curves is basically the classical "bell-shaped" curve as one might expect by the nearly constant recharge rate of 52 mm/yr after the first 1000 days of a rate of 87 mm/yr. The dashed curve is the BTC for a constant recharge rate of 54 mm/yr from zero to the end of the simulation.

- The solid curve in the bottom set of curves varies from that of the dashed curve because of the first 1000 days of pollutant distribution under a recharge rate of 87 mm/yr and because of daily variations of
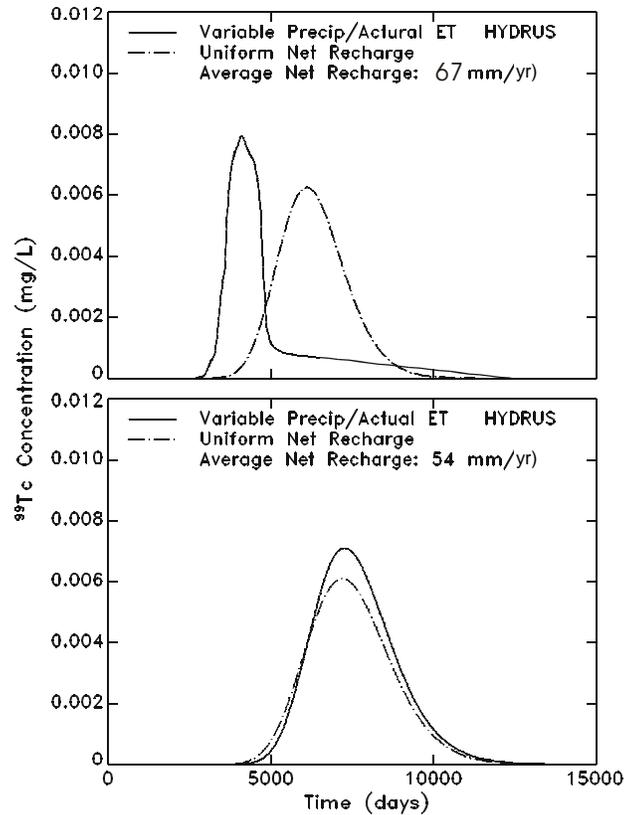
Figure F-4. Comparison of predicted ^{99}Tc breakthrough curves (through the 6 m layer) using the variable precipitation/actual ET versus uniform recharge rate in the HYDRUS Model. Average recharge rate is calculated as the mean net amount of precipitation and actual ET from 0 to 12,000 days. The net recharge varies between the two sets of curves due to the root-uptake scenario, (h_1, h_2, h_3).

precipitation and PET. The C_{peak} of the solid curve is 1.16 times that of the dashed curve, and the T_{peak} of the solid curve is 1.01 times that of the dashed curve. At the scale shown in Figure F-4, the daily and weekly "oscillations" are not apparent, but their cumulative effects are present.

- The relationship between the dashed curve in the bottom set, which reflects a nonuniform moisture distribution, and the corresponding uniform moisture content result is such that the C_{peak} decreases by 14% and the Tpeak increases 5.5% over those for the uniform case, based on the standard being the nonuniform case. These percentages are consistent with those found for the parameters K_d and D_L in Appendix E.

- The solid curve in the top set of curves in Figure F-4 does not possess the classic "bell-shape". This is primarily due to the nonlinear cumulative recharge shown in the top set of curves in Figure F-3. The average recharge rate is 87 mm/yr for the first 1000 days, 83 mm/yr for the next 4015 days, followed by 20 mm/yr for the next 2555 days, then 83 mm/yr for 4015 days, and finally 20 mm/yr for the last 2550 days.

- The first part of the solid curve in the top set is somewhat like that of the base case for HYDRUS given in Section 6, except the variable precipitation C_{peak} is 1.08 times higher and its T_{peak} 0.88 times smaller. After 5015 days, the average recharge rate drops sharply to 20 mm/yr, thus giving a long "heavy tail" to the distribution. At 7570 days the larger recharge rate kicks in again, producing a cutoff of the tail at about 12,500 days, or so.

- The dashed curve in the top set of Figure F-4 is the nonuniform moisture distribution BTC for a constant recharge rate of 67 mm/yr. Comparing this curve to results for the uniform moisture case, one sees that the C_{peak} decreases by 13.6% and the T_{peak} increases by 2.9% over those for the uniform case, based on the standard being the nonuniform case. These results are consistent with those of Appendix E.

F-6

References

Eagleson, P.S. 1970. <u>Dynamic Hydrology</u>. McGraw-Hill Book Co. New York, NY. 462 pp.

Jensen, M.E., R.D. Burman, and R.G. Allen. 1990. "Evapotranspiration and irrigation water requirements." <u>ASCE Manuals and Reports on Engineering Practice</u>. No. 70. American Society of Civil Engineers, NY. pp. 332.

Miller, R.W. and R.L. Donahue. 1995. <u>Soils in Our Environment</u>. 7th Edition. Prentice Hall, Englewood Cliffs, NJ. 649 pp.

Nobel, P.S. 1994. "Root-soil responses to water pulses in dry environments." In: <u>Exploitation of Environmental Heterogeneity by Plants: Ecophysiological Processes Above- and Belowground</u>. M.M. Caldwell and R.W. Pearcy, Eds. Academic Press. New York, NY. pp. 285-304.

Royo, A..R. 2000. "Desert Plant Survival." <u>DesertUSA Newsletter</u>. http://www.desertusa.com/du_plantsurv.html. 5 pp.

Šimúnek, J., K. Huang, and M.Th. van Genuchten. 1998. <u>The HYDRUS Code for Simulating the One-Dimensional Movement of Water, Heat, and Multiple Solutes in Variably-Saturated Media</u>. Research Report No. 144. U.S. Salinity Laboratory. USDA, ARS. Riverside, CA.

Yao, T-M. and J.M.H. Hendrickx. 1996. "Stability of wetting fronts in dry homogeneous soils under low infiltration rates." <u>Soil Sci. Soc. Am. J.</u> 60, 20-28.

Appendix G
The Impact of Considering a Layered Soil Column versus a Homogeneous Soil Column

In this appendix we are concerned with the impact on the flow and transport, and the sensitivity analyses of replacing the 6 m homogeneous layer (the "all" layer in Table 5-2) by the 9-layer soil column given in Table 5-2. It is recognized that these impacts will be *considerably less* than the impacts due to layering reported in Miyazaki et al. (1993) and Rockhold et al. (1997). However, the objective of the current impact analysis is to assess the differences of using the 9-layered soil column for the Las Cruces Trench Site versus the single all-layer soil column, and to decide if the use of one layer is comparable to the nine layers *at this site*.

As stated, Table 5-2 gives the soil hydraulic properties (K_s, θ_s, θ_r, α, β) at the Las Cruces Trench Site for the first 6m of the soil profile. The 6 m homogeneous layer used in the sensitivity analyses in Sections 6 and 7 is the layer with the hydraulic properties listed in the "all layer" row of the table. However, as seen in this table, the 600 cm layer is broken down into 9 sublayers, having different thicknesses and hydraulic properties. The biggest outlier of all the 9 layers is, as one would expect, the 15 cm thick surface layer which contains the most organic matter and is the most highly disturbed, both by natural and anthropogenic processes. The pathway through this surface layer represents only about 2.5 percent of the total pathway through the 600 cm layer; thus, its effect on the total passage of ^{99}Tc through the 6m vadose zone to the hypothetical water table is very minor. For the remaining eight layers, the range of values for the five soil properties about their base values (Section 6) and the corresponding maximum percentage deviation (based on the base value) are given below:

$$172 \text{ cm/d} < K_s = 270 < 334 \text{ cm/d}, \qquad 36.3\,\%,$$
$$0.294 < \theta_s = 0.32 < 0.343, \qquad 8.1\,\%,$$
$$0.071 < \theta_r = 0.08 < 0.091, \qquad 13.8\,\%,$$
$$0.027 \text{ cm}^{-1} < \alpha = 0.055 < 0.070 \text{ cm}^{-1}, \qquad 50.9\,\%,$$
$$1.383 < \beta = 1.51 < 1.711, \qquad 13.3\,\%.$$

The sensitivity results derived for the HYDRUS Code in Section 6, a code which can handle layered soil columns, show that of these five parameters, K_s is the least sensitive, followed closely by α; and β is the most sensitive, followed by θ_s and then by θ_r. The quantity β appears to be about twice as sensitive as θ_s, and θ_s about twice as sensitive as θ_r. Combining these relative sensitivity results with the above ranges and percent deviations, one sees that calculating the breakthrough curves (BTCs) for ^{99}Tc using the layered profile should not depart too radically from the homogeneous layer calculations.

Figure G-1 illustrates one set of differences between the homogeneous-layer calculations and the layered-soil calculations, using the HYDRUS Code. The comparative results are for three different values of the distribution coefficient K_d shown in the figure (0.001, 0.007, 0.019 ml/g). For both the layered and uniform soil profiles, the *nonuniform soil moisture content* was used, i.e., the Richards Equation was solved for constant recharge rate q. For the uniform layer case, the base values in Section 6 were used (i.e., the base values for q, ρ, D_L, D_w, K_s, θ_s, θ_r, α, β). For the layered case, the various values of K_s, θ_s, θ_r, α, and β in Table 5-2 were used, along with the base values of q, ρ, D_L, and D_w given in Section 6.

The results in this figure indicate that the C_{peak} values for the layered soil are less than those for the uniform layer, while the values for T_{peak} and T_{MCL} are greater. Considering the parameters which are the most sensitive (β, θ_s, θ_r), the changes in the outputs due to θ_s and θ_r are in the opposite directions to those for β. Thus, in the first three layers (0 to 205 cm), θ_s and θ_r tend to reduce C_{peak} and increase T_{peak} and T_{MCL} over those for the uniform layer case, while β has the opposite effect. In the next two layers (205 to 305 cm), all three parameters tend to increase
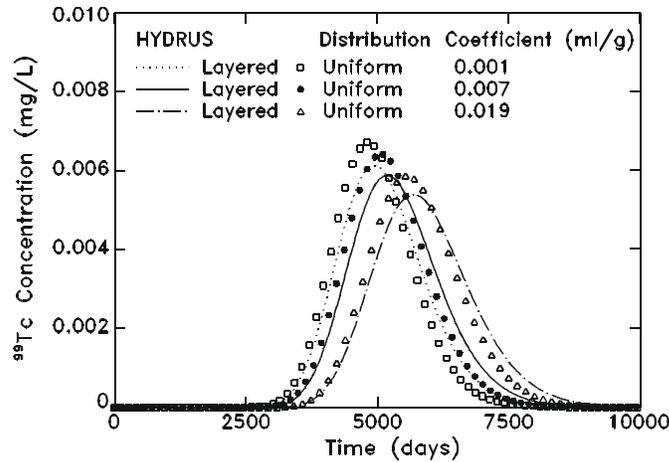
Figure G-1. Sensitivity of ^{99}Tc breakthrough (through the unsaturated zone with a water table at a depth of 6 m) to the distribution coefficients in a layered soil and in a uniform soil using the HYDRUS Model.

C_{peak} and decrease T_{peak} and T_{MCL}. In the layer from 305 to 370 cm, θ_s and β tend to increase C_{peak} and decrease T_{peak} and T_{MCL}, while θ_r has the opposite effect. In the final three layers (370 to 600 cm), β tends to decrease C_{peak} and increase T_{peak} and T_{MCL}, while the effects due to θ_s and θ_r are fairly close to those of the uniform case. From this collection of "facts," it is difficult to dogmatically say how the layered and uniform cases should compare. Thus, relying on the computations, one arrives at the following results, where percentages are based on the layered results as being the standard and decreases/increases are related to changes from the uniform case:

K_d (ml/g)	C_{peak}	T_{peak}	T_{MCL}
0.001	9.9% decrease	3.4% increase	2.4% increase
0.007	9.5% decrease	2.7% increase	2.2% increase
0.019	9.0% decrease	2.7% increase	2.0% increase

As suggested above, the differences between the results for the uniform soil and the layered soil are not too great. And because of this, it seems reasonable to expect the sensitivity studies given in this report for the 6m homogeneous layer are also applicable for the layered soil described in Table 5-2. The differences in C_{peak} are assumed to be within 10% of one another and those for T_{peak} and T_{MCL} are assumed to be around 3 to 4%, or less, of one another. However, as initially stated, these conclusions will ***not be valid*** if the layering is of the type considered by Miyazaki et al. (1993) and Rockhold et al. (1997), layering with significant changes in hydraulic properties from layer to layer in the soil column.

References

Miyasaki, T., S. Hasegawa and T. Kasubuchi. 1993. Water Flow in Soils. Marcel Dekker, Inc., New York, NY, 296 pp.

Rockhold, M.L., C.S. Simmons and M.F. Fayer. 1997. "An analytical solution technique for one-dimensional, steady vertical water flow in layered soils." Water Resour. Res. 33(4):897-902.

Appendix H
A Detailed Analysis of Nonequilibrium Sorption of Pollutants, Mainly for the Radionuclide ^{90}Sr

Thibodeaux (1996) states that the validity of the local equilibrium assumption (LEA) in solid-liquid soil reactions depends on the degree of interaction between the macroscopic transport processes of water flow and hydrodynamic dispersion, and the microscopic processes of molecular diffusion and sorbed-solute distribution in conjunction with soil aggregate size. When the rate of change of solute mass during microscopic sorption processes is fast relative to bulk flow, the interaction is nearly instantaneous, comparatively speaking, and it conforms with the LEA. Deviations from local equilibrium occur as the interactions of the solute with the porous media become increasingly time dependent with respect to the time scales of the bulk flow. This divergence also occurs as soil aggregates increase in size and complexity, and the pore-class heterogeneity increases. In the present case, the transport of radionuclides through the unsaturated zone is taking place under the influence of a very low annual recharge rate, which leads to a hydrodynamic dispersion of only two times that of molecular diffusion. Under these conditions, sites that were in local equilibrium at higher recharge rates will still be in local equilibrium. Some new sites where nonequilibrium conditions existed or no liquid-solid reactions occurred at higher recharge rates will now become under the LEA, while other new sites will pass from no action sites to nonequilibrium sites, and some will be nonequilibrium sites under both the higher and lower flows. Thus, the adsorption-desorption cycle of a given pollutant through a given soil profile has a variety of characteristic time scales dependent upon the type of liquid-solid reaction mechanisms at the various sites in the soil matrix. Therefore, it seems reasonable that for "all" recharge flows one considers nonequilibrium sorption as well as equilibrium conditions.

H.1 A Simplified Version of the Transport Equations

Although there are other models (see Section 3.6), the system used in CHAIN 2D and HYDRUS is a two-site (equilibrium-nonequilibrium) model developed by van Genuchten and his colleagues (van Genuchten and Wagenet, 1989; Toride et al., 1993). The one-dimensional version of the transport equations using this model (i.e., the HYDRUS Code) is given in Section 2 and Appendix D. It is this version that is used to generate results for the current appendix. However, for purposes of discussion and argument, the following simplified set of transport equations for the liquid phase pollutant concentration, c, and the nonequilibrium solid phase concentration, s, is considered:

$$\frac{\partial c}{\partial t} + \frac{q}{\theta + \rho f K_d} \frac{\partial c}{\partial z} = \frac{\theta \tau_w D_w + D_L |q|}{\theta + \rho f K_d} \frac{\partial^2 c}{\partial z^2} - \mu c - \frac{\rho}{\theta + \rho f K_d} D/P , \tag{H-1}$$

$$\frac{\partial s}{\partial t} = D/P - \mu s , \tag{H-2}$$

where μ is the radioactive decay rate for both s and c, and D/P is a decay/production, sorption transfer function defined by

$$D/P \equiv \omega \left[(1\text{-}f) K_d \, c - s \right]. \tag{H-3}$$

The quantity, f, is a parameter fixed by the soil structure. When $f = 1$, there are no nonequilibrium sorption sites in the soil and when $f = 0$, there are no equilibrium sorption sites. When $0 < f < 1$, there are both equilibrium and nonequilibrium sites. The quantity, ω, is the first-order rate constant for nonequilibrium sorption in inverse time units. Thus, we have two new input parameters for the nonequilibrium sorption process, (ω, f).

When $D/P = 0$ (i.e., the nonequilibrium sites act as equilibrium sites), these transport equations reduce to the following:

$$\frac{\partial c}{\partial t} + \frac{q}{\theta + \rho f K_d} \frac{\partial c}{\partial z} = \frac{\theta \tau_w D_w + D_L |q|}{\theta + \rho f K_d} \frac{\partial^2 c}{\partial z^2} - \mu c \, , \tag{H-4}$$

$$s = (1 - f) K_d c \, . \tag{H-5}$$

Equations (H-4) and (H-5) define the situation when there are no nonequilibrium sites, which occurs when $f = 1$; or if $0 \leq f < 1$, the equations define the situation when ω is sufficiently large so as to dominate the effect of the decay rate, μ.

H.2 The Transport of ^{99}Tc with a $K_d = 0.007$ ml/g

As a first example of Equations (H-1) and (H-2), let us consider the transport of ^{99}Tc through the 6 m soil column. The initial distributions of (c,s) in the soil profile are taken as zero, and a source of c is postulated at the surface. For ^{99}Tc, the decay rate, μ, has a very small effect on the breakthrough curves (BTCs) since lifetimes for these curves in the given system are from 10,000 days to 12,000 days for the default K_d of 0.0007 ml/g, while the half-life of ^{99}Tc is 2.1×10^5 years. Thus the important decay/production in these two equations is D/P and not μ. As the process begins, $t > 0$, pollutant c begins to be spread throughout the water in the soil profile. This then produces a source of s via the D/P term; thus, s begins to be spread throughout the soil matrix in the column. As long as s is less than $(1 - f)K_d c$, D/P is a sink term for c and a source term for s. If s is greater than $(1 - f)K_d c$, then D/P is a source term for c and a sink term for s. Since the only other term in the s-equation is a very small sink term (i.e., μs), s will approximately be equal to $(1 - f)K_d c$ for sufficiently large ω. Thus, under sufficiently high sorption rates ω, we have the "equilibrium" condition:

$$s \cong (1 - f)K_d c \, . \tag{H-6}$$

Equation (H-6) shows that for low K_d-pollutants, the amount of material adsorbed at the nonequilibrium sites for any one time is very small, while for high K_d-pollutants, the opposite is usually true. Consequently, even though the low-q problems considered in this report may partially violate the LEA, the resultant effect of nonequilibrium sorption can still be very small if the pollutant in question (i.e., ^{99}Tc) has a very small K_d.

Using the HYDRUS Code with the nonuniform distribution for θ and the base values of Section 6 for the other 10 standard input parameters, the BTCs of ^{99}Tc for different values of (ω, f) were derived. One set of BTCs were obtained for $f = 0.47$ and $\omega = 0.003, 0.032,$ and 0.320d^{-1}. Another set of BTCs were obtained for $\omega = 0.032 \text{d}^{-1}$ and $f = 0.27, 0.47, 0.67$. These five curves were compared with the equilibrium case, $f = 1$ and $\omega = 0$, given by the solid curve in the top set of curves in Figure E-2. It should be noted that when one is comparing such sets of curves, Equations (H-1) and (H-2) are not exactly the ones solved by the HYDRUS Code since θ is not constant but is variable with depth as shown in Figure E-1. However, for order-of-magnitude arguments, Equations (H-1) to (H-6) are adequate.

Considering Equations (H-1) and (H-2), one sees that the parameters (ω, f) affect three processes (terms): advection, diffusion, the decay/production term D/P. When s reaches its equilibrium value of $(1-f)K_d c$, the D/P term is turned off and the s-distribution will track the c-distribution if c and s do not again get out of balance. This tracking is such that when $s = (1-f)K_d c$, the c-distribution is the distribution that occurs when there are no nonequilibrium sites. That is, the existence of active nonequilibrium sites requires an s-distribution which is not equal to the equilibrium sorption condition given by $(1-f)K_d c$.

For ^{99}Tc, with its default K_d of 0.007 ml/g and its large half-life, the c- and s-distributions should not get out of balance once they are in balance. Further, the transfer of material between solution and the soil matrix is relatively small for the (ω, f) given above:

$$\left[(1 - f) \, K_d c\right]_{max} \cong 0.51\% \text{ of c(t) .} \tag{H-7}$$

These results are verified when the "nonequilibrium" ^{99}Tc BTCs for the five combinations of (ω, f) mentioned above are compared with one another and with the equilibrium case for $(\omega, f) = (0, 1)$. All of these BTCs are within 1% or 2% of one another at any given time. Thus, for a soil profile of 6 m, the nonequilibrium formulation given in Equation (H-1) and (H-2) reduces to an equilibrium formulation for a radionuclide with a K_d of 0.007 ml/g and a half-life of 76,650,000 days, if ω is sufficiently large.

H.3 The Transport of ^{99}Tc with a K_d = 1.0 ml/g

For illustrative purposes, we next considered ^{99}Tc with a K_d equal to unity and (ω, f) equal to $(0.032d^{-1}, 0)$, $(0.032d^{-1}, 0.47)$ and $(0, 1)$. The results of these numerical experiments were basically the same as the K_d of 0.007 ml/g results (i.e., nonequilibrium conditions quickly approach equilibrium conditions), even though the maximum amount of material transferred between solution and soil matrix is much greater than that given in Equation (H-7):

$$\left[(1 - f) \, K_d c\right]_{max} = 100\% \text{ of c(t),} \tag{H-8}$$

Table H-1 summarizes both sets of results (i.e., K = 0.007, 1.0 ml/g) for three selected times and concentration pairs (c, s) for the ^{99}Tc BTCs. The equilibrium cases are given by the pair $(\omega, f) = (0,1)$, while the "nonequilibrium" cases are given by the pairs $(\omega, f) = (0.032, 0.47)$ and $(0.032, 0)$. Columns headed by c and s are rounded off calculated values from the HYDRUS Code, while the column headed by $(1-f)K_d c$ is a check to see if c and s are in equilibrium sorption balance. To round-off error, for both K_d values of 0.007 and 1.0 ml/g, all times, and a half-life of 76,650,000 days, the equilibrium and "nonequilibrium" BTCs are the same and the c– and s–distributions are in

Table H-1.   Comparison of Nonequilibrium and Equilibrium Results for ^{99}Tc BTCs for K_d Values of 0.007 and 1.0 ml/g.

Radionuclide	K_d ml/g	μ (d^{-1})	ω (d^{-1})	f	Time (d)	c mg/L	$(1-f)K_d c$ mg/kg	s mg/kg
Technetium								
^{99}Tc	0.007	9.043 x10^{-9}	0	1	3750	0.00105	0	0
					5005	0.00646	0	0
					6250	0.00227	0	0
	0.007	9.043 x10^{-9}	0.032	0.47	3750	0.00111	4.12 x 10^{-6}	4.12 x 10^{-6}
					5005	0.00644	2.39 x 10^{-5}	2.39 x 10^{-5}
					6250	0.00222	8.24 x 10^{-6}	8.19 x 10^{-6}
	1	9.043 x10^{-9}	0	1	40,000	3.67 x 10^{-4}	0	0
					46,500	6.22 x 10^{-4}	0	0
					60,000	1.38 x 10^{-4}	0	0
	1	9.043 x10^{-9}	0.032	0.47	40,000	3.67 x 10^{-4}	1.94 x 10^{-4}	1.90 x 10^{-4}
					46,500	6.12 x 10^{-4}	3.24 x 10^{-4}	3.24 x 10^{-4}
					60,000	1.38 x 10^{-4}	7.31 x 10^{-5}	7.35 x 10^{-5}
	1	9.043 x10^{-9}	0.032	0	40,000	3.67 x 10^{-4}	3.67 x 10^{-4}	3.63 x 10^{-4}
					46,500	6.02 x 10^{-4}	6.02 x 10^{-4}	6.01 x 10^{-4}
					60,000	1.38 x 10^{-4}	1.38 x 10^{-4}	1.40 x 10^{-4}

equilibrium sorption balance through the formula $(1-f)K_d c = s$. In addition, one sees a slight drop in the C_{peak} (at t = 46,500d) for the $K_d = 1.0$ ml/g case from 6.22×10^{-4} mg/L for the equilibrium case $(\omega, f) = (0, 1)$, to 6.12×10^{-4} mg/L for $(\omega, f) = (0.032, 0.47)$ to 6.02×10^{-4} mg/L for $(\omega, f) = (0.032, 0)$.

H.4 The Transport of ^{90}Sr with a $K_d = 1.0$ ml/g

The third case that we considered was the base case scenario for ^{90}Sr; this radionuclide has a default K_d of 1.0 ml/g and a half-life of 10,585 days. Thus, one would expect significant decay over the lifetime of the BTCs for this radionuclide. Figure H-1a shows the BTCs for the concentrations of ^{90}Sr in solution for the parameter pairs $(\omega, f) = (0, 1)$, $(0.032d^{-1}, 0.47)$, and $(0.032d^{-1}, 0)$. The BTCs for these three parameter pairs are basically equal, which means that the two "nonequilibrium" cases, (ω, f), $(0.032d^{-1}, 0.47)$, and $(0.032d^{-1}, 0)$, are the same as the equilibrium case $(\omega, f) = (0, 1)$. Further, Figure H-1b shows that the D/P term is essentially zero for all three parameter pairs (this is trivially so for $\omega = 0$ and $f = 1$):

$$D/P = \omega\left[(1 - f)K_d\ c - s\right] \cong 0, \text{ for all time t.} \tag{H-9}$$

The s-distributions for $f = 0$ and 0.47 track those of the c-distributions through the relationship $s = (1 - f) K_d c = (1 - f)c$.

The results in Table H-1 and those shown in Figure H-1ab support the claim that nonequilibrium sorption has very little effect for the low recharge rates considered $(0.014 \leq q \leq 0.032$ cm/d), for the sorption reaction rates which range over $0.003 < \omega < 0.32d^{-1}$, and for the specific radionuclides considered in this report, with K_d values that range from 0 to 5 ml/g. This claim is further supported by the magnitude of the coefficients in Equations (H-1) and (H-2). For example, in the ^{90}Sr case, the coefficients for $(\omega, f) = (0.032d^{-1}, 0.47)$ are as follows:

(a)

(b)
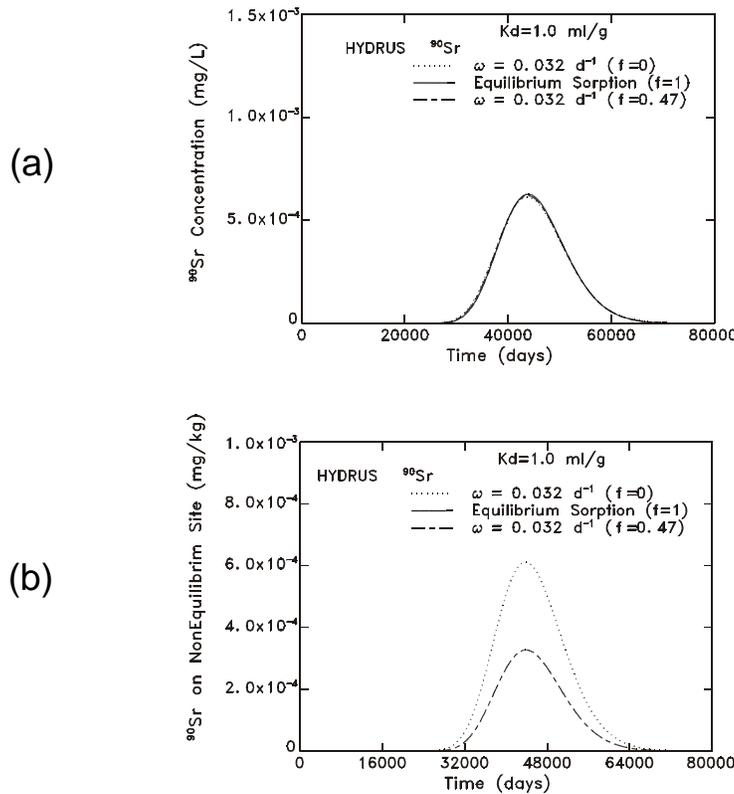
Figure H-1. The c- and s distribution of Equations (H-1) and (H-2) for ^{90}Sr for $(\omega, f) = (0, 1)$, $(0.032\ d^{-1}, 0.47)$, $(0.032d^{-1}, 0)$. Distributions were derived by the HYDRUS Code, (a) gives the concentration in solution and (b) gives the concentration on the soil matrix.

Equation	Radioactive Decay	Sorption Decay	Nonhomogeneous Sorption Term
Eq. (H-1)	$-6.55 \times 10^{-5}c$	$-3.01 \times 10^{-2}c$	$+5.67 \times 10^{-2}s$
Eq. (H-2)	$-6.55 \times 10^{-5}s$	$-3.20 \times 10^{-2}s$	$+1.70 \times 10^{-2}c$

From these coefficients, we note that the radioactive decay term is negligible as compared to the transfer of ^{90}Sr between solution and soil matrix. Thus, even though the radioactive decay greatly reduces the C_{peak} values of the ^{90}Sr BTCs over their lifetimes of 65,000 to 80,000 days, this decay has little influence on the much faster adsorption/ desorption processes. Further, as shown in Figures H-1a and H-1b, the nonequilibrium sorption process is sufficiently fast that the D/P term goes to zero and the nonequilibrium sites, in reality, become equilibrium sites. A more detailed analysis is given in the following paragraphs.

H.5 The Transport of ^{90}Sr with a K_d = 1.0 ml/g, f = 0, and Varying Sorption Rates

We have found that the nonequilibrium sorption sites for ^{99}Tc, in essence, acted as equilibrium sites for the low recharge rates considered in this report when the sorption rates ω are taken to be equal to or greater than 0.003d^{-1}. In addition, the nonequilibrium sorption sites for ^{90}Sr acted as equilibrium sites for a sorption rate ω of 0.032d$^{-1\cdot}$. Therefore, the question that arises is the following: At what sorption rates ω will these systems truly possess nonequilibrium sites that are **not** in equilibrium balance with the liquid phase concentration? We answered this question for ^{90}Sr, whose K_d value is taken as 1.0 ml/g and whose decay rate μ is given as 6.55×10^{-5}d^{-1}. However, the reader should be aware that the values of ω for which ^{90}Sr possesses "true" nonequilibrium sites in this Las Cruces soil may be physically unrealistic. The current exercise was conducted to both understand this module of the HYDRUS Code and to indicate the range of values for ω that are required to unbalance equilibrium sorption conditions for the very low recharge rates considered in this report.

For the radionuclide, ^{90}Sr, with a K_d = 1.0 ml/g and an f = 0 (i.e., no equilibrium sorption sites, only nonequilibrium sites), Equations (H-1) and (H-2) become:

$$\frac{\partial c}{\partial t} + v \frac{\partial c}{\partial z} = D \frac{\partial^2 c}{\partial z^2} - \mu c - \frac{\rho}{\theta} \omega(c\text{-}s) , \tag{H-10}$$

$$\frac{\partial s}{\partial t} + (\omega + \mu)s = \omega c , \tag{H-11}$$

where the coefficients (v,D) are defined by

$$v = q/\theta, \quad D = \tau_w D_w + D_L \left|q\right|/\theta . \tag{H-12}$$

Equation (H-11) is a is a first order, linear, nonhomogeneous equation for s where s(z,0) is taken to be zero, as stated in Section H.2. Solving Equation (H-11) results in the following:

$$s(z,t) = \omega \int_0^t \exp\left[-(\omega + \mu)(t - \eta)\right] c(z,\eta) \, d\eta . \tag{H-13}$$

Combining Equations (H-10) and (H-13) produces the following linear, integrodifferential equation for the liquid phase concentration c:

$$\frac{\partial c}{\partial t} + v \frac{\partial c}{\partial z} = D \frac{\partial^2 c}{\partial z^2} - \mu c +$$

$$+ \frac{\rho\omega}{\theta} \left[\omega \int_0^t \exp\left[-(\omega + \mu)(t - \eta)\right] c(z,\eta) \, d\eta - c \right] . \tag{H-14}$$

The integral term in Equation (H-14) radically changes the system defined by Equation (H-4) by introducing a "history" dependence in the evolution of the liquid phase concentration. This integral term shows that the value of $c(z,t)$ at any point z in the soil column not only depends on the current time, but also depends on the entire history of the evolution of $c(z,\eta)$ from the initial time $\eta = 0$ to the current time $\eta = t$ at the point z in question. As we have seen in Section H.2, this integral term loses its historic dependence if ω is sufficiently large. But what happens if ω is sufficiently small? To answer this question, we let ω equal a sequence of values from $6.5 \times 10^{-6} d^{-1}$ to $6.5 \times 10^{-1} d^{-1}$, remembering that μ equals $6.55 \times 10^{-5} d^{-1}$.

Before considering the results obtained from the HYDRUS calculations, two comments are worth emphasizing:

(1) Equations (H-10) to (H-14) represent a "stripped-down" version of the HYDRUS Code used to simulate the transport of ^{90}Sr with parameters (K_d, f) set equal to (1.0, 0). The HYDRUS Code uses a variable soil moisture, $\theta(z)$, in the simulation, while the "stripped-down" version does not. Equations (H-10) to (H-14) are only used for explanatory and argumentative purposes.

(2) The "stripped-down" version of the HYDRUS Code (although f need not be zero) has been recently solved by Drake et al. (2002), though the use of Laplace Transformations, the theory of residues, and the Bromwich Integral in the complex plane. The z-domain was defined by $0 \le z \le L$, the source at $z = 0$ was a variable stepwise-continuous function, and the condition at $z = L$ was a variable flux of pollutants. The exact solution is in the form of a single definite integral involving elementary functions of the independent variables (z,t) and the system parameters.

Figures H-2a and H-2b depict the c- and s-distributions at the bottom of the 6 m soil column for the sequence of ω values listed in the above paragraph. Figure H-2a gives the usual BTCs for the concentration of ^{90}Sr in solution at the hypothetical water table (i.e., the bottom of the 6 m column). These BTCs show the usual "bell-shape" for $\omega \ge 6.5 \times 10^{-4} d^{-1}$ (keep in mind that Figure H-2a is a semi-log plot), but are radically different from the "bell-shape" for $\omega = 6.5 \times 10^{-6} d^{-1}$ and $6.5 \times 10^{-5} d^{-1}$. For these lowest two values of ω, the "history" term in Equation (H-14) has the greatest effect. Figure H-2b gives the corresponding concentration curves (CCs) for the solid phase at the water table level of 6 m. As with the BTCs, the CCs show a characteristic "bell-shape" for $\omega \ge 6.5 \times 10^{-4} d^{-1}$, and a non "bell-shape" for the lowest two ωs. In fact, as ω increases in size one can see, by careful analysis of the curves in Figures H-2a and H-2b, that the BTCs approach the CCs. That is, as ω increases, the nonequilibrium sites "convert" to equilibrium sites, the "history" term in Equation (H-14) becomes less effective, and Equations (H-1) and (H-2) change over to Equations (H-4) and (H-5).

Table H-2 reinforces the above conclusion. In this table we have listed the peak values of the BTCs and CCs at the 6 m water table, C_{peak} and S_{peak}, respectively, and their corresponding times to T_{peak}. The values for the BTCs and CCs are quite different for the lowest two ω values, while from ω equal to $6.5 \times 10^{-4} d^{-1}$ and higher, the values for the BTCs begin to quickly approach those for the CCs. For $\omega \ge 0.032 d^{-1}$, the BTCs and CCs tend to give the same results. This means that the nonequilibrium sites become equilibrium sites (or act like equilibrium sites) for the low recharge rates used in this analysis whenever the sorption rate $\omega \ge 0.032 d^{-1}$ and the pollutant is ^{90}Sr. For other pollutants with different K_ds and decay rates, μ, this limiting sorption rate will vary, but the general trend is valid.

The final reinforcement of the above conclusion was made by considering the time evolution of the c- and s-distributions throughout the entire 6 m soil column. Figures H-3 to H-6 give the liquid phase concentrations (the "a" figures) and the solid phase concentrations (the "b" figures) throughout the soil column (0 for the surface and -600 cm for the water table) for various fixed times and various values of the sorption rate ω. Figure H-3 is for a rate ω of $6.5 \times 10^{-5} d^{-1}$. It is obvious that the c- and s-distributions are not in balance, and nonequilibrium sorption conditions *do exist*. An interesting observation is that the earlier time distributions for c have the classic "bell-shape," while the later time distributions tend to lose this shape (also see the dotted curve in Figure H-2a). The reason for the non-bell-shapes is that the "history" term in Equation (H-14) has had more time to accumulate the effects from earlier distributions and has thus changed the classic diffusion equation. Figure H-4 is for a rate ω of $6.5 \times 10^{-4} d^{-1}$. These distributions also indicate the existence of nonequilibrium conditions for the earlier time curves; while for the later time curves, the c-distributions are rapidly approaching those of the solid phase, which indicates the approach of equilibrium sorption at all sites in the soil matrix. Figure H-5 is for a rate ω of $6.5 \times 10^{-3} d^{-1}$. As one can easily see, the shapes of the c-distributions are nearly the same as those for the s-distributions; however, the peaks of the s-distributions are slightly greater than those of the c-distributions at the earlier times. As time increases the peaks for both sets of distributions approach one another and the sorption sites approach equilibrium. In addition, both sets of curves exhibit the classic "bell-shape" which indicates the reduced roll of the "history" term in Equation (H-14). The
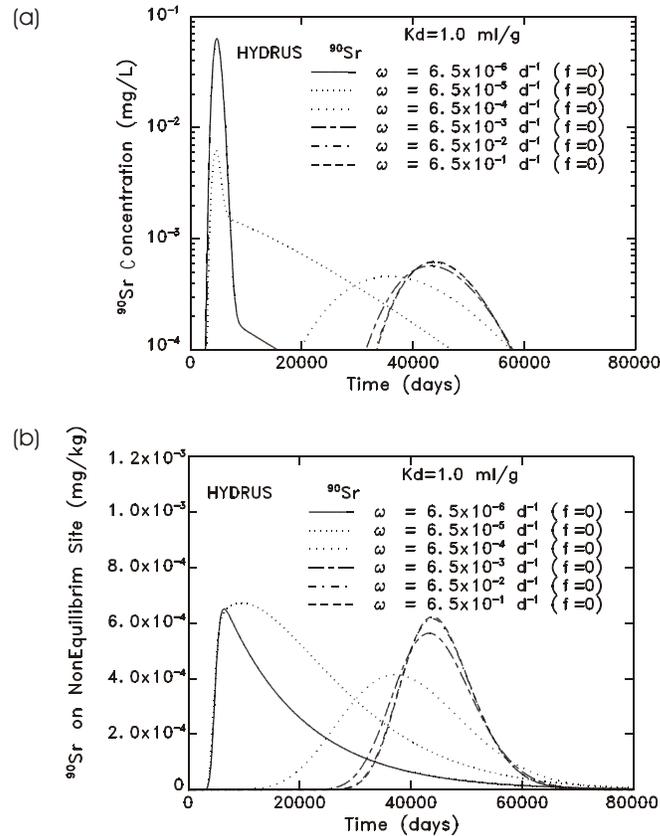
Figure H-2. (a) Breakthrough curves for the liquid phase concentration at the 6 m level. (b) Concentration curves for the nonequilibrium solid phase at the 6 m depth. Curves for $\omega = 6.5 \times 10^{-2}d^{-1}$ and $6.5 \times 10^{-1}d^{-1}$ are basically the same for both (a) and (b).

Table H-2. Liquid Phase and Solid Phase Peak Concentrations at the Hypothetical Water Table for a Sequence of Sorption Rates, along with the Corresponding Times to Arrive at Those Peaks.

Sorption Rate, ω (d^{-1})	Solid Phase Concentration		Liquid Phase Concentration	
	S_{peak} (mg/kg)	T_{peak} (d)	C_{peak} (mg/L)	T_{peak} (d)
6.5×10^{-6}	6.5×10^{-4}	6,300	6.3×10^{-2}	4,900
$*6.5 \times 10^{-5}$	6.7×10^{-4}	9,500	6.2×10^{-3}	4,700
6.5×10^{-4}	4.1×10^{-4}	37,100	4.6×10^{-4}	35,200
6.5×10^{-3}	5.6×10^{-4}	43,100	5.7×10^{-4}	43,200
$**3.2 \times 10^{-2}$	6.2×10^{-4}	43,500	6.2×10^{-4}	43,500
6.5×10^{-2}	6.2×10^{-4}	43,500	6.2×10^{-4}	43,500
6.5×10^{-1}	6.2×10^{-4}	43,500	6.2×10^{-4}	43,500

* Decay Rate μ for ^{90}Sr is $6.55 \times 10^{-5}d^{-1}$.
** Data from Figure H-1.

final sets of distributions are given in Figure H-6, which are for $\omega = 6.5 \times 10^{-2}d^{-1}$; the curves for $\omega = 6.5 \times 10^{-1}d^{-1}$ were found to be "graphically" equivalent to those for $\omega = 6.5 \times 10^{-2}d^{-1}$. As one can see, for all times greater than or equal to 2000 days, the c- and s-distributions are the same, and there are no nonequilibrium sites within the soil column.

References

Drake, R.L., J-S. Chen and D.G. Jewett (2002). "An exact solution for the assessment of nonequilibrium sorption of radionuclides in the vadose zone." Waste Management 2002 Conference. February 24-28, 2002, Tucson, AZ. Available from *www.wmsym.org/wm02* (click on WM'02 Proceedings).

Thibodeaux, L.J. 1996. Environmental Chemodynamics: Movement of Chemicals in Air, Water, and Soil. 2nd Edition. John Wiley & Sons, Inc. New York, NY. 593 pp.

Toride, N., F.J. Leij, and M.T. van Genuchten. 1993. "A comprehensive set of analytical solutions for nonequilibrium solute transport with first-order decay and zero-order production." Water Resour. Res. 29(7), 2167-2182.

van Genuchten, M. Th., and R.J. Wagenet. 1989. "Two-site/two-region models for pesticide transport and degradation: theoretical development and analytical solutions." Soil Sci. Soc. Am. J. 53, 1303-1310.

Figure H-3. Liquid phase concentration curves (a) and solid phase concentration curves (b) for ^{90}Sr, for various times and for $\omega = 6.5 \times 10^{-5}d^{-1}$, where zero depth is the surface and -600 cm is the hypothetical water table.

Figure H-4. Liquid phase concentration curves (a) and solid phase concentration curves (b) for ^{90}Sr, for various times and for $\omega = 6.5 \times 10^{-4}d^{-1}$, where zero depth is the surface and -600 cm is the hypothetical water table.

Figure H-5. Liquid phase concentration curves (a) and solid phase concentration curves (b) for ^{90}Sr, for various times and for ω = 6.5 x 10^{-3}d^{-1}, where zero depth is the surface and -600 cm is the hypothetical water table.
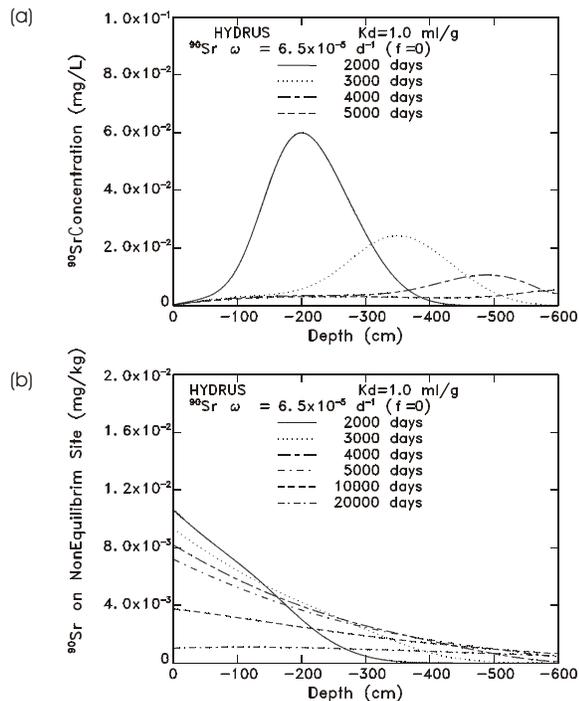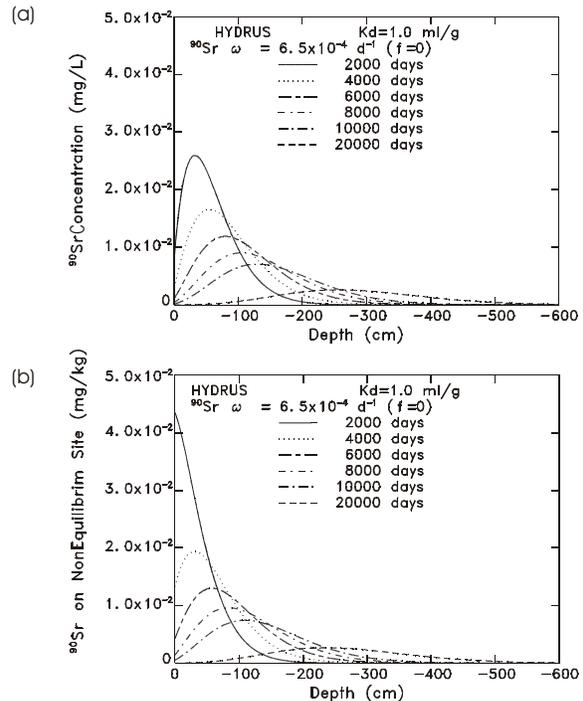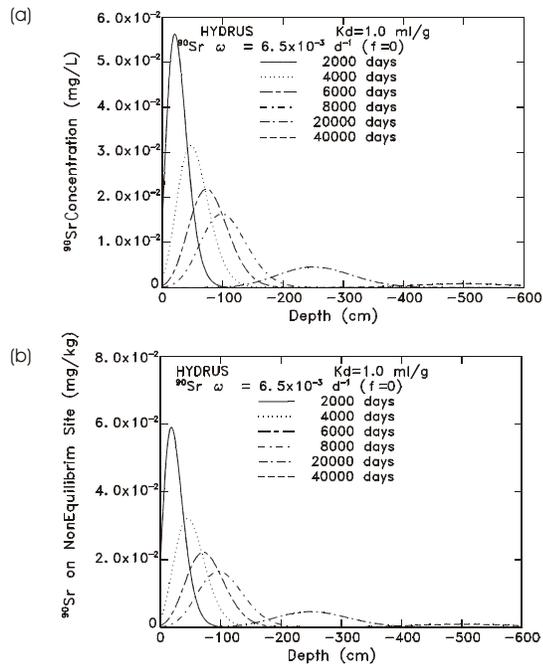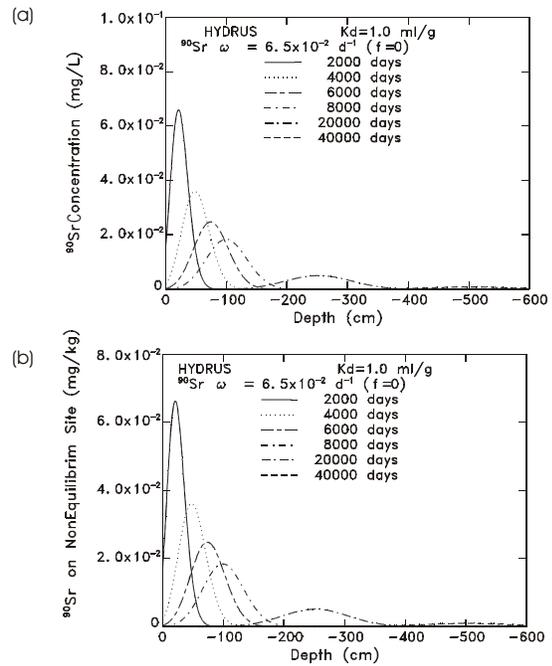
Figure H-6. Liquid phase concentration curves (a) and solid phase concentration curves (b) for ^{90}Sr, for various times and for ω = 6.5 x 10^{-2}d^{-1}, where zero depth is the surface and -600 cm is the hypothetical water table.

Appendix I
Results from the Transport and Fate of Other
Radionuclides Not Considered in the Main Text

The fate and transport of radionuclides in a finite soil column (e.g., the five parent radionuclides listed in Section 5.1 passing through the 6 m soil column considered in this report) are strongly influenced by the distribution coefficient, K_d, the radioactive decay rate, μ, and the recharge rate, q. One could imagine that there exists some decay-mobility scale (DMS) that represents the basic characteristics of a radionuclide as it passes through the finite column. For example, for the *smaller values of the DMS*, the radionuclide could be long-lived and highly mobile in the soil column, and thus have characteristics somewhat similar to a conservative species, Region I of the curve in Figure I-1. In this figure, the ordinate is the concentration, C, at the bottom of the soil column, normalized by the concentration, C_o, of the source at the top of the column, the ordinate being denoted as $[C/C_o]_B$. The values of $[C/C_o]_B$ for Region I of the curve, which are less than one, represent diffusive dilution but very little dilution due to radioactive decay. For the *larger values of DMS*, the radionuclides could be short-lived and highly immobile in the soil column, thus producing small values of $[C/C_o]_B$ as shown in Region III of the curve in Figure I-1. The radionuclides with intermediate half-lives and values of K_d would be characterized by the **intermediate values of DMS** and Region II of the curve. However the exact form of the DMS is unknown, but its qualitative properties are as represented in Figure I-1. One reason a DMS is difficult to quantify is the fact that K_d is a lumped parameter which represents many unknown geochemical processes in natural soil columns. Thus, a K_d value for a given radionuclide is not unique but is highly dependent on soil structure, texture, and geochemistry (U.S. EPA 1999a,b; 2000a,b). Consequently, a DMS value for a given radionuclide would not be expected to be unique either. But, the qualitative trends stated above, and shown in Figure I-1, are potentially correct, and have value in relating diffusive dilution and radioactive decay to pollutant travel time.
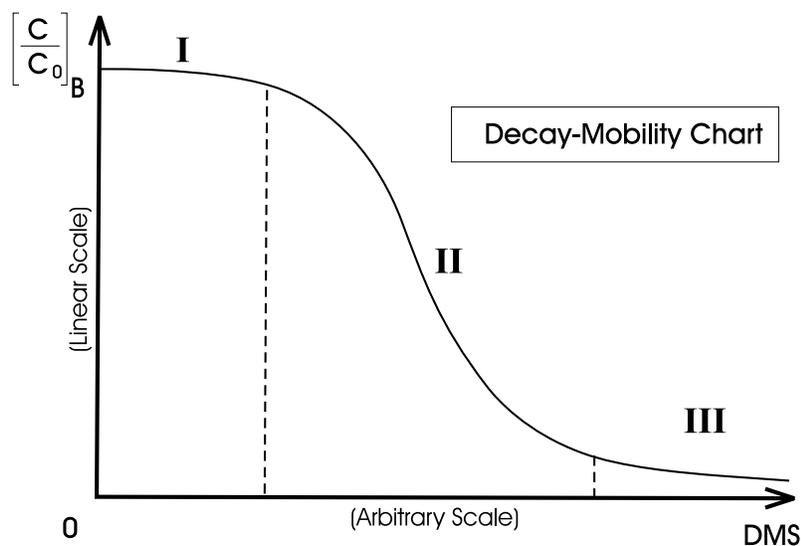

Figure I-1. The normalized concentration of a radionuclide at the bottom of a soil column (the source being at the top of the column) versus a hypothetical decay-mobility scale (DMS), where I represents highly mobile, long-lived species, III represents highly immobile, short-lived species, and II represents species with intermediate mobilities and half-lives.

The five parent radionuclides given in Section 5.1, along with their default K_d values and their half-lives listed in Figure 5-1, can be located "on the curve" in Figure I-1 for this report's 6 m, homogeneous soil column. These proposed locations are as follows:

- ^{99}Tc and ^{238}U are represented by Region I;
- Travel time through the 6 m column for ^{238}U is about 5 times greater than that for ^{99}Tc, thus diffusive dilution is much greater for ^{238}U than for ^{99}Tc;
- ^{3}H is represented by the left-hand side of Region II;
- ^{90}Sr is represented by the right-hand side of Region II; and
- ^{238}Pu is represented by Region III.

This appendix reports the results of two sets of simulations illustrating the validity of the placement of the five parent radionuclides on the curve in Figure I-1. Using the CHAIN and FECTUS Codes, the differences between the transport and fate of a parent and that of a daughter are displayed for ^{99}Tc and its daughter, ruthenium ^{99}Ru, for the 6 m, homogenous soil column. The other set of calculations used the CHAIN Code to compute the C_{peak} - and T_{peak}- values for the breakthrough curves (BTC's) at the 6 m level, for each of the five radionuclides under the influence of a range of recharge rates, thus verifying the proposed locations of the radionuclides "along the curve" in Figure I-1.

I.1 The CHAIN Governing Equations

The CHAIN Equations covering the transport and fate for both these comparative exercises are as follows:

$$\frac{\partial c}{\partial t} + \frac{q}{\theta + \rho K_d} \frac{\partial c}{\partial z} = \frac{\theta D}{\theta + \rho K_d} \frac{\partial^2 c}{\partial z^2} - \mu c \ , \tag{I-1}$$

$$\frac{\partial c^*}{\partial t} + \frac{q}{\theta + \rho K_d^*} \frac{\partial c^*}{\partial z} = \frac{\theta D}{\theta + \rho K_d^*} \frac{\partial^2 c^*}{\partial z^2} - \mu^* c^* + \frac{\theta + \rho K_d}{\theta + \rho K_d^*} \mu c \ , \tag{I-2}$$

where c is the concentration of the ***parent*** in mg/L and the asterisked (*) quantities represent those for the ***daughter***. Using the base values for (q, θ, ρ, D) given in Section 6, the default values of K_d for the radionuclides given in Section 5, and the half-lives given in Figure 5-1, the coefficients for the advection term, the diffusion term, and the sink term in Equation (I-1) can be evaluated. These coefficients for the five radionuclides are given in Table I-1. The relationship between μ and the half-life, $t_{1/2}$, is given by:

$$\mu = \left(\log_e 2\right) \div t_{1/2} \ . \tag{I-3}$$

Table I-1 shows that as K_d increases from 0 to 5 ml/g, the seepage velocity (advection term coefficient) decreases by a factor of 54, as does the diffusion term coefficient. Even though the diffusive mechanism decreases greatly, it may still be very important because the great decrease in seepage velocity allows the diffusion to act over a longer time, as exemplified by the following:

Radionuclide	(600 cm) ÷ (Advection Term Coefficient)
^{3}H	4,000 d
^{99}Tc	4,300 d
^{238}U	21,000 d
^{90}Sr	46,500 d
^{238}Pu	216,600 d

Table I-1. Coefficients of the Advection, Diffusion, and Sink Terms in Equation (I-1).

Radionuclide	Initial Concentration in Recharge Water C_0 (mg/L)	Default Value K_d (ml/g)	Half-Life $t_{1/2}$ (d)	First-Order* Decay Rate μ (d^{-1})	Advection Term* Coefficient $\dfrac{q}{\theta + \rho K_d}$ (cm/d)	Diffusion Term* Coefficient $\dfrac{\theta D}{\theta + \rho K_d}$ (cm^2/d)
Tritium ^{3}H	1.1 x 10^{-7}	0	4380	1.5825x10^{-4}	0.15000	1.00000
Technetium ^{99}Tc	1.25 x 10^{-2}	0.007	76,650,000	9.043x10^{-9}	0.13962	0.93077
Uranium ^{238}U	417	0.4	1.6425x10^{12}	4.2201x10^{-13}	0.02857	0.19048
Strontium ^{90}Sr	2.0 x 10^{-1}	1	10,585	6.5484x10^{-5}	0.01290	0.08602
Plutonium ^{238}Pu	1.0 x 10^{-7}	5	32,120	2.1580x10^{-5}	0.00277	0.01848

> *   q, θ, ρ, and D are assigned the base values in Section 6;
> K_d is assigned values given in Column Three;
> μ is obtained from half-life $t_{1/2}$ using Equation (I-3).

Comparing the times, (600 cm ÷ advection term coefficient), with the half-lives listed in Table I-1, one observes that the first-order decay rate μ will probably be most important for the transport and fate of ^{238}Pu through the 6 m layer, followed by that of ^{90}Sr, followed by that of ^{3}H. Because of the very long half-lives for ^{99}Tc and ^{238}U, their decay rates are not very important over the 6 m layer with respect to the BTCs of these parents. However, with respect to the production of the daughter, ^{99}Ru from ^{99}Tc and ^{234}U from ^{238}U, these very small decay rates may be important.

I.2 Breakthrough Curves for ^{99}Tc and It's Daughter, ^{99}Ru

For the decay chain, ^{99}Tc → ^{99}Ru, ^{99}Tc has a very low decay rate μ which has negligible effect on the BTC for ^{99}Tc over the 6 m depth of the current simulation. However, this low decay rate does produce a small amount of the stable radionuclide, ^{99}Ru, while the ^{99}Tc moves from its surface source (of a 1,000 days duration) down through the 6 m soil column. The lifetime of the moving source of ^{99}Ru equals the lifetime of the ^{99}Tc BTCs for the given recharge rate q = 0.0024 cm/d. This lifetime is equal to or less than 10,000 days while the half-life of ^{99}Tc is about 76,650,000 days. The travel time for ^{99}Ru through the layer is much greater than that for ^{99}Tc because the K_d for ^{99}Ru is 5 ml/g versus that of 0.007 ml/g for ^{99}Tc. However, the travel time for ^{99}Ru through the 6 m layer should be on the same order as that of ^{238}Pu, namely about 200,000 days, since the K_d values of ^{99}Ru and ^{238}Pu are taken to be equal. However, ^{238}Pu has a significant decay rate (^{238}Pu → ^{234}U), while ^{99}Ru is stable; μ^* in Equation (I-2) is zero for ^{99}Ru. Since FECTUZ has a different θD-value than CHAIN (see Equation I-2), these two codes were used to see the effects of diffusion on the BTCs of ^{99}Ru for the 6 m layer. The diffusion term coefficient for FECTUZ is about 2/3 that of CHAIN.

The relative magnitude of the concentration c* of ^{99}Ru produced by the decay of ^{99}Tc can be obtained from Equation (I-2) if one ignores all terms except the source term and the time derivative of c*:

$$c^* \cong 1.8 \times 10^{-10} \int_0^t c(t)dt \; . \tag{I-4}$$

The integral term in Equation (I-4) can be approximated from the BTC for ^{99}Tc under the influence of a 0.024 cm/d recharge rate, as given in Figure I-2b. We can roughly approximate the area under this curve as given by 0.001 mg/L times 10,000 d. Thus, the concentration of ^{99}Ru at 10,000 d is equal to 1.8 x 10^{-9} mg/L by Equation (I-4). The FECTUZ/CHAIN result given in Figure I-2a is very nearly equal to this value at t = 10,000 d. Thus, over the first 10,000 d of the evolution of ^{99}Ru, the dominant term in Equation (I-2) is the source of ^{99}Ru being produced by the decaying ^{99}Tc.
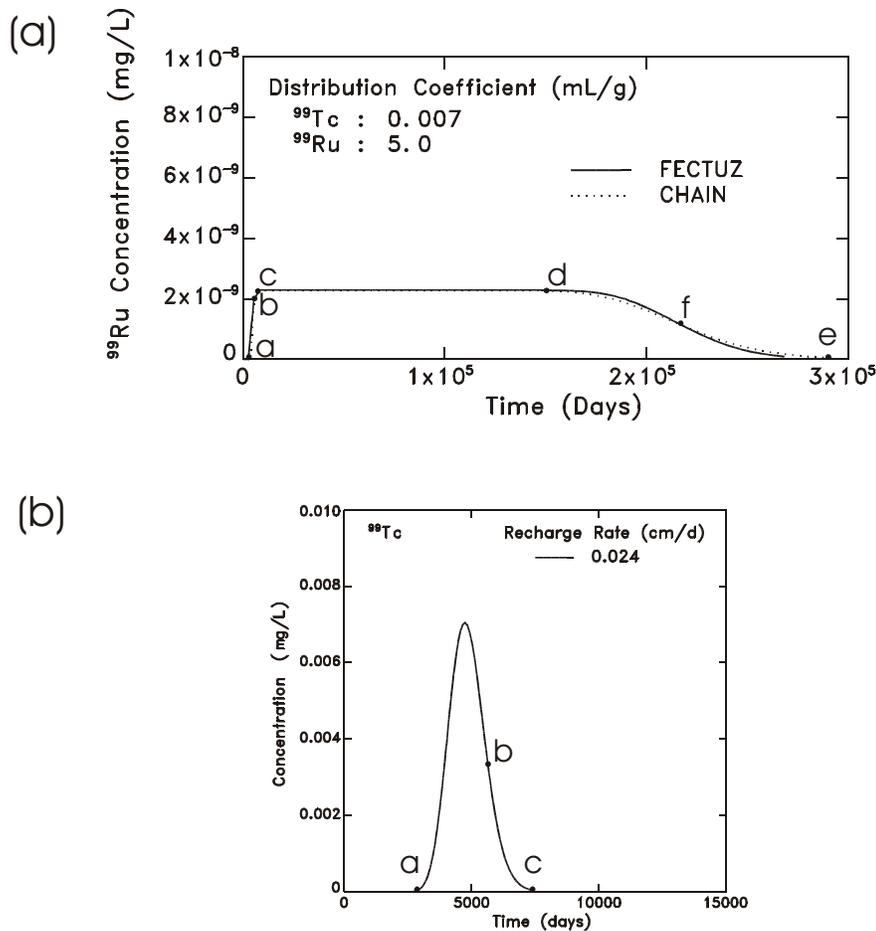
Figure I-2. (a) Breakthrough curves of the daughter product, [99]Ru, from the ^{99}Tc decay using the CHAIN and FECTUZ Models for base case simulation, and (b) the breakthrough curve for [99]Tc. The text will explain a, b, c, d, e and f.

Figures I-2ab, as stated above, show the BTC's at the 6 m soil depth for the parent (^{99}Tc in Figure I-2b) and for the daughter ([99]Ru in Figure I-2a) using the CHAIN and FECTUZ Codes for the base case simulation given in Section 6. The salient points, a, b, c, d, f, e, in the two graphs represent key features in the evolution of the two BTC's. *Point a* represents the beginning of the ^{99}Tc BTC for either the CHAIN or FECTUZ simulation. Since [99]Ru is continually being generated by ^{99}Tc, although very slowly, Point a also represents the initiation of the [99]Ru BTC. From Point a to Point b, the [99]Ru BTC sharply rises as shown in Figure I-2a. *Point b* on the ^{99}Tc BTC is close to the inflection point of the "bell-shaped" curve. At *Point c* on the ^{99}Tc BTC, the remaining mass of the ^{99}Tc released by the surface source during its 1000 day lifetime has moved out of the 6 m thick soil layer. Point c is also the time that the [99]Ru BTC first reaches its maximum value. The times (a,b,c) are roughly equal to (2700, 5600, 7800) days. Because of the large K_d of 5 ml/g for [99]Ru, there is still a reservoir of this stable radionuclide in the 6 m soil column. As seen by both the CHAIN and FECTUZ Codes, this reservoir produces a constant, or nearly constant, peak in the BTC from *Point c to Point d* (a total time interval of more than 140,000 days). From *Point d to Point e* in Figure I-2a, one notes the classical "bell-shaped" curve as the [99]Ru BTC goes from a maximum value at Point d to zero at about Point e. The only major difference between CHAIN and FECTUZ (and this is pretty small) occurs between *Points d and e*. Between *Points d and f,* the FECTUZ result is above that of CHAIN; the reverse is true from *Point f to e*. This is reasonable since FECTUZ has less diffusion than that of CHAIN. There is also a very slight difference (in the right direction) in the models from Point a to Point b. The magnitude of this difference is hard to quantify graphically.

Overall, the CHAIN and FECTUZ Codes tell a reasonable and consistent story concerning the evolution of parent and daughter radionuclides through a 6 m, homogenous soil column, with a uniform, 1000 d source of the

parent at the top of the column. However, the evolutions of parent and daughter species can be quite complex in two-dimensional and three-dimensional, heterogeneous soil columns, as pointed out in Section 3.6 (Oldenburg and Pruess, 1996).

I.3. The Sensitivity of the Five Parent Radionuclides to Recharge Rate

Figures I-3 (a to e) illustrate the sensitivity of the transport and fate of the five parent radionuclides through the 6 m, homogenous soil column to a variable recharge rate, q, using the CHAIN Code for the simulation. The five sets of curves are given in order of increasing default K_d values. As indicated by Equation (I-1), these K_d values govern the rates of pollutant passage through the 6 m layer. In fact, a good representation of characteristic times of passage
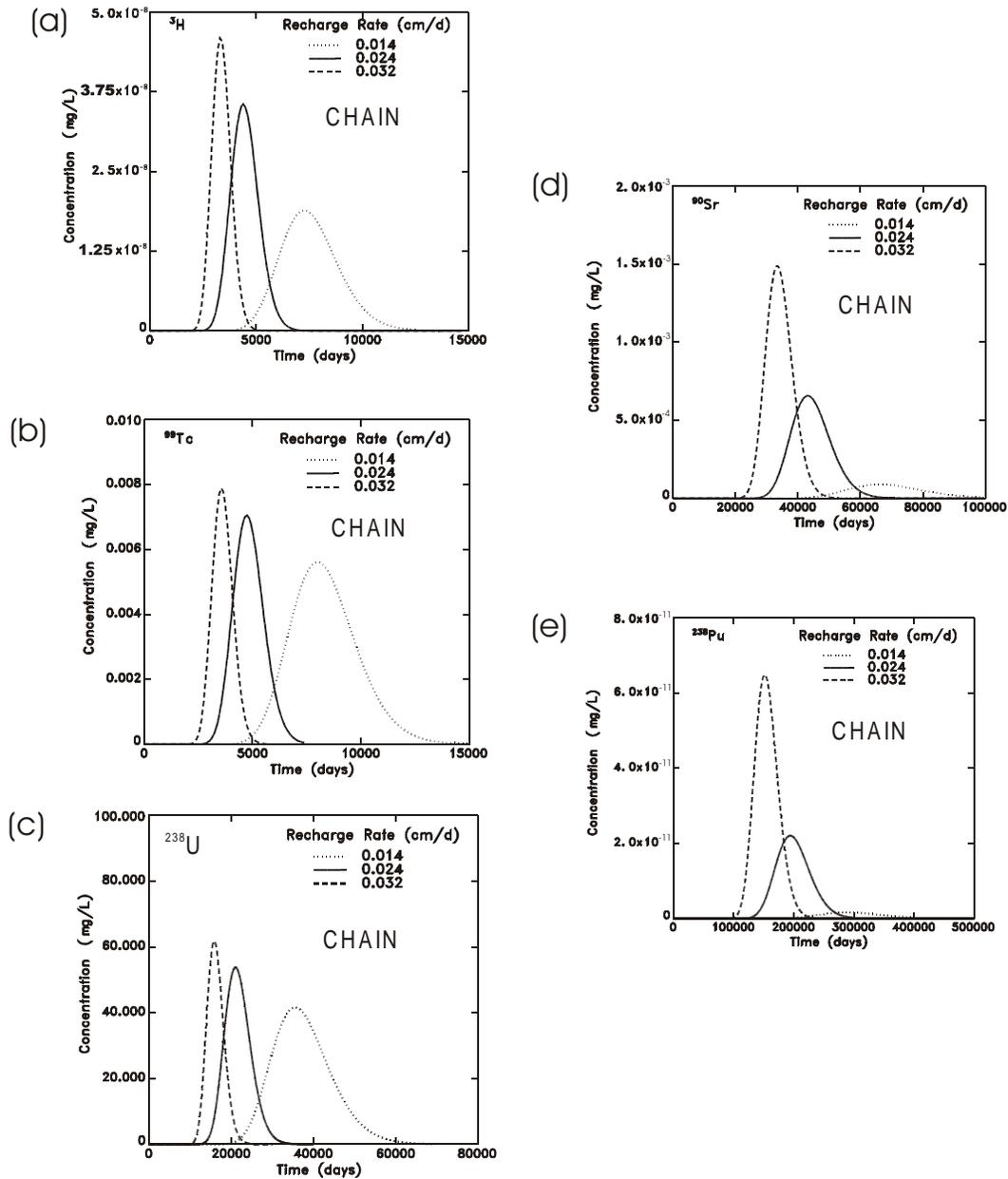

Figure I-3. Sensitivity of radionuclide transport through the unsaturated zone to recharge rate (q) using the CHAIN Model: (a) Tritium ^{3}H; (b) Technetium ^{99}Tc; (c) Uranium ^{238}U; (d) Strontium ^{90}Sr; and (e) Plutonium ^{238}Pu.

I-5

can be obtained from the quotient 600 cm ÷ v, where v is the seepage velocity, or coefficient of the advection term in Equation (I-1):

$$v = \frac{q}{\theta + \rho K_d} \quad .$$

(I-5)

These characteristic times are listed in Table I-2 for the five radionuclides and the three recharge rates q. Also listed in this table are the normalized peaks of the BTCs shown in Figures I-3 (a to e). These peaks are normalized by the respective source concentrations of the radionuclides given in Table I-1. Corresponding to these normalized C_{peak} values are the times to peak concentration, T_{peak}, given in the last column. One should note the rather close correspondence between the "characteristic time" values and the values of T_{peak} given in Table I-2. The final column to note in this table is the "type of decay." The descriptors given in the table can be made more explicit from the log-log plot of $C_{peak} \div C_0$ versus T_{peak} in Figure I-4.

To further illuminate the results in Table I-2 and Figure I-4, we introduce a ***relative diffusion factor (DIF)*** and ***a relative decay factor (DEC)***. The value of DIF is defined as the quotient of the species T_{peak} for q = 0.024 cm/d divided by the T_{peak} for the highly mobile radionuclide, ^{3}H, at a q = 0.024 cm/d. The value of DEC is defined as the quotient of the species T_{peak} for q = 0.0024 cm/d divided by the species decay half-life. Table I-3 lists these factors for the five parent radionuclides. As DIF increases, the amount of diffusive dilution increases, while an increase in DEC produces an increase in the amount of radioactive decay. Using these two factors, the locations of the five curve segments in Figure I-4 can be easily explained:

- The diffusive dilutions of ^{3}H and ^{99}Tc are nearly equal since their DIF values are nearly equal, and the time ranges of their curve segments are nearly the same.

- The curve segment for ^{3}H is below that for ^{99}Tc because ^{3}H has significantly decayed over the time interval, while the decay of ^{99}Tc has been insignificant, although not zero as seen in Figure I-2a.

- The curve segment for ^{238}U, as that of ^{99}Tc, has only experienced insignificant decay, but is lower than the curve segments for ^{99}Tc and ^{3}H, and further to the right, because its DIF is almost five times that of ^{99}Tc and ^{3}H. The ^{238}U's normalized concentrations are lower only because of diffusive dilution.

Table I-2. C_{peak} Normalized by Source Concentration C_0 and T_{peak} for Each Radionuclide and for Three Recharge Rates.

Radionuclide	*Type of Decay	Recharge Rate q (cm/d)	**Characteristic Time (600cm) ÷ v (d)	***Normalized C_{peak} $C_{peak} \div C_o$	T_{peak} (d)
Tritium ^{3}H	Significant	0.014	6860	1.72×10^{-1}	7300
		0.024	4000	3.23×10^{-1}	4400
		0.032	3000	4.18×10^{-1}	3300
Technetium ^{99}Tc	Very Little	0.014	7370	4.49×10^{-1}	8000
		0.024	4300	5.64×10^{-1}	4750
		0.032	3225	6.31×10^{-1}	3560
Uranium ^{238}U	Very Little	0.014	36,000	9.98×10^{-2}	35,500
		0.024	21,000	1.29×10^{-1}	21,000
		0.032	15,750	1.48×10^{-1}	15,900
Strontium ^{90}Sr	Very Significant	0.014	79,715	4.47×10^{-4}	66,100
		0.024	46,500	3.28×10^{-3}	43,100
		0.032	34,875	7.44×10^{-3}	33,200
Plutonium ^{238}Pu	Very Significant	0.014	371,145	1.66×10^{-5}	287,000
		0.024	216,600	2.20×10^{-4}	194,000
		0.032	162,375	6.48×10^{-4}	152,000

*Type of Decay with respect to the 6 m soil column.

** v = seepage velocity = $\dfrac{q}{\theta + \rho K_d}$.
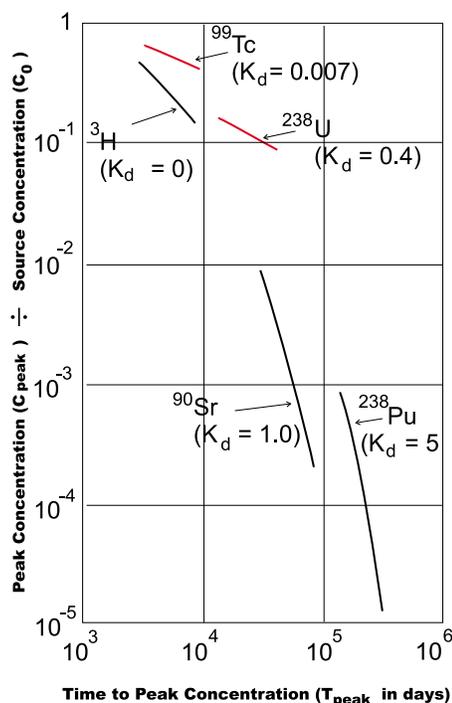
*** C_o = Concentration at Source, in Table I-1.

Figure I-4. $C_{peak} \div C_o$ versus T_{peak} in days for five radionuclides, showing the effects of various K_d values and various decay rates, where the time intervals of the curve segments are determined by the range of discharge rates for the 6 m soil column.

- The curve segments for ^{90}Sr and ^{238}Pu are both much lower and to the right of those ^{3}H, ^{99}Tc and ^{238}U because their DEC values are much larger and their DIF values are also much larger. This means that their normalized concentrations are lower than the other three species because of both greater diffusion and greater decay.

- The curve segment for ^{238}Pu is lower and further to the right of that of ^{90}Sr since its DIF is four and one-half times that of ^{90}Sr and its DEC is about one and one-half times that of ^{90}Sr. This means that over comparable time segments (i.e., the T_{peak} values for the range of q for the 6 m soil column) more of the ^{238}Pu has diffused and decayed than that of ^{90}Sr.

Table I-3. The Relative Diffusion Factors and the Relative Decay Factors for the Five Parent Radionuclides.

Radionuclide	*Type of Decay	For Recharge Rate, q = 0.024 cm/d	
		Relative Diffusion Factor	Relative Decay Factor
Tritium ^{3}H	Significant	1.000	1.005
Technetium ^{99}Tc	Very Little	1.080	0.000
Uranium ^{238}U	Very Little	4.773	0.000
Strontium ^{90}Sr	Very Significant	9.795	4.072
Plutonium ^{238}Pu	Very Significant	44.091	6.040

*Type of Decay with respect to the 6 m soil profile.

References

Oldenburg, C.M. and K. Pruess. 1996. "Mixing with first-order decay in variable-velocity porous media flow." Transport in Porous Media. 22:161-180.

U.S. EPA. 1999a. Understanding Variations in Partition Coefficients, K_d, Values: Model, Methods of Measurement, and Application of Chemical Reaction Codes. Volume I. EPA 402/R-99/004A. Office of Radiation and Indoor Air & Office of Solid Waste and Emergency Response. U.S. EPA. Washington, DC.

U.S. EPA. 1999b. Understanding Variations in Partition Coefficients, K_d, Values: Review of Geochemistry and Available Kd Values for Cadmium, Cesium, Chromium, Lead, Plutonium, Radon, Strontium, Thorium, Tritium, (^{3}H), and Uranium. Volume II. EPA 402/R-99/004B. Office of Radiation and Indoor Air and Office of Solid Waste and Emergency Response. U.S. EPA. Washington, DC.

U.S. EPA. 2000a. Soil Screening Guidance for Radionuclides: User's Guide. EPA 540/R-00/007. Office of Radiation and Indoor Air and Office of Solid Waste and Emergency Response. U.S. EPA. Washington, DC.

U.S. EPA. 2000b. Soil Screening Guidance for Radionuclides: Technical Document. EPA 540/R-00/006. Office of Radiation and Indoor Air and Office of Solid Waste and Emergency Response. U.S. EPA. Washington, DC.

EPA

United States
Environmental Protection
Agency

National Risk Management
  Research Laboratory
Cincinnati, OH 45268

Official Business
Penalty for Private Use
$300

EPA/600/R-02/082
July 2002